Thompson, Catriona M.A. (2019) *The biochemical and biophysical characterisation of protein antibiotics targeting Pectobacterium spp. and Streptococcus agalactiae.* PhD thesis.

https://theses.gla.ac.uk/41021/

Copyright and moral rights for this work are retained by the author

A copy can be downloaded for personal non-commercial research or study, without prior permission or charge

This work cannot be reproduced or quoted extensively from without first obtaining permission in writing from the author

The content must not be changed in any way or sold commercially in any format or medium without the formal permission of the author

When referring to this work, full bibliographic details including the author, title, awarding institution and date of the thesis must be given

Enlighten: Theses
https://theses.gla.ac.uk/
research-enlighten@glasgow.ac.uk

University of Glasgow

The Biochemical and Biophysical Characterisation of Protein Antibiotics Targeting *Pectobacterium* spp. and *Streptococcus agalactiae*

Submitted to the University of Glasgow for the degree of Doctor of Philosophy

Catriona M. A. Thompson

Submitted 28/09/18

Institute of Infection, Immunity and Inflammation

College of Medical Veterinary and Life Sciences

University of Glasgow

Acknowledgements

Firstly, I would like to thank both Professor Daniel Walker and Professor Olwyn Byron for their continuous support and encouragement throughout this project. They allowed me to take my PhD in my own direction and to develop as a scientist, whilst always letting me ask the stupid questions.

To the excellent pals I have made along the way, you are brilliant in every way and you have all truly made these 3 years the best I have had. Thank you to the end office for the helpful discussions, unhelpful discussions and snack box. You have always made coming into work a joy. Thank you to members of the Walker lab past and present who have been both great friends and great mentors.

To my family who have always been my biggest supporters, I am not sure what I would do without you. And to Shona, the best of cats, who was here from beginning to end and who chose to sleep on every draft of this thesis.

This work was supported by a BBSRC Westbio DTP studentship.

Disclaimer

I declare that, unless explicitly stated, this work was performed solely by the author and has not been submitted for any other degree at the University of Glasgow.

Catriona M. A. Thompson

28/09/18

Abstract

Food security is the idea by which a population has enough food to sustain itself without famine. A large number of factors can influence the stability of food production, including diseases caused by microorganisms. *Pectobacterium* spp. is one of the leading causes of soft rot disease, resulting in crop losses both pre- and post-harvest.

Bacteriocins are potent narrow spectrum protein antibiotics which target closely related bacteria to the producing strain. Ferredoxin-containing bacteriocins produced by and targeted towards *Pectobacterium* species have both a different domain organisation and uptake mechanism to all known Gram-negative bacteriocins. This work has shown that pectocins are able to pass through the outer membrane of *Pectobacterium* spp. by parasitising the ferredoxin uptake receptor, FusA. This uptake requires the pectocins to be flexible in order to pass through the lumen of the barrel and enter the periplasm. This work has shown an interaction between FusB and pectocin M1, suggesting a novel mechanism of uptake.

Streptococcus agalactiae is the causative agent of disease in a wide range of hosts, ranging from human neonates to farmed Tilapia. *S. agalactiae* infection has a detrimental effect on the dairy industry each year as it is the leading cause of mastitis in cattle. As well as this, the prevalence of *S. agalactiae* in farmed fish has resulted in large numbers of infected fish and subsequently the infection of consumers.

Bacteriocins produced by Gram-positive bacteria are often small modified peptides which target the peptidoglycan layer or cytoplasmic membrane of the target cell. However, a small number of protein bacteriocins produced by Gram-positive bacteria have been discovered, with the best characterised of these being lysostaphin. It has been shown that bacteriocins similar to lysostaphin are also produced by other Gram-positive bacteria, such as zoocin A produced by *Streptococcus zooepidemicus*. Prior to this work a novel protein bacteriocin produced by and targeted towards *S. agalactiae*, named agalacticin A, was discovered. It was predicted that this bacteriocin was similar in structure and

function to zoocin A. This work has gone some way to structurally characterising agalacticin A, showing a two-domain structure joined by a flexible linker region allowing for the two domains to move independently. As well as this it has shown the importance of the histidine residues at the predicted active site confirming the similarities between agalacticin A and zoocin A. Together this work has gone some way to showing the potential of agalacticin A as a novel therapeutic.

Altogether this work has characterised three novel bacteriocins active against pathogenic bacteria to gain a better understanding of their structure, mechanism of action and uptake.

Abbreviations

Å	Angstrom
A_{nm}	Absorbance (wavelength in nanometres)
AA	Amino acid(s)
AUC	Analytical ultracentrifugation
BCCM	Belgian co-ordinated collections of microorganisms
BHI	Brain-heart infusion
bp	Base pair
CD	Circular dichroism
CFU	Colony forming units
CSP	Chemical shift perturbation
Da	Dalton
D_2O	Deuterated water
dH2O	Distilled water
DLS	Diamond light source
DTT	Dithiothreitol
EB	Elution buffer produced by Qiagen
EDTA	Ethylenediaminetetraacetic acid
ENM	Energetic node modelling
EOM	Ensemble optimisation modelling
g	Gram(s)
GBS	Group B streptococcus
h	Hour(s)
HCl	Hydrochloric acid
HPLC	High pressure liquid chromatography
HSQC	Heteronuclear single quantum coherence
i(q)	Scattering angle intensity
IPTG	Isopropyl β-D-1-thiogalactopyranoside
IUTD	Intrinsically unstructured translocation domain
kb	Kilobase(s)
kDa	Kilodalton (s)
keV	Kilo electron volt(s)
kV	Kilovolt(s)
L	Litre(s)
LB	Lysogeny broth
LDAO	Lauryldimethylamine oxide
LPS	Lipopolysaccharide
M	Moles
MALS	Multi-angle light scattering
mAU	Milli absorbance units
MgCl2	Magnesium chloride
$MgSO_4$	Magnesium sulphate
min	Minute(s)
ml	Millilitres
mM	Millimolar
MOPS	3-(N-morpholino)propanesulfonic acid

NAG	N-acetylglucosamine
NaCl	Sodium chloride
NAM	N-acetylmuramic acid
ng	Nanogram(s)
nM	Nanomolar
Nm	Nanometres
NMR	Nuclear magnetic resonance
OD	Optical density
p.p.m.	Parts per million
PBS	Phosphate buffer saline
PCR	Polymerase chain reaction
PDB	Protein data bank
PMF	Proton motive force
q	Scattering angle
RE	Restriction enzyme
R_g	Radius of gyration
rpm	Revolutions per minute
RT	Room temperature
S.O.C.	Super optimal broth
SANS	Small angle neutron scattering
SAXS	Small angle x-ray scattering
SCRI	Scottish crop research institute
SDM	Site-directed mutagenesis
SDS	Sodium dodecyl sulphate
SDS-PAGE	Sodium dodecyl sulphate–polyacrylamide gel electrophoresis
SEC	Size exclusion chromatography
SV	Sedimentation velocity
TRD	Target recognition domain
Tris	Tris(hydroxymethyl)aminomethane
TSA	Tryptone soya agar
UV	Ultraviolet
V	Volt(s)
w/v	Weight per volume
WT	Wild-type
Δ	Deletion
µF	Microfarad
µg	Microgram
µM	Micromolar

Table of Contents

List of Tables

List of Figures

List of Accompanying Material

Chapter 1 Introduction

1.1 Food security

Food security is the idea that an entire population has enough viable food to sustain itself without famine. Hunger and malnutrition are prevalent with more than 800 million people suffering worldwide [1] and this number is ever increasing as the population increases. There are a large number of factors that affect the stability of crop production including crop diversity, susceptibility to diseases, phytopathogens such as bacteria and fungi, and lack of nutrient rich soil are a few of the environmental factors that can affect the production of good quality crop plants in many countries around the world [1,2].

Plant pathogens destroy at least 10% of crop plants every year [2–4] with a further 6-12% being lost post-harvest [2,3]. This crop loss can be devastating as a large proportion of a population can be dependent on a single crop species [3]. It is important therefore to develop novel methods to prevent diseases within crop plants in order to increase the amount of viable food produced.

Bacteria can cause a wide-range of diseases affecting both plant and animal species [5,6]. There are a large number of both Gram-positive and negative bacteria that can be detrimental to the health of domesticated animals such as farmed cattle and fish [5,7]. One organism which can infect a wide range of host species is *Streptococcus agalactiae*, also known as Group B *Streptococcus* (GBS). GBS is an opportunistic human pathogen which is the major causative agent of neonatal sepsis [8,9]. Moreover, GBS is one of the leading causes of mastitis in cattle, which in turn has a significant impact on milk production [5]. Not only does this organism infect cattle, but GBS infection can also have a detrimental impact on the populations of farmed fish, particularly those grown in south Asian countries [7]. The first line of defence against GBS infection is the use of β-lactam antibiotics, such as penicillin, however the overuse of these to treat human disease and in aquaculture is leading to an increase in the development of resistant bacterial populations therefore the development of novel control strategies is essential [10,11].

1.2 Bacteria targeted in this work

1.2.1 *Pectobacterium* spp.

Plant pathogens employ one of two methods to invade host tissue: stealth or brute-force [12]. Pathogens that rely on living plant tissue as a nutrient source, such as *Pseudomonas* spp., employ stealth mechanisms to maintain an infection and avoid the host immune system [12]. However, necrotrophs, such as *Pectobacterium* spp., employ a brute-force method of infection as they do not require living plant tissue to gain nutrients [12]. *Pectobacterium* spp. are aggressive phytopathogens characterised by their large arsenal of plant cell-wall degrading enzymes and ability to macerate plant tissue causing necrosis [12]. Maceration of plant tissue is particularly damaging to crops pre- and post-harvest, as even if the infection can be treated the crop plants are still likely to be unusable due to the necrosis that may have occurred during infection [3,13].

The two species within the *Pectobacterium* genus are *P. atrosepticum* and *Pectobacterium carotovorum* which have a narrow and broad host range respectively [14]. *P. atrosepticum* is a prolific pathogen which infects only S*olanum tuberosum* (potato) both in the field (blackleg) and during storage (soft rot) [15]. The characteristic symptoms of blackleg infection are black rot lesions which are wet and slimy in appearance, however under dry conditions these can appear as a yellow wilt in the stems and leaves [15]. Soft rot is confined to the tuber after harvest, the tuber tissue is macerated and becomes black when exposed to the air [15].

The spread of infection most commonly occurs through interaction with infected tissue, as survival of *Pectobacterium* species in the soil is limited to a maximum of 6 months under ideal conditions [15]. The most likely cause of disease transmission is through the release of bacteria into the soil after the planting of infected seed potatoes and the subsequent soil water contamination [15]. Once in the soil *Pectobacterium* spp. can colonise the roots of the host and utilise the vascular system to enter the plant tissue, leading to colonisation and potentially infection [15].

In order for a successful infection to be established *Pectobacterium* spp. must colonise the plant tissue, grow and evade the hosts innate immune defences [13]. During colonisation *Pectobacterium* spp. acquires essential nutrients from the plant tissue, however once this supply of nutrients has been exhausted it is thought that this triggers the deployment of cell-wall degrading enzymes in order to overcome this nutrient deficiency [13]. Within a large majority of pathogenic bacteria the type III secretion system is relied upon to secrete effector proteins to evade the hose immune system [12], however it has been shown that some *Pectobacterium wasabiae* strains lack this system entirely [16] suggesting an alternative method of evasion. This lack of a type III system is not a universal trait of *Pectobacterium* species, with work showing that the presence of this system is essential for the early colonisation of potato leaf by *P. carotovorum* [17].

The prevention of soft rot within *S. tuberosum* has been achieved primarily through the breeding of partially resistant tubers. However, it has also been shown that pre-treatment of plants with calcium can reduce infection rates [15]. One of the most commonly used methods of disease prevention is the removal of diseased crops through careful inspection prior to certification [15]. Although this method is widely used the presence of latent infections within seed tubers is difficult to detect [15].

Preliminary work to examine the use of biological tools to combat *Pectobacterium* spp. infection began with the use of lytic bacteriophage particles [4]. Bacteriophages have been tested against a variety of soft rot pathogens and were shown to be successful at reducing bacterial load in tubers, however more work to develop this as a long-term prevention method against *Pectobacterium* infection is needed [18]. Several other methods of biocontrol have been investigated including the use of *Streptomyces* [19], carob extracts [20] and the disruption of quorum sensing [21], however, to date no definitive biocontrol strategy has been successfully implemented in the field.

1.2.2 *Streptococcus agalactiae*

GBS is a Gram-positive opportunistic commensal bacteria which causes disease in a wide range of host species [22]. The ability to colonise and persist in different hosts is dependent on a variety of virulence factors and adherence capacities as well as the ability to successfully form biofilms [22]. It has been shown that some sequence types of GBS have shown host specificity by remodelling their metabolism to suit their preferred host environment as well as tailoring their genome to best suit their preferred host [23]. Despite the adaptation of some GBS sequence types to a specific host, a large number of GBS strains are able to successfully colonize a range of both warm and cold blooded hosts with little change in their physiology [24].

GBS is a causative agent of both mastitis in cattle and streptococcosis in fish resulting in losses in both agricultural industries each year [5,25,26]. The prevalence of mastitis within the dairy industry is one of the leading causes of profit loss, with GBS being the primary causative agent of this disease [27]. Within recent years the number of GBS mastitis outbreaks has been reduced due to improved farming and control methods, however the passing of the organism between species still poses some risk to the industry [27].

GBS colonises the urogenital tract of up to 30% of healthy adults but can be transmitted vertically to neonates [28]. GBS can colonise neonates either *in utero* or during birth, with infections occurring in 1-2% of colonized new-borns [22]. Prophylactic treatment of GBS positive expectant mothers with ß-lactam antibiotics before or during labour has been shown to be an effective method of reducing the number of neonatal GBS infections [28]. Early onset infections generally occur within the first 6 days of life with symptoms typically presenting within the first 24 hours [29]. Infections within neonates can lead to the development of bacteraemia and meningitis which can lead to mortality [29].

In 2015, an outbreak of invasive GBS infection in non-pregnant adults was retrospectively associated with the consumption of uncooked fish colonised by the bacteria [30]. Recent years have seen an increase in GBS outbreaks within farmed fish species, resulting in the annual loss of 40 million dollars within the

industry [26]. The persistent asymptomatic colonisation by GBS within farmed Tilapia is a worldwide concern due to the transmission of the bacteria between colonised fish and humans, either through contact or consumption [26].

Within aquaculture an increased use and dependence on antibiotics for the successful rearing of farmed fish has resulted in an increase in the prevalence of antibiotic resistance within GBS strains [10]. There are two major concerns with the use of antibiotics in aquaculture: The prevalence of antibiotic residue in the edible tissues and the emergence of antimicrobial resistance in zoonotic pathogens [31]. Due to the nature of aquaculture large amounts of prophylactic antibiotics are used in both the water and food which has led to an increase in the presence of antibiotic resistance genes within bacteria isolated from farmed fish [32]. This prevalence of antibiotic resistance transmission between fish, mammals and humans is becoming a growing concern for both human health and food security [10,33].

The first approach to treating GBS infection is through the use of ß-lactam antibiotics, such as penicillin, however in recent years an increasing number of isolates have been shown to be resistant to this treatment method due to the alteration of peptidoglycan amino acids [11]. This is further complicated by the presence of resistance markers to alternative antibiotics, such as erythromycin, in as many as 50% of colonising isolates [34–36]. Due to the widespread prevalence of GBS worldwide, the development of novel antibiotics treatments has been examined for some time. Unfortunately, widespread prevalence and diversity has meant that no current vaccine is effective against all strains of GBS at present [22,37].

1.3 Bacteriocins

1.3.1 Bacterial competition

The competition for nutrients and the occupation of a niche are the focal point of the microbial competition machinery [38]. Bacteria have developed an arsenal of antimicrobial mechanisms in order to displace and outcompete neighbouring cells [39]. Microbes can compete indirectly through the consumption of resources, depleting the supply of nutrients and outcompeting

other members of the niche [39]. Direct competition occurs through the production of inhibitory substances which damage competing cells [39]. Bacteriocin production is widespread amongst both Gram-negative and Gram-positive bacteria in order to directly compete for nutrients and space [39–41].

Bacteriocins from Gram-positive bacteria are generally found to be small peptide antibiotics which target other Gram-positive bacteria usually from within the same genus [42]. In contrast, Gram-negative bacteriocins are more commonly found to be protein antibiotics targeting peptidoglycan synthesis, degrading nucleic acids or creating pores in the cytoplasmic membrane causing depolarisation [43]. The mechanism and uptake of bacteriocins has been of interest for many years as they are a good candidate for novel antibiotics due to their narrow spectrum and potency [44].

1.3.2 Peptide bacteriocins

Both Gram-positive and Gram-negative bacteria produce an array of antimicrobial compounds, including small peptides. Small peptide bacteriocins are most commonly produced by Gram-positive bacteria and can have a narrow or a broad spectrum [45]. One of the most well studied and widely used of these peptide bacteriocins is nisin. Nisin is a post-translationally modified peptide consisting of 34 amino acids (AA) which depolarises the cytoplasmic membrane to cause cell lysis [46]. Unlike most bacteriocins, nisin has a broad-spectrum and is able to target multiple Gram-positive bacteria [46]. Due to its potency against food-related pathogens nisin has been successfully implemented as a food preservative worldwide [47].

1.3.3 Colicins

Bacteriocins have been found to be produced by most, if not all, Gram-negative bacteria and are generally classified by their cytotoxic activity [48]. The most well studied group of Gram-negative bacteriocins are those produced by and targeted towards *Escherichia coli,* named colicins.

Unlike the bacteriocins of Gram-positive bacteria, Gram-negative bacteriocins have to cross the outer membrane of the target cell in order to cause cell lysis

[49,50]. For this to occur the bacteriocins must interact with at least one outer membrane receptor for translocation [51]. Colicins have a conserved three domain arrangement regardless of their mechanism of action or outer membrane receptor [43]. This structure consists of an N-terminal translocation domain which contains a disordered N-terminal intrinsically unstructured translocation domain (IUTD), a receptor binding domain and C-terminal cytotoxic domain, the nuclease type colicins also possess a C-terminal immunity protein which remains bound to the protein until translocation (Figure 1-1) [43].

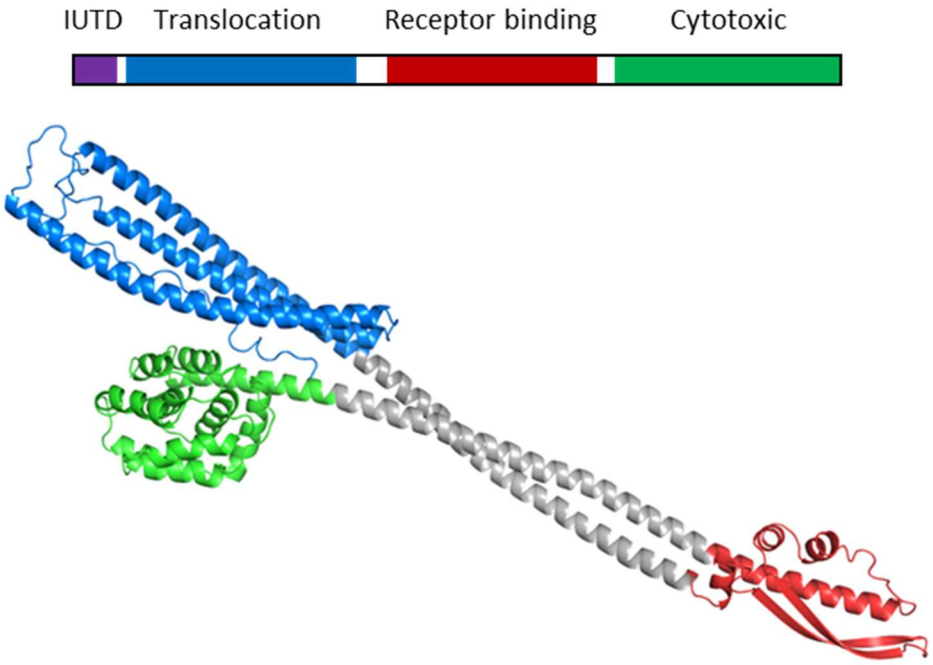

Figure 1-1 Schematic of colicin domain structure with the crystal structure of colicin Ia, a group B colicin, (PDB ID 1CII) used as an example model. The N-terminal intrinsically unstructured translocation domain (IUTD) in purple (not shown in crystal structure), followed by a translocation domain (blue), receptor binding domain (red) and cytotoxic domain (green). Group A colicins also possess a C-terminal immunity protein (not shown).

It has been shown that the majority of colicins require two outer membrane proteins for successful translocation [40,43]. The colicin primarily binds to an outer membrane receptor with high affinity, this outer membrane receptor is responsible for the anchoring of the colicin to the outer membrane and is the first interaction between the protein and the target cell [40].

Once bound to the cell, the translocation domain of the colicin interacts with a co-receptor. The N-terminal region of the colicin consists of a disordered region, known as the intrinsically unstructured translocation domain (IUTD), which can pass through the lumen of an outer membrane receptor or porin to interact with TonB or TolB in the periplasm, completing the translocon and initiating translocation [52].

Finally, the C-terminal domain of the colicin is the catalytic or cytotoxic domain. This domain is responsible for the lysis of the target cell, whether through pore-formation, DNase or RNase activity or by disrupting the synthesis of peptidoglycans [40,43]. Nuclease type colicins act by either degrading chromosomal DNA (e.g. colicin E9) or through the cleavage of RNA, either ribosomal 16S or tRNA (e.g. colicin E3 and E5 respectively) [53].

In contrast to the nuclease colicins, pore forming colicins are amongst the most structurally diverse of the colicins and their uptake is mediated by a variety of different outer membrane receptors [40]. The pore-forming domains are structurally similar and consist of a tightly packed bundle of α-helices which is able to rearrange itself upon contact with the cytoplasmic membrane in order to form a voltage-gated ion channel, destabilising the membrane and subsequently causing cell lysis [43].

Although colicins are the most well studied of the bacteriocins, the conserved domain structure can be seen in bacteriocins from other Gram-negative bacteria. Pyocins are bacteriocins produced by and targeted towards *Pseudomonas* species and have been seen to have a similar domain organisation [54]. This conserved organisation suggests a universal domain organisation of Gram-negative bacteriocins in order to parasitise existing nutrient uptake receptors [43,54,55].

1.4 Crossing the outer membrane

1.4.1 Mechanisms of bacteriocin uptake

The outer membrane of Gram-negative bacteria allows the selective passage of nutrients into the cell [56]. The selective uptake of proteins and nutrients has

led to the parasitisation of outer membrane uptake machinery by bacteriocins in order to enter the target cell [43]. Both Tol- and TonB-dependent bacteriocins possess an N-terminal IUTD which is known to be important for the uptake of colicins and pyocins into the periplasm of the target cell (Figure 1-2) [43,55].

The E-type colicins of *E. coli* utilise the Tol system to enter the cell through the recruitment of the periplasmic TolB protein. E-type colicins first interaction with the cell surface is the high affinity binding to BtuB, an outer membrane TonB-dependent receptor [50,57,58]. The receptor binding domain of colicin E3 has been shown to interact with the extracellular loops of BtuB [58]. This primary interaction is thought to be to coordinate the colicin close to the membrane surface in order for it to interact with its secondary receptor, OmpF [58].

The translocation domain of E-type colicins is important for the recruitment and occlusion of the OmpF porin [59]. The IUTD of the colicin is passed through the OmpF channel to recruit the periplasmic Tol complex, forming the translocon [52]. The interaction between TolB and the colicin connects the colicin to the proton motive force (PMF) of the inner membrane, triggering the release of the bound immunity protein and initiating cell entry [59].

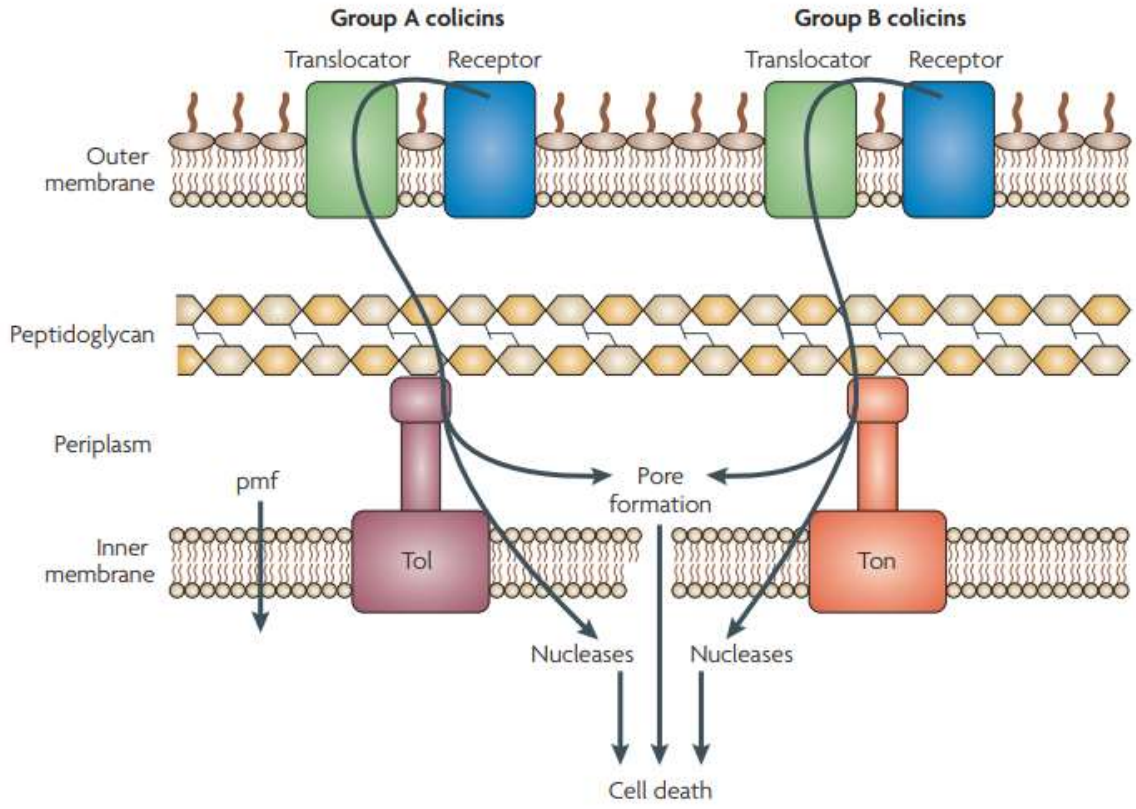

Figure 1-2 Schematic of translocation uptake systems of colicins into *E. coli*. Group A and B colicins utilise the Tol and Ton systems respectively, this diagram illustrated the uptake routes of each group into the target cell. Taken from [40] with reproduction rights obtained from the nature publishing group.

Colicin N is an unusual group A colicin which has been seen to only use the OmpF porin for uptake [60]. Like the other colicins, colicin N has the same three domain structure, however the receptor binding and translocation domains are much smaller than those of other group A colicins [60]. Unlike other colicins, the receptor binding domain of colicin N interacts with lipopolysaccharide (LPS) on the surface of the target cell rather than an outer membrane receptor [60,61]. Colicin N has a high affinity to OmpF, once bound the unfolded IUTD threads through the pore of OmpF to interact directly with TolA for translocation, though the exact mechanism for translocation still remains elusive [52,60,62].

Unlike the group A colicins, group B colicins interact with the inner membrane TonB-protein complex to gain entry into the cell [43]. TonB-dependent outer membrane receptors, such as BtuB, interact with the TonB protein complex

within the periplasm to harness the PMF for substrate uptake [63]. Therefore like the group A colicins, group B colicins also rely on the recruitment of the PMF by the IUTD to gain entry into the cell [63].

Pyocin S2 is a DNase type bacteriocin produced by and targeted towards *Pseudomonas* species and is known to parasitise the *Pseudomonas* FpvAI outer membrane receptor [63]. FpvAI is a TonB-dependent receptor that actively imports the iron-binding siderophore ferripyoverdine [63,64]. The interaction of pyocin S2 and FvpAI was seen to mimic the native substrate, ferripyoverdine, in both structure and receptor binding site [63]. The similarity of the pycocin S2 N-terminal domain to the natural substrate allows it to mimic the natural substrate upon interaction with FpvAI and thus induce the conformational change in the receptor needed for import (Figure 1-3) [63]. This conformational change allows for the interaction of the PMF-coupled TonB with the now exposed TonB-box of the FpvAI, promoting the partial unfolding and exit of the plug domain from the barrel [63]. Subsequently, a second copy of TonB interacts with the IUTD of pyocin S2 to pull the bacteriocin through the FpvAI channel after the plug domain is displaced [63].

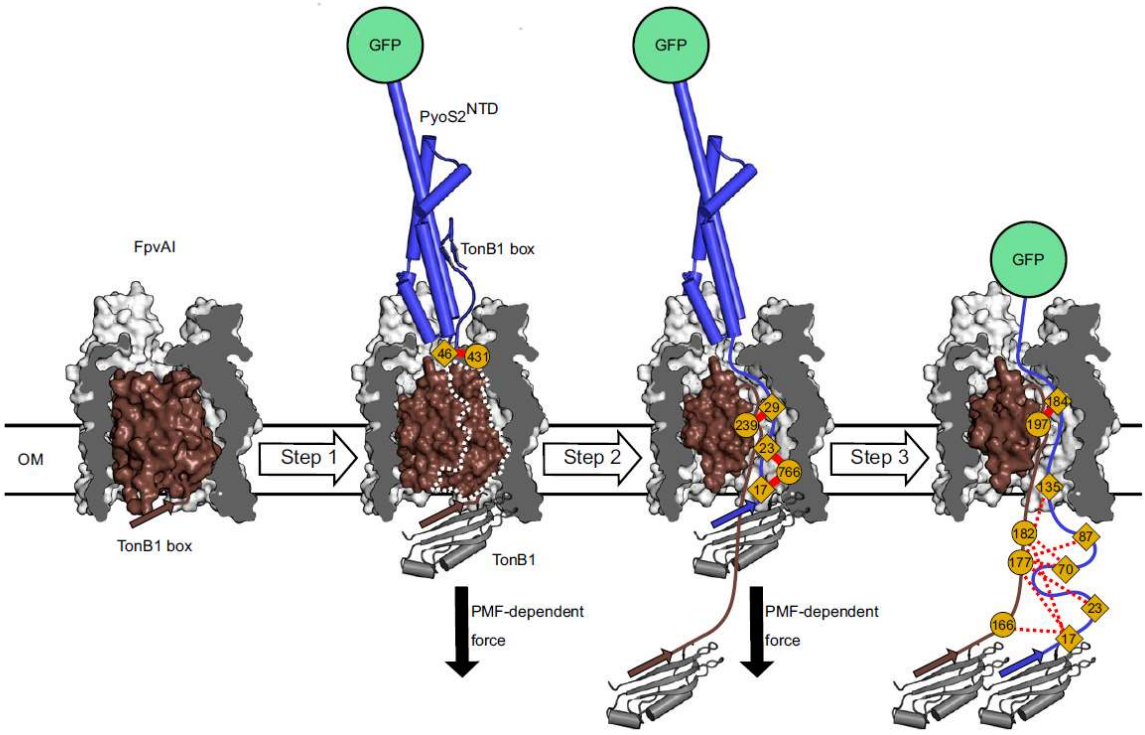

Figure 1-3 Model of Pyocin S2^{NTD} translocation through FpvAI as a model for TonB-dependent pyocin uptake. Pyocin S2^{NTD} mimics the native substrate ferripyoverdine and binds to TonB-dependent outer membrane receptor FpvAI. Substrate binding induces a conformational change and release of the TonB-box and partial unfolding of the plug domain by TonB. This allows the IUTD of pyocin S2 to recruit a second copy of TonB for translocation through the FpvAI lumen. Reproduced from [63] under a creative commons licence.

Unlike pyocin S2, colicin Ia recruits two copies of the same TonB-dependent receptor for uptake. The colicin Ia receptor (Cir) is both the primary binding site and the translocon which allows colicin Ia to enter the cell [65]. Colicin Ia binds with high affinity to Cir on the cell surface, it then locates a second copy of the Cir protein which is used for translocation into the periplasm [65]. Translocation of colicin Ia is dependent on both the presence of a functional Cir outer membrane protein and a functional TonB suggesting that TonB is also necessary for successful uptake (Figure 1-4) [65]. Despite the variation between outer membrane uptake receptors all bacteriocins appear to require the recruitment of the inner membrane PMF for translocation into the periplasm [52,63].

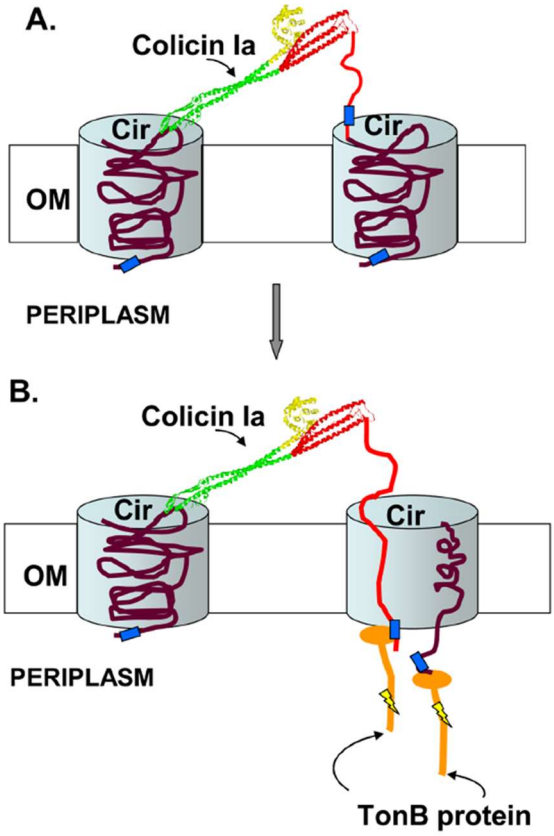

Figure 1-4 Model of colicin Ia receptor recruitment and uptake showing the interaction of colicin Ia with two Cir outer membrane proteins and interaction with TonB a) Binding of the second copy of Cir triggers the rearrangement of the TonB-box allowing for the plug domain to be partially unfolded, allowing for the IUTD of colicin Ia to pass through the lumen to interact with a second copy of TonB in the periplasm . Reproduced from [65] with the publishers permission.

1.4.2 TonB-dependent receptor structure

Gram-negative bacteria use outer membrane transporters dependent on the periplasmic TonB protein interaction to take up nutrients from the environment [66]. This family of receptors is highly conserved with an N-terminal "plug" domain of around 130-150 amino acids which is folded to occlude the C-terminal barrel of the receptor, which in turn is composed of 22 antiparallel ß-strands [66,67]. Despite a highly conserved structure the substrates of these outer membrane proteins vary from carbohydrates to vitamins [68]. Amongst this family are receptors utilised by bacteriocins, including BtuB, FepA and FhuA from *E. coli* (Figure 1-5) [67,69].

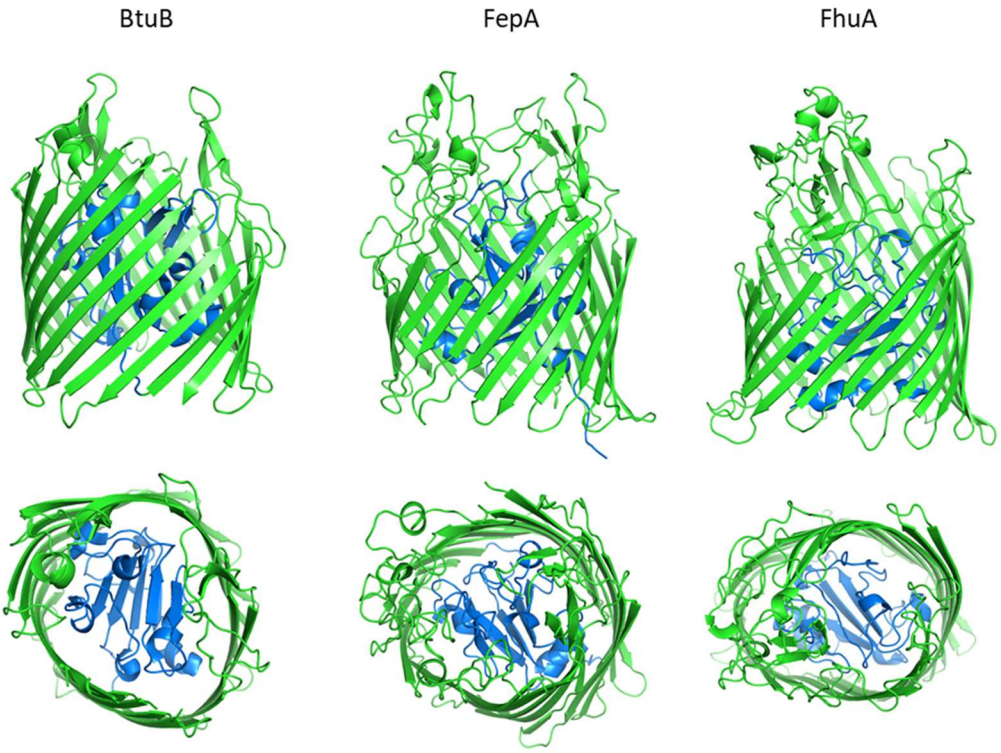

Figure 1-5 Crystal structures of three TonB-dependent receptors from *E. coli* showing their conserved structure. The N-terminal domain (blue) is shown to form a plug within the β-barrel (green) of BtuB (PDB ID 3RGM), FepA (PDB ID 1FEP) and FhuA (PDB ID 1BY3).

The extracellular loops of FhuA, FepA and BtuB are shown to be important for substrate interaction [70]. These extracellular loops show some degree of flexibility that may be important for interaction and coordination of the substrate [70]. Through the deletion of the extracellular loops of FhuA it was shown that these loops are essential for substrate interaction and uptake, but that the substrate binding site is not ubiquitous for all substrates [71]. Moreover this has been supported by studies of both BtuB and FepA which showed that the extracellular loops are essential for substrate uptake [72,73].

FhuA and BtuB are two of the most well studied of the *E. coli* TonB-dependent receptors and are involved in the uptake of siderophores and vitamin B_{12}, respectively. As well as this, both receptors are important for the uptake of colicins into the target cell [70,74]. The N-terminal plug domain of TonB-dependent outer membrane receptors occludes the barrel to prevent the transport of unwanted molecules into the cell, however it must be at least partially removed in order to allow substrate translocation [75,76]. The

mechanism and conformation in which the plug domain exits the barrel is not well understood. It has been suggested that the plug domain can completely unfold, partially unfold or remain folded when exiting the barrel [77–79]. Evidence is present for each of these theories, but to date the strongest evidence suggests that the plug domain partially unfolds and exits the barrel to allow for substrate uptake [63,76].

The examination of the TonB-BtuB complex using atomic force microscopy showed that the interaction of TonB with BtuB can facilitate the remodelling of the BtuB plug domain to allow for the uptake of its substrate, vitamin B_{12} [76]. The examination of FhuA has given support to this model of partial unfolding suggesting that this may be a conserved mechanism between TonB-dependent outer membrane receptors [78].

However, work examining other TonB-dependent proteins suggests that the plug domain may remain folded once it has exited the barrel. Work examining the structure of the plug domain of FepA suggests that it has the properties of an autonomous globular protein [80]. The FepA plug domain appears to have a hydrophobic core and charged and polar side chains suggesting that it might be stable in the absence of the C-terminal barrel, however it was shown to only be partially folded in solution [80]. Contrary to this, work examining TbpA from *Neisseria* spp. showed that the plug domain, although unable to interact with the substrate, remained folded and globular in the absence of the barrel, supporting the idea that the plug domain remains folded when exiting the barrel [77]. This discrepancy suggests that there may not be a universal mechanism of plug displacement within TonB-dependent receptors.

The plug domain of TonB-dependent outer membrane receptor may also be important for the interaction and translocation of the substrates into the periplasm. It has been shown that the plug domain of FepA can bind its substrate, ferric enterobactin, in the absence of the C-terminal barrel [80]. The substrate interaction with the extracellular binding sites is thought to drive the conformational change needed for import [80]. This is supported by the conformational change shown in the crystal structure of FhuA in the presence of its substrate, ferretin, showing a conformational change in the N-terminal

domain consistent with the unfolding of the TonB-box during substrate binding [77,81].

1.4.3 TonB complex

The PMF of the cytoplasmic inner membrane is harnessed for outer membrane substrate translocation by periplasmic proteins such as the TonB protein complex [82]. The TonB complex is comprised of three inner membrane proteins which are required for the active transportation of substances across the outer membrane of Gram-negative bacteria [82]. The energy transfer from the cytoplasmic membrane to the TonB-dependent outer membrane receptor is mediated by the 5-7 residue TonB-box located at the N-terminus of the receptor (appendix 1) [82]. It has been predicted that each TonB complex serves a large number of TonB-dependent receptors to allow substrate uptake rather than a 1:1 molar ratio of receptor to TonB complex [83]

TonB is a proline-rich protein which provides a functional link between the inner and outer membranes of Gram-negative bacteria [84]. TonB is anchored to the cytoplasmic membrane by an N-terminal transmembrane helix and has been shown to directly interact with the TonB-box of the outer membrane proteins [84]. TonB is a highly flexible protein making structural characterisation difficult, however it has been shown that TonB can extend across the periplasm in order to interact with the outer membrane receptors [83].

TonB is in complex with two cytoplasmic membrane proteins, ExbB and ExbD which enhance the efficiency of TonB-dependent uptake [85]. The crystal structure of ExbB shows the presence of a transmembrane domain consisting of three α-helices and a cytoplasmic 5 α-helix bundle [82]. ExbB forms a pentamer in the membrane creating a pore across the cytoplasmic membrane [82]. ExbD is thought to be more similar in structure to TonB with an N-terminal membrane anchor and large periplasmic domain and is a dimer in both the presence and absence of TonB [82]. The pore formed by the ExbB pentamer is thought to be the site at which protons are translocated across the cytoplasmic membrane as well as anchoring ExbD within the membrane [82,85,86].

It has been shown that TonB interacts in an edge to edge manner with the TonB-box of the outer membrane receptor [67]. The β-sheet of TonB interacts with the extended TonB-box, the extension of which is known to be substrate mediated [67]. The N-terminal of the outer membrane receptor FhuA has been shown to be disordered and extend 15-20 Å into the periplasmic space in order to interact with TonB [67]. The interaction between the outer membrane protein and TonB is mediated by the presence and interaction of the TonB-box with the TonB protein in order to drive uptake of the substrate [67,87].

1.5 Targeting the peptidoglycan layer

1.5.1.1 Current antimicrobials

The peptidoglycan layer is an integral part of the bacterial cell structure and therefore a good antimicrobial target [56]. One of the most frequently used classes of antibiotics is the ß-lactams which interfere with assembly of the peptidoglycan layer [88]. ß-lactams interact with penicillin binding proteins preventing the successful construction of the peptide cross-bridges, destabilising the cell [89,90]. Vancomycin, a potent antibiotic against Gram-positive bacteria, inhibits cell wall synthesis by interacting with peptidoglycan precursors [91]. Peptidoglycan plays an essential role in maintaining the shape of both Gram-positive and Gram-negative cells [92]. Therefore the disruption of peptidoglycan synthesis or break-down of the peptidoglycan layer can lead to cell lysis [93].

1.5.1.2 Gram-positive protein bacteriocins and M23 metalloproteases

Within Gram-positive bacteria the number of protein bacteriocins that have been discovered and characterised is limited, with the majority found to be similar in both structure and function to M23 metalloproteases. The M23 metalloprotease are a family of zinc dependent peptidases which exhibit glycyl-glycine endopeptidase activity [94]. This family contains both bacteriocins and autolysins, such as LytM produced by *Staphylococcus aureus* which is known to cleave *Staphylococcal* peptidoglycan during cell division [94]. Recent work has shown a conserved active site within M23 metalloproteases consisting of three histidine residues, a tyrosine residue and an aspartic acid residue which co-

ordinate tetrahedrally around the zinc ion present in the active site (Figure 1-6) [94]. This work also suggested the importance of a tyrosine residue at the active site which has been shown to be important for activity [94]. The co-crystallisation of LytM in the presence of a substrate analogue has identified the substrate binding site as well as suggesting a proposed mechanism by which the water molecule is recruited into the active site by the histidine residues [94].

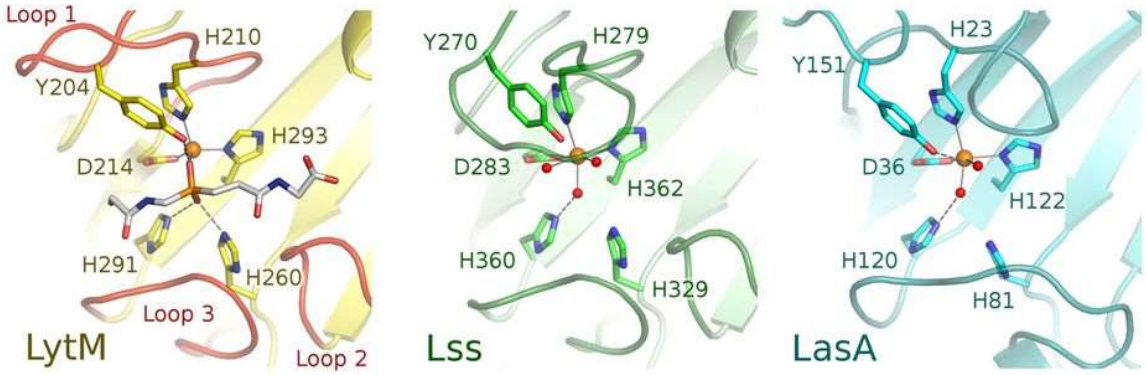

Figure 1-6 Conserved active site of LytM, Lysostaphin (LSS, PDB ID 4QPB) and LasA from *Pseudomonas aeruginosa* (PDB ID 3IT5). Structures of the active site of three M23 metalloproteases showing the conserved histidine, aspartic acid and tyrosine residues coordinating the zinc ion (orange) with the substrate analogue bound to LytM shown in white. Taken from [94] under the creative commons licence.

The mostly widely studied of the Gram-positive protein bacteriocins is lysostaphin, an M23 metallopeptidase produced by *Staphylococcus similins* which has activity against *S. aureus* [95]. Lysostaphin is similar in structure and function to autolysins such as LytM, having a conserved active site and mechanism of action. In contrast, lysostaphin is released from the producing strain to target other *Staphylococcal* species within the same niche [94,95]. It has been known for some time that lysostaphin is a bacteriolytic agent with activity against *S. aureus* making it an important potential therapeutic [96]. Lysostaphin has proved to be an effective therapeutic *in vivo* when tested topically in rodent models and is currently undergoing clinical trials [95].

Structural characterisation of lysostaphin has shown it to be a two domain protein with an inter-domain flexible linker region joining the N-terminal catalytic domain with the C-terminal cell-wall targeting domain [95]. The lysostaphin catalytic domain is similar in structure to LytM with the

characteristic HXXXD and HXH motifs co-ordinating the zinc ion in the active site [95]. As with other M23 metalloproteases the active site is located in the substrate binding groove with the floor of the groove built by the ß-sheet and the wall made of unstructured loops [95].

The cell wall targeting domain of lysostaphin is thought to directly interact with the inter-peptide bridges within the peptidoglycan layer, although the exact interaction site is yet to be confirmed [95]. It has been shown that the cell wall targeting domain has a higher affinity for the stem peptide within the peptidoglycan than towards the glycine cross-bridges [97] suggesting that the initial contact between the cell wall targeting domain and the peptidoglycan does not occur at the cleavage site [97]. The C-terminal domain of lysostaphin is necessary for the targeting of the molecule to the cell wall of *S. aureus* [98]. Previous work has shown that the deletion of this targeting domain does not interfere with enzymatic activity but does abolish the lysis of *S. aureus* cells suggesting that it is essential for the correct functioning of lysostaphin [98].

The flexible inter-domain region of lysostaphin allows the two domains to move independently [95]. With the use of small angle X-ray scattering (SAXS) it was shown that the flexible linker allows the elongation and contraction of the protein with the two domains moving separately [97].

1.5.1.3 Zoocin A

Zoocin A (ZooA) is a bacteriocin produced by *Streptococcus equi* ssp. *zooepidemincus* and targeted towards other *Streptococcal* species. ZooA is similar in both structure and function to lysostaphin with an N-terminal catalytic domain and a C-terminal targeting domain [99,100]. The *zooA* gene and the gene encoding its immunity protein *zifA* are adjacent on the chromosome [101] with the *zooA* gene encoding a 285 amino acid (AA) ZooA pre-peptide. The pre-preptide includes a 27 AA leader sequence to allow for the translocation of ZooA across the cell membrane, it is presumed that this is cleaved at the cell surface resulting in the 262 AA active molecule [102].

The structure of both the N- and C-terminal domains of ZooA have been solved individually using NMR spectroscopy [99,100] showing an N-terminal domain

similar in structure to the catalytic domain of lysostaphin, and a unique C-terminal domain predicted to be involved in cell wall targeting [103]. Previous work has shown ZooA to be a peptidoglycan hydrolase targeted towards *Streptococcal* species [104]. Work by Heath et al (2004) suggested that ZooA is a D-alanyl-D-alanine endopeptidase which acts by hydrolysing the alanine cross-bridges present in the *Streptococcal* peptidoglycan layer [104,105].

The presence of *Streptococcus mutans* in multispecies biofilms can cause dental disease in humans [106]. It has been shown that treatment with ZooA can successfully reduce the number of *S. mutans* bacteria present in these biofilms suggesting it can be used as a novel treatment against *Streptococcus* species *in vivo* [106]. Furthermore, at sub-lethal concentrations ZooA can be used to permeabilise the membrane of *S. mutans* in order to deliver anti-sense oligonucleotides to the cytoplasm [107]. As lysostaphin is a successful antimicrobial it is predicted that similar bacteriocins, such as ZooA, are also promising antimicrobials.

1.5.1.4 Gram-negative bacteriocins targeting the peptidoglycan layer

Colicin M is a unique colicin that targets the renewal of the peptidoglycan layer to cause cell lysis [108]. Unlike the other colicins, colicin M acts by hydrolysing the peptidoglycan precursor lipid II [109], thus preventing the production of mature peptidoglycan. Since the discovery of colicin M, several other M-type bacteriocins have been characterised, for example pyocin M from *Pseudomonas* and BurM from *Burkholderia*, however no structures have been solved to date [110,111].

The crystal structure of colicin M showed that it has a three domain structure similar to the other colicins [112,113]. It consists of an N-terminal IUTD, a central domain which interacts with its outer membrane receptor and the C-terminal catalytic domain [108]. The N-terminal unstructured domain showed a higher degree of flexibility than the other two domains, with a high number of proline residues [108]. This highly flexible IUTD is found in other colicins as it contains the TonB- on Tol-box motif which interacts with the TonB or Tol proteins in the periplasm [43,108]. The central domain is globular and consists entirely

of alpha-helices and is predicted to be involved in uptake or in the interaction of colicin M with the inner membrane [108]. Finally, the C-terminal domain of colicin M is made up of both α-helix and ß-strand motifs and is enzymatically active (Figure 1-7) [108]. Although the exact mechanism by which M-type bacteriocins degrade lipid II remains unclear, mutagenesis studies have identified an essential motif ($DXYDX_5HR$) required for hydrolysis [41]. This motif can be found within the short ß-strand and loop at the C-terminal end of colicin M and is conserved within other M-type bacteriocins, such as those produced by *Pectobacterium* spp. and *Pseudomonas* spp. [41].

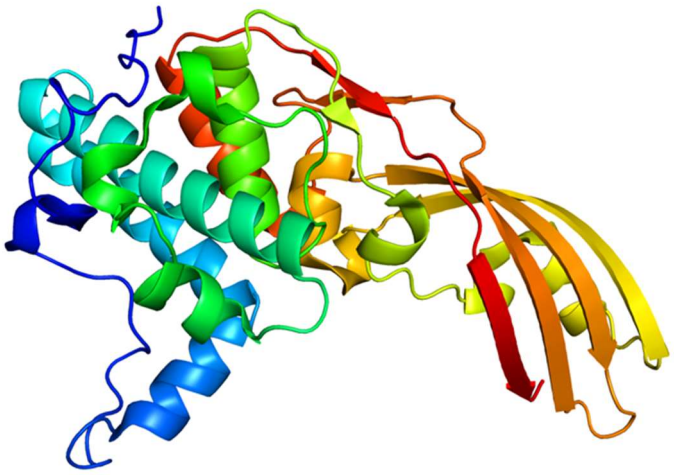

Figure 1-7 X-ray crystal structure of colicin M (PDB ID 2XMX) shown with the N-terminal as blue and the C-terminal as red.

Colicin M is a group B colicin and is dependent on the TonB system for uptake [108]. The N-terminal IUTD encodes a TonB-box like motif which has been shown to be necessary for successful uptake [108]. It is thought that this interaction allows for the removal of the plug domain of the outer membrane receptor FhuA to allow for colicin M to translocate into the periplasm [108]. Although the translocation domains of M-type bacteriocins are specific for their target organism, the cytotoxicity of the catalytic domain can indiscriminately target peptidoglycans from other Gram-negative bacteria as well as lipid II from Gram-positive bacteria [114,115].

As well as M-type bacteriocins, bacteriocins which cleave mature peptidoglycan causing cell lysis. One of these bacteriocins is pesticin from *Yersinia pestis*

which targets related bacteria in the same niche, including *Y. pestis* and *E. coli* strains [116]. Similarly to the colicins, the pesticin gene is plasmid encoded and the *pst* operon contains both the gene for the bacteriocin and the corresponding immunity protein (Pim) [116].

Like the colicins, pesticin is characterised by its three domain structure, an IUTD of ~40 amino acids at the N-terminus, followed by an elongated translocation domain consisting of both α-helices and ß-strands [116]. The cytotoxic domain of pesticin, located at the C-terminus, is unlike any known colicins and is more closely related to a phage lysozyme [116].

The structure of pesticin (Figure 1-8) is novel in many ways and does not resemble other proteins, with the N-terminal domain thought to be specifically folded to allow for the interaction with the outer membrane receptor FyuA [116]. The predicted mechanism of uptake is similar to that of the colicins, the interaction of the bacteriocin with the outer membrane receptor, the passage of the IUTD into the periplasm of the cell to interact with TonB and the subsequent uptake of the bacteriocin [116]. It has been shown that the IUTD is essential for the translocation of pesticin into the cell which supports this model [116].

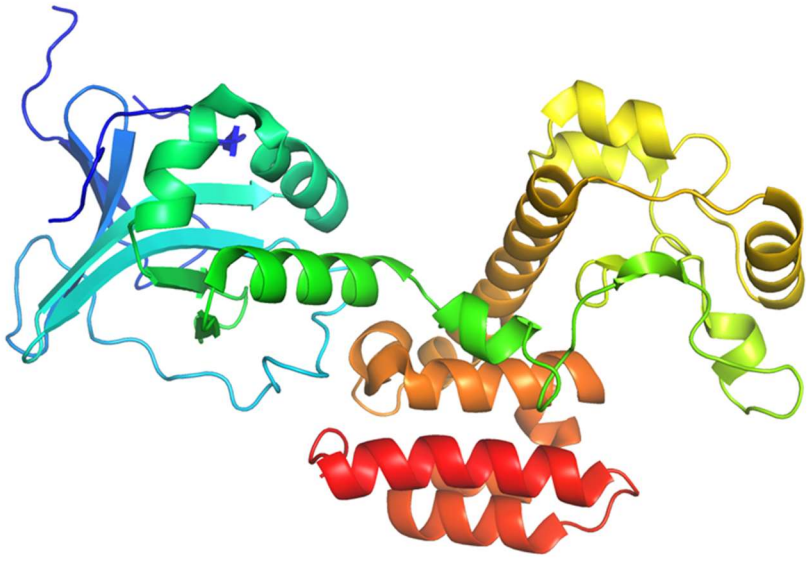

Figure 1-8 X-ray crystal structure of pesticin (PDB ID 4AQN) with the N-terminus shown in blue and the C-terminus in red.

The cytotoxic domain of pesticin is unique and similar to that of a phage lysozyme with additional secondary structure elements [116]. Structural unfolding has been shown to be necessary for the uptake of pesticin, this flexibility is uncommon amongst bacteriocins and suggests a potential novel mechanism of translocation [116].

1.5.2 Ferredoxin-containing bacteriocins

Bacteriocins, such as colicins and pyocins, have a conserved domain structure for binding, translocation and cytotoxicity with an N-terminal IUTD needed for uptake [43,52,57]. However, the recent discovery of ferredoxin-containing pectocins suggests a novel entry mechanism for bacteriocins in the absence of an IUTD [117].

Ferredoxins are small, soluble proteins that function as electron carriers in bacteria, plants and animals [118,119]. These proteins are characterised by the presence of an iron sulphur cluster, however the number of elements within this cluster differs depending on the organism with bacterial ferredoxins typically containing either one or two [4Fe-4S] clusters [120]. Plant-type ferredoxins are characterised by the presence of a [2Fe-2S] cluster and are part of the chloroplast electron transport chain (Figure 1-9) [121]. They are the first soluble electron acceptor within the stromal side of the chloroplast and are essential for the distribution of electrons to different metabolic pathways [119].

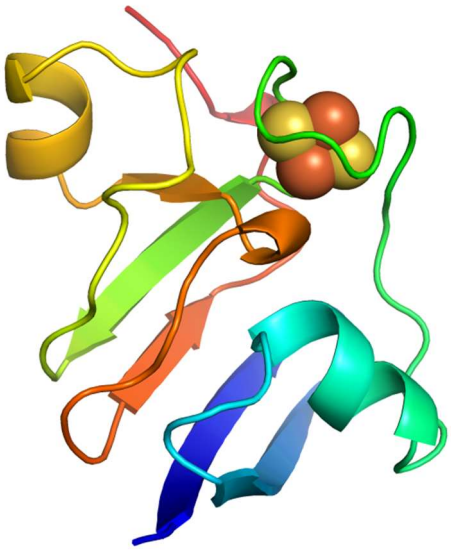

Figure 1-9 Structure of spinach (*Spinacia oleracea*) ferredoxin showing the positioning of the iron-sulphur cluster. Structure of spinach ferredoxin showing the position of the iron-sulphur cluster (spheres) within the loop, the N-terminus is shown in blue and the C-terminus in red (PDB:1A70).

Plant-type ferredoxins are distinguished by their small size with a mass of ~10 kDa and the conserved nature of their amino acid sequence and structure between organisms, including cyanobacteria and higher plants [119,122]. Structurally ferredoxins are composed of three to five ß-strands forming a ß-sheet and up to three α-helices with the [2Fe-2S] cluster located near the C-terminal end of the protein [119]. The [2Fe-2S] cluster is tetrahedrally coordinated by four cysteine residues and is surrounded by hydrophobic residues [119]. This is in contrast to the rest of the protein which contains a large number of charged residues important for binding partner interaction [119].

Ferredoxin-containing pectocins (hereafter pectocins) are a novel class of bacteriocins produced by and targeted towards *Pectobacterium* species. To date three pectocins have been discovered: pectocin M1, M2 and P. Pectocins share an N-terminal domain which is homologous to spinach ferredoxin II [117]. The crystal structure of pectocin M2 showed structural similarities to both spinach ferredoxin II at the N-terminal and a C-terminal cytotoxic domain homologous to colicin M (Figure 1-10) [123].

Although the N-terminal domain of pectocins appears to be specific to *Pectobacterium* species, the cytotoxic domain of the protein has a broader killing spectrum if expressed within the cell [114]. Recent work has shown that the periplasmic expression of pectocin M1 within *E. coli* can cause cell death by the successful cleavage of lipid II subsequent cell lysis [114,124].

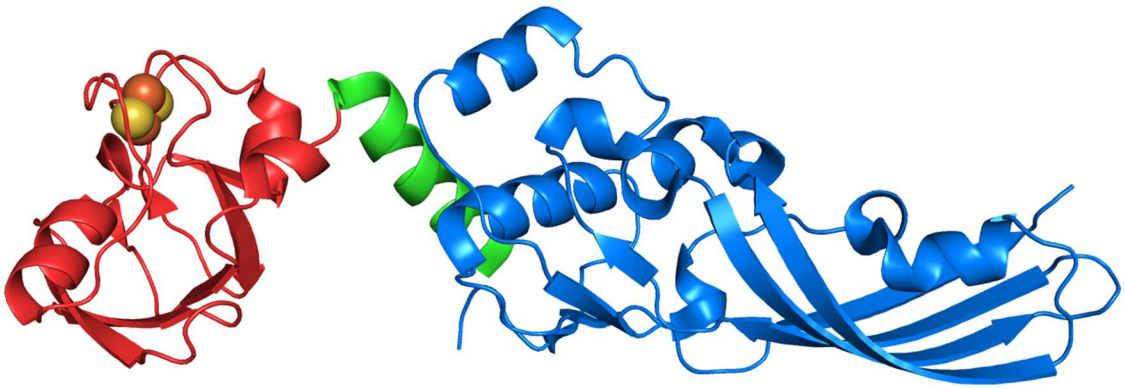

Figure 1-10 Crystal structure of pectocin M2 in the elongated conformation. Pectocin M2 (PDB ID 4N58) with the ferredoxin N-terminal domain shown in red, flexible linker region in green and the cytotoxic domain homologous to colicin M shown in blue

Unlike colicins which are plasmid encoded, pectocins are chromosomally encoded on the genome of *Pectobacterium carotovorum* [117]. However, similar bacteriocins can be found in the genomes of several other plant pathogenic species, such as *Dickeya chrysanthemi* (Figure 1-11). Pectocins are unique amongst the known Gram-negative bacteriocins as they lack an N-terminal IUTD suggesting a novel uptake mechanism for these bacteriocins [117].

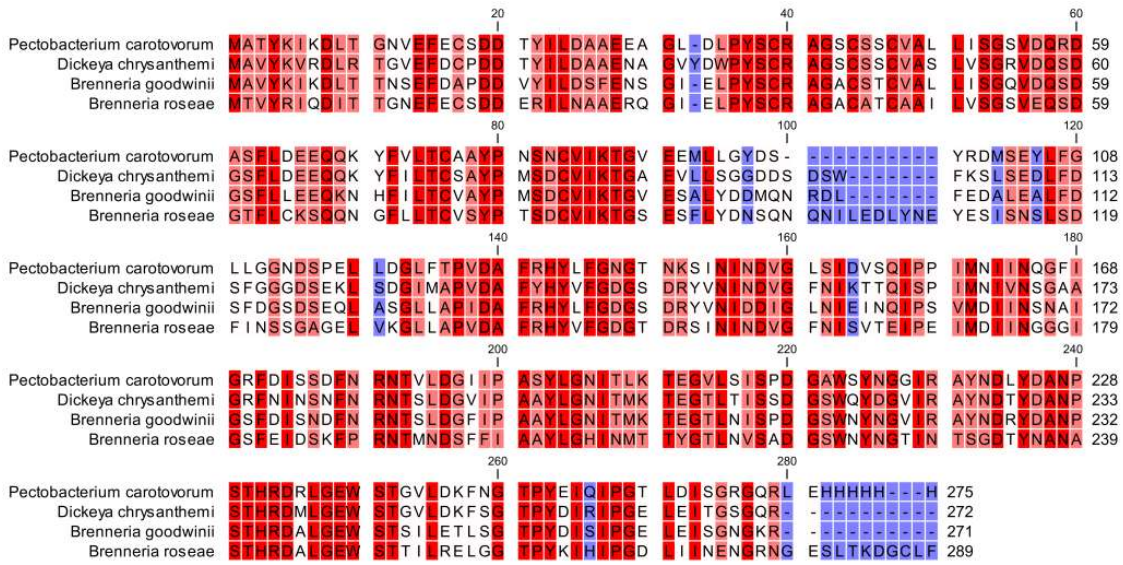

Figure 1-11 Sequence alignment for pectocin M1 homologues in closely related phytopathogens Amino acid sequence alignments showing homology between pectocin M1 from *P. carotovorum* and hypothetical bacteriocins from three related species with conserved residues shown in red and non-conserved residues in blue. Residues which are shared between three species are shown in pink and those shared in two species are highlighted in white. Alignment performed using CLC workbench.

It is known that Gram-negative bacteriocins parasitise existing nutrient receptors for uptake [51], however the uptake of a bacteriocin without the deployment of an IUTD is highly unusual [43,117]. The high resolution structure of pectocin M2 has shown that it is flexible and can be found in multiple conformations in solution [123]. The lack of an IUTD means that pectocins are unable to make direct contact with the Tol or TonB complexes within the periplasm to facilitate uptake [123], however the acquisition of an analogous substrate of the receptor allows the pectocin to utilise the target cells uptake machinery for translocation without the IUTD [123,124]. The N-terminal domain of the pectocins, as mentioned above, is homologous with spinach ferredoxin II, a host protein [117] and it has been shown that this allows the pectocins to parasitise the ferredoxin outer membrane receptor, FusA, in order to enter the periplasm [124]. FusA is found in all *Pectobacterium* species, with homologues seen in the genomes of closely related species [124]. This suggests a potential conserved mechanism of ferredoxin and ferredoxin-containing bacteriocin uptake in plant pathogenic bacteria.

1.5.3 Ferredoxin uptake system in *Pectobacterium* spp.

The ferredoxin uptake system (*fus)* in *Pectobacterium* spp. consists of four proteins, FusA, FusB, FusC and FusD and is thought to be necessary for the uptake and processing of ferredoxins acquired from host cells during infection [124,125] (Figure 1-12). To date the crystal structures of two of these proteins have been solved [124,126]. This operon can be seen within several soft rot bacteria, with the *fusA* and *fusC* homologues in *Dickeya dadantii* being some of the most highly upregulated during infection [124,127].

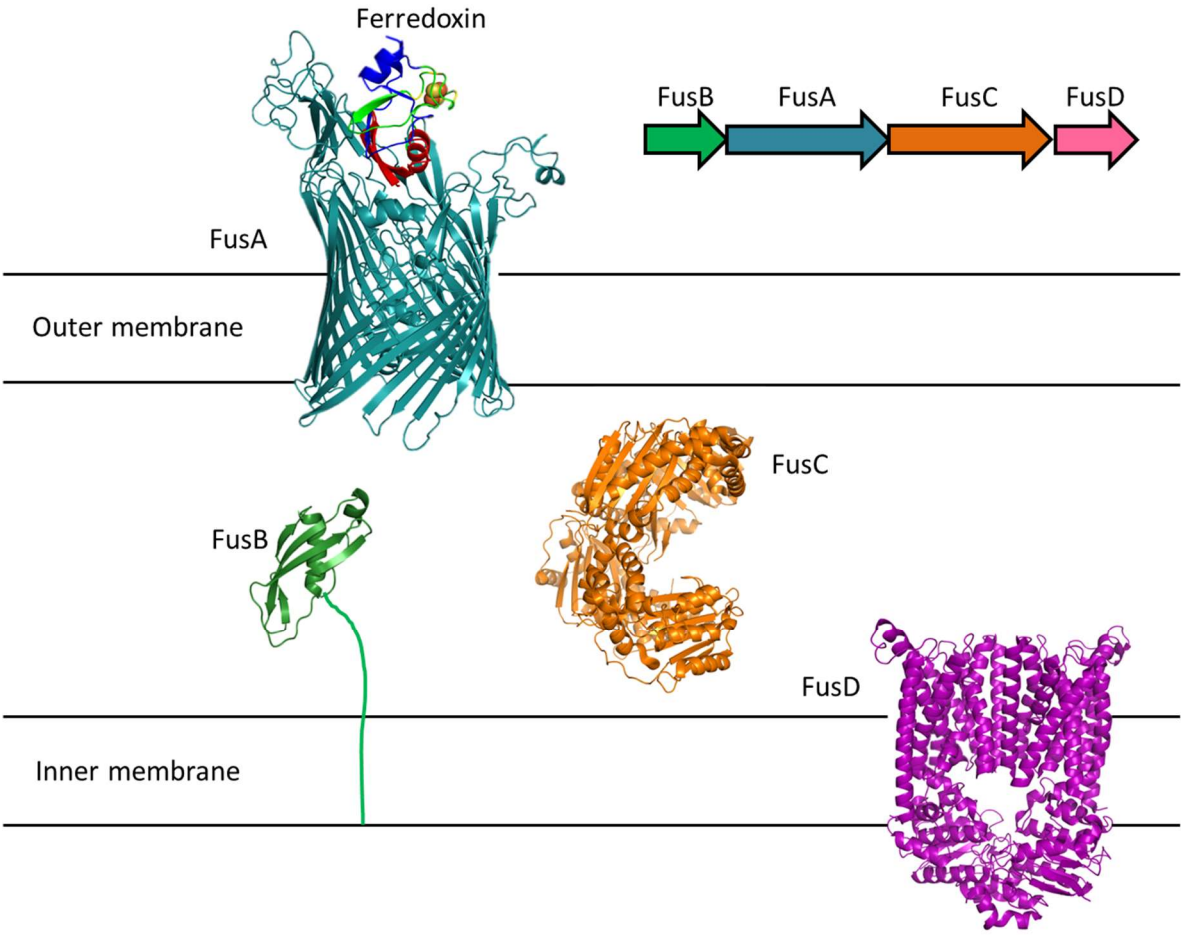

Figure 1-12 Schematic representation of the organisation of the Fus system in *Pectobacterium* cells. Operon organisation and predicted positions of the Fus proteins the membranes and periplasmic space of *Pectobacterium* spp. showing the solved crystal structure of FusA (PDB ID 4ZGV) and FusC (PDB ID 6BRS) with Phyre2 models representing FusB and FusD. Adapted from [124–126] under a creative commons licence.

FusA is an outer membrane TonB-dependent receptor found in *Pectobacterium* species. This outer membrane receptor has the characteristic structure of TonB-

dependent outer membrane receptors with an N-terminal plug domain and a C-terminal barrel consisting of 22 transmembrane antiparallel ß-strands [124]. The extracellular loops of FusA are larger than those of other TonB-dependent receptors found in related species such as *E. coli* [124]. These extracellular domains largely consist of ß-sheet and non-regular secondary structure elements and are thought to be highly flexible [124]. The larger of these two extracellular loops as well as the N-terminal plug domain extend into the extracellular environment, it is therefore predicted that these may be involved in substrate coordination and binding [124].

Once ferredoxin has translocated into the periplasm of *Pectobacterium* cells it is processed by FusC to release the [2Fe-2S] cluster [125]. The FusC crystal structure shows that it is a four domain zinc dependent protease found in a "clamshell" structure [126]. The active site is found in the centre of the protein and is responsible for the processing of plant-type ferredoxins [125,126]. The presence of the substrate in the centre of the clamshell structure induces a conformational change in which the FusC closes around the ferredoxin via the C-terminal segment of the substrate [126]. FusC cleaves ferredoxin at two specific peptide bonds releasing the central iron coordinating loop which can then be taken up into the cytoplasm, presumably by FusD [125].

So far it is known that FusA and FusC are necessary for the uptake and processing of ferredoxins in *Pectobacterium* species, however the roles and interactions of the other two proteins within the operon are unknown [124,125]. FusB is predicted to be homologous to TonB and it is not known whether it interacts with the TonB-box of FusA or with the substrate to aid with translocation. FusD it is predicted to be an ABC inner membrane transporter, similar to BtuCD, due to the presence of ATP-binding motifs present in the amino acid sequence [128]. It is therefore predicted that it will facilitate the transport of the cleaved ferredoxin into the cytoplasm [125].

1.6 The study of proteins in solution

1.6.1 The principles of small angle scattering

Small angle scattering (SAS) is a well-established technique which can be used to examine both ordered and disordered proteins in solution [129]. SAS allows for proteins in a multitude of conformations and orientations to be examined and therefore the in solution state of a particle to be deduced [129]. Unlike X-ray crystallography, SAS allows for the characterisation of a conformationally heterogenous samples as well as flexible and intrinsically disordered proteins [129].

There are two major types of small angle scattering used within the study of proteins: small angle neutron scattering (SANS) and small angle X-ray scattering (SAXS), the principles of which are largely similar. Both types of SAS rely on the deviation of incoming radiation from its incident path once it comes into contact with a macromolecule (Figure 1-13) [130]. This deviation (q) is measured using a detector, at a set distance, which measures both the angle and the intensity at the angle (i(q)).

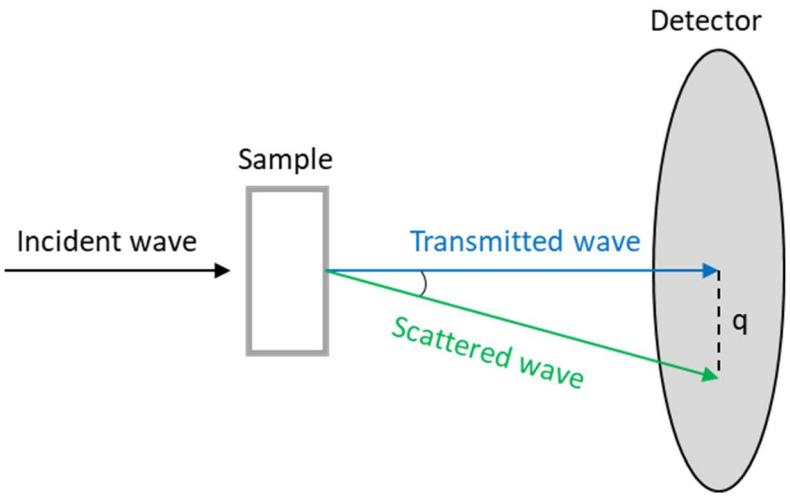

Figure 1-13 Schematic representation of small-angle scattering. The incident wave (either X-rays or neutrons) interacts with the sample and the angle at which it scatters (2θ) is denoted as q. (Adapted from [131]).

In order to examine the 'true' scattering of a protein corrections are made for a variety of physical fluctuations, such as normalising for the incident flux [130]. Once the data has been corrected the scattering of the solvent is subtracted from the scattering of the sample to give only the scattering data for the protein in solution [129,130].

SAXS can be used to examine both soluble and insoluble proteins, however due to the tendency of detergent micelles to scatter in a similar way to proteins these proteins are more often examined using SANS. SANS can be used to visualise detergent solubilised proteins in solution by matching out the detergent using deuterated water. Using a ratio of water and deuterated water (D_2O) a contrast match point for the detergent can be found in which the scattering length density of the solvent is the same as the detergent [132,133]. This allows for the protein to be analysed without visualising the micelle. Both methods however are useful in examining protein conformation in solution.

Previously, measurements were taken of a stationary sample within a cuvette meaning that the protein sample needed had to be in a singular oligomeric state for the data to be analysed. However, the development of size-exclusion chromatography small angle scattering (SEC-SAS) has allowed for complex or transiently self-associating systems to be separated *in situ* [134,135].

1.6.2 Shape and flexibility analysis of a molecule

SAS can be used to examine the properties of a given macromolecule in solution to determine if a predicted or *in crystallo* model is a good representation of the proteins behaviour and conformations within solution. Moreover, the ability to examine proteins within solution allows for their flexibility and conformational changes to be examined more closely.

The Guinier region is the linear region observed at low scattering angles allowing for the extrapolation of the data to the scattering intensity at 0 (i(0)) [129,131] . Investigation of the Guinier region of the SAXS scattering curve yields information about both the i(0), which is proportional to the molecular weight,

and the radius of gyration (R_g) which yields information about the inter-electron distances within the particle [130,136].

The shape and order of a protein can also be examined using a dimensionless Kratky plot which is normalised for both mass and concentration. If the data forms a Gaussian distribution, with the peak of the distribution occurring around $qR_g = \sqrt{3}$ (~1.73), it suggests that the particle is ordered and globular. If the $qR_g^2(I(q)/I(0))$ continues to increase as the qR_g increases, this suggests that the particle is intrinsically disordered and flexible [129]. In this way a particle can be characterised as globular, elongated or highly disordered. Comparison of the Kratky-Debye and Porod-Debye plots simultaneously allows for the particle to be classified as compact or flexible [129,137] . By examining which data set plateaus at the highest q value in the low q range the particle can be deemed to be either compact or flexible [138]. Together this can determine if a particle is flexible in solution, and if so does this flexibility come from a flexible region within a folded protein or due to the nature of a highly disordered protein [139,140].

1.6.3 Low-resolution structural modelling and Computational methods of flexibility analysis

A low-resolution structural envelope of a protein can be created based on the pair set distribution of the radial distances between electrons (SAXS) or neutrons (SANS) within the particle (p(*r)*) through an indirect Fourier transformation of the scattering data [129,141]. The maximum distance within the particle is calculated and *ab initio* modelling can be used to create a low resolution envelope of the protein in solution [141]. In order to construct this model a sphere with a radius equal to half the maximum particle dimensions (D_{max}) is filled with smaller spheres either belonging to the particle or the solvent [141]. Using DAMMIF, an algorithm is used to determine which small spheres belong to the particle and fit the scattering data [141]. This process is done up to 23 times and the final models are averaged to give the final low resolution envelope of the particle [141]. High resolution models or structures obtained from X-ray crystallography can be compared with these low-resolution envelopes to determine if they are similar in size and shape to known or predicted structures.

As mentioned above SAS is a useful tool for examining the flexibility of proteins in solution, however, like X-ray crystallography, this flexibility is not always shown in structural models. The advantage of SAS is that it can provide information about intrinsically flexible proteins or proteins which contain interdomain flexible linker regions. However, due to the flexibility of these molecules in solution it is assumed that the experimental data is an average of unknown conformers in solution [142].

Ensemble optimisation modelling (EOM) can be used to determine which conformations from a large pool of randomly generated models best fits the experimental SAS data [142]. EOM creates a large pool of available conformations and a sub-set of these conformers are selected by the fit to the experimental SAS data [139]. Previous work examining pectocin M2 used EOM to determine that pectocin M2 can be found in multiple conformations in solution, with the structure of two of these conformations being solved using X-ray crystallography [123].

1.7 Aims

The threat to food security has led to the need to develop novel biocontrol strategies to feed an ever-growing population. This project aims to further understand the structure and function of novel bacteriocins from *Pectobacterium* species and GBS to potentially develop them as novel therapeutics. This project aims to characterise a novel bacteriocin from GBS to understand the enzymatic activity as well as the structure of the protein. As well as this it aims to elucidate the uptake mechanism of ferredoxin-containing bacteriocins, the role of the proteins within the *fus* operon in bacteriocin uptake and the structural and biochemical properties of the bacteriocins themselves.

Chapter 2 Materials and Methods

2.1 Chemicals used

Unless otherwise stated all chemicals and reagents used in this study were procured from Sigma Aldrich, Thermofisher or Promega.

2.2 Culture of bacteria used in this study

2.2.1 *Pectobacterium atrosepticum* strains

All *P. atrosepticum* strains were cultured in lysogeny (LB) liquid broth (5% yeast, 10% tryptone, 10% sodium chloride) or on LB solid agar (LB broth with 1.5% agar). All cultures were grown at 28-30^{o}C with liquid cultures shaken at 180 rpm.

Strain	Relevant characteristics	Source
P. atrosepticum		
LMG2386	Isolated from *Solanum tuberosum* (stem rot)	BCCM
SCRI1043	Isolated from *Solanum tuberosum* (tuber soft rot)	SCRI
LMG2386 Δ*fusA*	Knock-out of FusA gene	Grinter et al. (2016)

2.2.2 *Streptococcus agalactiae* strains

GBS strains were cultured on Columbia agar supplemented with 5% sheep's blood (SGL) or TSA supplemented with 5% sheep's blood (E&O laboratories) at 37^{o}C. GBS strains were grown in BHI broth (Oxoid) at 37^{o}C, shaking at 180 rpm.

Table 2-1 *Streptococcus* strains used in this study

Strain	Relevant characteristics	Source
STIR CD01 (ST7)	Isolated from Mullet, serotype Ia	Kuwait
MRI Z1-354 (ST67)	Isolated from Cattle, serotype Ia	Denmark
MRI Z2-197 (ST7)	Isolated from Cattle	United Kingdom
MRI Z2-366 (ST263)	Isolated from Tilapia, serotype III	Vietnam
STIR CD25 (ST263)	Isolated from Tilapia, serotype III	Thailand

2.2.3 *Escherichia coli* strains

All *E. coli* strains were commercially available laboratory strains and grown in the appropriate antibiotics at 37°C.

Table 2-2 *E. coli* strains used in this study

Strain	Relevant characteristics	Source
DH5-α	F- Φ80lacZΔM15 Δ(lacZYA-argF) U169 recA1 endA1 hsdR17(rk-, mk+) phoA supE44 thi-1 gyrA96 relA1 λ	Invitrogen
BL21 (DE3)*	F$^-$*ompT* *hsd*S$_B$ (r_B^-, m_B^-) *galdcmrne*131 (DE3)	Invitrogen
BL21 (DE3) pLysS	F–, *ompT*, *hsd*S$_B$ (r_B–, m_B–), *dcm*, *gal*, λ(DE3), pLysS, Cm^r.	Promega

2.2.4 Antibiotics used in culturing

All antibiotics used in this study were procured from Melford or Sigma Aldrich.

Table 2-3 Antibiotics used in this study

Antibiotic	Final Concentration	**Solvent**
Ampicillin	100 µg µl^{-1}	Water
Kanamycin	50 µg µl^{-1}	Water
Chloramphenicol	32 µg µl^{-1}	Ethanol

2.2.5 Plasmids used in this study

Table 2-4 Plasmids used in this study

Plasmid	Relevant characteristics	Source
p*fusA*2386	*fusA* gene from *P. atrosepticum* LMG2386 synthesised for complementation	DNA 2.0
p*fusA*2386$_{N151A}$	As above with an N151A mutation	This study
p*fusA*2386$_{Y155A}$	As above with an Y155A mutation	This study
p*fusA*2386$_{P157G}$	As above with an P157G mutation	This study
p*fusA*2386$_{F376A}$	As above with an F376A mutation	This study
p*fusA*2386$_{F378A}$	As above with an F378A mutation	This study
p*fusA*2386$_{F380A}$	As above with an F380A mutation	This study
p*fusA*2386$_{N401A}$	As above with an N401A mutation	This study
p*fusA*2386$_{G489A}$	As above with an G489A mutation	This study
p*fusA*2386$_{N491A}$	As above with an N491A mutation	This study
pPCM1_pJ404	Plasmid containing codon optimised Pectocin M1 gene	DNA 2.0
pFRIB1043	Expression plasmid containing the *fusA* gene from *P. atrosepticum* SCRI1043 in a pET28a vector.	Rhys Grinter
p*fusB*$_{1043}$	FusB gene from *P. atrosepticum* SCRI1043 codon optimised for expression in *E. coli*	DNA 2.0
p*fusA*-Plug	pET21a vector plasmid containing AAs 29-210 of *fusA* from *P. atrosepticum* SCRI1043	This study
pPCM1$_{T3A}$	As above with a T3A mutation in pJ404	This study
pPCM1$_{K5A}$	As above with a Y4A mutation in pJ404	This study
pPCM1$_{K5A}$	As above with a K5A mutation in pJ404	This study
pPCM1$_{K7A}$	As above with a K7A mutation in pJ404	This study
pPCM1$_{N12A}$	As above with a N12A mutation in pJ404	This study
pPCM1$_{F15A}$	As above with a F15A mutation in pJ404	This study
pPCM1$_{E16A}$	As above with a E16A mutation in pJ404	This study
pPCM1$_{D19A}$	As above with a D19A mutation in pJ404	This study
pPCM1$_{C38A}$	As above with a C37A mutation in pJ404	This study
pPCM1$_{S52A}$	As above with a S25A mutation in pJ404	This study
pPCM1$_{R58A}$	As above with a R57A mutation in pJ404	This study
pPCM1$_{S60A}$	As above with a S60A mutation in pJ404	This study
pPCM1$_{E65A}$	As above with a E65A mutation in pJ404	This study
pPCM1$_{Y70A}$	As above with a Y70A mutation in pJ404	This study
pPCM1$_{K86A}$	As above with a K86A mutation in pJ404	This study
pPCM1$_{Y4AK5E}$	As above with a Y4A and K5E mutations in pJ404	This study
pPectocinP	Codon optimised Pectocin P sequence in pET100a with a TEV cleavable 6x histidine tag	GeneArt
pAgaA	pJ404 plasmid containing codon optimised agalacticin A gene	DNA 2.0
pAgaA$_{H23A}$	As above with H23A mutation in pJ404	This study
pAgaA$_{H108A}$	As above with H109A mutation in pJ404	This study
pAgaA$_{C67A}$	As above with C63A mutation in pJ404	This study

2.3 DNA manipulation

2.3.1 Polymerase chain reaction

50 µl reactions were set up for each polymerase chain reaction (PCR). Each reaction contained 20 ng of DNA, 1 x pfu turbo buffer, 40 mM dNTPs, 0.1 µM forward and reverse primer and 1-2.5 units of pfu turbo polymerase. The standard programme for a PCR reaction is as below (Table 2-5). A lower number of cycles were used for site-directed mutagenesis (SDM) whereas a higher number of cycles were used for amplification of genes for cloning.

Table 2-5 Standard PCR program used in this study

Temperature	Duration (m)	
95 ºC	5 minutes	
95 ºC	45 seconds	18/35 cycles
57 ºC	45 seconds	
68 ºC	1 min per kb +1 min	
68 ºC	5 minutes	

If no product was seen within the first reaction 10% DMSO and 2.5 mM $MgCl_2$ were added to subsequent reactions to enhance binding of oligos. Temperatures from 45-65ºC were also tested if necessary.

Table 2-6 List of primers used for sequencing reactions

Primer	Sequence (5'-3')	Use
FusA2386_Seq1_F	ATG AAT AAG AAC GTC TAT TTA ATG ATG	Sequencing first 500bp of *fusA* in LMG2386
FusA2386_Seq1_R	CTT AGC CGA AAT ATT ACT ATC	
FusA2386_Seq2_F	GAT AGT AAT ATT TCG GCT AAG	Sequencing bps 500-1000 of *fusA* in LMG2386
FusA2386_Seq2_R	CTG ATA TCC CGC CAG ACT GGT C	
FusA2386_Seq3_F	GAC CAG TCT GGC GGG ATA TCA G	Sequencing bps 1000-1500 of *fusA* in LMG2386
FusA2386_Seq3_R	CGT TCA GAT TTT CCA AGA AGT C	
FusA2386_Seq4_F	GAC TTC TTG GAA AAT CTG AAC G	Sequencing bps 1500-2000 of *fusA* in LMG2386
FusA2386_Seq4_R	GAA GTA AGT ATC CAC ACT CAG G	
FusA2386_Seq5_F	CCT GAG TGT GGA TAC TTA CTT C	Sequencing bps 2000+ of *fusA* in LMG2386
FusA2386_Seq5_R	TTA CCA GGT GTA AGC GAC GC	
PCM1_Seq_F	AGGAGGTAAAACATATGGCC	Sequencing PCM1 ORF in PCM1_pJ404 plasmid
PCM1_Seq_R	CTC GAG CTA GTG GTG ATG	
Zoo_Seq_F	AGG AGG TAA AAC ATA TGG ACA C	Sequencing Zoo ORF in Zoo_pJ404 plasmid
Zoo_Seq_R	GGT GGT GGT GGT GCT CTT TG	

Table 2-7 List of primers used for site-directed mutagenesis of plasmids

Primer	Sequence (5'-3')
Pectocin M1 (PCM1_pJ404) – all mutations are in the primer name	
PCM1_T3A_F	GGTAAAACATATGGCCGCGTACAAAATTAAAG
PCM1_T3A_R	CTTTAATTTTGTACGCGGCCATATGTTTTACC
PCM1_Y4A_F	AGG AGG TAA AAC ATA TGG CCA CGG CCA AAA TTA AAG ATC TGA CCG
PCM1_Y4A_R	CGG TCA GAT CTT TAA TTT TGG CCG TGG CCA TAT GTT TTA CCT CCT
PCM1_K5A_F	AAA ACA TAT GGC CAC GTA CGC AAT TAA AGA TCT GAC CGG TAA TG
PCM1_K5A_R	CAT TAC CGG TCA GAT CTT TAA TTG CGT ACG TGG CCA TAT GTT TT
PCM1_K7A_F	GCCACGTACAAAATTGCAGATCTGACCGGTAATG
PCM1_K7A_R	CATTACCGGTCAGATCTGCAATTTTGTACGTGGC
PCM1_N12A_F	AAA GAT CTG ACC GGT GCT GTT GAG TTT GAG TGT TCG G
PCM1_N12A_R	AAC ACT CAA ACT CAA CAG CAC CGG TCA GAT CTT T
PCM1_S52A_F	TCG CGC TGT TAA TTG CCG GTT CTG TTG ATC AGC
PCM1_S52A_R	GCT GAT CAA CAG AAC CGG CAA TTA ACA GCG CGA
PCM1_Y70A_F	GGA TGA AGA ACA GCA AAA GGC CTT TGT CCT CAC CTG TGC
PCM1_Y70A_R	GCA CAG GTG AGG ACA AAG GCC TTT TGC TGT TCT TCA TCC
PCM1_K86A_F	GAA CAG CAA CTG TGT GAT CGC GAC CGG CGT GGA AGA AAT
PCM1_K86A_R	ATT TCT TCC ACG CCG GTC GCG ATC ACA CAG TTG CTG TTC
PCM1_Y4AK5E_F	AAA ACA TAT GGC CAC GGC CGA AAT TAA AGA TCT GAC CGG TAA
PCM1_Y4AK5E_R	TTA CCG GTC AGA TCT TTA ATT TCG GCC GTG GCC ATA TGT TTT
PCM1_D19A_F	CGA TAC GTA CAT CTT GGC TGC AGC AGA AGA GGC TG
PCM1_D19A_R	CAG CCT CTT CTG CTG CAG CCA AGA TGT ACG TAT CG

PCM1_R57A_F	GTT CTG TTG ATC AGG CTG ACG CGA GCT TCC TG
PCM1_R57A_R	CAG GAA GCT CGC GTC AGC CTG ATC AAC AGA AC
PCM1_S60A_F	CAG CGT GAC GCG GCC TTC CTG GAT GAA GAA C
PCM1_S60A_R	GTT CTT CAT CCA GGA AGG CCG CGT CAC GCT G
PCM1_E64A_F	GAG CTT CCT GGA TGC AGA ACA GCA AAA GTA CTT TG
PCM1_E64A_R	CAA AGT ACT TTT GCT GTT CTG CAT CCA GGA AGC TC
PCM1_F15A_F	GAC CGG TAA TGT TGA GGC TGA GTG TTC GGA CGA TAC
PCM1_F15A_R	GTA TCG TCC GAA CAC TCA GCC TCA ACA TTA CCG GTC
PCM1_E16A_F	CGG TAA TGT TGA GTT TGC GTG TTC GGA CGA TAC
PCM1_E16A_R	GTA TCG TCC GAA CAC GCA AAC TCA ACA TTA CCG
	***fusA* 2386 mutants (p*fusA*$_{2386}$)**
FusA_N151A_F	GTG AAT TGG GCT CGG CTC CTG ATG GAT ACA GCC
FusA_N151A_R	GGC TGT ATC CAT CAG GAG CCG AGC CCA ATT CAC
FusA_Y155A_F	GA ATC CTG ATG GAG CCA GCC CGA CCG ATT TAC CTG
FusA_Y155A_R	CAG GTA AAT CGG TCG GGC TGG CTC CAT CAG GAT TC
FusA_P157G_F	GAT GGA TAC AGC GGG ACC GAT TTA CCT GCT GGT GG
FusA_P157G_R	CC ACC AGC AGG TAA ATC GGT CCC GCT GTA TCC ATC
FusA_F376A_F	GAG CAT GAA TCT AAT GAG GCT ATT AGC TGG TTC CAC ACT GTT CC
FusA_F376A_R	CC CAG GAA CAG TGT GGG CCC AGC TAA TAA ACT CAT TAG ATT CAT
FusA_S378A_F	CAT GAA TCT AAT GAG TTT ATT GCC TGG TTC CAC ACT GTT CCT GGG T
FusA_S378A_R	A CCC AGG AAC AGT GTG GAA CCA GGC AAT AAA CTC ATT AGA TTC ATG
FusA_F380A_F	ATG AAT CTA ATG AGT TTA TTA GCT GGG CCC ACA CTG TTC CTG GG
FusA_F380A_R	CC CAG GAA CAG TGT GGG CCC AGC TAA TAA ACT CAT TAG ATT CAT
FusA_N401A_F	GGC AGA CTA CAA ACA GAG CTT CAC AGG TTGGTG GCT ATG
FusA_N401A_R	CAT AGC CAC CAA CCT GTG AAG CTC TGT TTGTAG TCT GCC
FusA_G489A_F	CCC GGT GAG CAG TTT GCT GCC ACT AAC ATAGTT TAC CCA G
FusA_G489A_R	CTG GGT AAA CTA TGT TAG TGG CAG CAA ACTGCT CAC CGG G
FusA_N491A_F	GTG AGC AGT TTG CTG GCA CTG CCA TAG TTTACC CAG CCC G
FusA_N491A_R	CGG GCT GGG TAA ACT ATG GCA GTG CCA GCAAAC TGC TCA C
	Agalacticin A mutants (pAgaA)
AgaA_H23A_F	GTT TTA ATG GTT ATC CGG GTG CTT GCG GCG TTG ATT ACG C
AgaA_H23A_R	GCG TAA TCA ACG CCG CAA GCA CCC GGA TAA CCA TTA AAA C
AgaA_C63A_F	GAC CGA TCT GGC TGG TAA CGC TGT TAT GAT CCA ACA TGC CG
AgaA_C63A_R	CGG CAT GTT GGA TCA TAA CAG CGT TAC CAG CCA GAT CGG TC
AgaA_H109A_F	CCG GTA TGG CGA CGG GTC CGG CCT TGC ACT TTG AGT TCC TG
AgaA_H109A_R	CAG GAA CTC AAA GTG CAA GGC CGG ACC CGT CGC CAT ACC GG

Table 2-8 List of primers used for amplification and cloning of genes.

Primer	Sequence (5'-3')	Use	RE site
FusA_Plug_NdeI	GCATACATATGGATGAAAATCAGCAG AAAAAC	Cloning the plug domain of FusA$_{1043}$ into pET21a	NdeI
FusA_Plug_XhoI	GCATACTCGAGTTTATCCAGCTTGGG ATCC		XhoI

2.3.2 Creation of mutants by site directed mutagenesis

Primers were designed to be ~40 bp in length with the initial and final bases to end on a C or G with the mutation in the centre of the primer, the reverse primer was the reverse complement of the forward primer with a melting temperature >70^{o}C.

PCRs were set up as in 2.3.1 and 1 µl of DpnI was added to the final PCR product and incubated for 1 hour at 37^{o}C. 5-10 µl of this reaction was transformed into 50 µl of DH5-α cells (see section 2.3.7) and 100 µl of the final product was spread onto LB agar plates with the appropriate antibiotics. If no colonies were seen then the remaining reaction was spread after 16 hours at room temperature (RT).

Plasmids were extracted from all colonies that grew (see 2.3.10) and mutations were confirmed by sequencing (Source Bioscience).

2.3.3 Purification of PCR fragments

PCR products were purified using a Qiagen PCR purification kit as per the manufacturer's instructions with the exception that the original DNA product was applied to the column twice and the elution buffer (EB) was incubated on the membrane for 5 minutes prior to elution. DNA concentrations were checked using a nanodrop 1000 spectrophotometer (Thermo Scientific).

2.3.4 Restriction enzyme digests

1 µg of DNA was digested for a minimum of 1 hour at 37^{o}C with 1 unit of enzyme in 1 x fast digest buffer (Promega) or Cutsmart buffer (NEB) depending on the enzyme manufacturer in a 50 µl total reaction volume. Plasmids were subsequently CipA (NEB) digested for 1 hour at 37^{o}C before ligation.

2.3.5 Purification of DNA from agarose gels

Gel slices were purified using a Qiagen gel purification kit as per the manufacturer's instructions with the exception that the original DNA product was applied to the column twice and the EB was incubated on the membrane for 5 minutes prior to elution. DNA concentrations were checked using a nanodrop 1000 spectrophotometer (Thermo Scientific).

2.3.6 Ligation reactions

Insert was added at a 1:3 molar ratio (plasmid:insert) to 50 ng of digested plasmid DNA. Products were ligated together using 400 units (1 µl) of T4 DNA ligase (NEB) in 1 x ligase buffer overnight at ~16ºC. 10 µl of the ligation reaction was transformed into competent cells (see section 2.3.7) and colonies were tested using both a restriction enzyme (RE) digest and PCR.

2.3.7 Creation and transformations of chemically competent *E. coli* cells by heat shock

DH5-α *E. coli* cells were inoculated 1:100 into 50 ml of LB broth and grown to OD_{600} ~0.4 at 37 ºC, 180 rpm. Cells were harvested at 4500 rpm, 4ºC for 10 minutes. Cells were resuspended in 25 ml of ice cold 0.1 M $CaCl_2$ and harvested again at 4500 rpm, 4ºC for 10 minutes. This was repeated twice more halving the resuspension volume each time. Cells were finally resuspended in 500 µl of ice cold 10% glycerol and 50 µl was used per transformation.

For known plasmids 2 µl of plasmid (~300 ng) was placed into 50 µl of cells. For ligation reactions or mutagenesis PCR reactions 5-10 µl was placed into 50 µl of cells.

Cells were incubated on ice for 30 minutes, followed by at 42ºC for 45 seconds followed by a further 5 minutes on ice. 300 µl of S.O.C. media was added and cells were incubated for 1-2 hours, 37ºC, and 180 rpm. After incubation 100 µl was plated onto LB agar with the corresponding antibiotic and incubated overnight at 37ºC.

2.3.8 Creation and transformation of electro-competent cells

P. atrosepticum strains were inoculated 1:100 into 50 ml of LB media and grown to OD_{600} ~0.4. Cells were harvested at 4500 rpm, 4 ^{o}C for 10 minutes. Cells were resuspended in 25 ml of ice cold sterile dH_2O and harvested again at 4500 rpm, 4 ^{o}C for 10 minutes. This was repeated twice, halving the resuspension volume each time. Cells were resuspended in 500 µl of ice cold 10% glycerol and 200 µl was used per transformation.

200 µl of cells and 5 µl of plasmid were added to a microporation cuvette and incubated for 2 minutes on ice. Cells were electroporated at 2.5 kV applied at a capacitance of 25 µF (Invitrogen) and incubated for 1-2 hours in 1 ml of S.O.C. media at 28^{o}C and 180 rpm. 150 µl was spread on an LB plate with the corresponding antibiotics and incubated for 24-48 hours at 28^{o}C with the remaining transformation left overnight at RT. If no small colonies had appeared overnight the rest of the transformation was harvested (4500 rpm) and spread onto an LB plate supplemented with the required antibiotic.

2.3.9 Electrophoresis

Agarose gel electrophoresis was used to separate DNA fragments for both PCR and plasmid verification. 1% agarose Tris-boric acid-EDTA gels were prepared with 0.1 µg ml^{-1} Sybrsafe (Invitrogen) to visualise the bands. Gels were imaged using the ChemiDoc system (Bio-Rad).

2.3.10 Plasmid DNA extraction

5 ml of overnight bacterial cultures were harvested at 14000 rpm for 3 minutes. PCR products were purified using a Qiagen mini-prep kit as per the manufacturer's instructions with the exception that the original DNA was applied to the column twice and the EB was incubated on the membrane for 5 minutes prior elution. DNA concentrations were measured using a nanodrop.

2.4 Bacteriocin toxicity assays

2.4.1 Spot-test overlay method

2.4.1.1 *Pectobacterium* spp.

LB agar with 200 µM bipyridine was overlaid with 5-20 ml of 0.8% agar inoculated with 100 µl of bacterial culture in mid log phase (OD_{600} 0.4-0.6) depending on the petri dish size. 2-5 µl of pectocin was spotted on in 3-fold dilutions. Δ*fusA* strains containing complementation plasmids were grown in broth supplemented with D-lactose (2% w/v) and the appropriate antibiotic. After incubation overnight, an overlay of 0.8% agar with a 10% PrestoBlue was added to each plate and incubated at RT for 10 minutes. Plates were imaged using the 546 nm filter on the Chemidoc. Prestoblue is a non-toxic resazurin based reagent which changes colour when metabolised by live cells [143], this was used to increase the contrast between zones of inhibition (blue) and live cells (pink) in order to better visualise the zones.

2.4.1.2 *Streptococcus agalactiae*

BHI agar plates were overlaid with 5 ml of 0.8% agar inoculated with 100 µl of mid-log phase bacterial culture (OD_{600} = 0.6). 2 µl of bacteriocin was spotted on in 3-fold decreasing concentrations from 0.3 mg ml^{-1} unless otherwise stated. Plates were incubated at 37°C overnight.

2.4.2 *Streptococcus* liquid growth assays

Cultures inoculated with a single colony were grown overnight at 37°C. 50 ml of BHI broth was inoculated at a 1:50 dilution and 200 µl was added to each well of a 96 well plate. Plates were incubated at 37°C, 180 rpm and readings taken every hour on a plate reader at OD_{630}. After 3 hours 10 µl of filter sterilised bacteriocin, mutants or ampicillin was added to the corresponding well and was incubated for a total of 8 hours with measurements taken at hourly intervals.

2.5 Recombinant protein expression

2.5.1 Soluble proteins

Recombinant proteins were expressed in *E. coli* BL21 (DE3) pLysS (Promega) cells, except for pectocin P which was expressed in BL21-star (DE3) cells. 2.5 or 5 L of LB was inoculated 1 in 50 with an overnight culture and grown to OD_{600} ~ 0.6 before induction. Bacterial cultures were induced with 0.1-0.3 mM IPTG and grown at 24-37°C for 3-16 hours (see Table 2-9 for details for individual proteins) depending on the optimal expression conditions for each protein.

Table 2-9 Induction conditions of proteins used in this study

Protein	Soluble/ insoluble	IPTG concentration	Induction temperature	Induction time
Pectocin M1 and mutants	Soluble	0.3 mM	25°C	16 hours
Pectocin P	Soluble	0.3 mM	30°C	6 hours
FusA Full length	Insoluble	0.1 mM	25°C	16 hours
FusA Plug	Soluble	0.3 mM	37°C	3 hours
FusB	Soluble	0.3 mM	37°C	3 hours
Agalacticin A and mutants	Soluble	0.3 mM	37°C	3 hours
FusA Barrel	Insoluble	0.3 mM	37°C	3 hours

Bacteria were harvested by centrifugation at 5000 rpm, 4°C for 15 minutes. Pellets were resuspended in 35 ml nickel binding buffer (20 mM Tris-HCl, 500 mM NaCl, 10 mM Imidazole, 5% glycerol, pH 7.5) supplemented with one complete protease inhibitor tablet (EDTA-free), 35 mg of lysozyme and 1 mg of DNAse I. After resuspension the bacteria were lysed by sonication on ice for 15 minutes at 12 mA for 15 seconds every minute. Soluble proteins were harvested by centrifugation at 18000 rpm for 20 minutes at 4°C.

Crude lysate was applied to a 5 ml His-trap HP column (GE healthcare) and eluted over a gradient 0-350 mM imidazole over 40 ml. Fractions were checked for the desired protein using gel electrophoresis and fractions containing the protein were dialysed into size exclusion chromotography buffer (50 mM Tris-HCl, 200 mM NaCl, 5% glycerol, pH 7.5) overnight at 4°C.

Dialysed samples were centrifuged for 10 minutes at 148000 rpm in a microfuge to remove any insoluble matter or aggregates. The supernatant was applied to a Superdex S75 (<40 kDa) or S200 (>40 kDa) size exclusion chromatography columns and fractions containing the desired protein were combined and concentrated as required.

2.5.2 Insoluble proteins

Insoluble proteins were purified from inclusion bodies from BL21 (DE3) pLysS cells. Cells were harvested and lysed (see for 2.5.1) and centrifuged at 18000 rpm, 20 minutes 4ºC to remove soluble proteins. The insoluble pellet was homogenised in 40 ml of 50 mM Tris-HCl, 1.5% LDAO, pH 7.5 using a tight-fitting homogeniser and incubated for 30 minutes at RT shaking. The insoluble material was then harvested as above. The pellet was again homogenised and harvested as before. The pellet was then washed in 50 mM Tris-HCl pH 7.5 and centrifuged again.

The pellet was homogenised in 40 ml denaturing buffer (10 mM Tris-HCl, 1 mM EDTA, 8 M Urea, 1 mM DTT, pH 7.5) and incubated at 56ºC for 30 minutes. The now soluble lysate was harvested at 8000 rpm for 10 minutes at 4ºC and then added dropwise to a rapidly stirring refolding buffer at RT (20 mM Tris-HCl, 1 M NaCl, 5% LDAO) at a 1:1 ratio. After refolding for 1.5 hours the proteins were dialysed overnight into 20 mM Tris-HCl, 500 mM NaCl, 10 mM imidazole and 0.1% LDAO.

Solubilised proteins were purified using a 5 ml His-Trap HP column (GE Healthcare) using the above dialysis buffer and was eluted using dialysis buffer with 350 mM imidazole. The eluted fractions were examined by SDS-PAGE to check for the desired protein and dialysed overnight in 50 mM Tris-HCl, 200 mM NaCl, and 0.1% LDAO. After dialysis the protein was applied to a Superdex S200 column and the purity assessed by SDS-PAGE.

2.5.3 SDS-PAGE

Tris-glycine SDS-PAGE gels were loaded with 5-10 µl of protein in 4x loading buffer and run until the ladder separation could be seen. Gels were incubated in coomaissie blue stain (0.2% Brilliant blue, 50% methanol, 10% acetic acid) for 30 minutes and destained in 10% methanol and 10% acetic acid for 2-4 hours.

Gels were either made in-house or pre-cast from Invitrogen. 12% gels were used for proteins of interest >40 kDa and 16% for proteins of interest <40 kDa.

2.6 *In vitro protein assays*

2.6.1 Nitrocefin assay

Nitrocefin is a ß-lactam which visibly changes in colour when it is hydrolysed by a ß-lactamase (see Figure 5-6) which can be representative of peptidoglycan hydrolysis. This visible colour change can be measured at an absorbance of 490 nm and therefore is a quantitative method to assess ß-lactamase activity.

Stocks of nitrocefin were dissolved in 10 mM potassium phosphate buffer pH 5.8 to a final concentration of 46 mM. 50µl of stock nitrocefin (230 µM) was added to 10 ml of 50 mM Tris-HCl, pH 7.5 and stored at 4ºC until needed.

50 µl of Nitrocefin was incubated with 15 µg, 7.5 µg, 3.7 µg and 1.87 µg of agalacticin A in a final volume of 100 µl. Samples were placed in a 96 well plate and absorbance at 490 nm was measured every 20 seconds for 30 minutes using a microplate reader (El_x 808_{IU}, Bio-Tek instruments Inc). Samples were kept at 37ºC with light shaking before each measurement

2.6.2 *Micrococcus* degradation assay

Micrococcus lysodeikticus (Sigma) lyophilised cells were resuspended in Tris–HCl pH 7.5 at a 0.01% w/v. 160 µl *Micrococcus* solution was incubated with 10 µl lysozyme (5 mg ml^{-1} and 2.5 mg ml^{-1}) and pectocin P (20 mg ml^{-1} and 10 mg ml^{-1}) and pectocin M1 (10 mg ml^{-1}). Degradation of *M. lysodeikticus* peptidoglycan

was measured at 450 nm for 3 hours in a microplate reader (see 2.6.1) with measurements taken every 30 seconds with light shaking before each measurement.

2.7 Biophysical techniques

2.7.1 Small-angle X-ray scattering

All small angle x-ray scattering (SAXS) data was collected at the B21 beamline at Diamond Light Source (Harwell, UK) using both size exclusion chromatography (SEC-SAXS) and a sample injection robot (bioSAXS). Data was collected at a detector distance of 4 m with a flux of 12.4 keV. All data analysis was performed using ScÅtter3 (Rambo, DLS) and verified using ATSAS [144].

For bioSAXS measurements, buffers were measured before and after sample measurements and an average buffer measurement was subtracted from the scattering data. For SEC-SAXS samples 50 frames of buffer before elution were used as the buffer measurement and subtracted from the sample.

For SEC-SAXS 45µl of protein (>5mg ml^{-1}) was injected into a SHOdex KW-402.5 (<50kDa proteins) or KW-403 (>50kDa proteins) column and scattering measurements taken every 3 seconds. 30 µl bioSAXS samples were measured at 1-10 mg ml^{-1} unless otherwise stated in 2-fold dilutions. The concentration showing the least radiation damage, as measured by excess kurtosis of each frame, was used for further analysis.

The self-association or aggregation was measured by analysing the Guinier region of each scattering curve. Curves in which no Guinier region could be analysed were excluded. Particle shape and foldedness were analysed by raising examining q^x i(q) vs q^x where x= 1-4 and using dimensionless Kratky analysis qR_g^2 (I(q)/I(0) vs qR_g where R_g is the radius of gyration. The p(*r*) distribution allowed for the calculation of the maximum particle dimensions (D_{max}). This distribution was used to create a dummy atom model envelope using DAMMIF [141].

2.7.2 Small angle neutron scattering

Small angle neutron scattering (SANS) experiments were carried out on D22 (ILL, Grenoble) at a detector distance of 5.6 m. 180 µl of $FusA_{1043}$ was measured in a 0.5 mm quartz cuvette for 10 minutes at a 5.6 m length. Samples were measured in 5.5% D_2O and reduced by Anne Martel (Beam line responsible). Data was analysed as for the SAXS analysis using ATSAS [145].

2.7.3 Ensemble optimisation modelling

The ensemble optimisation modelling (EOM) web interface was used [139] to model 10 000 independent models and plot hypothetical SAXS curves for each predicted model. Domain 1 was kept in its original PDB co-ordinates in order to account for potential flexibility of the protein; however, domains 2 and 3 remained free. The determined R_g and D_{max} were plotted using Graph-pad prism. EOM was used to model the flexibility in pectocin M1, P and agalacticin A with the domains chosen shown below.

Table 2-10 Amino acid residues chosen for each domain to be modelled using EOM to examine the flexibility of each protein.

Protein	Domain 1	Domain 2	Domain 3
Pectocin M1	1-91	92-116	117-268
Pectocin P	1-94	95-124	125-318
Agalacticin A	1-132	133-164	165-274

2.7.4 CRYSOL modelling of SAXS data

Predicted models for pectocin M1 were created based on the crystal structures of its homologue pectocin M2 which has been crystalized in two conformations (PDB ID 4N58 and 4N59). Models were created using both I-TASSER and Phyre2 [146]. CRYSOL was used to create hypothetical scattering curves based on each of these models to determine whether the SAXS data may be made up of a mixed population of structures [147]. For pectocin P and agalacticin A the predicted flexibility models generated by EOM were used to calculate theoretical scattering curves for elongated and compact conformations.

2.7.5 Circular Dichroism

Protein spectra were measured in 50 mM Tris-HCl, 50-200 mM NaCl and 5% glycerol buffer at ~0.5 mg ml^{-1} for the far UV range and ~1 mg ml^{-1} for the near UV range with the data standardised to the absolute protein concentration. All spectra were obtained in a 0.2 mm path length quartz cuvette using a Jasco J-810 spectropolarimeter. Measurements were carried out by June Southall, University of Glasgow. Secondary structure estimates were made using both the CONTIN-LL and CDSSTR methods [148].

2.7.6 SEC-MALS

SEC-MALS experiments were conducted by June Southall, University of Glasgow. $FusB_{1043}$ was purified (as in 2.5.1) and concentrated to 30 mg ml^{-1}in 200 NaCl, 50 mM Tris-HCl, 5% glycerol pH 7.5 in HPLC grade dH_2O. $FusB_{1043}$ was loaded onto a Waters Xbridge BEH200 SEC 3.5µ7.8x300 column at a final concentration of 30, 10, 5 and 1 mg ml^{-1}.

2.7.7 Analytical ultracentrifugation

Sedimentation velocity (SV) data were acquired in a Beckman Coulter optima XL-I analytical ultracentrifuge using either an an-50 Ti eight-hole rotor or an an-60 Ti four holed rotor (Beckman Coulter). 360 µl of dialysate and protein solutions were loaded into 12 mm path-length charcoal-filled epon double sector centrepiece with sapphire windows.

SV data were gathered at 49000 rpm for ~18 hours with scans collected every 7 minutes (8 hole) or 3 minutes (4 hole) using absorbance optics at 280 nm and interference optics if necessary. Sample concentrations of 0.5 mg ml^{-1} to 3 mg ml^{-1} were measured depending on the 280 Δnm absorbance to ensure all absorbance was 0.5-1.5 mAU.

SEDNTERP was used to calculate the partial specific volume ($\overline{V}$) from the amino acid sequence, buffer density (ρ) and buffer viscosity (η) at both 20°C and 4°C.

For interacting systems average $\bar{V}$ of the components within the system was used. The values were used to analyse the data and can be found in Table 2-11.

Table 2-11 Details of proteins, buffers and corresponding parameters used in AUC data analysis for SV experiments

Protein	Temp.	Buffer (all pH 7.5)	Partial specific volume (ml/g)	Buffer density (g/ml)	Buffer viscosity (poise)
Agalacticin A	4 °C	50 mM Tris, 200 mM NaCl, 5% Glycerol	0.72186	1.0243	0.018828
	20 °C		0.73078	1.0225	0.012039
Pectocin M1	4 °C	50 mM Tris, 200 mM NaCl, 5% Glycerol	0.71818	1.0243	0.018828
	20 °C		0.72711	1.0225	0.012039
FusB	4 °C	50 mM Tris, 200 mM NaCl, 5% Glycerol	0.72027	1.0243	0.018828
	20 °C		0.72919	1.0225	0.012039

Sedimentation velocity data were analysed using SEDFIT to obtain experimental sedimentation coefficients using the continuous c(s) distribution model. Hypothetical sedimentation coefficients based on predicted models of each protein were calculated to compare with the experimental data using US-SOMO [149].

2.7.8 Crystallography

Initial crystallisation trials were set up using a Cartesian Honeybee 8+1 dispensing robot into 96 well plates via the sitting drop method with a reservoir volume of 80 µl and drop size of 0.5 µl protein and 0.5 µl of the reservoir solution by vapour diffusion. Proteins were screened in Morpheus, JCSG+, Midas and PACT trays from molecular dimensions. Trays were incubated at 16°C for >6 months and checked for crystal growth.

2.8 Plant Infections

2.8.1 Infection of *Solanum tuberosum* tubers

P. atrosepticum LMG2386 were grown in liquid culture overnight in LB broth, 200 µM bipyridine, 2% w/v D-lactose and ampicillin for complimented strains.

Bacteria were harvested at 4500 rpm for 10 minutes and resuspended in 1/5th the original growth volume in sterile 10 mM $MgCl_2$ or 10 mM $MgSO_4$.

The optical density of cultures was then corrected to A_{600} = 0.45 or 0.9, corresponding to ~5 x10^5 and ~10 x10^6 respectively. 100 µl of this standardised culture was placed onto the potato (*S. tuberosum,* Isle of Jura variety). Slices of around 1 cm in thickness were incubated for 72 hours in humid conditions at 28^{o}C.

For pectocin M1 tests were conducted with 500 µl of pectocin M1 at a total of 2.5, 0.5 and 0.1 mg was added 30 minutes prior to infection and further incubated until 72 total hours of infection had passed.

2.8.2 Infection of *Nicotiana benthamiana nahG*

Nicotiana benthamiana nahG plants (courtesy of Jonathan Jones, GAL Warwick) were grown for 4-6 weeks by William Rooney until the leaves were >3 cm in diameter. Leaves were harvested and were pressure infiltrated with 500 µl of *P. atrosepticum* cultures in 10 mM $MgCl_2$.

Pectocin M1 was administered by pressure infiltration at concentrations between 3 µM and 170 µM (0.1-5 mg ml^{-1}) in a total volume of 500 µl in 10 mM $MgCl_2$ 30 minutes prior to infection. Leaves were imaged using the ChemiDoc (Bio-Rad) to monitor cell lysis (white light).

Chapter 3 Biochemical and biophysical characterisation of ferredoxin-containing bacteriocins targeting *Pectobacterium* spp.

3.1 Introduction

Pectobacterium atrosepticum is a prolific pathogen of *Solanum tuberosum* (potato) and is responsible for the loss of both potato plants and tubers worldwide [3]. *P. atrosepticum*, like all *Pectobacterium* species, is characterised by the production of cell-wall degrading enzymes which cause damage to both the potato plants (blackleg) and tubers in storage (soft rot) [3,150]. In recent years three novel ferredoxin-containing bacteriocins targeted towards *P. atrosepticum* have been found: Pectocin M1, M2 and P [117,123]. As attempts are being made to reduce the amount of traditional pesticides being used, due to adverse effects on both health and the environment, the discovery of novel phytopathogen control strategies is crucial for food security [151].

Colicins and colicin-like bacteriocins possess an intrinsically unstructured translocation domain (IUTD) of 30-40 amino acids which is essential for uptake [40]. This IUTD passes through the lumen of an outer membrane receptor to interact with Tol or TonB for translocation [40,52,123]. Unlike other Gram-negative bacteriocins, pectocins do not possess an IUTD which suggests a novel uptake mechanism [117,123].

Ferredoxin-containing pectocins have an N-terminal domain homologous to a plant-type ferredoxin, specifically spinach ferredoxin II [117]. This N-terminal domain contains an iron-sulphur [2Fe-2S] cluster and it is thought that the gene encoding this domain may have been acquired by horizontal gene transfer from a host-species [117]. This N-terminal domain is thought to be necessary for uptake by the ferredoxin uptake receptor (FusA) found in *Pectobacterium* species [117,124].

Previous work has shown that pectocin M2 can be found in multiple conformations in solution, with the rigid C-terminal cytotoxic domain rotating around the N-terminal ferredoxin domain due to the presence of a flexible linker region (Figure 3-1) [123]. However, the most commonly found conformations are an elongate and bent form for which the X-ray crystallography structures were solved (Figure 3-1) [123].

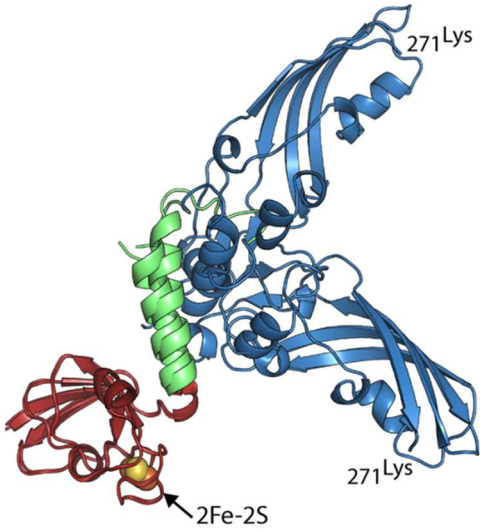

Figure 3-1 Pectocin M2 can be found in multiple conformations in solution. X-ray crystal structure of pectocin M2 in both the elongated and compact conformations (overlain at the N-terminus) showing the flexibility of the cytotoxic domain (blue) around the flexible linker region (green) with the ferredoxin domain shown in red (PDB IDs 4N58 and 4N59). Reproduced from [123] under a creative commons licence.

The FusA outer membrane receptor is required for the uptake of M-type pectocins [124]. The deletion of *fusA* prevents the uptake of pectocin M1 and subsequent cell lysis (Figure 3-2) with the complementation of *fusA* restoring the activity [123]. Docking models suggest that two separate conformations are required for receptor binding and uptake [124]. It is predicted that receptor binding can only occur in the folded conformation, but the elongated conformation is required for translocation due to the dimensions of the FusA barrel [124].

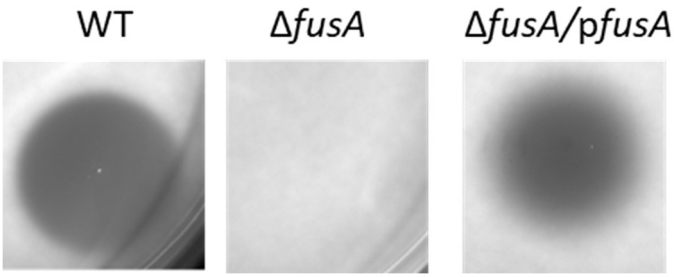

Figure 3-2 Uptake of pectocin M1 by *P. atrosepticum* LMG2386 is dependent on the presence of the FusA outer membrane receptor. WT, Δ*fusA* and Δ*fusA*/p*fusA* strains were grown to mid-log phase and overlain onto LB agar containing 200 µM bipyridine, 2% w/v D-lactose (as well as 100 µg ml^{-1} ampicillin for the complimented strain). 7 mg ml^{-1} of purified pectocin M1 was spotted and plates were incubated overnight at 28^{o}C. Plates were overlain with PrestoBlue to visualise the spots and images taken with the Chemidoc at 546 nm.

The three known pectocins share a conserved plant-type ferredoxin N-terminal domain, however the cytotoxic domains of the M-type pectocins and pectocin P are very different (Figure 3-3). Pectocin M1 and M2 share a conserved colicin M-type cytotoxic domain which is known to cleave lipid II [117,123]. However pectocin P has a cytotoxic domain which is similar to pesticin from *Yersina pestis* and T4 phage lysozyme, suggesting that it may act by hydrolysing peptidoglycan to cause cell lysis [116].

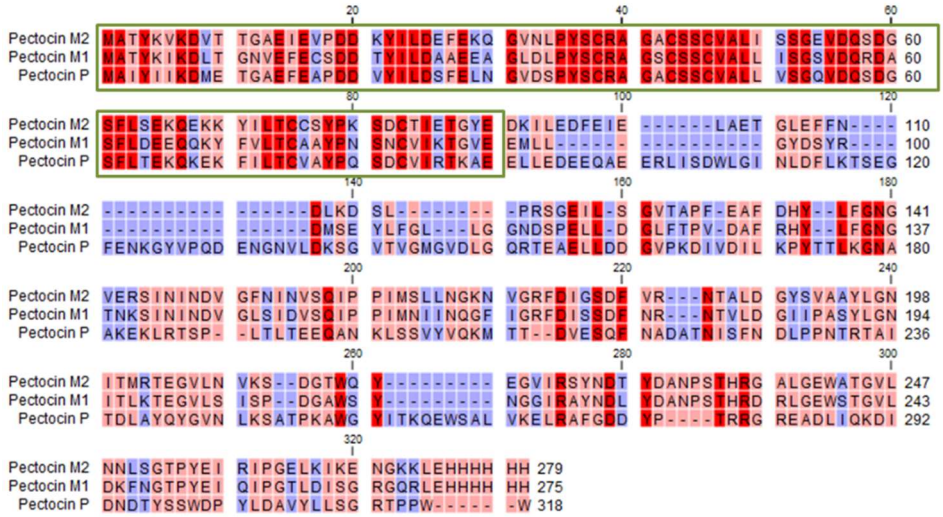

Figure 3-3: Amino acid sequence alignments of pectocins M2, M1 and P. Amino acid sequence alignment performed in CLC workbench aligning all three pectocins based on their primary structure with conserved residues highlighted in red, residues conserved between two proteins highlighted in pink and non-conserved residues highlighted in blue. The conserved ferredoxin binding domain is highlighted in green.

As pectocin M1 is a homologue of pectocin M2, it is predicted that it will also be flexible in solution to allow for it to bind and translocate into the periplasm of the target cell. However, as pectocin P has a different predicted structure its behaviour, binding and translocation mechanism are completely unknown. It is presumed that, due to the homology between the ferredoxin domains, pectocin P also uses the FusA receptor for uptake. This chapter aims to structurally characterise both pectocin M1 and pectocin P to further understand both their mechanism of action and the conformational changes necessary for translocation.

3.2 Results

3.2.1 Predicted model of pectocin M1

Like pectocin M2, pectocin M1 has a ferredoxin N-terminal domain with 58% sequence identity to spinach ferredoxin II, joined with a flexible linker region to a lipid II degrading cytotoxic domain with a 42% sequence identity to colicin M (Figure 3-4a). Pectocin M2 is found in multiple conformations in solution [123], therefore it is predicted that pectocin M1 will be similar in both structure and behaviour. Based on the X-ray crystal structures of pectocin M2, two models of pectocin M1 were created using Phyre2, with pectocin M1 in both a bent and elongated conformation (Figure 3-4b).

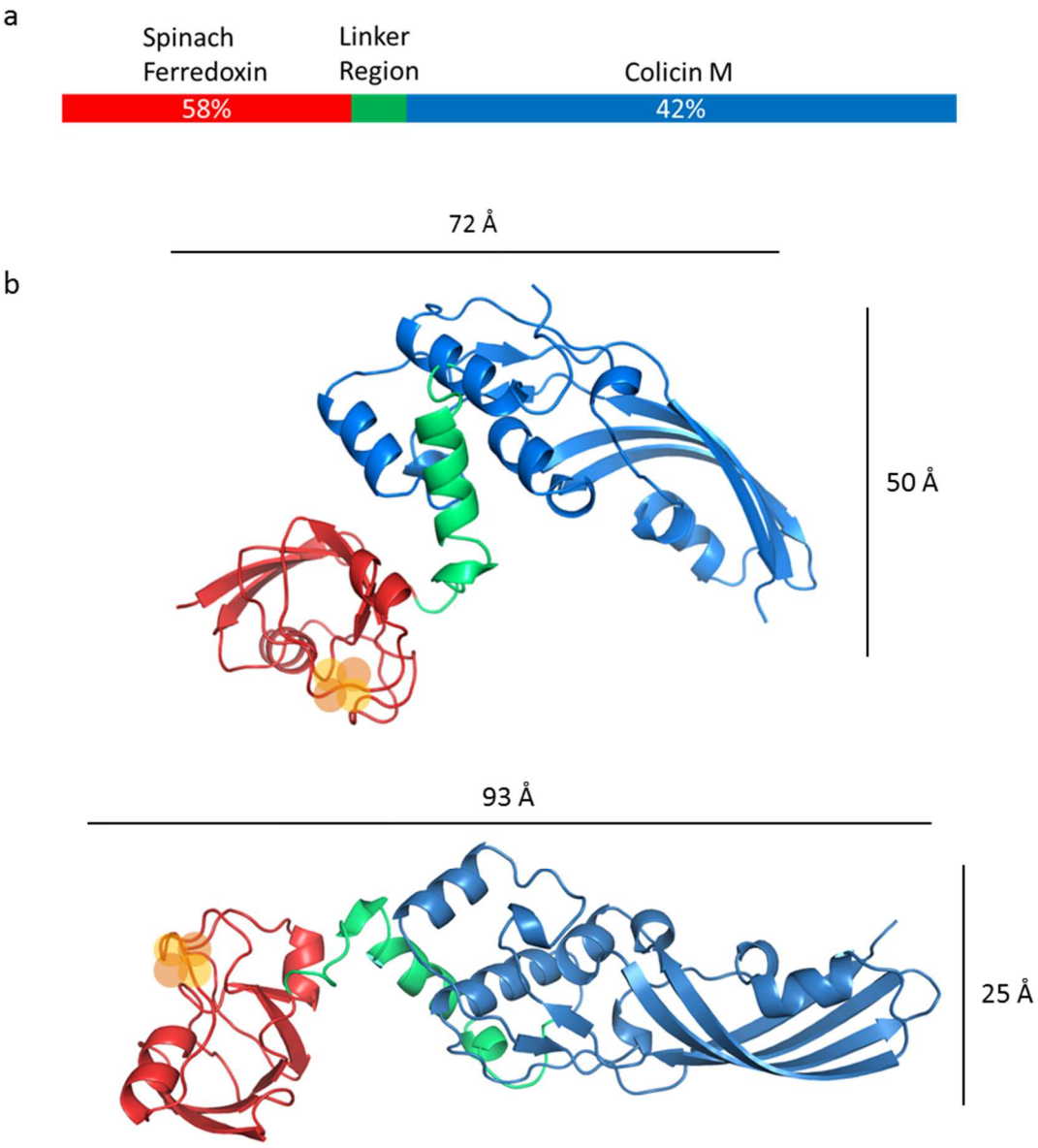

Figure 3-4 Cartoon representation of the structure of pectocin M1 and the domain homologies a) Cartoon representation of the domain structure of pectocin M1 showing sequence homology to both spinach ferredoxin and colicin M. b) Bent and elongated Phyre2 models of pectocin M1 based on homology with pectocin M1. The ferredoxin domain is shown in red, linker region in green and cytotoxic domain in blue with the predicted location of the iron-sulphur cluster represented by orange spheres.

3.2.2 SAXS analysis of pectocin M1

Pectocin M1 was examined using SEC-SAXS to determine if, like pectocin M2, it is both flexible and found in multiple conformations in solution. Scattering data from pectocin M1 were collected and frames with the highest signal within the SEC-SAXS peak were chosen for analysis (Figure 3-5a).

Analysis of the Guinier region (Figure 3-5b) showed that the sample was free of aggregation as the residuals were randomly distributed. An R_g of 23.6 Å was calculated for pectocin M1 which is smaller than the R_g for pectocin M2 which was found to be 27.4 Å, suggesting pectocin M1 may be found in a more compact conformation in solution. Extrapolation of the Guinier region to I(0) gives a molecular weight for pectocin M1 of 28.5 kDa, (calculated using SAXSMoW2 [136]) which is similar to the molecular weight of 30.3 kDa calculated from the amino acid sequence (using protparam [152]). This suggests that pectocin M1, like pectocin M2, is monomeric in solution.

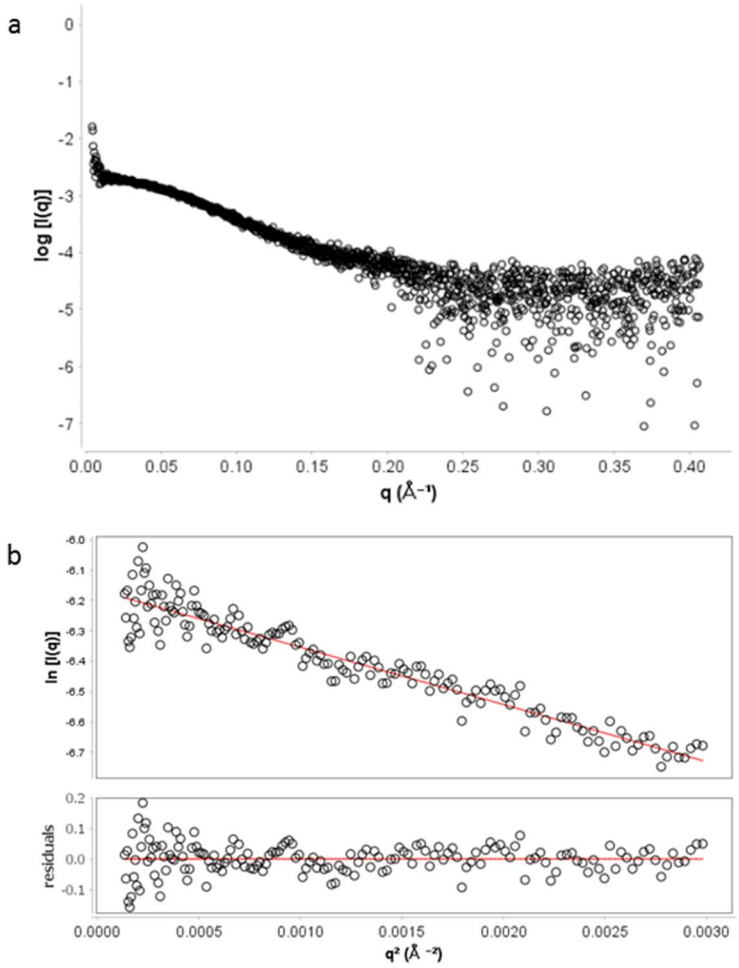

Figure 3-5 SEC-SAXS data for pectocin M1 a) q vs Log I(q). b) Guinier analysis of the low q range suggests a molecular weight of 28.5 kDa (calculated using SASMoW2 [136]) . Data was obtained using a Showdex kw- 402.5 column in 50 mM Tris-HCl, 200 mM NaCl, 5% Glycerol, and pH 7.5 with an initial concentration of pectocin M1 measured as 12.5 mg ml^{-1}.

3.2.3 Flexibility of pectocin M1 in solution

Kratky analysis for pectocin M1 showed that the peak of the distribution occurs around √3 (Figure 3-6a). This suggests that pectocin M1 is ordered and folded in solution. It also suggests that the particle is more likely to be globular in solution than elongated, which is consistent with the predicted bent conformation of pectocin M1.

As shown in Figure 3-6, the plateau in the scattering data for pectocin M1 occurs first in the Kratky-Debye (Figure 3-6b) plot and no plateau can be seen at any q

range in the Porod-Debye plot (Figure 3-6c). This suggests that the particle is flexible in solution, supporting the idea that pectocin M1 may be found in multiple conformations.

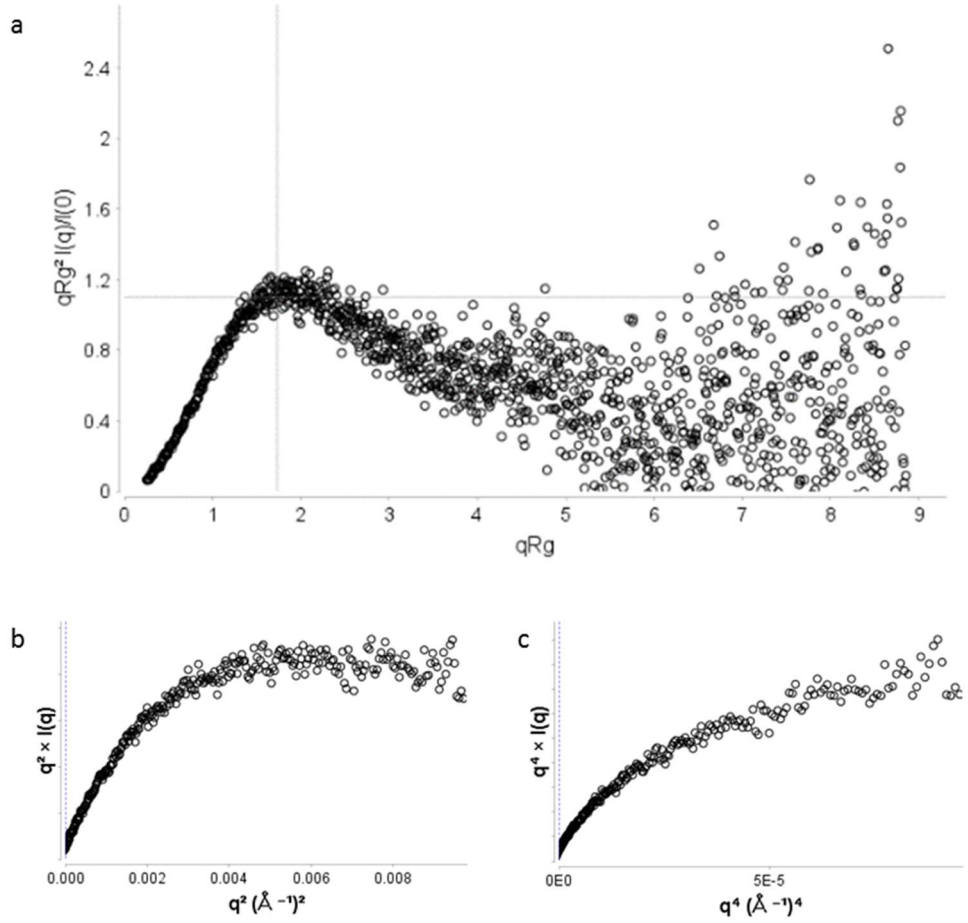

Figure 3-6 Flexibility analysis of pectocin M1 shows that it is both globular and flexible a) Dimensionless Kratky plot shows the peak of the data occurring around √3 (1.73 (as shown by the cross-hairs) suggests that pectocin M1 is globular in solution b) Kratky-Debye and c) Porod-Debye plots showing the plateau occurring first in the Kratky-Debye plot suggesting that pectocin M1 is flexible in solution.

3.2.4 Dummy atom modelling of pectocin M1

The maximum particle dimension (D_{max}) for pectocin M1 in solution was found to be 85 Å (Figure 3-7a), which is smaller than the D_{max} found for pectocin M2 at 96 Å [123]. The D_{max} at 85 Å is similar to that of the elongated model at ~92 Å in length (Figure 3-4), suggesting an intermediate conformation between the bent and elongated models may exist in solution. Using the p(*r*) distribution a predicted model of pectocin M1 in solution was created (Figure 3-7b).

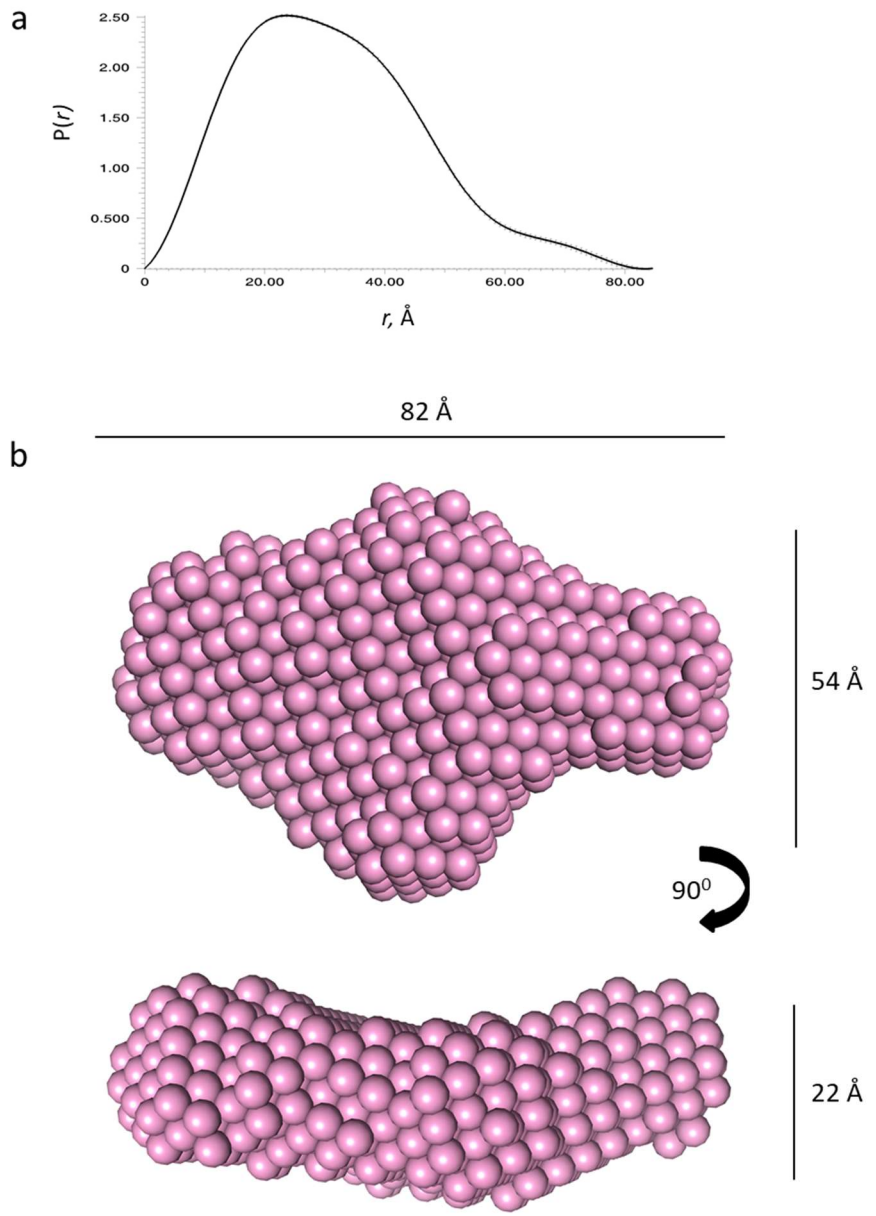

Figure 3-7 P(*r*) distribution for pectocin M1 SAXS data and DAMMIF model. a) p(*r*) distribution showing the inter-electron distances gives a D_{max} of 85 Å. b) DAMMIF model created from p(*r*) distribution with the two-dimensional measurements shown.

When compared with the individual models of pectocin M1, the DAMMIF model does not fit either individual model well. For a monodispersed single conformation population the p(*r*) distribution will represent the individual particle within solution, however if a particle is found in multiple conformations within solution the p(*r*) distribution represents the averaged particle [129]. Therefore, as the DAMMIF model does not represent either individual model, it was predicted that pectocin M1, similarly to pectocin M2, would also be found in more than one conformation in solution.

3.2.5 Pectocin M1 is in multiple conformations in solution

In order to determine if the experimental data could be better described by pectocin M1 in multiple conformations over either individual model, theoretical SAXS curves for both the globular and elongated conformations were created using CRYSOL [147]. The predicted scattering curve for each of the models was compared with the experimental data (Figure 3-8) and it can be seen that the bent conformation of pectocin M1 (Figure 3-8a) has a better fit to the experimental data with X^2 = 1.756 compared with the elongated model at X^2= 2.258 (Figure 3-8), although neither of these models describes the data very well.

Ensemble optimisation modelling (EOM) was used to determine whether the scattering data obtained could be explained better by a protein in multiple conformations. The model of pectocin M1 was separated into three domains (N-terminal ferredoxin, flexible region and C-terminal cytotoxic domain), the N-terminal domain was fixed in space and both the flexible linker and the C-terminal domains were unrestrained to allow for flexibility to be modelled. EOM creates a pool of randomly created conformations of the given protein and selects the conformations from that pool that best fit the experimental data [139].

The EOM data showed that an ensemble of conformations was better able to fit the experimental data (X^2 = 1.455) when compared with either conformation individually (Figure 3-8c), further supporting the idea that pectocin M1 is flexible in solution.

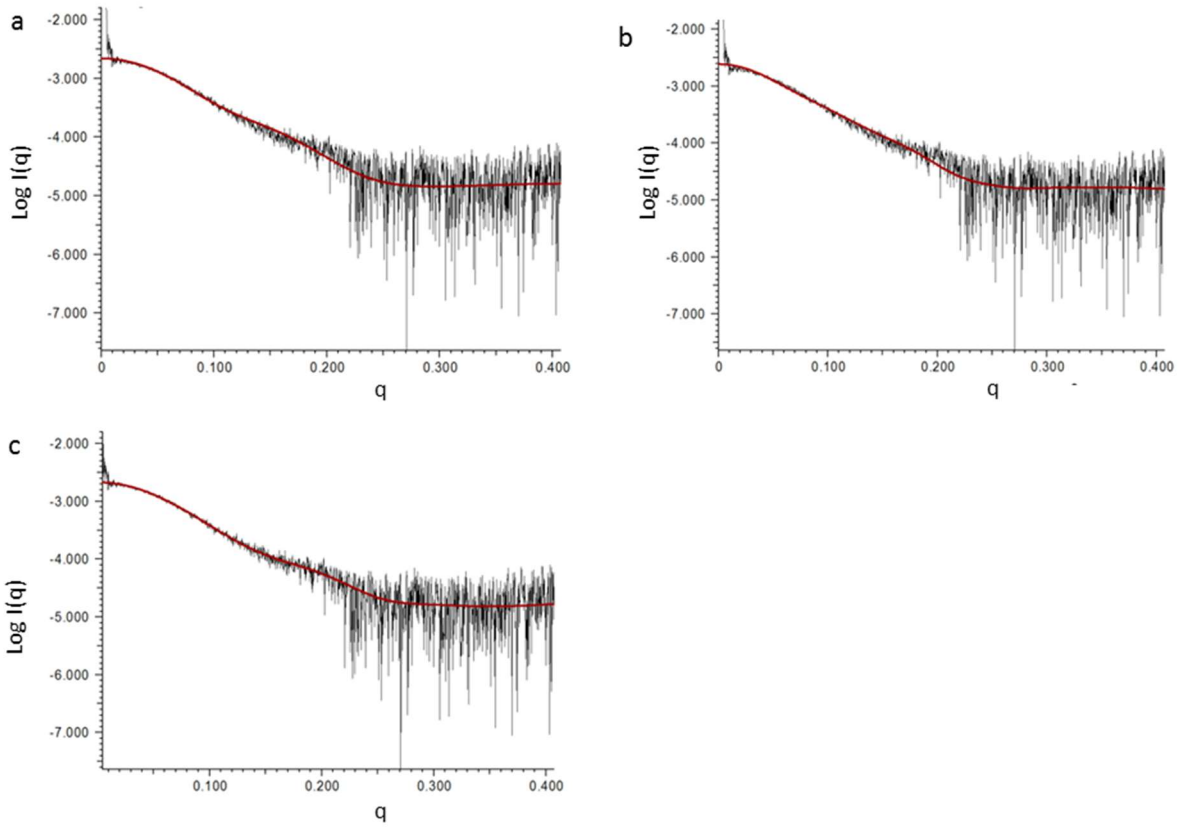

Figure 3-8 CRYSOL SAXS curve predictions for pectocin M1 in multiple conformations show that a mixed population is the best fit for the experimental data. CRYSOL predicted SAXS curves (red) were fit to the experimental SAXS data (black) for pectocin M1 shown in a a) globular conformation (X^2 = 1.756), b) elongated conformation (X^2=2.258) and c) mixed population (X^2= 1.455) as calculated by ensemble optimisation modelling.

As the EOM predicted SAXS curve showed the best fit the experimental data the selected models were examined in more detail. The D_{max} and R_g for each of the models were calculated and plotted to determine the most commonly occurring model dimensions. The pool of models had a range of maximum dimensions from 66.2 Å to 118.8 Å, however the models selected to fit the SAXS data (Figure 3-9a) show two distinct populations with peaks at 70 Å and 90 Å. Similarly, the models show two distinct populations when the R_g was measured, with peaks occurring at 22 Å and 26 Å (Figure 3-9b) which is consistent with the experimental data which gives an R_g of 23.6 Å. When compared with the predicted models of pectocin M1 these dimensions are consistent with the globular and elongated conformations respectively (Figure 3-10).

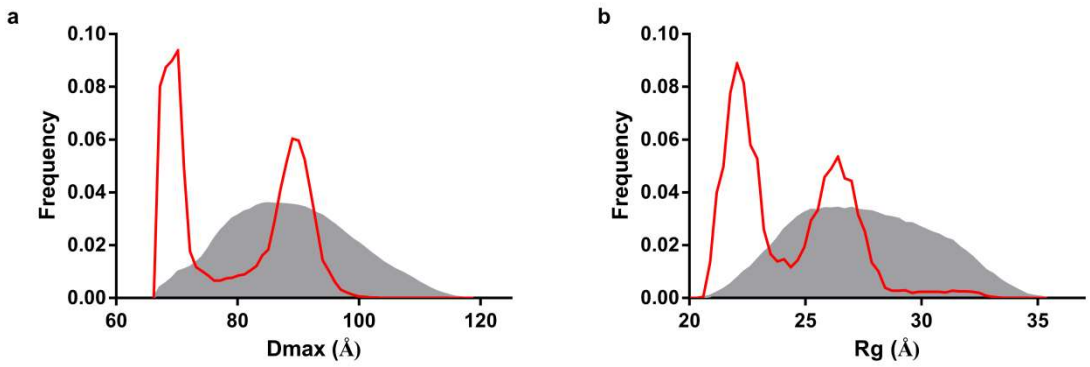

Figure 3-9 Ensemble optimisation modelling of pectocin M1 based on SAXS data shows that pectocin M1 is found in at least two conformations in solution. EOM predictions of a) maximum dimensions (D_{max}) and b) Radius of gyration (R_g) suggest that pectocin M1, like M2, is found in multiple conformations in solution. The maximum dimensions are consistent with the maximum dimensions of the predicted models. The pool of models is shown in grey with the population frequency shown in red.

In comparison to the D_{max} of the scattering data the elongated form of pectocin M1 has a larger D_{max} than the experimental data. Similarly, the bent conformation has a smaller D_{max}. This further supports the idea that the scattering data is an average of both the bent and elongate conformations of pectocin M1, as well as a potential intermediate conformation. In order to examine this further the ability to examine a single conformation of pectocin M1 would be beneficial.

Moreover, when compared with the DAMMIF model and it can be seen that the overall envelope does appear to fit both the globular and elongated forms of pectocin M1 (Figure 3-10). This data further supports the idea that pectocin M1 behaves in the same was as pectocin M2 in solution and can be found in multiple conformations.

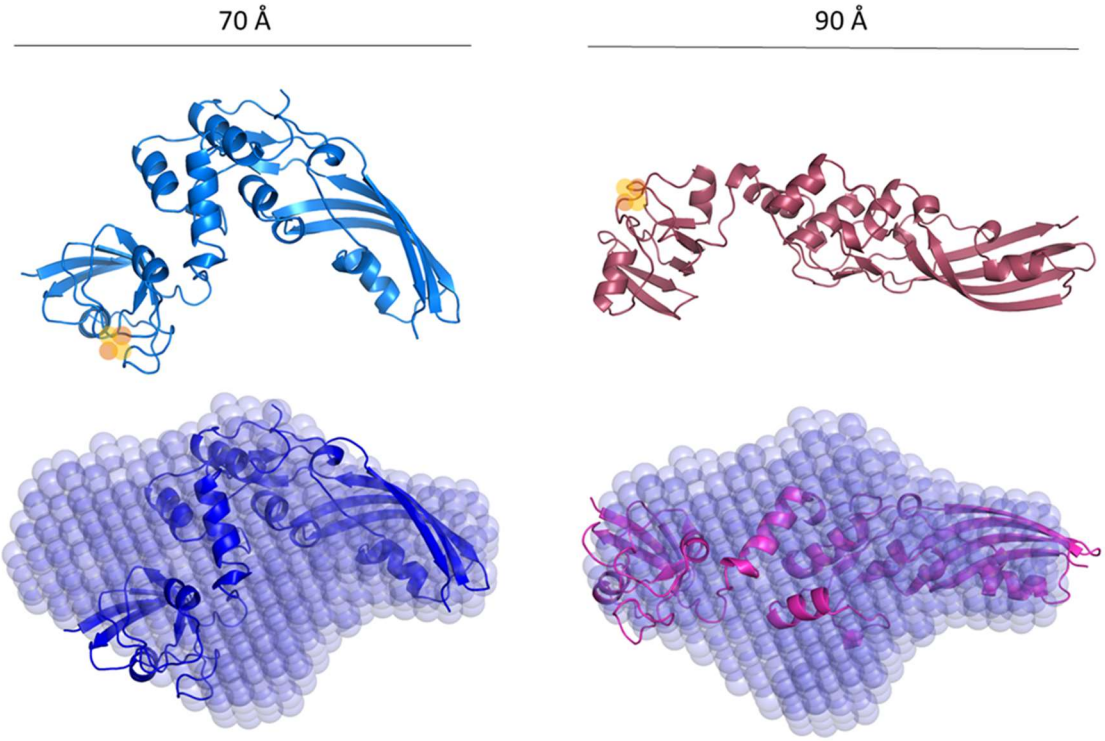

Figure 3-10 Dummy atom model (DAMMIF) of pectocin M1 in solution overlaid with pectocin M1 in two predicted conformations. Dimensions to show the D_{max} of both the globular (blue) and elongated (pink) conformations of pectocin M1. The DAMMIF model is overlaid with both the predicted globular and elongate conformations of pectocin M1 based on the high-resolution crystal structures of pectocin M2 [123] suggesting that pectocin M1 may also be found in two conformations.

3.2.6 Pectocin M1 crystallisation trials

The X-ray crystal structure of pectocin M2 was able to yield information as to its conformations in solution. Therefore, to assess the accuracy of the model and to examine its similarity to pectocin M2, crystallisation trials for pectocin M1 were conducted. Initial crystallisation screenings were set up for pectocin M1. Optimisation screens using PACT, Mopheus, Mem Gold and JCSG screening trays from Molecular dimensions, were set up and monitored for 10 months but did not yield any crystals.

3.2.7 Uptake and mechanism of action of pectocin P

3.2.7.1 Uptake of pectocin P

The N-terminal ferredoxin domain of pectocin M1 is known to interact with the FusA receptor (Chapter 4) and FusA is essential for pectocin M1 uptake (Figure 3-2). With respect to this, it is predicted that pectocin P, like pectocin M1, possesses the ferredoxin N-terminal domain to allow it to also parasitise the FusA receptor in *Pectobacterium* species, although this has not been previously demonstrated.

Initial spot tests showed that, at high concentrations, pectocin P is active against *P. atrosepticum* LMG2386 with a minimum inhibitory concentration of 8.13 µM (Figure 3-11), which is significantly less potent than pectocin M1 which is active down to nanomolar concentrations.

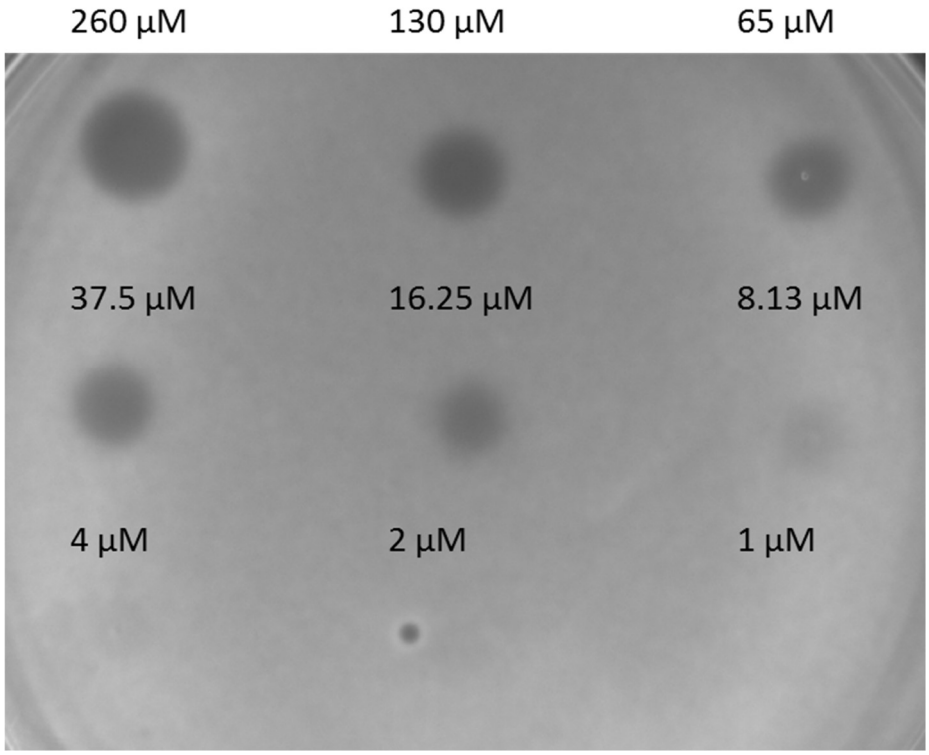

Figure 3-11 Pectocin P is active against of *P. atrosepticum* LMG2386. Pectocin P spotted LB agar containing 200 µM bipyridine with an overlay of *P. atrosepticum* LMG2386. Pectocin P was spotted in two-fold dilutions from 260 µM to 1 µM, showing a minimum inhibitory concentration of 8.13 µM. Plates were overlain with PrestoBlue and images taken with the Chemidoc at 546 nm.

Pectocin P was tested against wild-type (WT), Δ*fusA* and Δ*fusA*/p*fusA* strains in order to determine if FusA is essential for uptake. Spot tests showed that FusA is essential for the uptake of pectocin P due to the absence of cell lysis in the Δ*fusA* strain and the complementation of FusA restored activity (Figure 3-12).

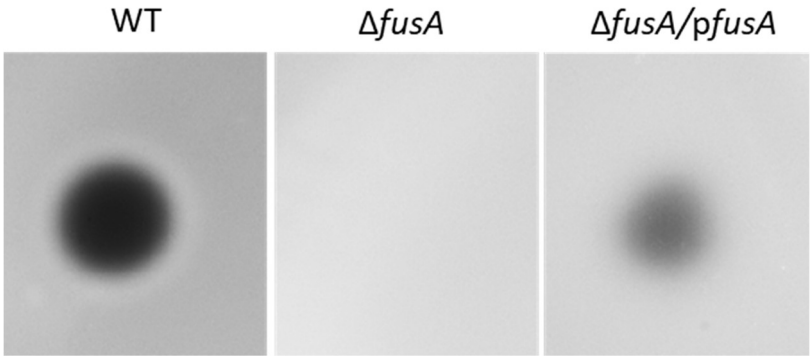

Figure 3-12 Pectocin P uptake is dependent on the presence of FusA. Pectocin P was spotted on 200 μM bipyridine, D-lactose and (100 μg ml $^{-1}$ ampicillin for complimented strain) LB agar at a concentration of 10 mg ml^{-1} (280 μM), a zone of inhibition can be seen clearly on the WT strain but there is no activity against the Δ*fusA* strain. Plates were overlain with PrestoBlue and images taken with the Chemidoc at 546 nm.

3.2.7.2 Predicted mechanism of action

Unlike the M-type pectocins, pectocin P has a cytotoxic domain which is homologous to that of pesticin from *Yersinia pestis* and lysozyme. These proteins break down the mature peptidoglycan of the target cell by hydrolysing the bond between the N-acetylmuramic acid (NAM) and N-acetyl-D-glucosamine (NAG). The important active site residues of pesticin have been identified as E178, T201 and D207 [49], which (Figure 3-13a) corresponding to residues E119, T142 and D148 of pectocin P respectively.

a

```
                    20                  40                  60
Pesticin    MSDTMVVNGS GGVPAFLESG STLSSYRPNF EANSITIALP HYVDLPGRSN FKLMYIMGFP 60
Pectocin P  MAIYIIKDME TGAE---FEA PDDVYILDSF ELNGVDS--P YSCRAGACSS CVALLVSG-Q 54
                    80                  100                 120
Pesticin    IDTEMEKDSE YSNKIRDESK ISKTEGTVSY EQK-ITVETG QEKDGVKVYR VMVLEGTIAE 119
Pectocin P  VD---QSDGS FLTE-KDKEK FILT--CVAY PQSDCVIRTK AEE------- --LLE----- 94
                    140                 160                 180
                                                            *
Pesticin    SIEHLDKKEN EDILNNNRNR IVLADNTVIN FDNISQLKEF LRRSVNIVDH DIFSSNGFEG 179
Pectocin P  -----DEEQA EERL------ --ISDWLGIN LD-------F LKTS------ --------EG 120
                    200                 220                 240
                        *                   *
Pesticin    FNPTSHFPSN PSSDYFNSTG VTFGSGVDLG QRSKQDLLND GVPQYIADRL DGYYMLRGKE 239
Pectocin P  FENKGYVPQD ENGNVLDKSG VTVGMGVDLG QRTEAELLDD GVPKDIVDIL KPYTTLKGNA 180
                    260                 280                 300
Pesticin    AYDKVRTAPL TLSDNEAHLL SNIYIDKFSH KIEGLFNDAN IGLRFSDLPL RTRTALVSIG 299
Pectocin P  AKEKLRTSPL TLTEEQANKL SSVYVQKMTT DVESQFNADA TNISFNDLPP NTRTAITDLA 240
                    320                 340                 360
Pesticin    YQKGFKLSRT APTVWNKVIA KDWNGLVNAF NNIVDGMSDR RKREGALVQK DIDSG----- 354
Pectocin P  YQYGVNLKSA TPKAWGYITK QEWSALVKEL RAFGDDYPTR RGREADLIQK DIDNDTYSSW 300

Pesticin    --------LL K------- 357
Pectocin P  DPYLDAVYLL SGRTPPWW 318
```

b

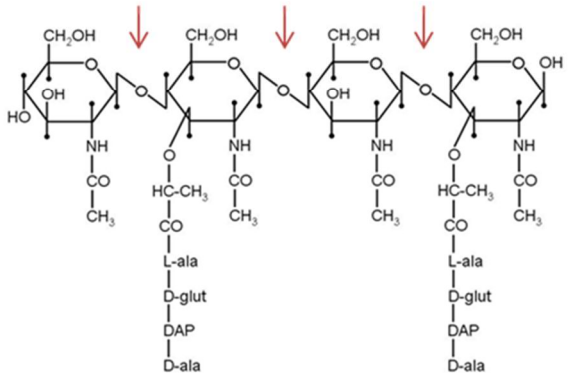

Figure 3-13 Protein sequence alignment of pesticin and pectocin P as well as an illustration of the mechanism of action of pesticin a) Protein sequence alignment performed in CLC showing similarity in some regions of the cytotoxic domain with the known catalytic residues of pesticin highlighted with an asterisk showing conservation of these amino acids in pectocin P and pesticin. b) Peptidoglycan structure shown with arrows showing the sites of hydrolysis by lysozyme, pesticin and predicted for pectocin P (image taken from cronodon.com).

Lysozyme has been extensively studied and its mechanism of action is well understood. It is known to hydrolyse the glyosidic bond between NAM and NAG in the peptidoglycan backbone (Figure 3-13b) [153]. The subdomains of lysozyme are known to close around the NAM ring in order for residues E11, E20 and T26 to interact with the substrate to catalyse the hydrolysis of the NAM-NAG bond [153].

It was therefore predicted that pectocin P would hydrolyse peptidoglycan in the same way as both lysozyme and pesticin (Figure 3-13b). Previous work to determine the mechanism of action of lysozyme has used the degradation of

Micrococcus lysodeikticus as a measure of enzymatic activity, the hydrolysis of the *M. lysodeikticus* peptidoglycan can be seen by a reduction of absorbance at 450 nm (Figure 3-14) [154].

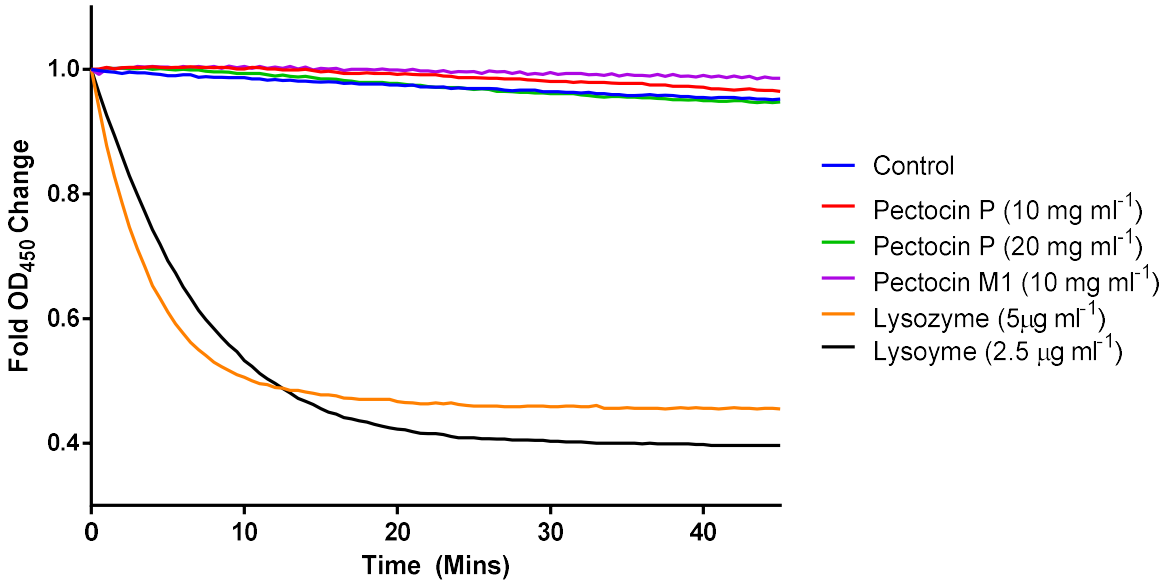

Figure 3-14 Graph showing fold-change of optical density (450 nm) for pectocin P. Proteins were incubated with *M. lysodeikticus* for 45 minutes and the optical density at 450 nm was measured at 30 second intervals. A reduction in absorbance is indicative of the breakdown of the *M. lysodeikticus* peptidoglycan layer. Substrate was incubated alone (blue) and with pectocin P at 20 mg ml^{-1} (green) , pectocin P at 10 mg ml^{-1} (red), pectocin M1 at 10 mg ml^{-1} (purple), 5 µg ml^{-1} lysozyme (orange) and 2.5 µg ml^{-1} lysozyme (black) .

Pectocin P was tested against *M. lysodeikticus* at several different concentrations with the highest two concentrations are shown here. When incubated with lysozyme the absorbance at 450 nm decreases rapidly over time before plateauing showing the effective hydrolysis of the peptidoglycan. In contrast, when incubated with pectocin P, no hydrolysis of the *M. lysodeikticus* peptidoglycan was observed (Figure 3-14). In parallel to this spot tests were carried out which confirmed the activity of recombinantly produced pectocin P *in vivo*, therefore the reduction in activity is assay specific rather than due to the complete loss of activity.

This lack of activity is surprising as pectocin P is similar in structure to lysozyme, however when pesticin was tested for activity against *M. lysodeikticus* it was

also unable to degrade the *M. lysodeikticus* peptidoglycan [116,155]. Therefore, as pectocin P is more closely related to pesticin the lack of activity may not necessarily mean that it does not hydrolyse peptidoglycans but rather this assay is an inconclusive way to measure it. Little is known about the conditions needed for pectocin P activity. It is possible therefore, that a conformational change is required for enzymatic activity and that this does not occur *in vitro*. Further work should be done to analyse the activity of pectocin P to conclusively determine its mode of action.

3.2.8 Structural characterisation of pectocin P

3.2.8.1 Predicted structure of pectocin P in solution

The high-resolution structure of pectocin P is yet to be solved and therefore homology models have been created using both Phyre2 and I-TASSER. Phyre2 models based on the homology of pectocin P to both the N-terminal of pectocin M2 and the C-terminal of pesticin combine to suggest a folded globular conformation (Figure 3-15b).

As pectocin P has less than 50% sequence identity with both homologues (Figure 3-15a), I-TASSER was used to create a model based on the primary amino acid sequence [156]. The I-TASSER model of pectocin P (Figure 3-15c) suggests a more elongated protein with less regular secondary structure, however both show the cytotoxic domain to be formed primarily of α-helices. The C-terminal domain of pectocin P shows a non-regular structure of 24 amino acids at the C-terminus. This C-terminal region contains a number of flexible amino acid residues (>50%) as well as three tryptophan residues and does not align with the pesticin sequence (Figure 3-13) suggesting it may be important for flexibility or activity.

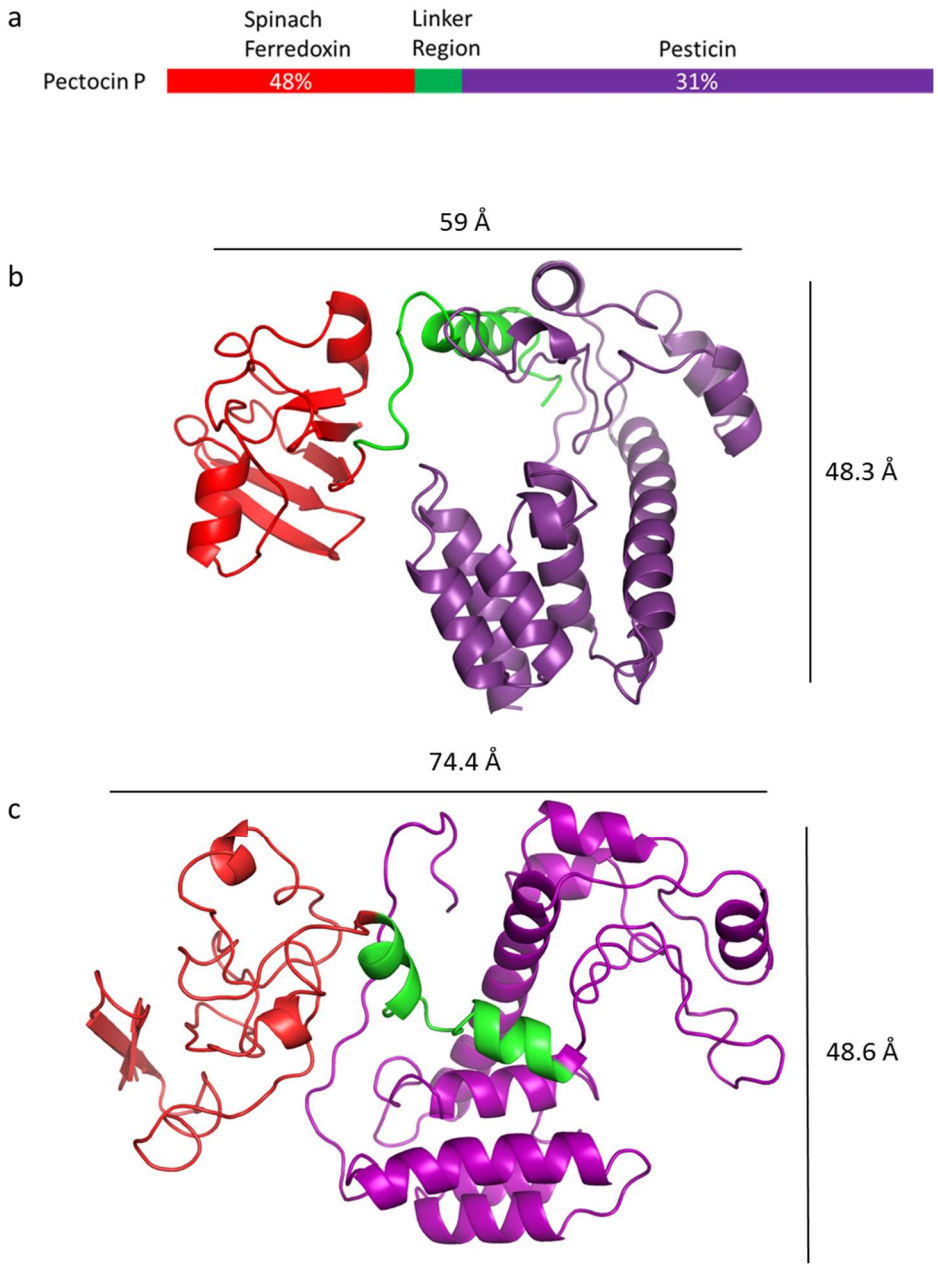

Figure 3-15 Sequence identity, Phyre2 and I-TASSER models of pectocin P. a) Cartoon representation of the domain structure of pectocin P showing the percentage sequence homology to both spinach ferredoxin and pesticin. b) Phyre2 combined model of the ferredoxin domain and cytotoxic domain of pesticin c) I-TASSER model of pectocin P with the N-terminal ferredoxin domain in red, flexible linker in green and the cytotoxic domain in purple.

3.2.8.2 Pectocin P is compact in solution

Pectocin P, like the M-type pectocins, consists of an N-terminal ferredoxin domain which is linked to a C-terminal cytotoxic domain by a linker region largely made up of flexible residues. In order to test the predicted models of pectocin P as well as determining if the two domains are indeed joined by a flexible linker region, pectocin P was examined by SEC-SAXS.

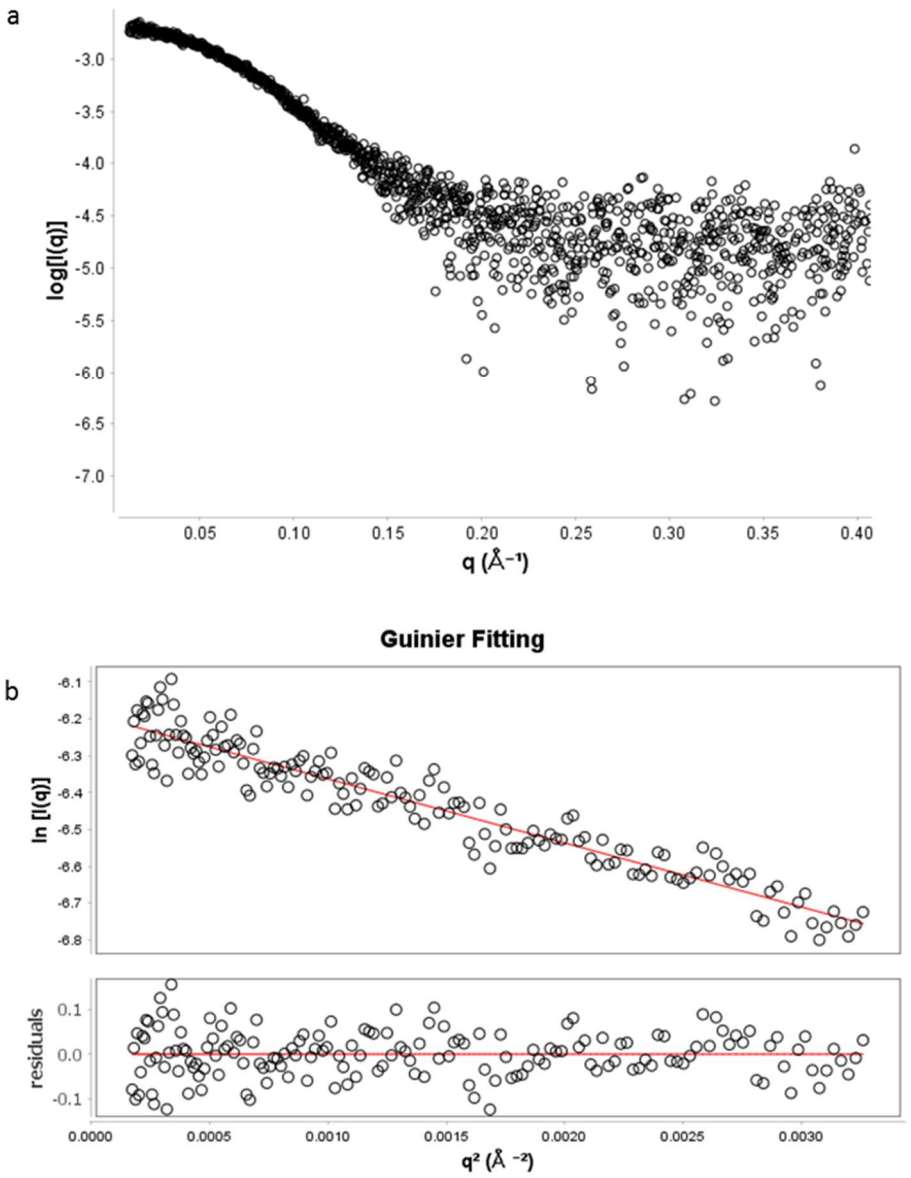

Figure 3-16 SEC-SAXS data for pectocin P a) Raw SAXS data for pectocin P shown as q vs Log I(q). b) Guinier region of pectocin P scattering data and residuals.

The Guinier region obtained from the SAXS data was analysed and showed that the sample was free from aggregation. The Guinier analysis yielded a radius of

gyration of 22.7 Å and the extrapolation to the I(0) gived a predicted molecular weight of 35.4 kDa with a which is almost identical to the molecular weight of 36 kDa calculated from the amino acid sequence (Figure 3-16) [136,152]. SAXS data for pectocin P was collected on multiple occasions and yielded similar results each time independent of concentration.

3.2.8.3 Pectocin P model is consistent with SAXS low-resolution models

Kratky analysis was performed to examine the shape and foldedness of pectocin P in solution. As mentioned previously the high number of flexible residues present suggests the presence of a flexible linker region joining the N- and C-terminal domains of pectocin P. This suggests that the C-terminal domain of pectocin P, like that of pectocin M1, may be able to move in relation to the N-terminal domain. This conformational change would allow pectocin P to become more elongated in order to pass through FusA into the periplasm.

The dimensionless Kratky distribution for pectocin P is seen to form a classical parabola shape with a peak occurring at $\sqrt{3}$ suggesting that pectocin P is globular in solution. This is consistent with both the Phyre2 and I-TASSER predicted structures. This is further supported by the Kratky-Debye and Porod-Debye analysis which clearly shows a plateau occurring first in the Porod-Debye when the scattering angle q is raised to the power of 4 and no plateau occurring in the Kratky-Debye plot, further supporting the model that pectocin P as a globular, inflexible and ordered particle (Figure 3-17).

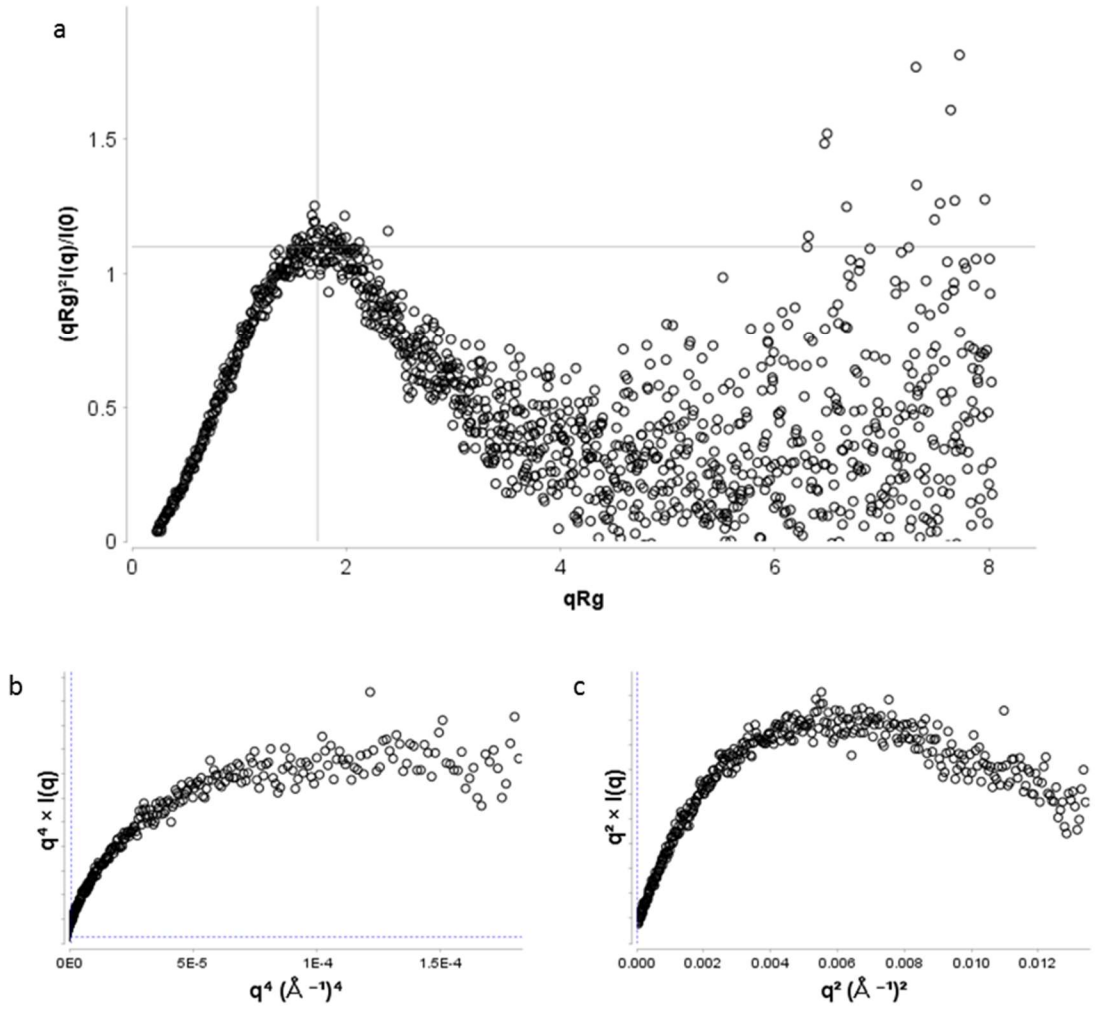

Figure 3-17: Flexibility analysis of pectocin P shows that it is globular in solution and inflexible. a) Dimensionless Kratky plot shows the peak of the data occurring around √3 suggesting pectocin P is globular in solution b) Porod-Debye and c) Krakty-Debye plots showing the plateau occurring first in the Porod-Debye plot further suggesting that pectocin P is globular and inflexible in solution.

The flexibility analysis confirms the Kratky analysis that pectocin P is compact and inflexible in solution. This does not necessarily mean that the particle cannot be found in more than one conformation but suggests that it is found in distinct conformations rather than being intrinsically flexible. It could also suggest that pectocin P is found in one conformation in solution and an interaction with another protein is required for a conformation change, or it could be that pectocin P is simply found in one conformation.

The p*(r)* distribution for pectocin P gave a maximum particle dimension of 73 Å and the parabola shape of the p*(r)* distribution further suggests that the particle

is globular in solution (Figure 3-18). Dummy atom modelling of pectocin P was performed with both DAMMIF [141] to create an overall *ab initio* envelope and GASBOR to create an *ab initio* chain model [157].

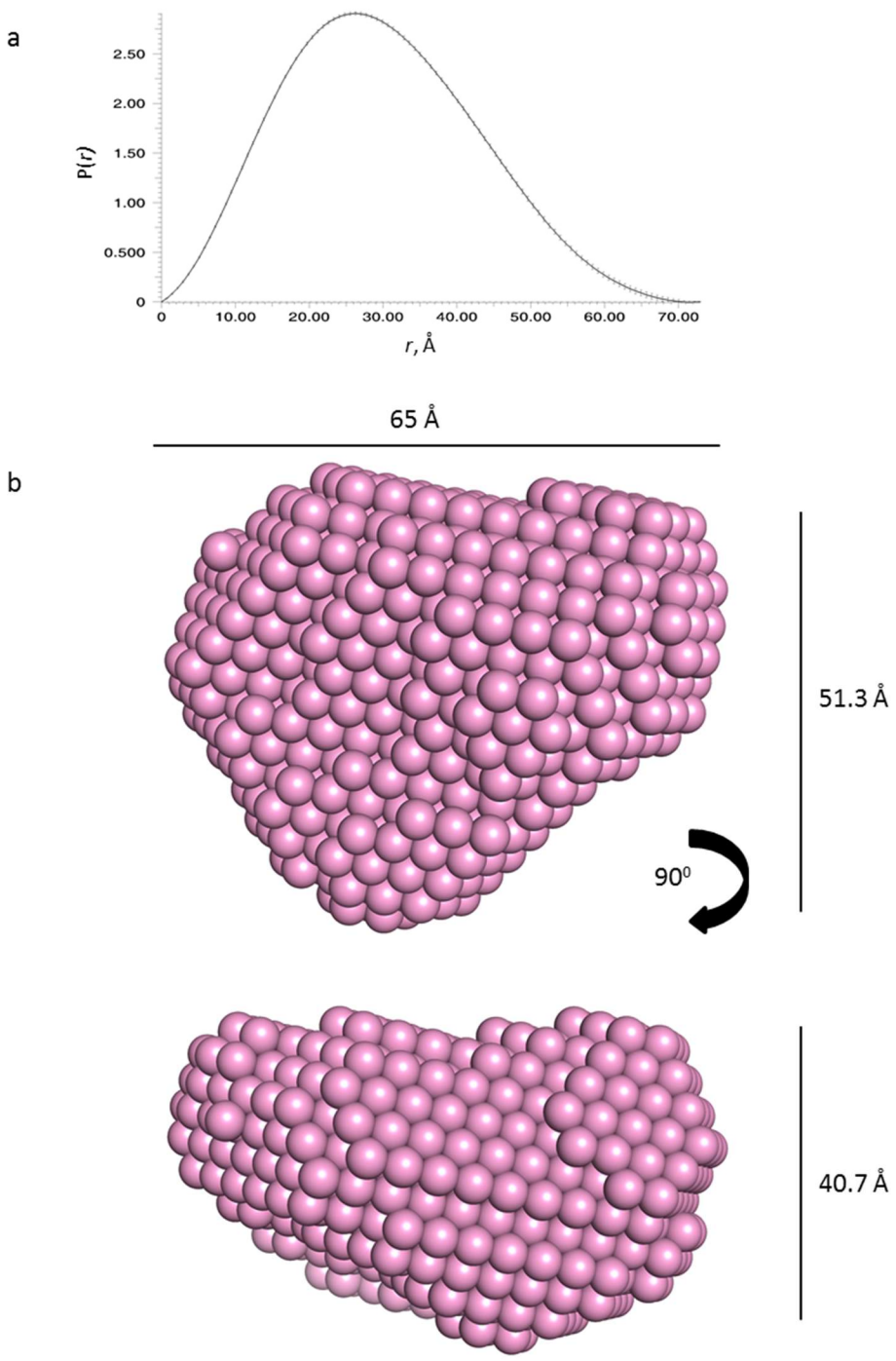

Figure 3-18 P*(r)* distribution of pectocin P in solution suggests it is globular in solution. a) Pair-set p*(r)* disribution of pectocin P shows gives a maximum dimension of 73 Å b) DAMMIF model of pectocin P created from the p*(r)* distribution showing the two dimensional measurements of the envelope.

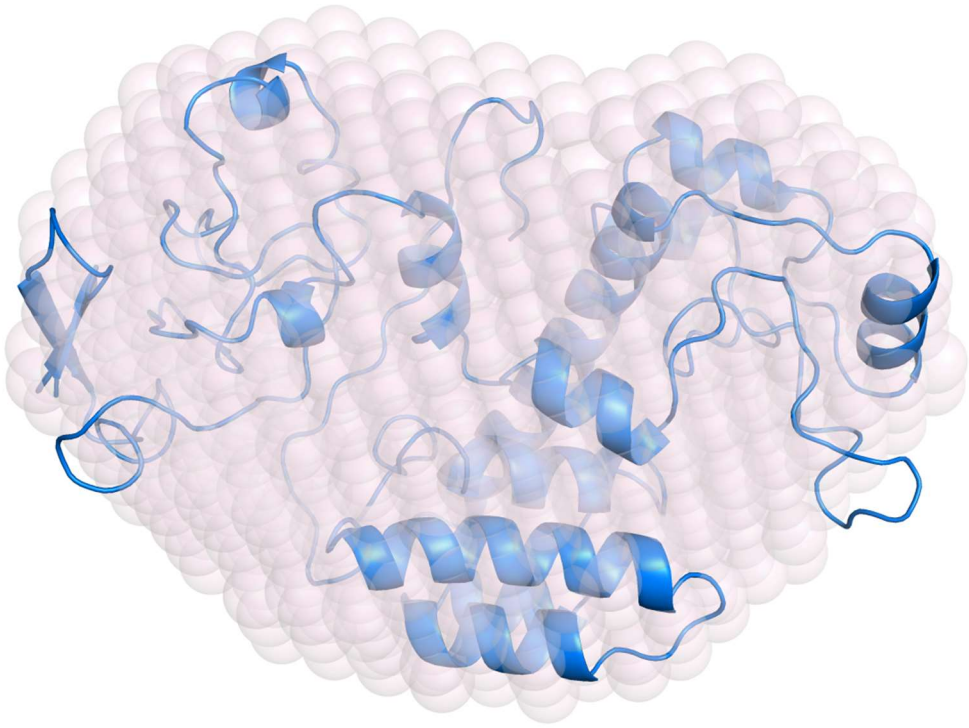

Figure 3-19 Dummy atom model (DAMMIF) of pectocin P overlaid with I-TASSER predicted model of pectocin P. Pectocin P dummy atom model (pink) based on SAXS data overlaid with I-TASSER predicted model (blue) suggests that pectocin P is compact and globular in solution which is consistent with the I-TASSER model. Overlay was performed using SUPCOMB [158].

It can be see that the predicted globular structure of pectocin P fits with the predicted envelope of the protein suggesting that the I-TASSER model is a good structural prediction for pectocin P (Figure 3-19). However, this does not support the hypothesis that pectocin P exists in multiple conformations in solution as the averaged dummy atom models clearly correspond to only one conformation.

3.2.8.4 Pectocin P must exist in an unfolded conformation in solution in order to utilise the FusA receptor

As shown in Figure 3-12, the uptake of pectocin P is dependent on the presence of the FusA outer membrane receptor. However, by examining the SAXS

structure of pectocin P and the predicted structure dimensions it is clear that these dimensions would not be able to pass through the lumen of the FusA barrel. The lumen of FusA is 35 Å in diameter and therefore any protein passing must have a diameter smaller than this. At the widest point of the cytotoxic domain pectocin P is approximately 50 Å in the conformation consistent with the SAXS data.

Therefore, computational modelling of pectocin P was performed to examine whether a possible elongated conformation is consistent with the SAXS data. The only solution which would explain the passing of pectocin P through the lumen of the FusA barrel is a highly elongated conformation resembling that of the elongated forms of pectocin M1 and M2. This would provide the right dimensions to enter the cell whereas all other solutions could not explain this. Pectocin P was separated into 3 domains and an ensemble of conformations modelled using EOM (as described in 3.2.5)

Primarily an elongated model of pectocin P was created with EOM and the fit of the globular, elongated and combined models were compared with the experimental SAXS curve using CRYSOL. It can be seen from the data that the best overall fit of the data (X^2= 0.178) is the combination of conformations (Figure 3-20c). However, this is very similar to the fit of the globular conformation alone (X^2=0.179), suggesting that the majority of proteins within the sample are likely to be in a globular conformation (Figure 3-20a). Contrastingly, an elongated conformation of pectocin P does not fit the data with a (X^2= 0.248) suggesting that this is the least likely conformation in solution (Figure 3-20b).

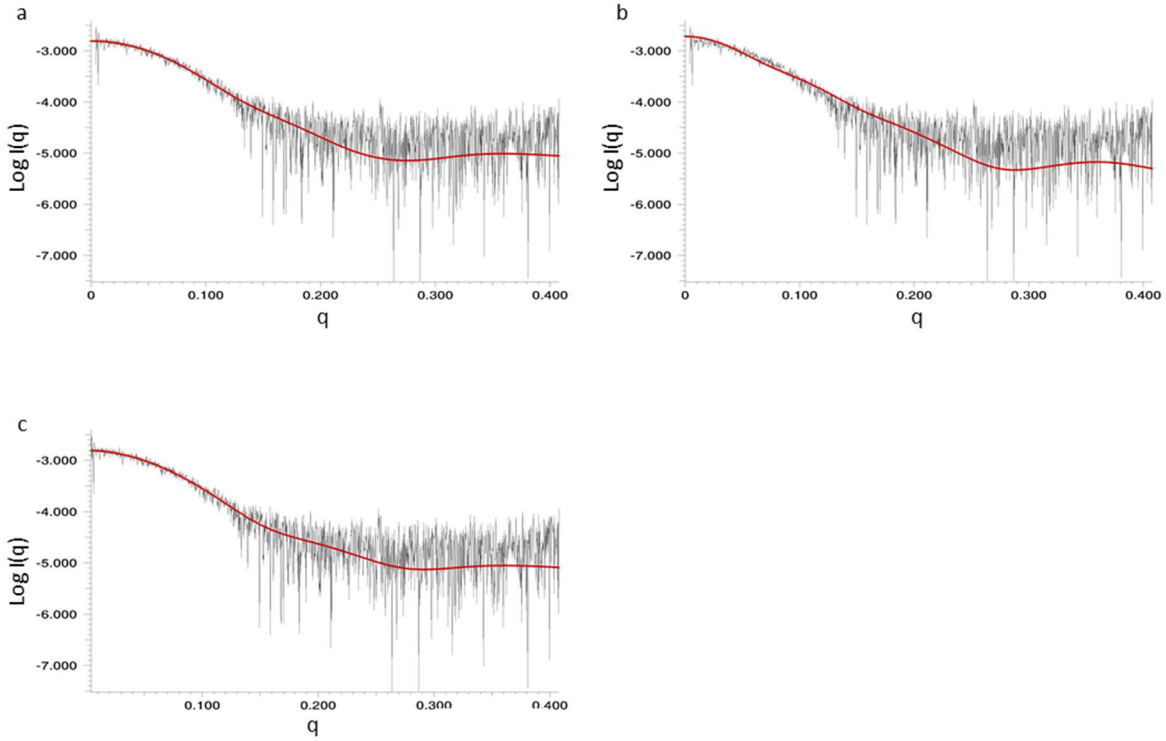

Figure 3-20 Theoretical SAXS curves created by CRYSOL comparing pectocin P in multiple conformations to experimental SAXS data. Theoretical SAXS curves generated by CRYSOL (red) overlain with the experimental SAXS data for pectocin P (black) for a) globular (X^2= 0.179), b) elongated (X^2= 0.248) and c) EOM modelling of a mixed population (X^2= 0.178)

The population used to create the EOM fit to the SAXS data was modelled and the selected population further examined. The maximum dimensions of the pool of models created ranged from 59-111 Å however the range of models selected to fit the SAXS data was less clear cut than pectocin M1. The models can be grouped into two populations with the first having the highest peak at a D_{max} of 67 Å, which is consistent with the SAXS experimental data. However, there is also a small population of models with a D_{max} of approximately 105 Å, which corresponds to an elongated model of pectocin P that is predicted to be necessary for uptake (Figure 3-21a). These results are further confirmed when the R_g is examined (Figure 3-21b) showing a peak around 21.7 Å, similar to the experimental R_g of 22.7 Å and a second peak at 30.2 Å, suggestive of an elongated conformation.

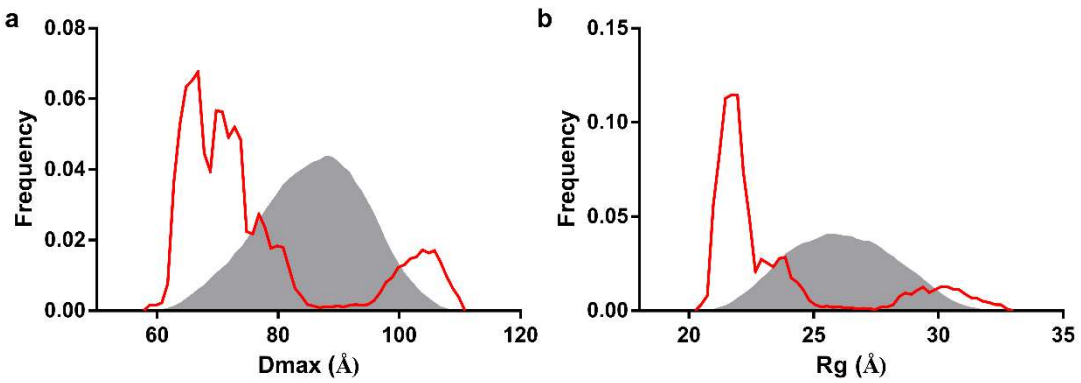

Figure 3-21 Ensemble optimisation modelling of pectocin P based on SAXS data shows that pectocin P is found in multiple conformations in solution. EOM predictions of a) D_{max} and b) R_g suggest that pectocin P is found in multiple conformations in solution. The pool of models is shown in grey with the population frequency shown in red.

As the EOM modelling of pectocin P suggests a small population of proteins in an elongated conformation the dimensions of this elongated model were assessed to confirm if it would be small enough to enter *P. atrosepticum* cells through the FusA barrel. While the dimensions of the globular model (Figure 3-22) are greater than the lumen of the FusA barrel, in an elongated conformation the dimensions modelled show that the rotation of the cytotoxic domain around the flexible linker region gives a dimension of 28.4 Å which is smaller than the FusA barrel and therefore would allow uptake.

Pectocin P, like pectocin M1, must elongate in order to have dimensions compatible with FusA uptake. Through the use of SAXS and EOM it has been shown that an elongated conformation of pectocin P is consistent with the in solution data, and in turn the predicted elongated model is consistent with the dimensions needed to pass through the FusA lumen. This work goes some way to confirming the predicted structure models of pectocin P, however the solving of a high-resolution crystal structure would be beneficial. Unfortunately to date attempts at this have been unsuccessful.

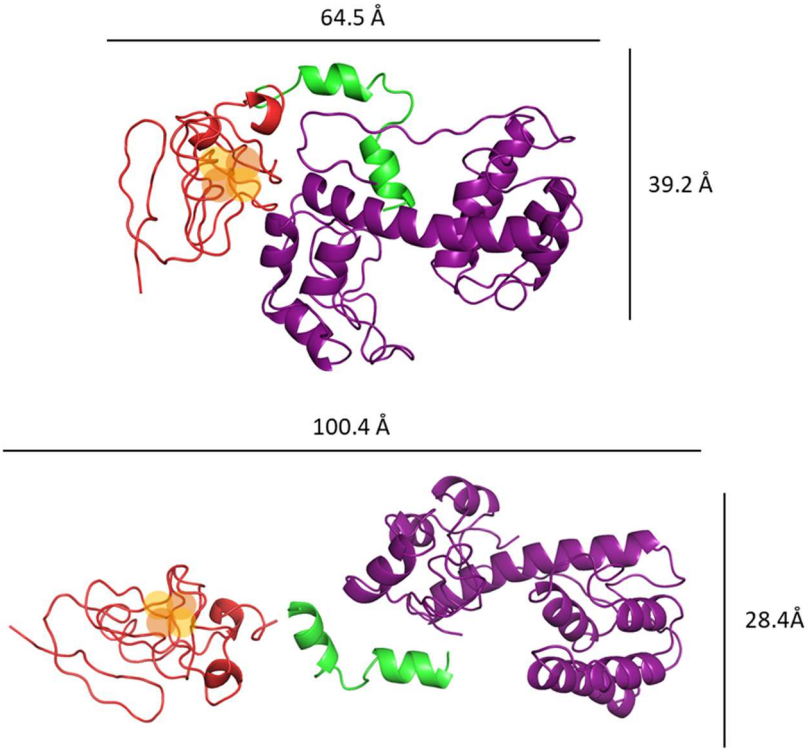

Figure 3-22 Models created by EOM showing the predicted conformations of pectocin P in both a globular and elongated form. Models of pectocin P were created showing it in both a globular and elongated conformation with the N-terminal ferredoxin domain shown in red, flexible linker in green and cytotoxic domain shown in purple. The predicted position of the iron-sulphur cluster is shown in orange.

3.3 Discussion

All three pectocins have been shown to parasitise the FusA receptor in *P. atrosepticum* to enter the target cell. The proteins are composed of an N-terminal ferredoxin domain and a C-terminal cytotoxic domain joined by a flexible linker region. Previous work has shown that the cytotoxic domain of pectocin M2 can rotate around the N-terminal domain due to the presence of this flexible linker and that this leads to multiple conformations in solution [123]. It was therefore predicted that all pectocins would act this way.

This work has shown that both pectocin M1 and pectocin P are flexible monomeric proteins which are active against *P. atrosepticum* LMG2386. Both of these pectocins are dependent on the FusA outer membrane receptor for uptake into the cell and therefore must be found in an elongated conformation in order to pass through the lumen of the barrel. SAXS data confirmed that both

pectocins are indeed found in multiple conformations in solution. Scattering data suggests that pectocin M1 is found in both an elongated and bent conformation in solution. For pectocin P, only a small population of the SAXS data could be accounted for by an elongated conformation. As pectocin P is much less readily found in an elongated conformation it may be that an interaction with another protein promotes this conformation or that this elongated conformation is disadvantageous or requires more energy to maintain.

The flexibility of pectocin M1 is unusual when compared with other M-type bacteriocins, for example it has been shown before that pyocin M is rigid in structure and shows little flexibility [123]. This work, similarly to previous work, has shown that pectocins, particularly M-type pectocins are highly flexible in nature [123]. Unlike other M-type bacteriocins pectocins possess a flexible inter-domain linker region around which the domains can move [123]. This region is necessary for the flexibility of the pectocins and for the conformational changes needed for uptake.

Ferredoxin-containing pectocins are unique amongst the bacteriocins of Gram-negative bacteria as, to date, they are the only known bacteriocins which have acquired a host-protein homologue to translocate into the cell. It has been shown previously that bacteriocin translocation is dependent on the presence of an IUTD and its subsequent interaction with the Tol or TonB system [40,159]. Contrastingly, pectocins use the presence of the N –terminal ferredoxin domain to interact with the outer membrane receptor and enter the cell. Although pectocins are a novel group of bacteriocins they are not unique to *Pectobacterium* species. Alignment searches have shown that ferredoxin-containing bacteriocins with similar M-type cytotoxic domains can also be found in other related species such as *Brenneria goodwinii* and *Dickeya chrysanthemi*. Future work to characterise these related proteins and their uptake systems may suggest a conserved route of entry into plant pathogenic bacteria that could be a potential antibiotic target.

Chapter 4 The role of the *fus* operon in the uptake of ferredoxin-containing pectocins and virulence

Disclaimer: Initial *pfusA* mutagenesis PCRs for AAs 151-380 were performed by Dr Khedidja Mosbahi, C38A mutation was created by Rhys Grinter and SEC-MALS experiments and analysis were performed by June Southall at the University of Glasgow protein facility.

4.1 Introduction

The first line of defence for Gram-negative bacteria is the presence of an outer membrane surrounding the cell. Membrane proteins are crucial for the uptake of solutes and proteins, as well as signal transduction [160]. One family of outer membrane transporters are the TonB-dependent outer membrane receptors characterised by their conserved N-terminal plug domain and C-terminal barrel formed of 22 antiparallel ß-strands [161]. TonB-dependent receptors import a wide variety of nutrients, ranging from small vitamins to carbohydrates [76,162,163]. A number of TonB-dependent receptors are necessary for the uptake of siderophores, such as ferric pyoverdine produced by *Pseudomonas aeruginosa* and taken up by the TonB-dependent FpvAI [164].

TonB-dependent receptors are required for the uptake of many bacteriocins as well as their natural substrates [50]. Bacteriocin translocation begins with the interaction of the receptor binding domain to an outer membrane receptor, such as BtuB [40]. A well understood mechanism of translocation is that of pyocin S2 which is known to parasitise the *Pseudomonas aeruginosa* FpvAI receptor in order to enter the cell [63]. The receptor binding domain of pyocin S2 interacts with the extracellular loops of FpvAI mimicking the substrate, and inducing a conformational change in the N-terminal plug domain [63]. This conformational change induces the extension of the TonB-box, interaction with TonB in the periplasm and subsequent partial unfolding of the N-terminal plug domain [63]. The rearrangement of the plug domain allows for the intrinsically unstructured translocation domain (IUTD) of pyocin S2 to pass through the lumen of FpvAI to interact with a second copy of TonB and its subsequent translocation into the periplasm [63] (diagram of uptake shown in Figure 1-3) .

A newly discovered member of this family of ß-barrel receptors is FusA which is responsible for the uptake of plant-type ferredoxins into the periplasm of *Pectobacterium* cells (Figure 4-1a) [124]. This protein is encoded on an operon containing three other proteins (FusB, FusC and FusD) thought to be essential in the uptake of ferredoxins [124] (Figure 4-1). This operon can be found in several other plant pathogenic species including *Dickeya* species. As well as this, similar proteins can also be found in many other Gram-negative bacteria including

prolific mammalian pathogens such as *Yersinia* spp. and *Escherichia coli* (Figure 4-1) [124].

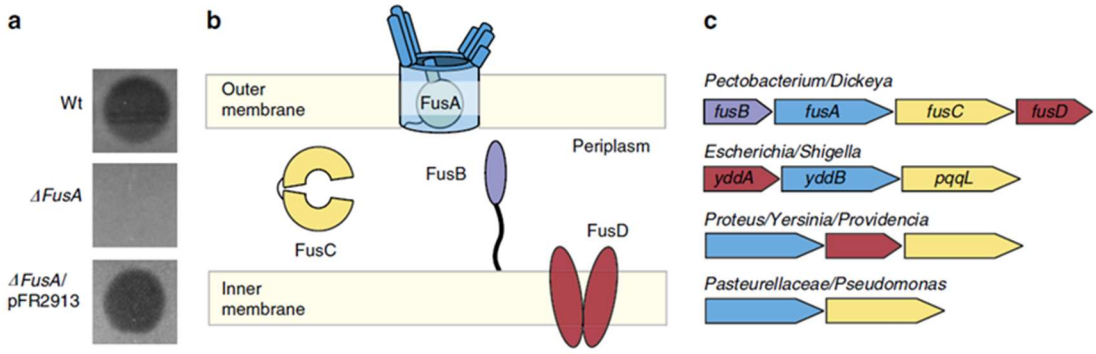

Figure 4-1 FusA is essential for pectocin M1 uptake and is part of the *fus* operon in *Pectobacterium spp.* a) Spot test showing that FusA is essential for pectocin M1 uptake in *Pectobacterium atrosepticum* LMG2386 under iron limiting conditions. b) Schematic diagram of the predicted cellular locations of the proteins encoded by the *fus* operon. c) Cartoon representation of the genetic organisation of the *fus* operon in *Pectobacterium* species and homologous genes from a subset of human pathogenic bacteria. Reproduced from [124] under a creative commons licence.

FusA is an essential part of the uptake system for both ferredoxins and ferredoxin-containing bacteriocins which have acquired the N-terminal ferredoxin domain in order to parasitise this receptor [124]. This parasitisation of an outer membrane receptor is not unusual in bacteriocin uptake, colicins routinely parasitise existing outer membrane proteins to enter the target cell [51]. The structure of FusA from *Pectobacterium atrosepticum* SCRI1043 has been solved previously (Figure 4-2) and the potential interaction sites between pectocin M1 and FusA examined by NMR spectroscopy [124].

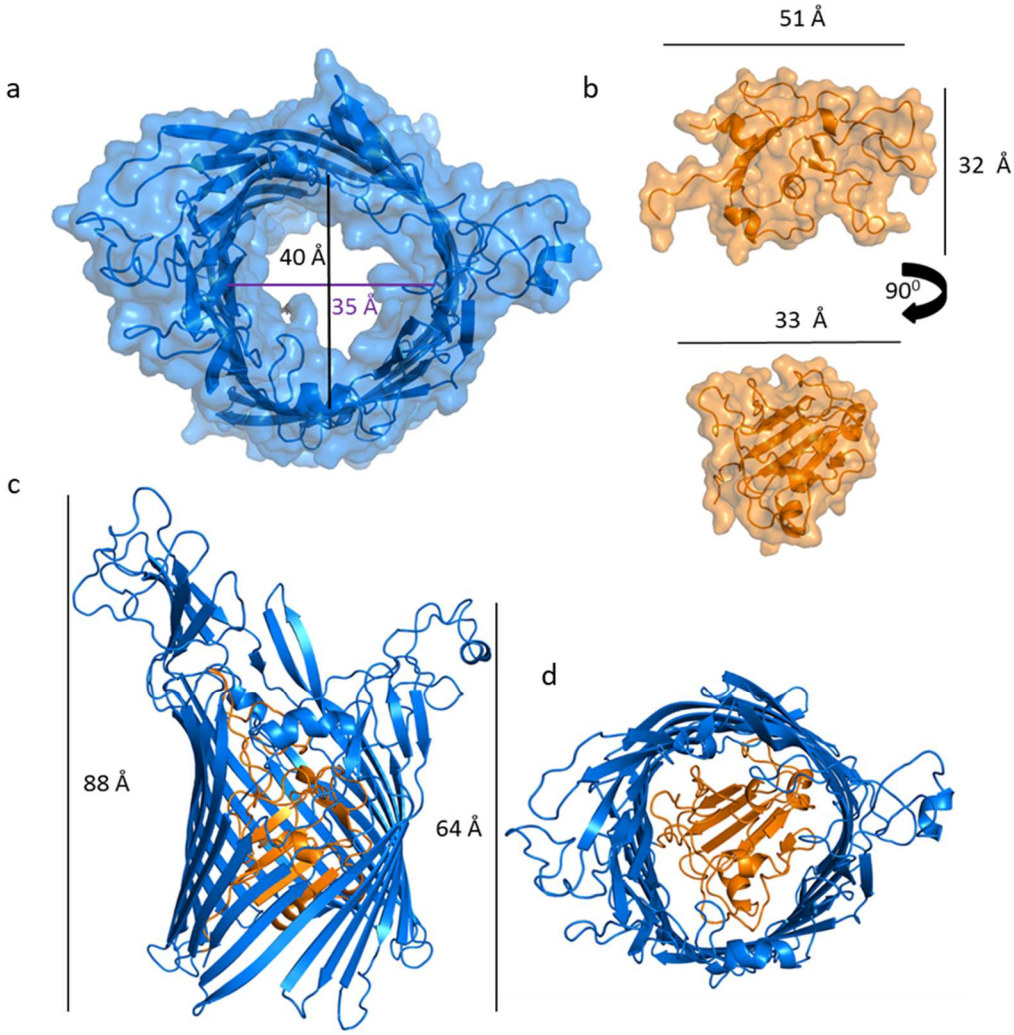

Figure 4-2 $FusA_{1043}$ crystal structure showing the dimensions of the plug domain (orange) and the lumen of the barrel (blue) (PDB ID 4ZGB). a) Top view of the C-terminal barrel domain of $FusA_{1043}$ showing both cartoon represenations of the secondary structure as well as the surface view. The dimensions of the internal of the barrel are shown. b) N-terminal plug domain of $FusA_{1043}$ showing two-dimensional maximum measurements. c) Cartoon representation of $FusA_{1043}$ with the two-dimensional maximum measurements of the protein showing the discrepancy in length due to the larger extracellular loops. d) Top view of $FusA_{1043}$ showing the plug domain occluding the barrel.

The first protein encoded on the *fus* operon is a TonB homologue, referred to as FusB, which is presumed to be located in the periplasm. TonB is a periplasmic protein which is known to interact with the TonB-box of TonB-dependent receptors in the periplasm [69,165]. As *Pectobacterium* spp. genomes encode copies of TonB it is not known whether FusB will interact with FusA or whether it has evolved to interact with the ferredoxin or ferredoxin-containing bacteriocin to aid with translocation.

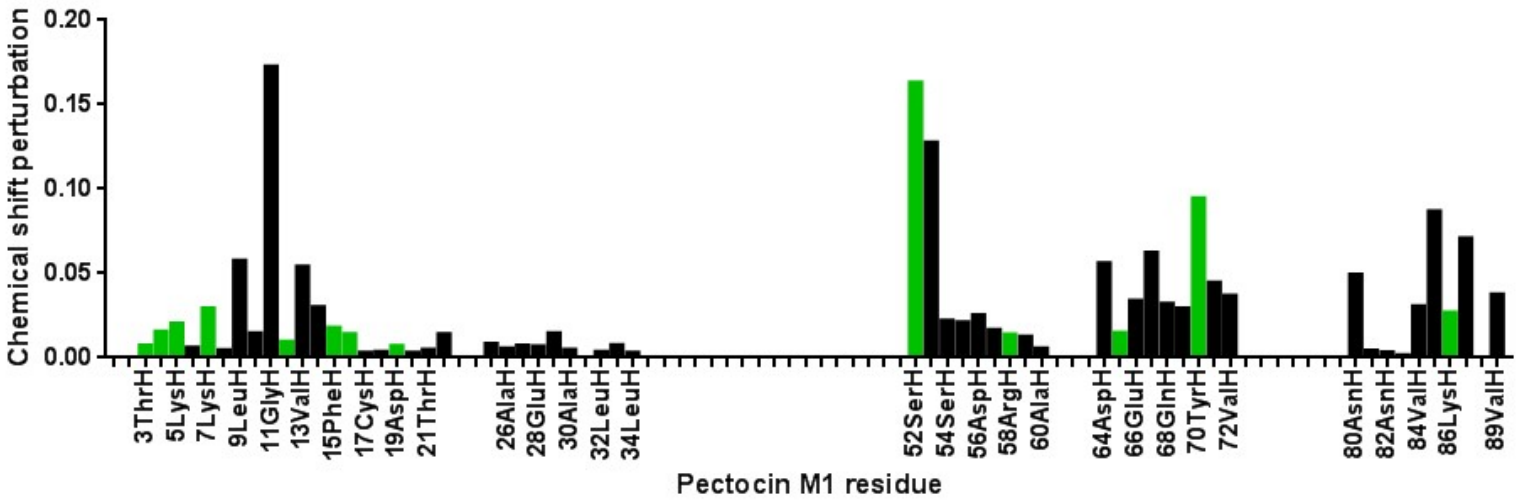

Figure 4-3 Graphical representation of the chemical peak shifts from the ferredoxin region of pectocin M1 with the addition of FusA. Chemical shift perturbations were measured with the addition of FusA at a 1:1 molar ratio. Residues highlighted in green are those selected for alanine screening. Adapted from Grinter et al (2016) and reproduced here under a creative commons licence.

It has been shown that the uptake of pectocin M1 and plant-type ferredoxins is dependent on the presence of FusA in the outer membrane [124]. Previous work performed by Grinter et al. (2016) examined the interaction of the N-terminal domain of pectocin M1 with FusA from *P. atrosepticum* SCRI1043 ($FusA_{1043}$) using NMR spectroscopy to determine a potential site of interaction. The HSQC spectra of ^{15}N labelled pectocin M1 chemical shifts were measured and the chemical shift perturbation for each residue shown in Figure 4-3 [124]. It can be seen in the graphical representation that there are five regions which show chemical changes during interaction, with all showing notable chemical shifts over 0.02 p.p.m in all of these sites, with the exception of residues 25-34. HADDOCK modelling based on the NMR data suggested an interaction between the N-terminal domain of pectocin M1 with the extracellular loops of FusA (Figure 4-4) [124].

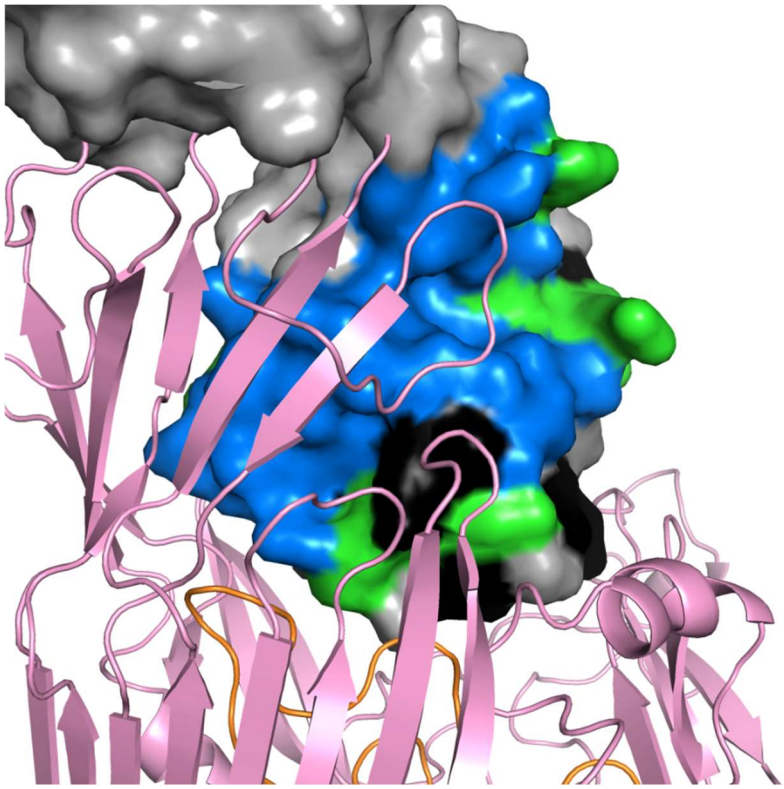

Figure 4-4 HADDOCK modelling of N-terminal of pectocin M1 with FusA suggests both a continuous biding site and the interaction with the extracellular loops of FusA NMR data suggests the presence of a continuous binding site. Residues showing a CSP of >0.02 p.p.m. shown in blue, 0.01-0.02 p.p.m shown in green and <0.01 p.p.m shown in black.

The aim of this chapter is to examine the interaction of pectocin M1 with proteins encoded on the *fus* operon in *P. atrosepticum* and subsequent uptake. This chapter primarily aims to determine how pectocin M1 and FusA interact *in vivo* and confirm the interaction sites of both proteins. Secondly pectocin M1 is a large folded protein with no IUTD, therefore this chapter aims to understand the mechanism by which pectocin M1 translocates into the periplasm. Finally, pectocins have the potential to be used as novel therapeutics within the field, therefore the final aim is to elucidate under what conditions they may be used in novel anti-infective strategies using both chimeric proteins and plant infection models.

4.2 Results

4.2.1 Interaction sites between pectocin M1 and FusA

4.2.1.1 Pectocin M1 binding site

NMR spectroscopy data suggests five potential groups of residues that may be important in receptor binding. In order to assess this, large or charged surface residues from four of these groups were chosen as candidates for site-directed mutagenesis (SDM). The residues chosen were: T3, Y4, K5, K7, N12, F15, E16, D19, C38, S52, R58, E65, Y70, and K86. Individual residues (highlighted in Figure 4-3) were mutated by PCR on the expression plasmid and purified using both nickel and size exclusion chromatography. Wild-type (WT) pectocin M1 and pectocin M1 mutants were tested against *P. atrosepticum* LMG2386 in order to examine their activity and minimum inhibitory concentrations. Preliminary experiments suggested that Y4 and K5 may be important residues for receptor interaction and therefore a double mutant was also created to see whether changing both of these would have a more drastic effect on activity loss. The lysine residue in this mutation was changed to a glutamic acid in order to reverse the charge in the residue position to increase the potential disruption of the binding site.

The mutation at position C38 is used in this instance as a negative control. The alteration of this residue to an alanine disrupts the binding of the iron-sulphur

cluster and prevents correct folding of the protein. This mutant is therefore unable to interact with and be taken up by FusA (Appendix 3).

Several different concentrations of the mutants were tested, and a representative image is shown in (Figure 4-5) in which the mutants were spotted on in 3-fold dilutions with a starting concentration of 1 μM. There is a reduction in activity on the mutation of T3, K5, K7, F15, and K86 to alanine, with mutations at K86 and F15 showing the greatest decreases in activity when mutated to alanine.

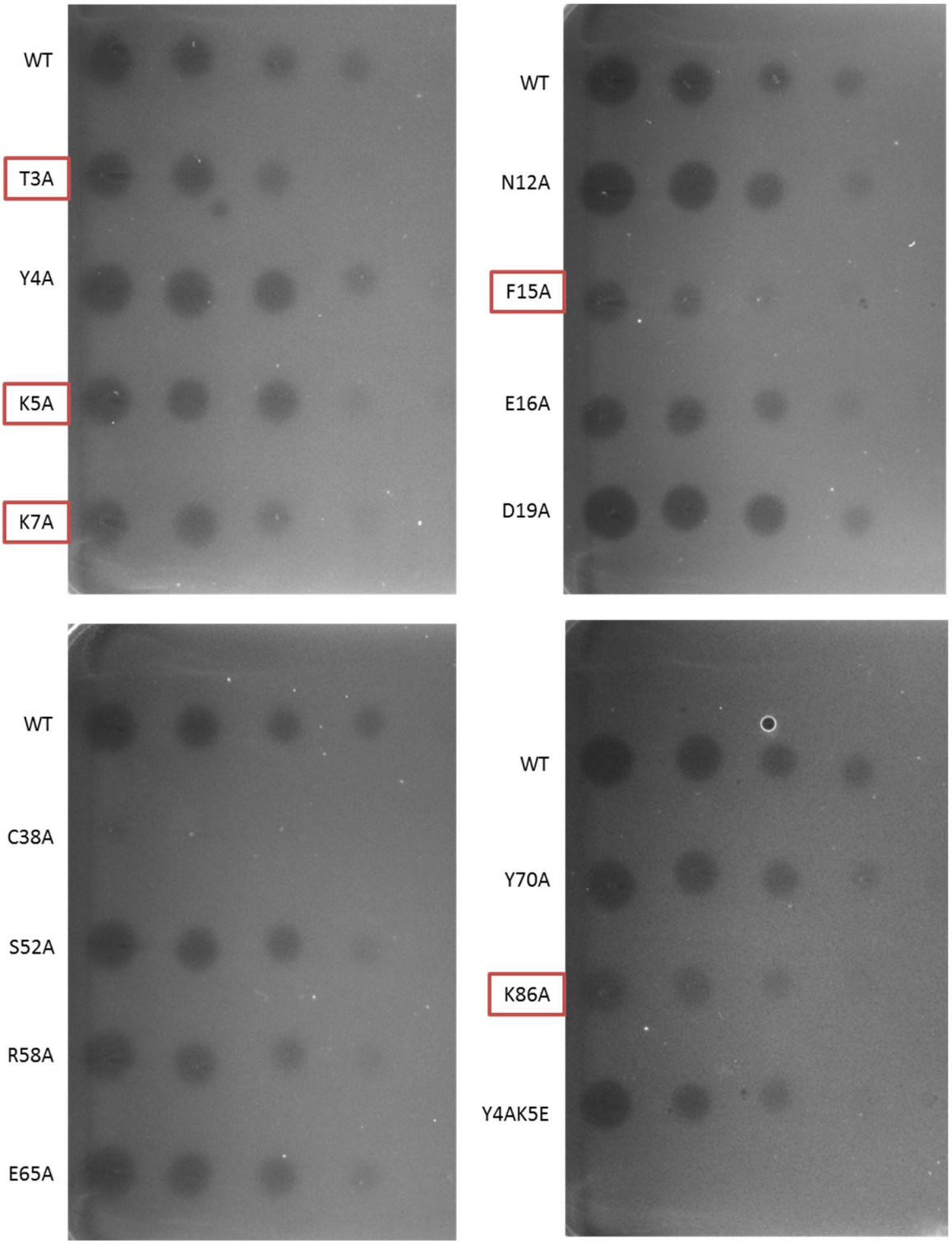

Figure 4-5 Spot tests comparing the potency of pectocin M1 mutants against *P. atrosepticum* LMG2386 under iron limiting conditions. Pectocin M1 and mutants were spotted onto an overlay of *P. atrosepticum* LMG2386 in 3-fold dilutions from a starting concentration of 1 μM (from left to right) to compare the minimum inhibitory concentration as compared with the wild-type of each mutant under iron limiting conditions. Residues showing a reduction in activity are highlighted.

A small reduction in minimum inhibitory concentration was seen for all mutants, with the exception of D19A and Y4A which were both active to the same concentration as the wild-type (representative image shown in Figure 4-5). Although the reduction in activity was small for each mutation it does suggest that these residues may be important for the interaction of pectocin M1 with FusA. Each of the mutated residues are either charged or large which further suggests that they may be important for binding as well as giving support to the NMR spectroscopy data which also suggested the presence of a continuous charged binding site (Figure 4-6) [124].

As, ideally all surface residues would be interesting to test, low fidelity PCR mutagenesis was performed to create random mutations within the ferredoxin region of pectocin M1, however this was unsuccessful. Future work could focus on creating multiple combinations of mutations to compare the potency of double amino acid substitutions to examine the effect this would have on binding affinity and potency.

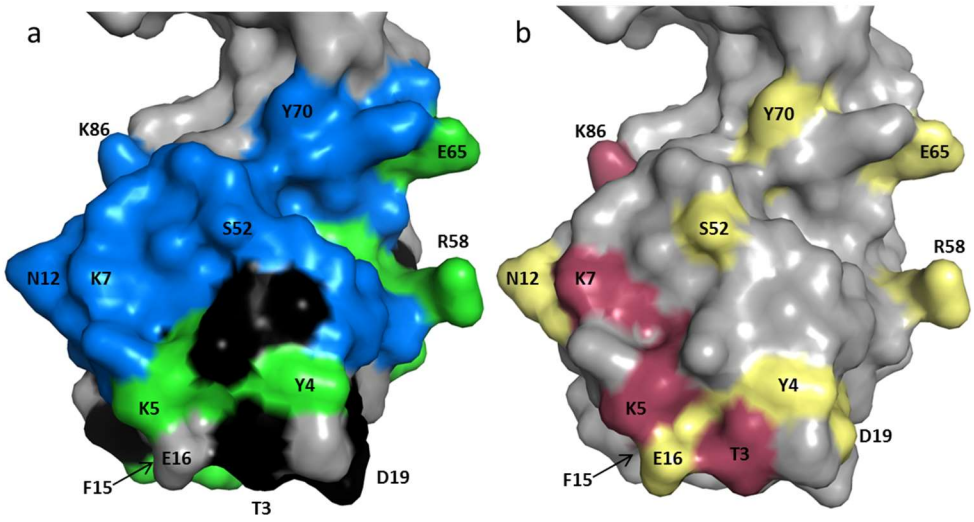

Figure 4-6 Surface representation of the predicted N-terminal domain of pectocin M1 showing the predicted binding sites. a) Surface of the N-terminal domain of pectocin M1 showing the residues predicted to be important for FusA interaction due to the CSP shifts determined using NMR and reproduced from Grinter et al 2016 under a creative commons licence. Residues showing a CSP change of >0.02 p.p.m. are shown in blue, 0.01-0.02 p.p.m. are shown in green and those with a CSP <0.01 p.p.m. are shown in black. b) Surface of the N-terminal domain highlighting residues chosen for SDM with those showing a decrease in potency shown in red and those residues thought to unimportant for the FusA-pectocin M1 interaction shown in yellow. A full view of this is shown in appendix 2.

When examined on the model of pectocin M1 the amino acids suggest a binding surface on the opposite face of the N-terminal domain to the iron-sulphur cluster (Figure 4-6). The SDM conducted in this study has shown that, with the exception of the phenylalanine in position 15, the residues that are involved in receptor binding are charged (lysine) and polar (threonine) in agreement with the NMR data suggesting a continuous binding surface consisting of these charged and polar residues. However, the SDM also suggests potential interaction sites outwith this predicted continuous binding site, such as the threonine in position 3. When these residues are examined, in relation to the interaction model, an interaction between pectocin M1 and the long extracellular arm of FusA and a potential interaction with the N-terminal plug domain is predicted (Figure 4-2).

4.2.1.2 CD spectra analysis of mutants

Pectocin M1 mutants were analysed by far and near UV circular dichroism (CD) in order to compare the secondary and tertiary structures respectively to determine whether it was likely that the reduction in activity was due to the individual mutations or incorrect folding of the protein. Those mutants which showed a reduction in activity and two that show little to no change in activity were measured.

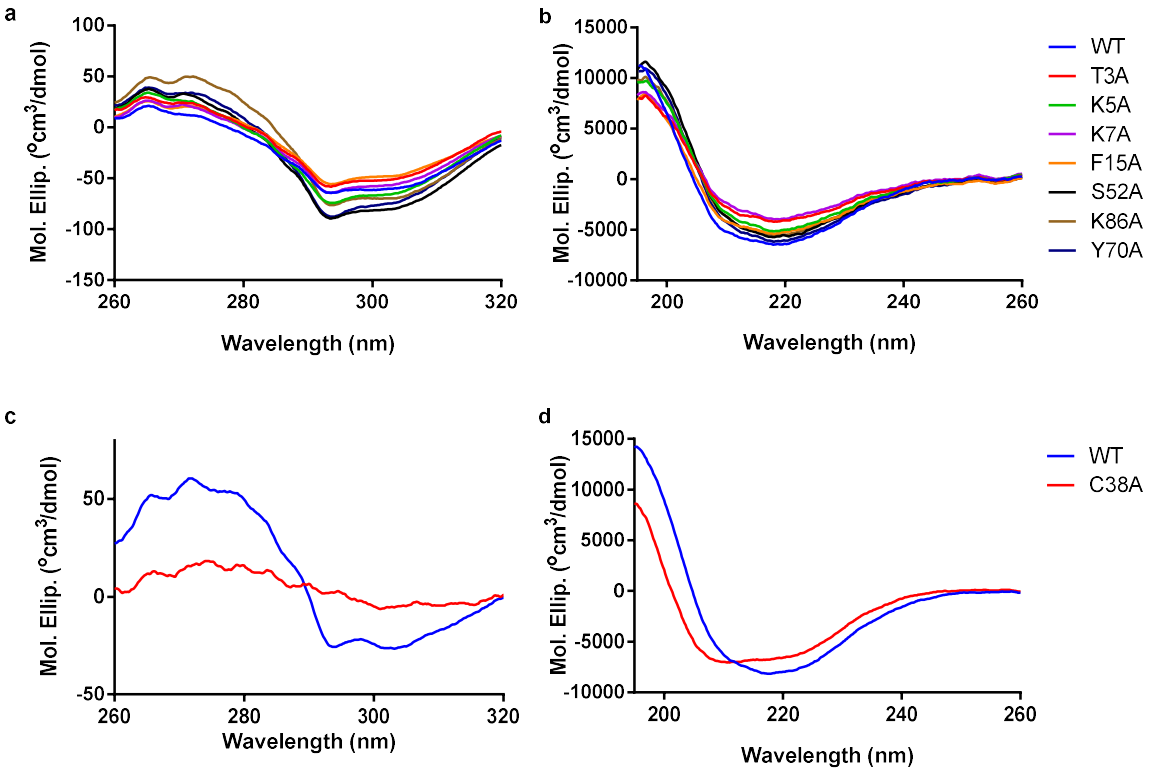

Figure 4-7: Far and near UV spectra of pectocin M1 and single amino acid mutants. Pectocin M1 (blue) has the same spectra in both the far and near UV spectra as T3A (red), K5A (green), K7A (purple), F15A (orange), S52A (black) Y70A (dark blue) and K86A (brown) shown at near (a) and far (b) UV. The CD spectra of pectocin M1 (blue) was compared with that of C38A (red) showing the discrepancy in both near (c) and far (d) spectra suggesting incorrect folding of the protein due to the lack of the iron-sulphur cluster.

The CD spectra of each mutant tested had a similar spectrum to that of the WT and therefore it is likely that reduction in activity is due to the individual mutation rather than protein misfolding (Figure 4-7). It can be seen that the spectra for C38A (Figure 4-7c and d) suggests protein misfolding compared with the WT. This amino acid is essential for the co-ordination of the iron-sulphur cluster and therefore the iron-sulphur cluster is not present in this mutant (appendix 3).

4.2.1.3 Binding site mutagenesis FusA

As docking modelling of pectocin M1 and FusA suggested an interaction between pectocin M1 and the extracellular loops of the FusA receptor, and potentially the

N-terminal plug domain these sites were selected as candidates for SDM screening. Mutations were created using SDM on the inducible p*fusA*$_{2386}$ plasmid and confirmed by sequencing. The subsequent p*fusA*$_{2386}$ plasmids were expressed in the Δ*fusA* cells under a lactose inducible promoter and the susceptibility of complimented strains to pectocin M1 was tested using spot test assays.

The residues chosen for SDM were based on their relative location within the FusA$_{1043}$ crystal structure and, like pectocin M1, based on their size and charge. Nine initial residues were chosen to be mutated: N151, Y155, P157, F376, S378, F380, N401, G489 and N491. All residues were mutated to an alanine residue, with the exception of P157 which was mutated to a glycine residue in order to minimise the effect on the secondary structure. The positioning of each of these residues can be seen in Figure 4-8, residues F376-F380, N401A, G489A and N491A are positioned on the larger of the two extracellular domains of FusA whereas N151-P157 are positioned on the plug domain of FusA.

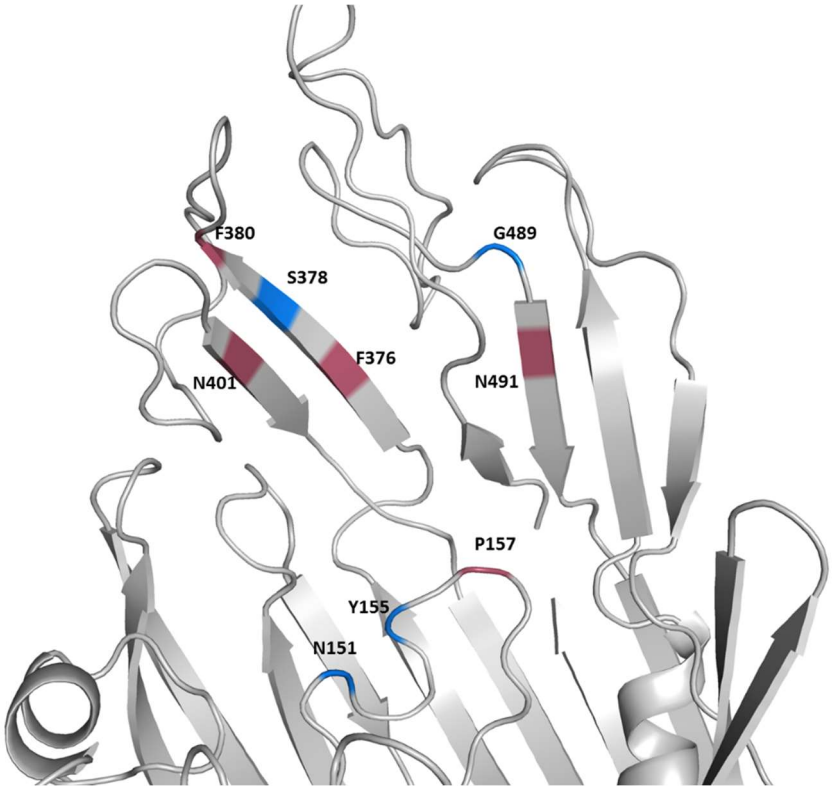

Figure 4-8 Predicted structure of FusA$_{2386}$ highlighting the residues chosen for mutagenesis. Residues chosen for mutagenesis are coloured, with those in red showing an increase in the MIC of pectocin M1 (red) and those showing little or no increase shown in blue.

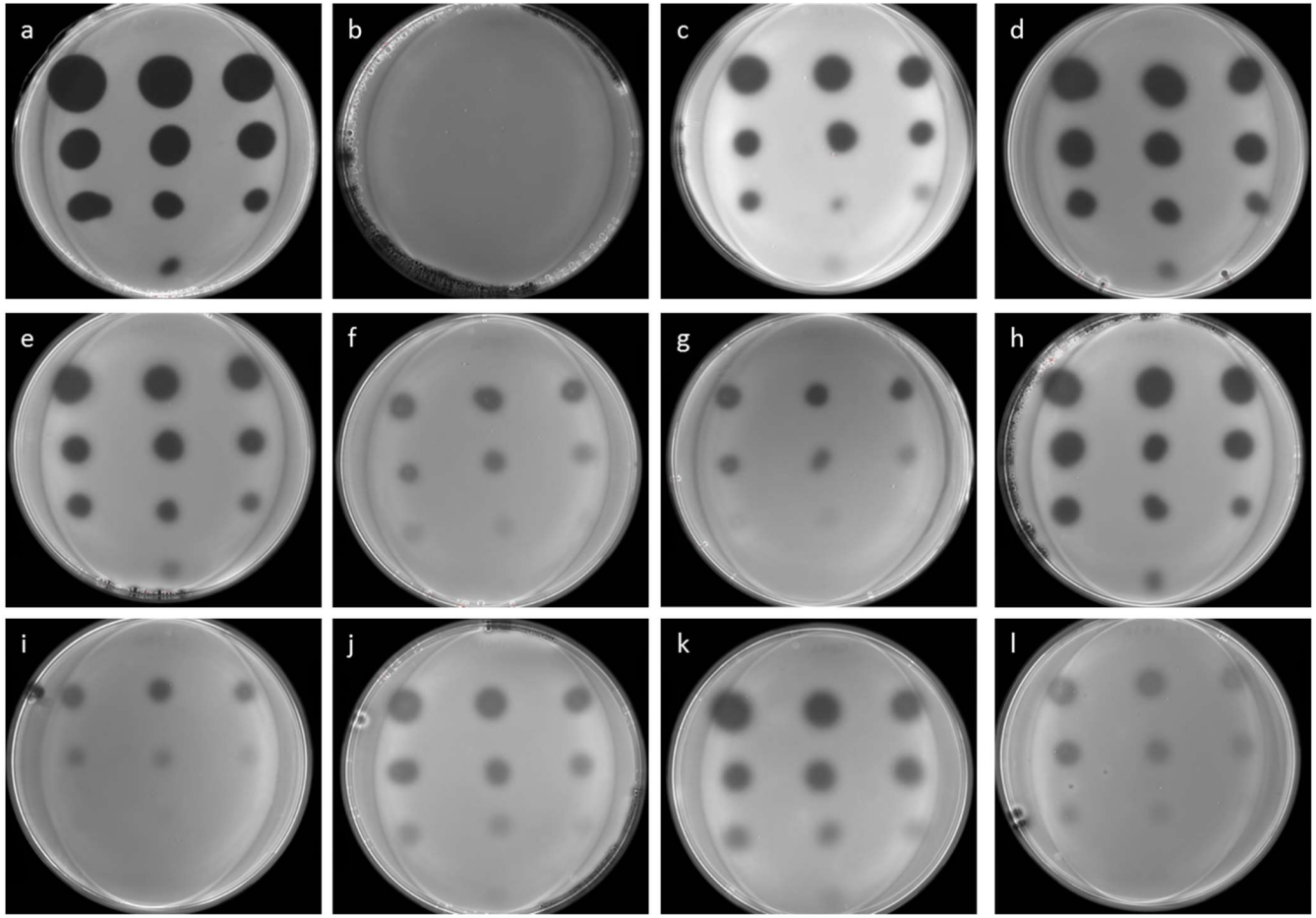

Figure 4-9 Pectocin M1 potency was tested against the FusA mutants expressed in *P. atrosepticum* LMG2386 Δ*fusA*. Pectocin M1 at 340 μM 3-fold decreasing concentrations was spotted onto LB agar supplemented with 2% w/v D-lactose, 200 μM bipyridine, (100 μg ml^{-1} ampicillin for complimented strains). Pectocin M1 was tested against a) WT *P. atrosepticum* LMG2386, b) Δ*fusA* c) Δ*fusA*/p*fusA* d) Δ*fusA*/p*fusA*$_{N151A}$ e) Δ*fusA*/p*fusA*$_{Y155A}$ f) Δ*fusA*/p*fusA*$_{P157G}$ g) Δ*fusA*/p*fusA*$_{F376A}$ h) Δ*fusA*/p*fusA*$_{S378A}$ i) Δ*fusA*/p*fusA*$_{F380A}$ j) Δ*fusA*/p*fusA*$_{N401A}$ k) Δ*fusA*/p*fusA*$_{G489A}$ l) Δ*fusA*/p*fusA*$_{N491A}$

The complementation of *fusA* using an inducible plasmid restores the uptake of pectocin M1 (Figure 4-8c*),* however this complemented strain is not as susceptible to pectocin M1 as the WT. It can also be seen that each of the mutants is susceptible to pectocin M1, however there is a reduction in the potency of pectocin M1 for mutations both in the long extracellular domains and a residue positioned on the N-terminal plug domain (P157G, Figure 4-9f). The reduction in binding can be seen with mutations F376A and F380A in particular (Figure 4-9g and I respectively), with a small reduction in potency seen for N401A and N491A (Figure 4-9j and l respectively). The reduction of activity is indicative that these loops are important for substrate interaction. This supports the current model of substrate interaction and uptake, however as the expression levels may vary between each of the strains this may also cause variation. Therefore, although it is indicative more work is needed to quantify the expression levels to determine if this reduction in activity is indeed due to the mutation.

To further examine the interaction between pectocin M1 and FusA *in vitro* analytical size exclusion chromatography (SEC) was used. Pectocin M1 was incubated with an equal concentration of either $FusA_{1043}$ or the $FusA_{1043}$ plug domain alone in order to examine if a complex could form *in vitro*. Analytical SEC showed the presence of a high molecular weight species when pectocin M1 and FusA were mixed together (Figure 4-10a). This confirms the interaction between FusA and pectocin M1 *in vitro*, giving support to the *in vivo* data.

The plug domain of $FusA_{1043}$ and pectocin M1 were mixed together in order to determine if there was an interaction *in vitro* as predicted by the SDM results. The plug domain has molecular weight of 20 kDa, as calculated by the amino acid sequence, which is smaller than that of pectocin M1 at 30 kDa. However, it can be seen in Figure 4-10b that the plug domain alone has a higher molecular weight than pectocin M1, suggesting self-association. This self-association has been seen in SAXS, making it difficult to examine the plug domain in solution. Analytical SEC therefore does not suggest an interaction between pectocin M1 and the plug domain due to the presence of two peaks overlaying with the individual species. This data does not support the idea that the plug domain interacts with pectocin M1, however it is possible that the self-association of the

plug domain disrupts any potential interaction. In order for this to be successfully assessed the plug domain would need to be monomeric in solution.

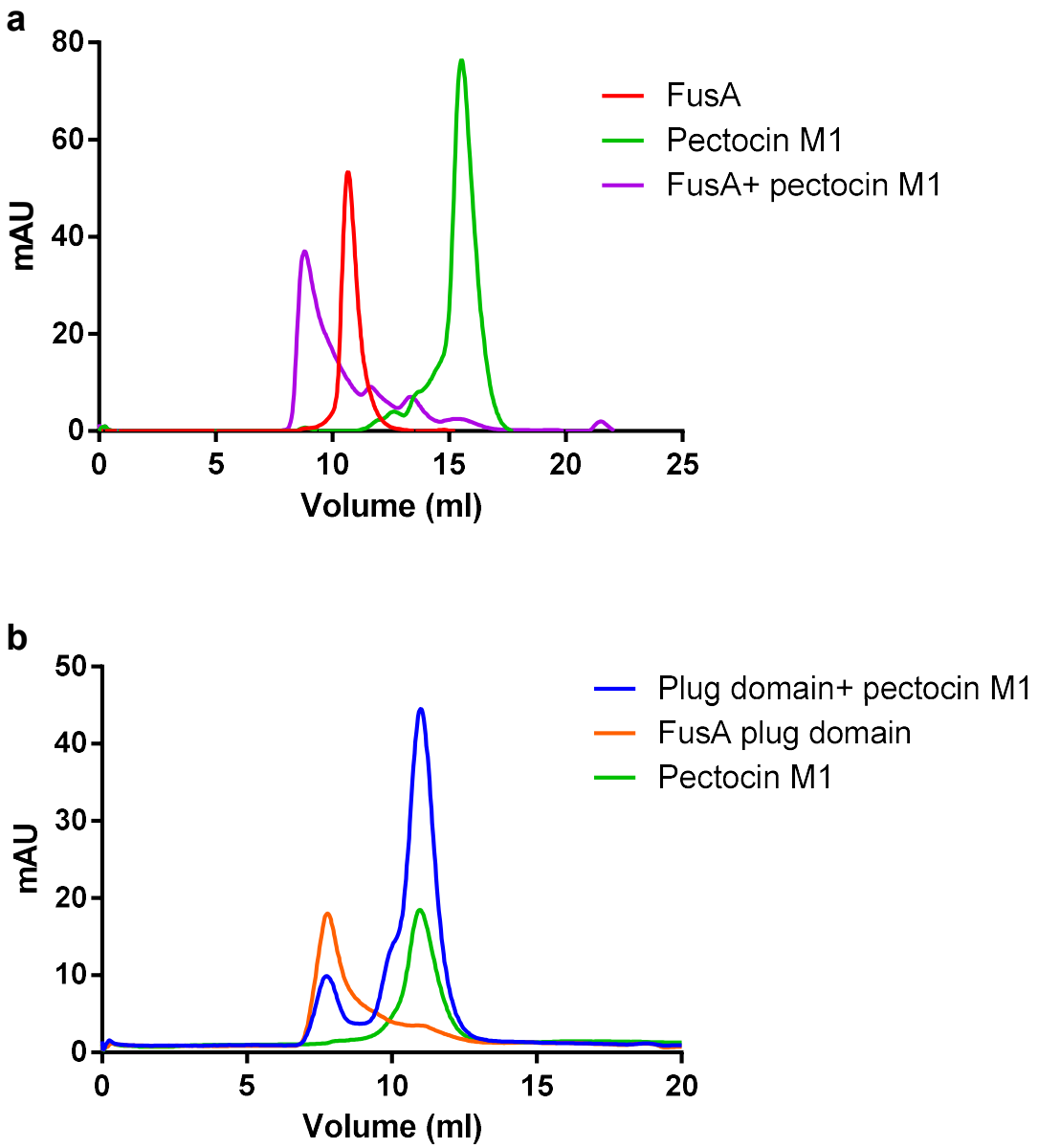

Figure 4-10 Analytical size exclusion chromatography showing an interaction between pectocin M1 and the FusA. a) Analytical SEC of pectocin M1 (green), FusA (red) and a 1:1 molar ratio of pectocin M1 and FusA in complex (purple) using a Superdex S200 10/30L column. b) Analytical SEC of pectocin M1 (green), the N-terminal plug domain of FusA alone (orange) and a 1:1 molar ratio of pectocin M1 and the plug domain (blue) using a Superdex S75 10/30L column. Both experiments were performed at RT in 50 mM Tris-HCl, 200 mM NaCl, 5% glycerol and 0.01% LDAO, protein concentrations varied from 40-200 μM depending on absorbance at 280 nm.

4.2.2 Uptake of pectocin M1 into the periplasm

4.2.2.1 FusA plug domain exits the barrel and remains folded

The mechanism by which the N-terminal plug domain is removed from the barrel of the TonB-dependent receptors is still poorly understood. Some work has been done to support both the hypothesis that the plug exits the barrel whilst remaining folded and other work supports the theory that the plug domain unfolds or partially unfolds to exit the barrel [63,76,77].

The dimensions of FusA and pectocin M1 suggest that the plug domain of FusA would have to be completely removed from the barrel in order for the substrate to pass into the periplasm. At the widest point pectocin M1 is 29 Å (Figure 3-4) in diameter which is slightly smaller than the lumen of FusA at 35 Å (Figure 4-2). Therefore, there are two possible conformational changes: the plug domain of FusA completely unfolds to allow for substrate uptake, or the plug remains globular and exits the barrel in a folded conformation.

Small-angle neutron scattering (SANS) was used to determine the behaviour of FusA in solution. SANS data for FusA was collected in a quartz cuvette for 10 minutes at a detector distance of 5.6 m (Figure 4-11a). The Guinier region of FusA was examined and the sample did not show any signs of aggregation. The p(*r*) distribution for FusA was determined giving a D_{max} of 185 Å which is much larger than the predicted dimensions of FusA with the plug domain inside the barrel (Figure 4-11b).

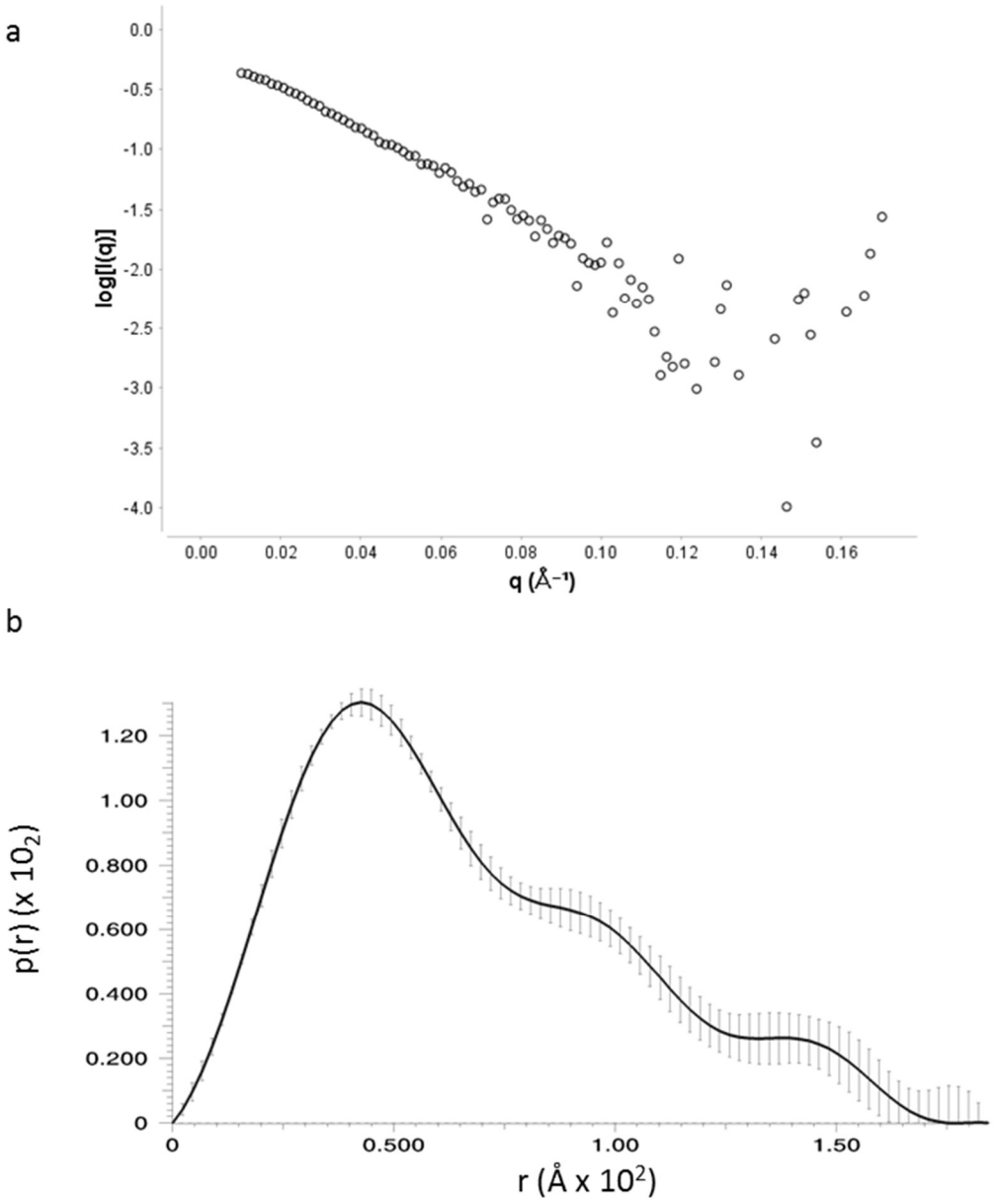

Figure 4-11 SANS data for FusA$_{1043}$ a) Scattering data for FusA$_{1043}$ showing log I(q) vs q b) p(*r*) distribution for FusA$_{1043}$ showing a maximum dimension of 185 Å. Experimental data was collected at 6^{o}C in a quartz cuvette at a concentration of 8 mg ml^{-1} in 5.5% D_2O in a buffer of 0.1% LDAO, 50 mM Tris-HCl, 100 mM NaCl pH 7.5 for 10 minutes.

As with SAXS data a dummy atom (DAMMIF) model of FusA in solution was created. The DAMMIF model, although larger in dimension than the crystal structure, suggests that the plug domain exits the barrel in a globular form (Figure 4-12). This construct of FusA was sent for N-terminal sequencing showing the first five N-terminal amino acids were STPTS (appendix 1c). These confirm that the FusA$_{1043}$ protein was lacking both signal sequence and predicted TonB-

box, suggesting that the small globular region is likely to be due to the plug domains exit from the barrel (Appendix 1).

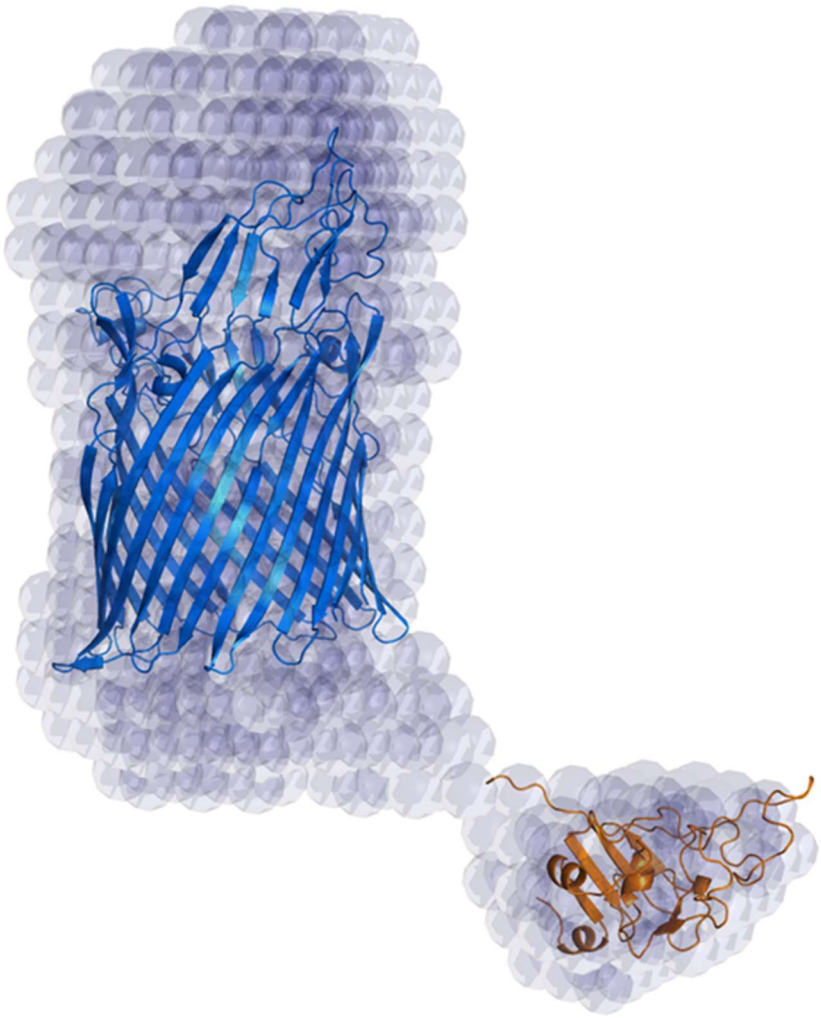

Figure 4-12 DAMMIF model suggest that $FusA_{1043}$ plug domain exits the barrel and remains globular. DAMMIF model (purple) overlaid with the N-terminal plug domain (orange) and the barrel (blue). Overlay performed using SUPCOMB [166].

In order to confirm this, constructs of both the N-terminal plug domain alone (AA 27-208) and the barrel alone (AA 209-863) were generated, expressed and purified. The plug domain could be successfully purified in the absence of the barrel which gives support to the plug exiting and remaining folded [77]. Both constructs were analysed by SANS, however neither yielded usable data.

As the plug domain of FusA is soluble and able to be purified on its own it was analysed using SAXS under several different conditions, however these revealed that the plug domain self-associates potentially due to the hydrophobicity of some residues which associate with the C-terminal barrel. This self-association has previously been seen in SEC (Figure 4-10) as the plug domain is larger in solution than the monomeric pectocin M1.

4.2.2.2 Characterisation of FusB

FusB is predicted to be a member of the TonB protein family and to interact with the predicted TonB-box of FusA (Appendix 1). TonB proteins are characterised by a flexible N-terminal domain and a folded C-terminal domain which interacts with the TonB-box of TonB-dependent receptors. As TonB has a largely disordered and flexible N-terminal a high-resolution structure of the entire protein is yet to be solved.

The N-terminal domain is flexible in order to span the periplasm to interact with the TonB-box of the outer membrane receptor. The disorder of this region makes biophysical characterisation of TonB difficult due to its flexibility. Models of FusB created by I-TASSER support the idea that it is a largely disordered and unstructured protein with a C-terminal globular domain (Figure 4-13).

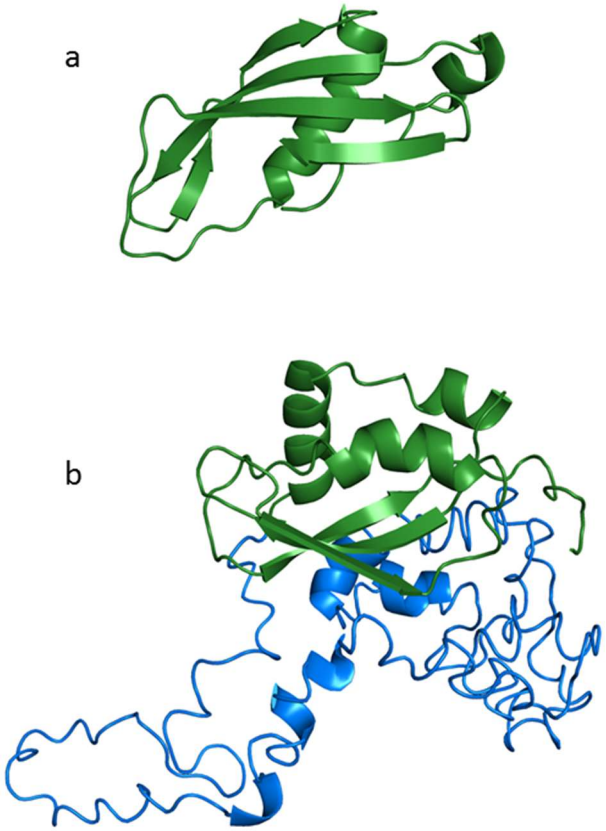

Figure 4-13 Models of FusB showing a folded C-terminal domain and a flexible N-terminal domain a) Phyre2 model of the C-terminal domain of FusB b) I-TASSER model of FusB with the folded C-terminal domain shown in green and the flexible N-terminal domain in blue.

This model is consistent with the predicted and solved structures of TonB within related organisms such as *E. coli* as it has the irregularly structured N-terminal region and a structured C-terminal domain with ß- sheet that is in the predicted interaction interface based on the known interacting sites of TonB [167]. Due to the high levels of predicted flexibility and the lack of homologous structures corresponding to the N-terminal domain, these models are unreliable predictions of structure.

In order to test the flexibility and potential structure of FusB in solution it was examined by SAXS. Unfortunately, despite testing several conditions and multiple attempts, the absence of a Guinier region in each of the scattering curves prevented further analysis. Although this generally suggests aggregation in samples it is important to note that for largely disordered or elongated particles it is often the case that Guinier analysis can be problematic [129].

Therefore, it is unclear whether this inability to analyse the Guinier is due to aggregation or disorder.

As biophysical characterisation by SAXS proved difficult, FusB was examined using AUC in order to assess whether, like TonB, it can be found as a dimer in solution [168,169]. Sedimentation velocity (SV) was used to examine if FusB is found in one or more oligomeric states in solution. The predicted sedimentation coefficient of the predicted I-TASSER structure was calculated using US-SOMO [149], however as the I-TASSER model is likely to be unreliable due to the flexibility of FusB, these were only used as a guide.

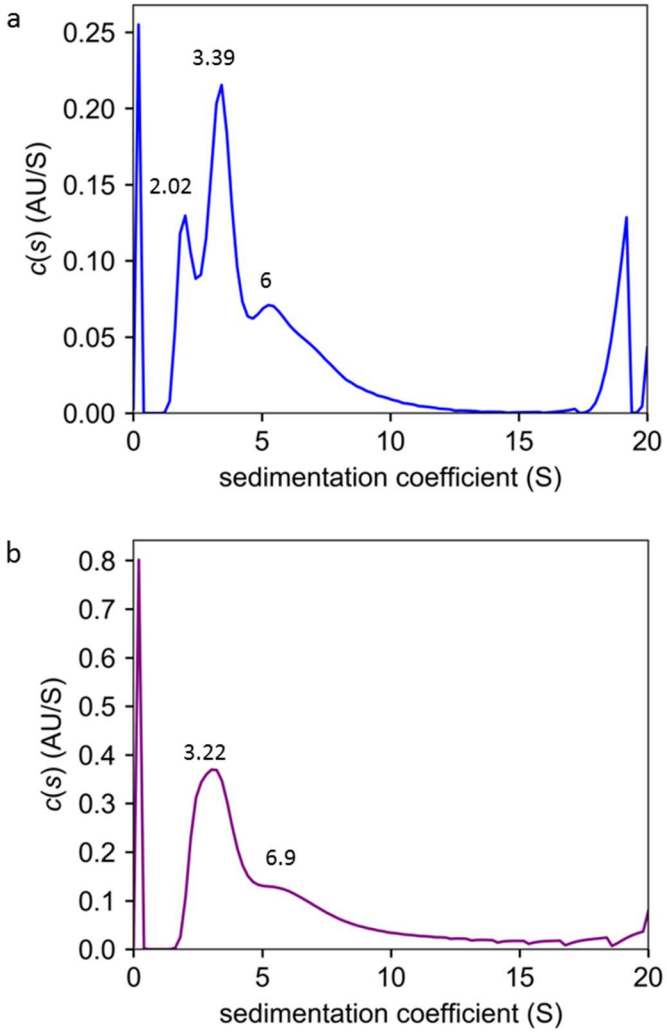

Figure 4-14 Sedimentation velocity data suggest that FusB can be found as both a monomer and a dimer in solution. Continuous c(s) distribution of FusB in 200 mM NaCl, 50 mM Tris-HCl, 5% glycerol pH 7.5 at 49000 rpm, 4°C at a concentration of a) 4 mg ml^{-1} and a)1 mg ml^{-1} suggests the presence of multiple populations in solution. Peaks are labelled with the corresponding sedimentation coefficient.

The sedimentation coefficient for each distinct peak was calculated by area under the distribution for a single peak to give the sedimentation coefficient for each discrete population and oligomeric state [170]. The distribution of FusB suggests that it can exist as both a monomer with a sedimentation coefficient of 3.22 and a dimer with a sedimentation coefficient of 6.9 (Figure 4-14). The tail of the distribution may suggest the presence of an aggregate which has been seen by SAXS despite thorough centrifugation. The c(s) distribution at a higher concentration of FusB suggests three populations with a sedimentation coefficient of 2.02, 3.39 and 6 respectively. The distribution of these peaks could suggest two or more conformations of FusB in solution (Figure 4-14). As FusB is predicted to be largely flexible and disordered it is possible than some of the conformations are elongated which would decrease the sedimentation coefficient in comparison with the globular and compact particles of the same mass.

The interacting state has been further examined by SEC-MALS which showed a proportion of the sample was aggregated. The results suggest that FusB self-associates with peaks giving a molecular weight of 56 kDa and 25.6 kDa which are similar to the calculated molecular weight 29 kDa calculated from the amino acid sequence (Figure 4-15). This suggests that as the concentration of FusB increases so does the self-association. It is well documented that *in vitro* TonB can form a dimer but when interacting with a substrate it becomes monomeric, this *in vitro* interaction seen above suggests that FusB may act in a similar way to TonB *in vitro* [87,168].

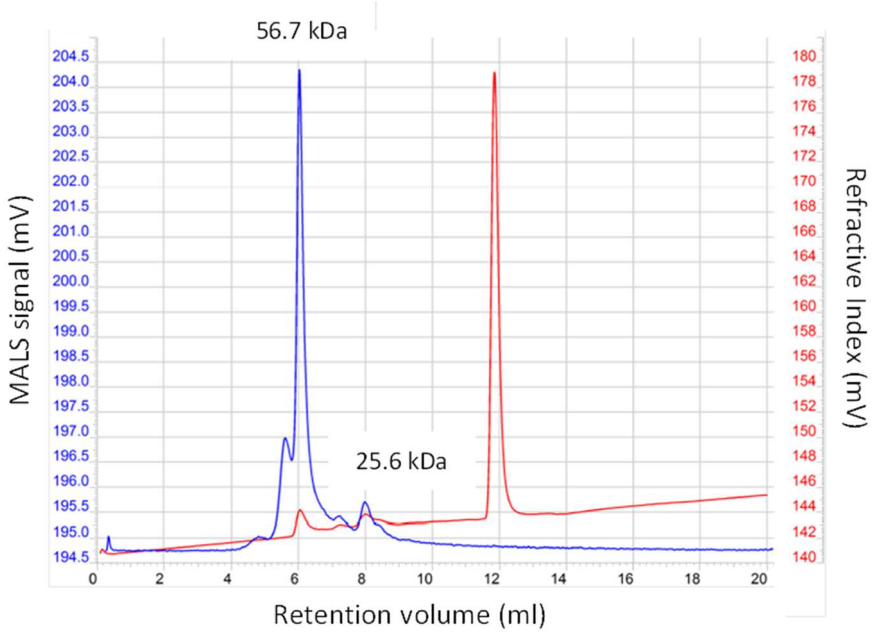

Figure 4-15 SEC-MALS data suggests FusB can be found as both a monomer and a dimer in solution SEC-MALS data was collected using a Waters Xbridge BEH200 SEC 3.5µ 7.8x300 column in 200 mM NaCl, 50 mM Tris-HCl, 5% glycerol pH 7.5 with 10 mg ml^{-1} of FusB loaded.

4.2.2.3 Interaction between FusB and pectocin M1

The absence of an IUTD within ferredoxin-containing bacteriocins suggests a novel mechanism of uptake. It is known that pectocin M1 interacts with FusA in order to enter the cell, however the exact mechanism of translocation is still unknown. It was predicted therefore that pectocin M1 may interact with FusB in the periplasm in order to harness the PMF of the inner membrane.

Sedimentation velocity (SV) was used to examine the interaction between FusB and pectocin M1. As pectocin M1 and FusB have similar molecular weights but are predicted to have very different conformations within solution, SV allowed for the separation of these distinct species. Pectocin M1 and FusB were incubated together for 2 hours prior to sedimentation at a variety of ratios, however only a 1:1 molar ratio is shown here (Figure 4-16).

Each of the peaks here integrated to calculate the sedimentation coefficient for each population. The continuous c(s) distribution for pectocin M1 alone (Figure 4-16a) showed a broad single peak with an sedimentation coefficient of 2.02. Whereas FusB alone, as shown previously, shows two peaks suggesting that it can

be found as a monomer and a dimer in solution (Figure 4-16b). Surprisingly, when mixed together at a 1:1 molar ratio a sedimentation coefficient of 1.522 was calculated, showing a single peak (Figure 4-16c).

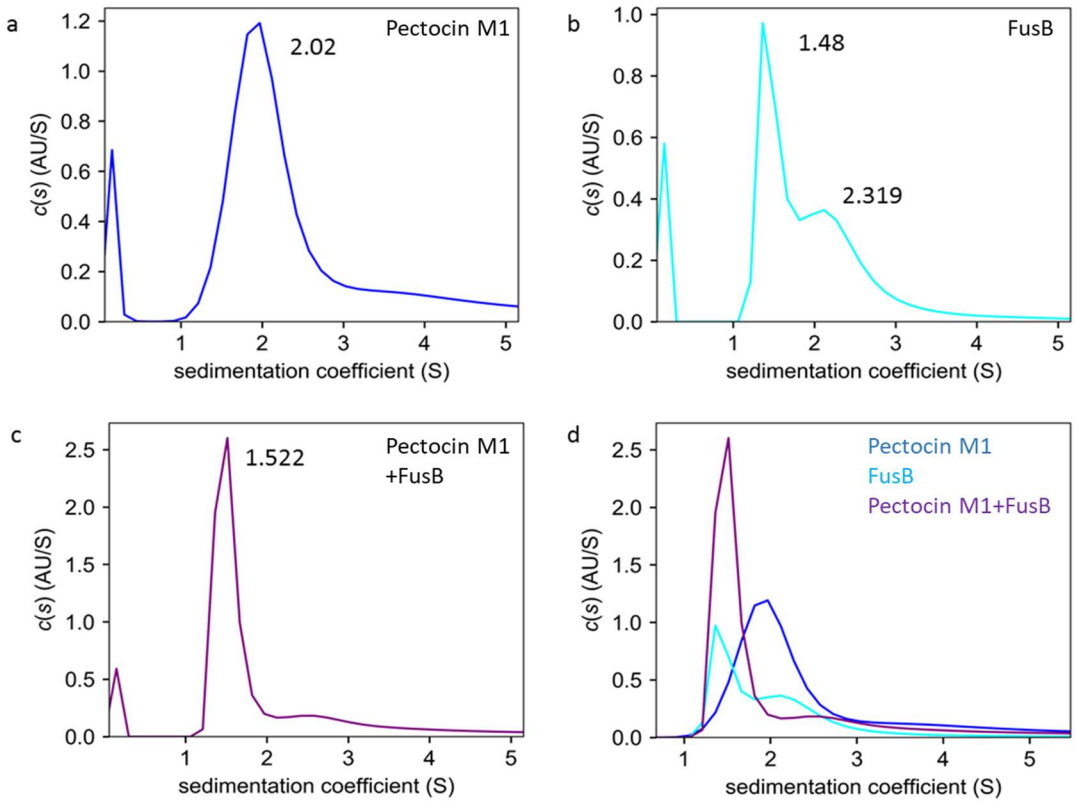

Figure 4-16 Sedimentation velocity continuous c(s) distribution of pectocin M1 and FusB individually and in complex suggests an interaction. c(s) distributions of a) Pectocin M1 (33 μM) b) FusB (99 μM) c) Pectocin M1 and FusB in a 1:1 molar ratio (33 μM of each) and d) an overlay showing the *s* shift. The sedimentation coefficients of each peak are shown on a-c.

The shift in the c(*s*) distribution cannot be explained by a simple shift to all monomeric proteins as the pectocin M1 and FusB peaks do not overlap due to their difference in shape, despite the same molecular weight (Figure 4-16d). Moreover, as FusB has a low absorbance at 280 nm a 3-fold concentration was measured alone in order to visualise the sedimentation profile of the protein, therefore the increase in absorbance can only be explained by the interaction of pectocin M1 and FusB.

The change in sedimentation coefficient when pectocin M1 and FusB are mixed together strongly suggests the interaction between the two proteins *in vitro*. As pectocins do not possess an IUTD containing a TonB-box they were thought to be unable to interact with TonB or FusB in the periplasm. However, this work has shown that despite the lack of a TonB-box pectocin M1 can interact with FusB *in vitro*. This work goes some way to supporting the idea of a novel uptake mechanism of ferredoxin-containing bacteriocins, suggesting they have found a novel mechanism of uptake in order to enter the target cell. However, more work showing the interaction *in vivo* is necessary to confirm the importance of this interaction for translocation.

4.2.3 Fus system as a potential antibiotic target

4.2.3.1 Pectocin M1$_{\text{PhiLOV II}}$ chimera

Pectocin M1 has been shown to be an effective antimicrobial against a number of *Pectobacterium* strains under iron limiting conditions [117]. As well as this pectocin M1 has been shown to enhance the growth of some strains in the same way as spinach ferredoxin, showing that resistant strains can still take up the bacteriocin [117]. The N-terminal domain of pectocin M1 is known to interact with FusA in order for the bacteriocin to be taken up, therefore it has the potential to be used as a delivery method for small molecules or antibiotics. In order to test whether the N-terminal domain of pectocin M1 would be able to interact with FusA in the absence of the cytotoxic domain, a pectocin M1 – PhiLOV II chimera (pectocin M1$_{\text{PhiLOV II}}$) was created by joining the N-terminal domain of pectocin M1 to PhiLOV II (Figure 4-17a) [171,172]. The predicted structure of the chimera showed that it was likely to be small enough to pass through the lumen of the FusA (Figure 4-17b) and the fluorescence of the chimeric protein suggested that the C-terminal PhiLOV II domain was correctly folded (Figure 4-17c).

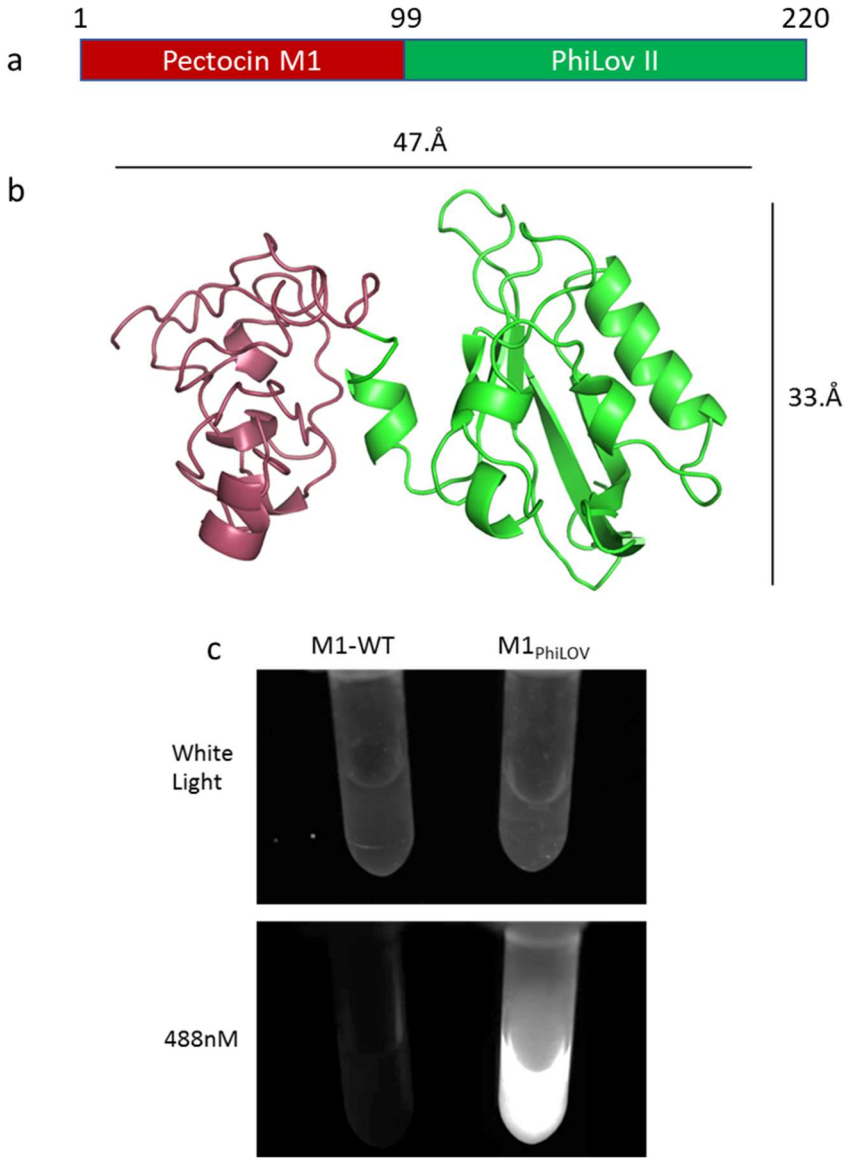

Figure 4-17 Pectocin M1$_{PhiLOV\ II}$ chimera of the N-terminal domain of pectocin M1 and the PhiLOV II protein. a) Schematic to show the construction of the chimera protein from pectocin M1 and PhiLOV II b) I-TASSER model of pectocin M1$_{PhiLOV\ II}$ with the N-terminal pectocin M1 domain in red and the PhiLOV II domain shown in green. c) Image taken under both white light and ultra-violet light (488 nm) showing the fluorescence of the chimera in comparison to the wild-type pectocin M1 suggesting the protein is correctly folded.

4.2.3.2 Uptake of Pectocin M1$_{PhiLOV\ II}$ into the cell

The receptor interaction and uptake of pectocin M1$_{PhiLOV\ II}$ was primarily tested using competition assays on LB agar supplemented with 200 µM bipyridine. The chimera and WT pectocins were spotted next to each other at equal molarities and volumes on a lawn of *P. atrosepticum* LMG2386 in order to determine if they compete for the same uptake receptor (Figure 4-18).

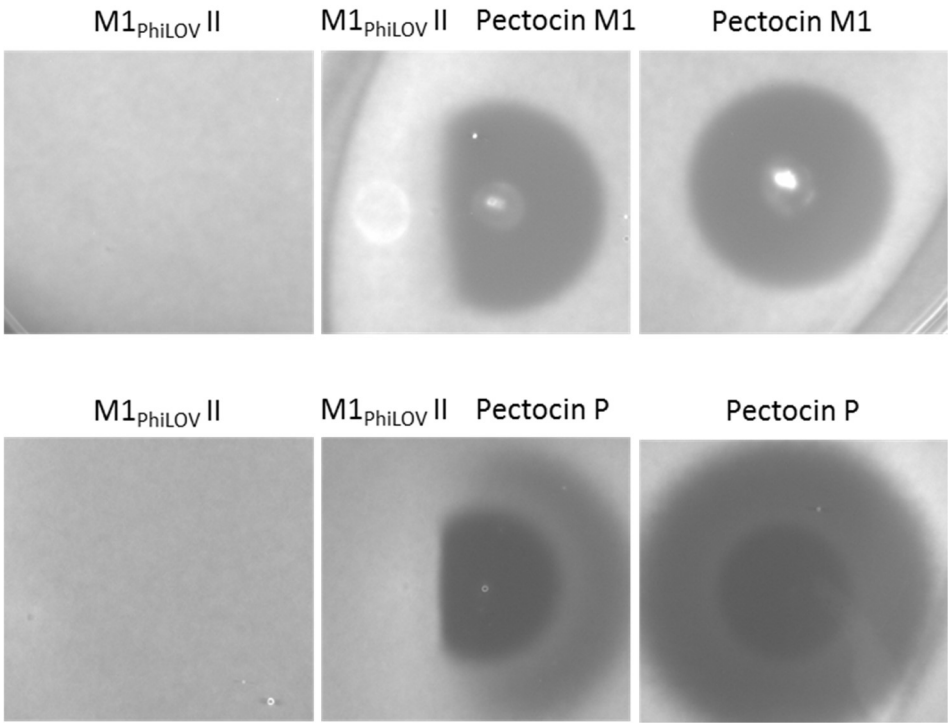

Figure 4-18 Competition assay showing pectocin M1, pectocin P and pectocin M1$_{PhiLOV\ II}$ compete for the same receptor (FusA) in *P. atrosepticum* LMG2386. Spots of 5 µl at 5 mg ml^{-1} were spotted onto a lawn of *P. atrosepticum* LMG2386 on LB agar with 200 µM bipyridine. Plates were overlain with PrestoBlue and images taken at 546 nm using a Chemidoc system.

When spots of pectocin M1$_{PhiLOV\ II}$ were placed next to either pectocin M1 or pectocin P it can be seen that a semi-circular zone of inhibition occurs. This suggests that the two proteins are competing for the same uptake receptor, in this case FusA. This data suggests that the presence of the N-terminal domain of pectocin M1 is sufficient for receptor binding. The limiting factor for this novel approach would be the size of the barrel of FusA, however this suggests that small antimicrobials which are otherwise unable to enter the cell could enter with the addition of the N-terminal pectocin M1 domain. In order to confirm this, experiments using a cytotoxic C-terminal domain would confirm the ability of the chimera to enter the cell. This would also confirm the potential of the N-terminal domain as a delivery system in *Pectobacterium* spp., for example small some antibiotic, such as vancomycin, are unable to cross the bacterial outer membrane to reach their target, in this case the peptidoglycan layer, therefore a delivery mechanism could enable them to be effective against a wider range of pathogens as well as specifically targeted to a specific genus.

4.2.3.3 Pectocin M1$_{PhiLOV\ II}$ structural characterisation by SAXS

It was shown in chapter 3 that both pectocin M1 and P are flexible and that this flexibility is likely to be necessary for uptake. In order to examine the structure and flexibility of Pectocin M1$_{PhiLOV\ II}$ scattering data was collected using SEC-SAXS (Figure 4-19a). Analysis of the Guinier region (Figure 4-19b) showed that the sample was free from aggregation and gave an R_g of 22.3 Å. Extrapolation of the Guinier region gives an estimated molecular weight of 26 kDa (calculated using SASMoW2 [136]) which is similar to the calculated weight from the amino acid sequence of 24.7 kDa (calculated using ProtParam [152]).

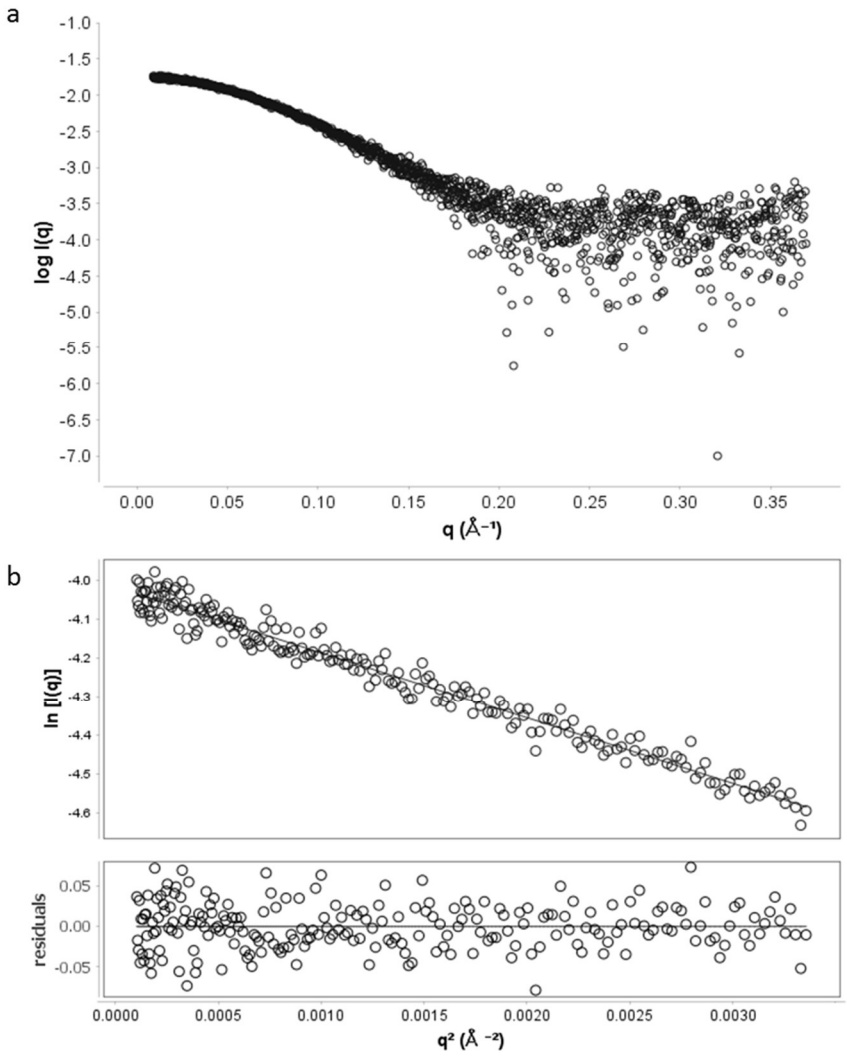

Figure 4-19 SAXS scattering data for pectocin M1$_{PhiLOV\ II}$ and Guinier analysis a) q vs Log I(q) scattering data at 5.2 mg ml^{-1} b) Gunier region of the scattering curve showing no aggregation and giving a predicted Rg of 22.4 Å and I(0) of 0.0179

Kratky analysis of pectocin $M1_{PhiLOV\ II}$ in solution shows the peak of the distribution occurs around √3 (Figure 4-20a) suggesting that the protein is globular in solution. This is similar in to the model of the chimera, shown in Figure 4-17b, which is shown to be compact and not elongated.

By analysing the data with both the Kratky-Debye and Porod-Debye the particle can be classed as either compact or flexible in solution when the low q range is examined. When the low q range was examined it can be seen that the plateau occurs first in the Porod-Debye plot, suggesting that the particle is compact and inflexible in solution (Figure 4-20b and c).

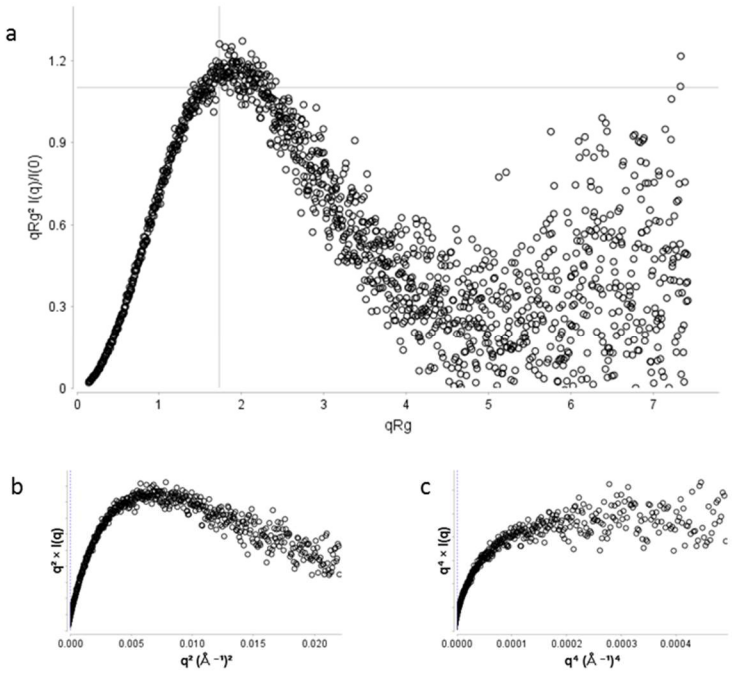

Figure 4-20 Flexibility analysis of Pectocin $M1_{PhiLOV\ II}$ suggests it is both globular and compact in solution. a) Kratky plot shows the peak occurring around √3 (shown by the crosshairs) suggesting that the particle is globular in solution. The Kratky-Debye (b) and Porod-Debye (c) plots suggest that the particle is compact in solution as the plateau occurs first in the Porod-Debye plot (q = 0.1491).

The structural analysis of pectocin $M1_{PhiLOV\ II}$ chimera suggests it is structurally globular and inflexible, however in conjunction with the biochemical data this suggests that as the chimera has dimensions small enough to pass through the barrel. Dummy atom modelling (Figure 4-21) suggests that the protein may be

able to elongate as the p(*r*) distribution gave a maximum dimension of 78 Å which is larger than that of the model.

Together, this data suggests that the pectocin $M1_{PhiLOV\ II}$ is compact in solution and inflexible. This suggests that flexibility found in pectocins is not necessary for the initial receptor interaction, however it may be required for translocation.

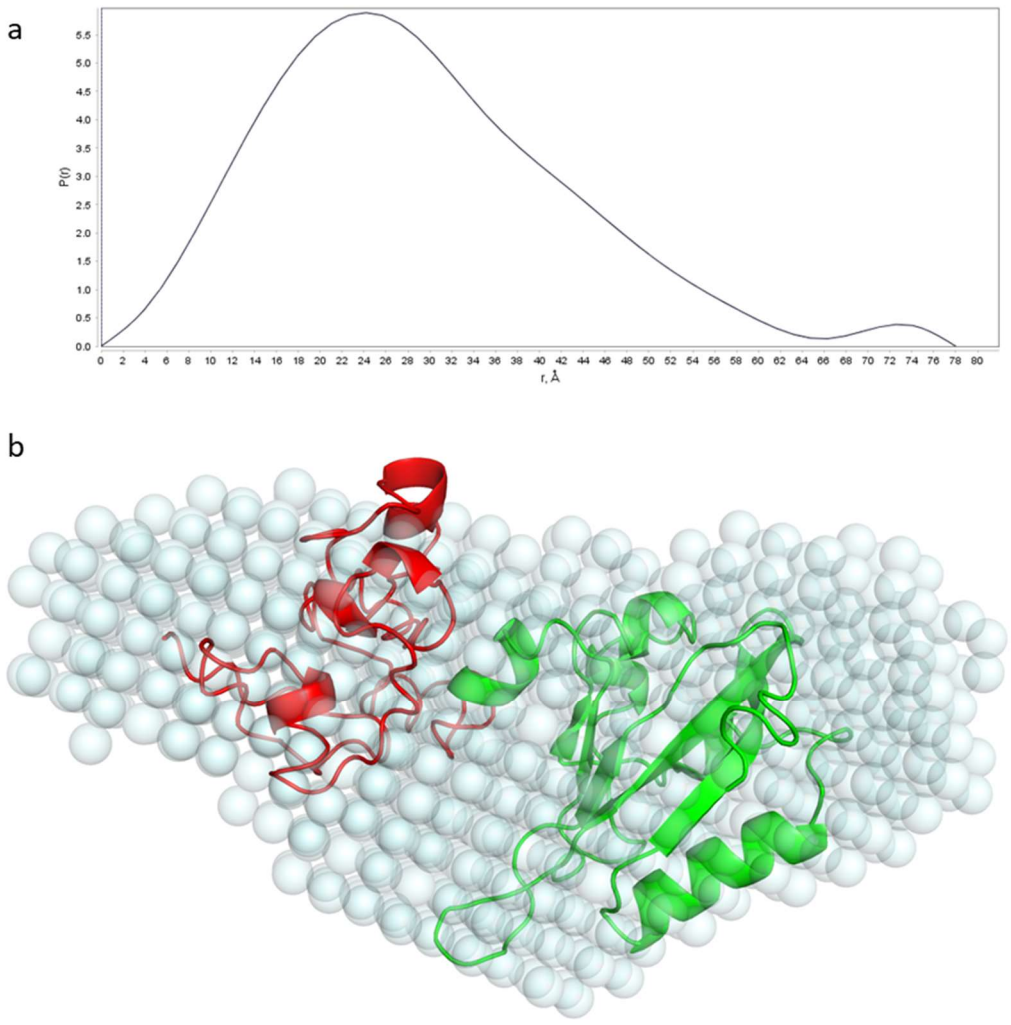

Figure 4-21 DAMMIF model of pectocin $M1_{PhiLOV\ II}$ suggests possible elongation. a) p(*r*) distribution of Pectocin $M1_{PhiLOV\ II}$ giving a D_{max} of 78 Å b) Pectocin $M1_{PhiLOV\ II}$ DAMMIF model (blue) based on SAXS data overlaid with the I-TASSER predicted model of the chimera with the N-terminal of pectocin M1 shown in red and the C-terminal PhiLOV II domain shown in green. Overlay was performed using SUPCOMB [158].

4.2.4 The role of the *fus* system in virulence

The uptake of iron is essential for the growth of *Pectobacterium* spp. and is often scarce during infection [173]. It is proposed that the *fus* operon has evolved in order to take up ferredoxins from the host species during infection. It was considered that FusA may be important for virulence and the absence of this protein would impact the ability of *P. atrosepticum* LMG2386 to successfully infect both plant and tuber tissue.

During a bacterial infection salicylic acid levels within plant tissue will increase at both the infection site as well as throughout the plant to activate the hosts defences [174]. NahG is a salicylate hydroxylase which breaks down salicylic acid and therefore increases the susceptibility of the plants to non-host pathogens [174]. The use of *N. benthamania* with the presence of the *nahG* gene was used as a model organism for *P. atrosepticum* black-leg infection as it was more susceptible and showed more classical signs of infection than wild-type *N. benthamania*.

In order to examine the potential for *P. atrosepticum* LMG2386 to infect plant tissue *Nicotiana benthamiana nahG* leaves were pressure infiltrated with ~0.5 or 1 x10^6 *P. atrosepticum* LMG2386 grown in LB with 200 µM bipyridine and 2 % w/v D-lactose overnight (with the addition of 100 µM ampicillin for Δ*fusA*/p*fusA*). Initial trials of wild-type *N. benthamania* infection showed no infection by *P. atrosepticum* LMG2386 and therefore strain of *N. benthamania* lacking the *nahG* gene was used as an infection model for subsequent experiments due to its increased susceptibility.

Infection of plant tissue showed that *P. atrosepticum* LMG2386 can successfully degrade *N. benthamania nahG* tissue through enzymatic maceration (Figure 4-22). These results show that the outcome of infection is the same for leaves infected with *P. atrosepticum* strains in both the presence and absence of the *fusA* gene, therefore showing that FusA does not impact virulence. Lighter patches on the leaves are indicative of cell lysis as the light passes through the degraded tissue, a representative image is shown in Figure 4-22.

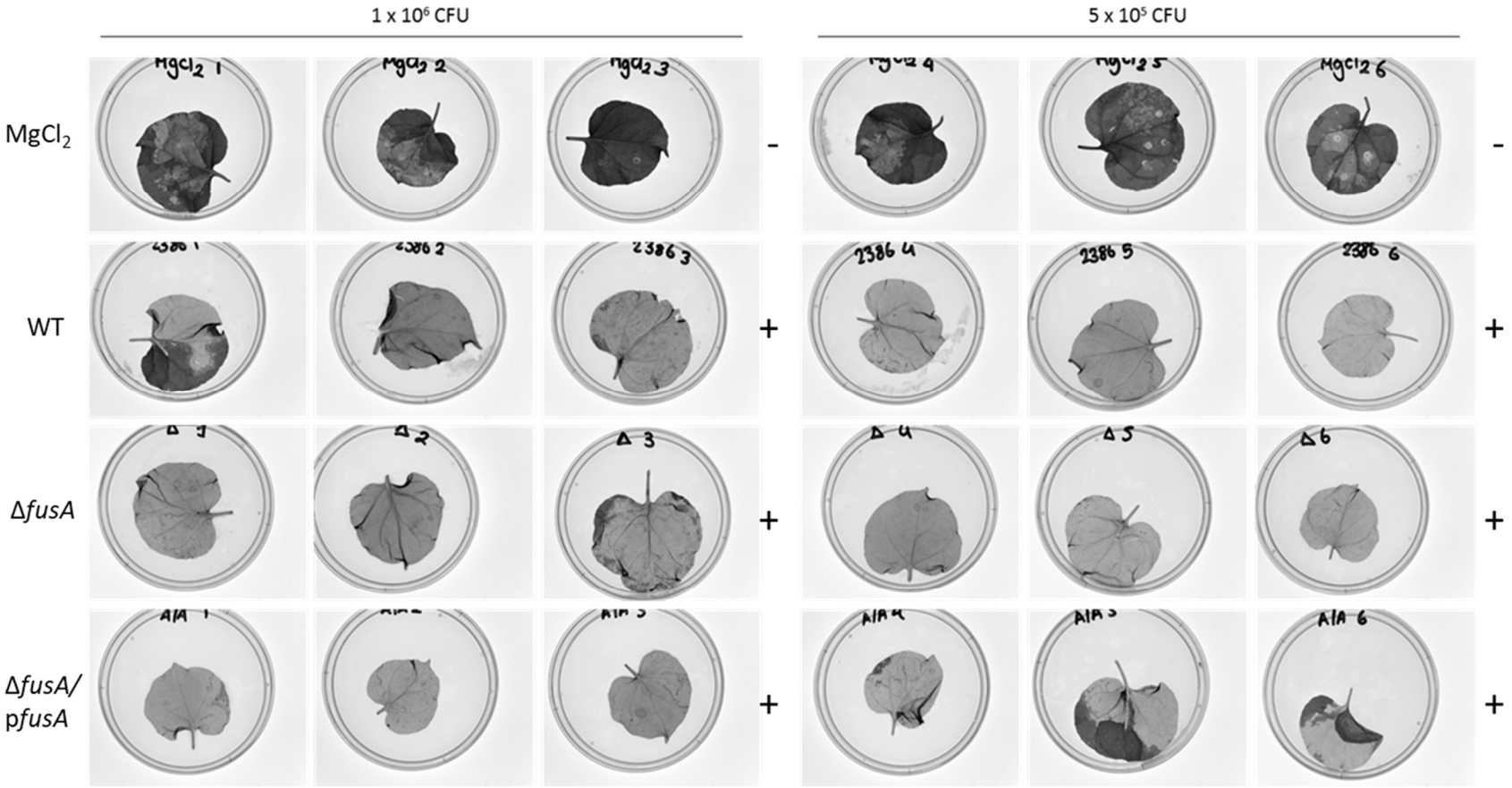

Figure 4-22 Representative images of infected *N. benthamania nahG* with *P. atrosepticum* LMG2386 and incubated at 28 °C for 72 hours. Leaves were pressure infiltrated with 500 µl *P. atrosepticum* LMG2386 WT, Δ*fusA* and Δ*fusA*/p*fusA* resuspended in $MgCl_2$ at two inoculums (1 x10^6 and 5 x10^5 CFU). Leaves were imaged with a Chemidoc system with degraded tissue shown as a lighter grey and intact leaf tissue as a darker grey. Tissue damage is indicated with no tissue maceration (-) and complete tissue maceration (+) shown. No intermediate levels of infection were observed, experiment was performed in triplicate with a representative image shown.

To further test the role of FusA in infection the virulence of each strain was tested against *S. tuberosum* tissue as this is a natural host species of *P. atrosepticum* LMG2386. Tuber slices were infected with *P. atrosepticum* LMG2386 and incubated at 28°C for 72 hours and examined. After infection tuber tissue exhibits the classical symptoms of soft rot infection with degraded tissue seen to be darker in colour. The tuber tissue was also observed to have lost all structural integrity due to maceration by cell-wall degrading enzymes. The outcome of infection was same for *P. atrosepticum* LMG2386 WT, Δ*fusA* and Δ*fusA*/p*fusA* (Figure 4-23). This further suggested that the presence of FusA is not essential for virulence as the absence does not create a fitness cost during tuber or leaf infections.

Previous work has shown that *P. atrosepticum* LMG2386, unlike other *Pectobacterium* species, does not show enhanced growth in the presence of plant-type ferredoxins under iron limiting condition [117]. This, in conjunction with these results, suggests that *P. atrosepticum* LMG2386 may be employing other iron sequestering mechanisms and therefore the removal of one is unlikely to completely disrupt virulence. It would be interesting to determine if the *fus* system is essential for virulence in other *Pectobacterium* species which more readily use the host ferredoxins as an iron source.

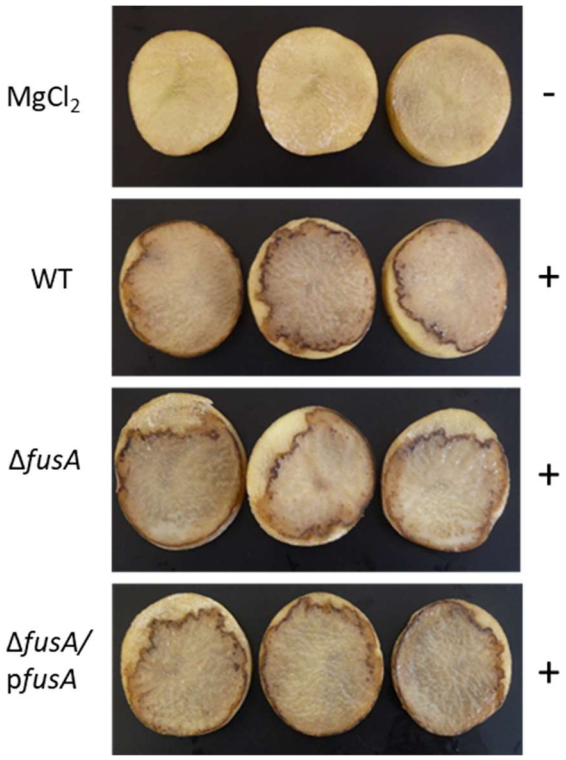

Figure 4-23 Representative image of *S. tuberosum* slices of 1 cm in thickness were inoculated with 500 µl of *P. atrosepticum* LMG2386 in 10 mM $MgSO_4$ at 1 x10^6 and incubated for 72 hours at 28 ºC. No sign of infection (-) and greater than 80% maceration (+) are indicated. Experiment was performed in triplicate with a representative image shown, no intermediate stages of infection were observed in any replicate.

4.2.5 Pectocin M1 as a potential pesticide

P. atrosepticum LMG2386 is a major pathogen of potatoes (*S. tuberosum)* however innate resistance against this pathogen varies between individual varieties of potato. It has been shown in this study that the Jura variety of potatoes is susceptible to *P. atrosepticum* LMG2386 infection. *P. atrosepticum* is known to cause necrosis in both tuber and leaf tissue *in planta* and therefore it was predicted that pre-treatment with pectocin M1 could prevent infection with *P. atrosepticum* LMG2386 [2,175]. As pectocin M1 has been shown to reduce cell growth and cause cell lysis down to nanomolar concentrations it was predicted to be effective at low concentrations *in vivo*.

Infections of ~1 x10^6 CFUs of bacteria were characterised previously for both tuber and leaf infections with *P. atrosepticum* LMG2386 WT, Δ*fusA* and Δ*fusA*/p*fusA* (4.2.4). This model was used to determine whether pre-treatment

with recombinant pectocin M1 could potentially be used as a preventative treatment for *P. atrosepticum* infection *in vivo*. Potato tubers were sliced at a thickness of 1cm and were treated with 500 µl of pectocin M1 in 10 mM $MgCl_2$ 30 minutes prior to infection and incubated for 48 hours at 28°C.

Table 12: Levels of infection in both tuber and leaf infections after treatment with pectocin M1. Leaves and tubers were pre-treated 30 minutes prior to infection with pectocin M1 (0.1-2.5 mg) and challenged with *P. atrosepticum LMG2386* WT, Δ*fusA,* Δ*fusA*/p*fusA* or $MgCl_2$ as a mock infection. Results shown indicate no infection (-), maceration of <50% of the tissue (+), maceration of 50-80% of the tissue (++) and maceration of >80% of the tissue for the total tuber mass. Experiments were performed in duplicate. (representative images shown in Figure 4-24 and Figure 4-25)

	Tubers				Leaves	
	no treatment	**2.5 mg**	**0.5 mg**	**0.1 mg**	**no treatment**	**2.5 mg**
$MgCl_2$	-	-	-	-	-	-
WT	++	++	+	+	+++	+++
Δ*fusA*	+++	+++	+++	+++	+++	+++
Δ*fusA*/p*fusA*	++	+++	+	++	+++	+++

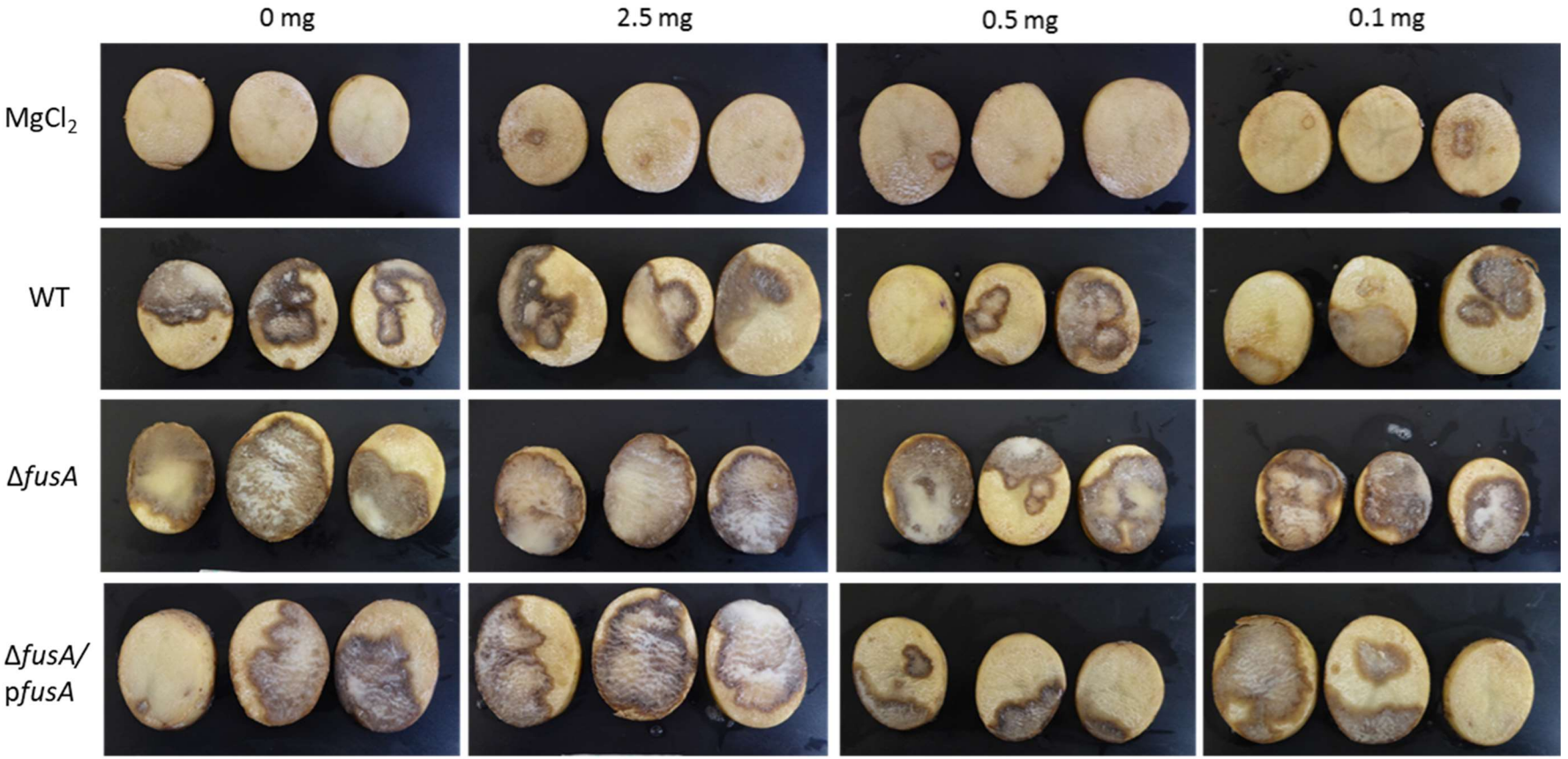

Figure 4-24 Pectocin M1 treatment of *S. tuberosum* with different concentrations of pectocin M1 comparing *P. atroseptcium* LMG2386 WT, Δ*fusA* and Δ*fusA*/p*fusA* strains. Tuber slices were pre-treated with pectocin M1 at 2.5, 0.5, 0.1 and 0 mg total protein 30 minutes prior to infection. Tubers were then inoculated with 10 mM $MgCl_2$ or 1 x10^6 CFUs of *P. atrosepticum* wild-type (WT), Δ*fusA* and Δ*fusA*/p*fusA*. Tubers were incubated at 28^{o}C for 48 hours. Experiment was performed in duplicate with a representative image shown.

Pre-treatment of potato tubers (Figure 4-24) showed that although the lesions caused by *P. atrosepticum* infection appear to be slightly reduced with the addition of pectocin M1 these results are inconclusive. The difference in treatment response between the WT and ΔFusA strains does suggest a reduction in bacterial load with the addition of pectocin M1. However, as lesions are also smaller in the absence of treatment this may not be indicative of successful treatment.

CFU counts were initially taken before and after infection in order to quantify the number of bacteria within an infected tuber slice to determine if there was a reduction in bacterial load. However due to the lack of resistance and no effective selective media for *P. atrosepticum,* the *P. atrosepticum* colonies could not be easily distinguished from contaminants. An effective way to tackle this would be to introduce an antimicrobial marker however this could potentially have a fitness cost and may reduce the level of infection. Additionally, it would be beneficial to examine the longevity of pectocin M1 in plant tissue over several days to determine if it is broken down by proteases or remains active over a long period of time.

4.2.5.1 Pectocin M1 as a potential treatment for *P. atrosepticum* infection using *N. benthamania* as a model organism.

Preliminary trials showed that pressure infiltration with pectocin M1 in 10 mM $MgCl_2$ was the most effective method of pre-treatment before infection. Pre-treatment with the addition of a surfactant was also tested, however with this method it was difficult to determine the concentration of pectocin M1 administered.

Leaves were pre-treated with pectocin M1 30 minutes before inoculation. *N. benthamania nahG* leaves were subsequently infected with *P. atrosepticum* LMG2386 WT, Δ*fusA* and Δ*fusA*/p*fusA* strains after pre-treatment and incubated for 48 hours and imaged using the white-light filter on the Chemidoc.

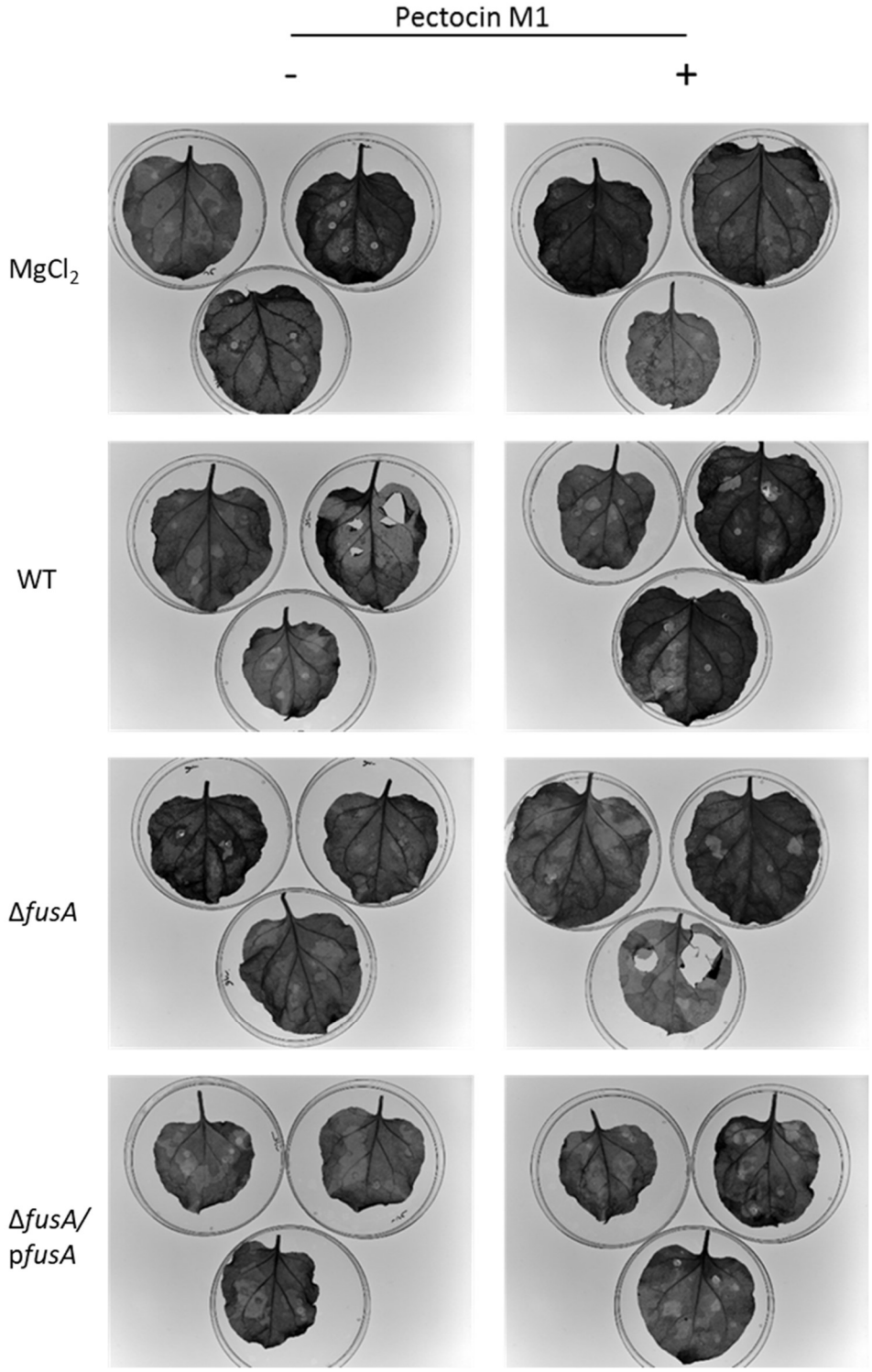

Figure 4-25 *N. benthamania* infection with *P. atrosepticum LMG2386* after 30 minutes of pre-treatment with 1 mg pectocin M1. Leaves were incubated for 24 hours at 28°C after infection with $MgCl_2$, *P. atrosepticum* WT, Δ*fusA* and Δ*fusA*/p*fusA* respectively.

Uninfected leaves ($MgCl_2$) showed no signs of cell lysis and leaves were intact, however some tissue damage was observed at the points of infiltration. It can be seen in Figure 4-25 that pre-treatment with pectocin M1 was ineffective in

clearing the infection. In the leaves infected with WT *P. atrosepticum* LMG2386 there was a small reduction in the amount of leaf tissue damage however the lack of complete eradication of the infection or the lack of a substantial difference in damage made it difficult to reach any conclusions (Figure 4-25).

As with the tuber infections, colony counts were performed from leaf sections however it was difficult to draw conclusions from the data collected. Primarily due to the lysis of the plant cells it was difficult to collect consistent samples from macerated tissue. Moreover, the bacteria counted were presumed to be *P. atrosepticum* however it was clear from the colony morphologies that there were other bacterial species present which were also seen in small numbers on the control leaves despite the lack of infection.

Furthermore, it is unclear whether pectocin M1 is broken down by host proteases and the host immune response. Western blotting was used to try and determine this however the level of protein in the leaf tissue after infection was too low to be detected in this manner. The most efficient way to use pectocin M1 as a treatment method against infection would be to express the protein *in planta* under a constitutive promoter so that the presence of pectocin M1 in the leaf tissue prevents an infection from being established.

4.3 Conclusions

Prior to this work it was known that pectocin M1 is taken up into the periplasm of *Pectobacterium* cells through the ferredoxin uptake receptor, FusA as the absence of this receptor eliminates the ability of pectocin M1 to enter the cell and cause cell lysis. It was further proposed that pectocin M2 could only interact with FusA in the folded conformation based on docking models of the ferredoxin domain of pectocin M1 and previous NMR work [124].

This work has furthered the understanding of the uptake and interaction of pectocin M1 with the FusA receptor. It has been shown that the long extracellular domain of FusA, as well as the N-terminal plug domain, interacts with pectocin M1 *in vivo*. Through the use of SDM the location of residues important for uptake were identified on both FusA and pectocin M1 suggesting a

binding interface between the two proteins and mutagenesis studies have given support for the current model of pectocin M1-FusA interaction.

Furthermore, this work has allowed the model of pectocin M1 uptake to advance as it has been shown that the substrate interacts with the periplasmic FusB *in vitro*. Future work will focus on successfully deleting the *fusB* gene in order to test if this protein is essential for uptake and examine the interacting sites through the use of NMR spectroscopy and subsequent SDM. The current model of pectocin M1 uptake therefore now consists of the binding of pectocin M1 to the long extracellular domain of FusA and the removal of the FusA N-terminal plug domain to allow for pectocin M1 to enter the cell and interact with FusB. It is unknown if pectocin M1 interacts with any other periplasmic proteins or immediately goes onto interact and cleave its substrate, lipid II (illustrated in Figure 4-26).

The use of pectocin M1 as a novel antibiotic has been shown to be ineffective in the current *in vivo* studies; however, this is likely due to the concentrations of proteins used. Future work should focus on developing and refining pectocin M1 as a novel antibiotic and examining if there are reductions in bacterial load when pectocin M1 is used. The current studies are limited in that the CFU counts at the end of an infection are difficult to determine due to the lack of selection media for *P. atrosepticum*. For future wok, it would be beneficial to select for *P. atrosetpicum* to accurately measure the bacterial load, this could be done through the introduction of an antibiotic resistance marker.

Finally, the production of a pectocin M1 chimera protein that can successfully interact with FusA shows that the N-terminal domain of pectocin M1 has the potential to be used to deliver small proteins into *Pectobacterium* spp. and has the potential to be developed as a new delivery tool for antimicrobials. Altogether this work has advanced our understanding of ferredoxin and ferredoxin bacteria uptake.

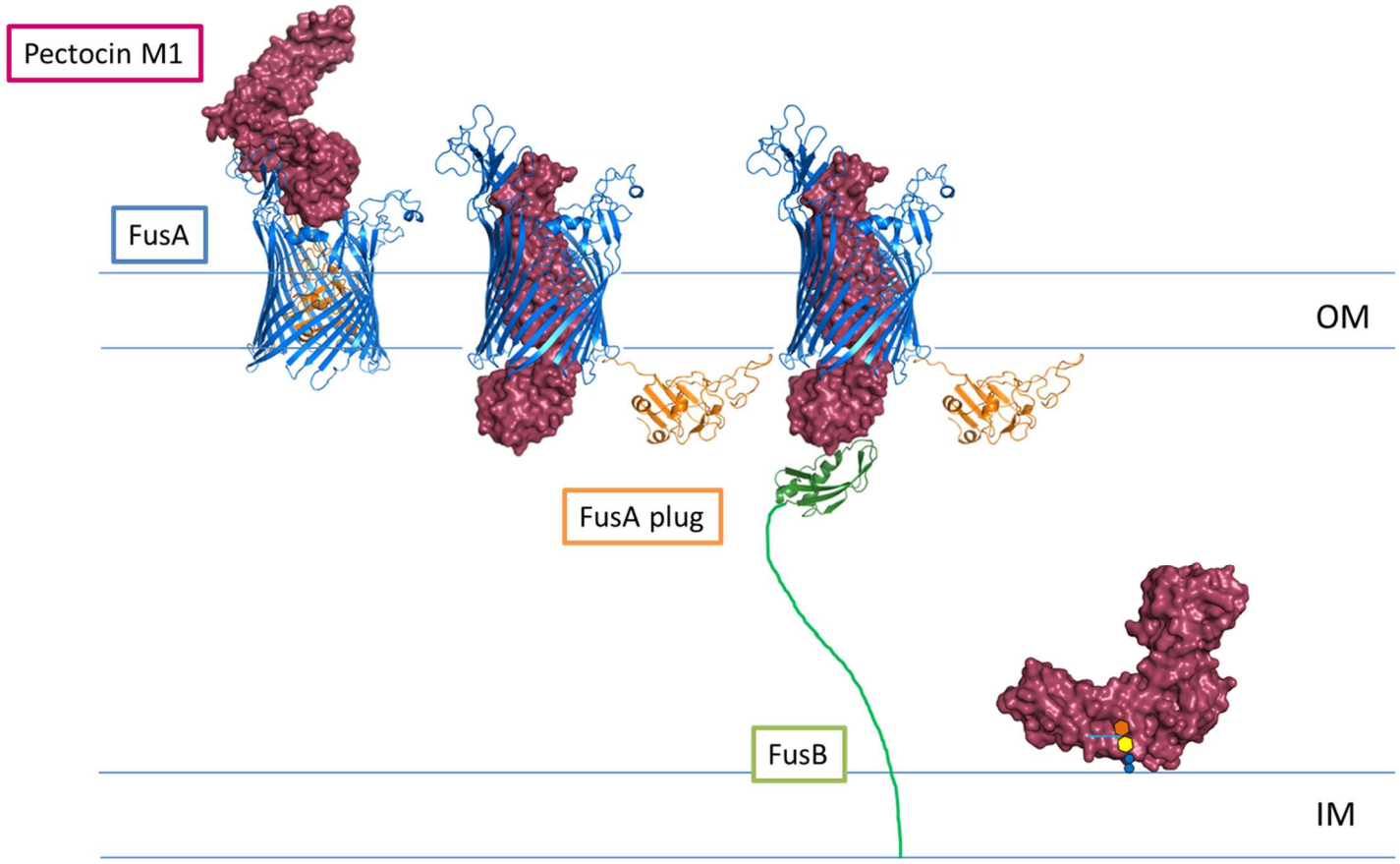

Figure 4-26 Schematic diagram showing the current predicted model of pectocin M1 uptake into *P. atrosepticum* cells. Model shows pectocin M1 (red) interacting with the FusA outer membrane receptor (blue) in the bent conformation. A conformational change occurs to allow pectocin M1 to pass through the lumen of the FusA barrel with the plug removed from the barrel, predicted to be in a folded conformation (orange). Pectocin M1 is then predicted to interact with FusB (green) in the periplasm in order to go on and cleave lipid II anchored in the inner membrane, potentially in the bent conformation as suggested in [176].

Chapter 5 Biochemical and Biophysical Characterisation of Agalacticin A

Disclosure: Agalacticin A was discovered by Sakramanee Krajangwong; initial testing of strains and all *Galleria mellonella* model work was performed by her. All other work presented here was performed by the author.

5.1 Introduction

GBS is a Gram-positive bacterium which is a causative agent of infections in a broad range of host species. GBS causes a wide-range of diseases from mastitis in cattle to neonatal infections in humans and streptococcosis in fish [26,29,177]. These diseases can have devastating consequences to human health, food security and production worldwide. GBS is resistant to several antibiotics and the overuse of antibiotics in farming means that antimicrobial resistance is increasing [10]. Therefore, the discovery of novel antibiotics to target GBS is essential.

Bacteriocins of Gram-positive bacteria are commonly peptide antibiotics [178]. The most well characterised of these peptide antibiotics is nisin, a commonly used food preservative produced by *Lactococcus lactis* and part of the lantibiotics family of bacteriocins [47]. The active form of nisin A is a 34 amino acid polypeptide which contains several post-translationally modified amino acids [179]. Nisin prevents successful cell wall synthesis and consequently cell lysis [180]. This lantibiotic has a relatively broad spectrum of killing and can target a large number of Gram-positive bacteria, including *Listeria* and *Clostridia* species [47]. Despite their broad-spectrum, lantibiotics are largely ineffective against Gram-negative pathogens due to their highly impermeable outer membrane [47].

Although the majority of Gram-positive bacteriocins discovered are peptide antibiotics, there is a class of narrow spectrum protein antibiotics, termed bacteriolysins, which are more similar to those found in Gram-negative bacteria [178]. Lysostaphin is a peptidase that is released by *Staphyloccoccus simulans* and targeted towards other *Staphylococcal* species, specifically *S. aureus* [96,181].

Lysostaphin belongs to the M23 metalloprotease family which are characterised by their ability to hydrolyse peptide linkages within the peptidoglycan layer during cell division and their requirement for a zinc ion in the active site [182]. A well characterised M23 metalloproteases is LytM, an autolysin from *S. aureus* which is very similar in structure and function to the catalytic domain of

lysostaphin [94]. Unlike lysostaphin, LytM is an autolysin which is responsible for peptidoglycan hydrolysis during cell division [94]. Lysostaphin and LytM are very similar in structure, with homologous active sites, both containing HXXXD and HXH motifs and a zinc ion at the active site [94,181].

ZooA (ZooA) is a bacteriocin produced by and targeted towards *Streptococcus epi ssp. zooepidemicus* and is similar in both structure and function to lysostaphin [104,183,184]. ZooA has an N-terminal cytotoxic domain which is structurally similar to both lysostaphin and LytM acts by hydrolysing peptidoglycan [94,99,183]. Similarly to lysostaphin, ZooA has a unique C-terminal target recognition domain (TRD) which is specific for the target organism, in this case *Streptococcus* species [94,97].

The TRD of ZooA is presumed to be necessary in order for it to specifically target the *Streptococcus* peptidoglycan layer. Recent work has suggested that this domain interacts with the tetrapeptide and alanine cross-bridges of the peptidoglycan layer positioning the bacteriocin on the cell surface [103]. Structural and sequence comparisons show that ZooA, LytM and lysostaphin share a show a conserved HXXXD, HXH active site (Figure 5-1). It can be seen in the sequence alignment that, unlike both LytM and lysostaphin, the cytotoxic domain of ZooA is at the N-terminus rather than the C-terminus of the protein. However previous work has shown that ZooA targets D-alanyl-D-alanine peptide bonds [104] and the D-alanyl-L-alanine bonds [100] within the peptidoglycan layer, this is in contrast to the activity of lysostaphin which is known to cleave the glycine-glycine cross-bridges of *Staphylococcal* peptidoglycan [97,104]. The preference for D-alanyl-D-alanine bonds and the ability to cleave nitrocefin suggests that ZooA is more similar in activity to a penicillin binding protein or ß-lactamase [104].

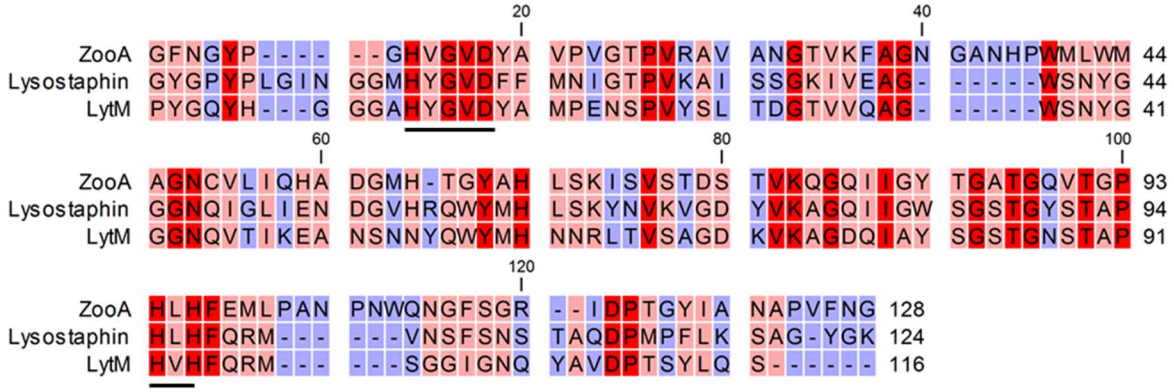

Figure 5-1 Amino acid alignment of conserved active sites of ZooA, lysostaphin and LytM. The conserved active site motifs are underlined with conserved residues in all three proteins in red, residues conserved in two proteins in pink and non-conserved residues in blue. Alignment of ZooA AA 37-162, lysostaphin AA 265-389 and LytM AA 199-315.

Recently a bacteriocin produced by GBS was discovered which is thought to be similar in structure and function to ZooA. This novel bacteriocin, named agalactitcin A, was shown to be targeted towards *S. agalactiae* strains when plated in direct contact with the producing strain (MRI Z2:09). This bacteriocin is predicited to be similar to zoocin A from *S. zooepidemicus* and therefore a potential novel therapeutic. The aim of this chapter is to characterise this bacteriocin, named agalacticin A, both biochemically and biophysically to examine its structure and mode of action.

5.2 Results

5.2.1 Agalacticin A

Agalacticin A and ZooA have a 58% sequence identity and show a high degree of sequence similarity in both the cytotoxic domain and TRD (Figure 5-2a). A molecular weight of 30.385 kDa was calculated for agalactin A from the amino acid sequence. This calculated weight is almost identical to the calculated weight of ZooA at 30.617 kDa (using protparam [152]). This, along with a high sequence similarity suggests a homology between ZooA and agalacticin A.

Both domains of ZooA have been structurally determined by NMR independently [99,183,184] and the overlapping region suggests a flexible linker joining the two domains. The recently solved NMR structure of ZooA (PDB ID 5KVP and 2LSO) suggests some regular secondary structure in the TRD, however the predicted model of agalacticin A suggests little regular secondary structure when modelled using I-TASSER [156]. This may be due to the lack of known homologues rather than the true lack of regular secondary structure suggesting that the model of this domain may be unreliable. However, the cytotoxic domain is similar in structure to that of both lysostaphin and LytM, consisting largely of ß-sheet.

When modelled the N-terminal cytotoxic domains of agalacticin A appears to be highly similar to the NMR structure of ZooA. This similarity is supported by the amino acid sequence alignment (Figure 5-2a). However, the TRD of each protein appears to be structurally dissimilar despite 50% sequence similarity (Figure 5-2b). The difference between the C-terminal domains may be due to their specificity to *Streptococcal* species, their lack of regular secondary structure or poor modelling of the Agalacticin A TRD due to the lack of known homologues.

a

b

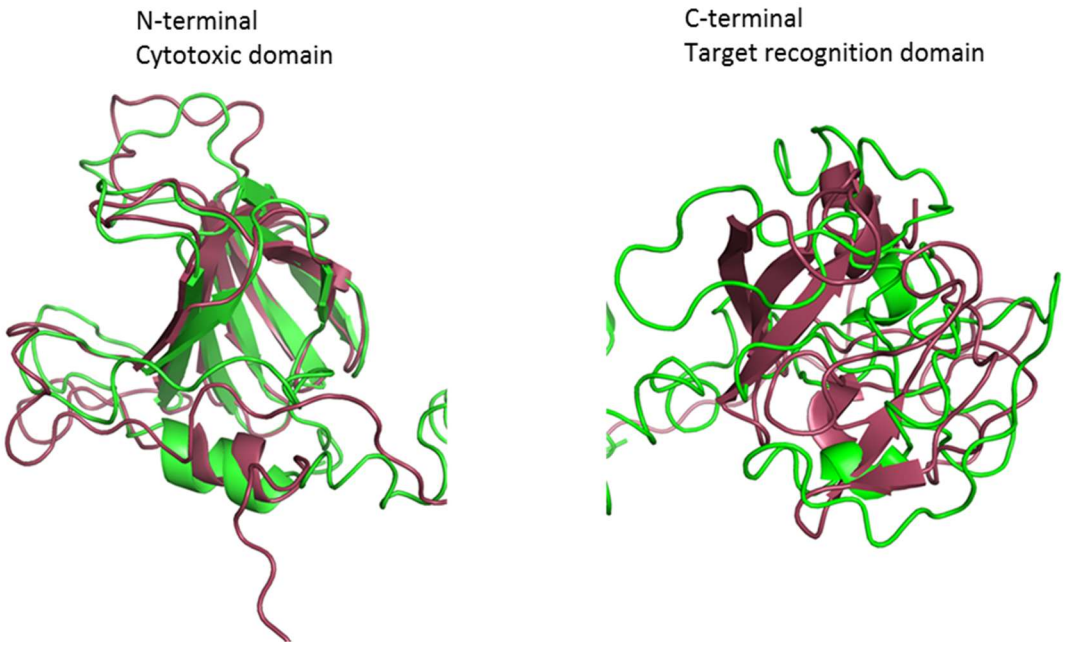

Figure 5-2 Sequence and structural alignments of agalacticin A from *S. agalactiae* and ZooA from *S. zooepidemicus*. a) Amino acid sequence alignment performed in CLC workbench with conserved residues shown in red. b) Structural sequence alignment of the I-TASSER model of agalacticin A (green) compared to the NMR structures of ZooA (pink). The N-terminal cytotoxic domain (PDB ID 5KVP) and the C-terminal target recognition domain (PDB ID 2LS0) performed in PyMOL. The alignment shows agalacticin A AA 1-146 align with the cytotoxic domain of ZooA and AA 164-272 align with the target recognition domain.

5.2.2 Agalacticin A is active against *S. agalactiae strains*

GBS are prevalent worldwide pathogens that cause disease in a wide range of hosts. Within recent years the prevalence of GBS isolates with either single or multidrug resistance is increasing [33]. Due to the wide host range it is important that novel antimicrobials can be used against a variety of isolates. The novel bacteriocin agalacticin A was recombinantly produced and was found to be effective against human, bovine and fish isolates.

Three strains were chosen for this work due to the diversity of their host species and sequence type (ST); STIR CD01 (fish, ST7), MRI Z1-354 (bovine, ST7) and MRI Z2-197 (bovine, ST67) hereafter known as CD01, 354 and 197 respectively. Preliminary work had shown that each of the strains chosen were susceptible to agalacticin A at nanomolar concentrations (Figure 5-3) with agalacticin A inhibiting growth at 250 nM in MRI Z1:354 and growth of both MRI Z2:197 and STIR CD01 inhibited at a concentration as low as 125 nM.

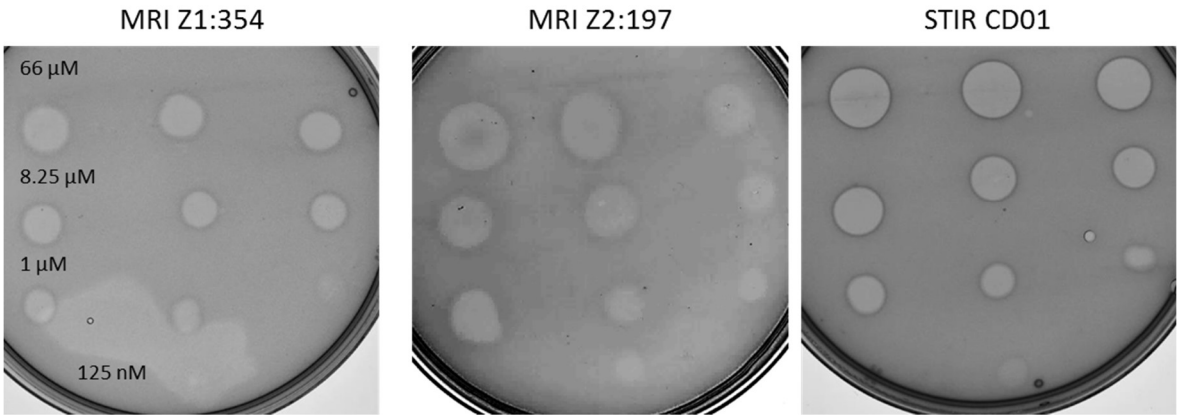

Figure 5-3 Spot test overlay of three GBS isolates with agalacticin A spotted at 2-fold dilutions from 66 µM to 125 nM. Overlay of GBS in 0.8% agar onto BHI agar incubated with 2 µl spots of agalacticin A overnight at 37°C.

The potency of agalacticin A in liquid culture was tested at a final concentration of 3 µM. Cells were grown to mid-log phase prior to the addition of agalacticin A and growth was monitored for a total of 8 hours. It can be seen in all strains (Figure 5-4) that growth was inhibited after the addition of agalacticin A.

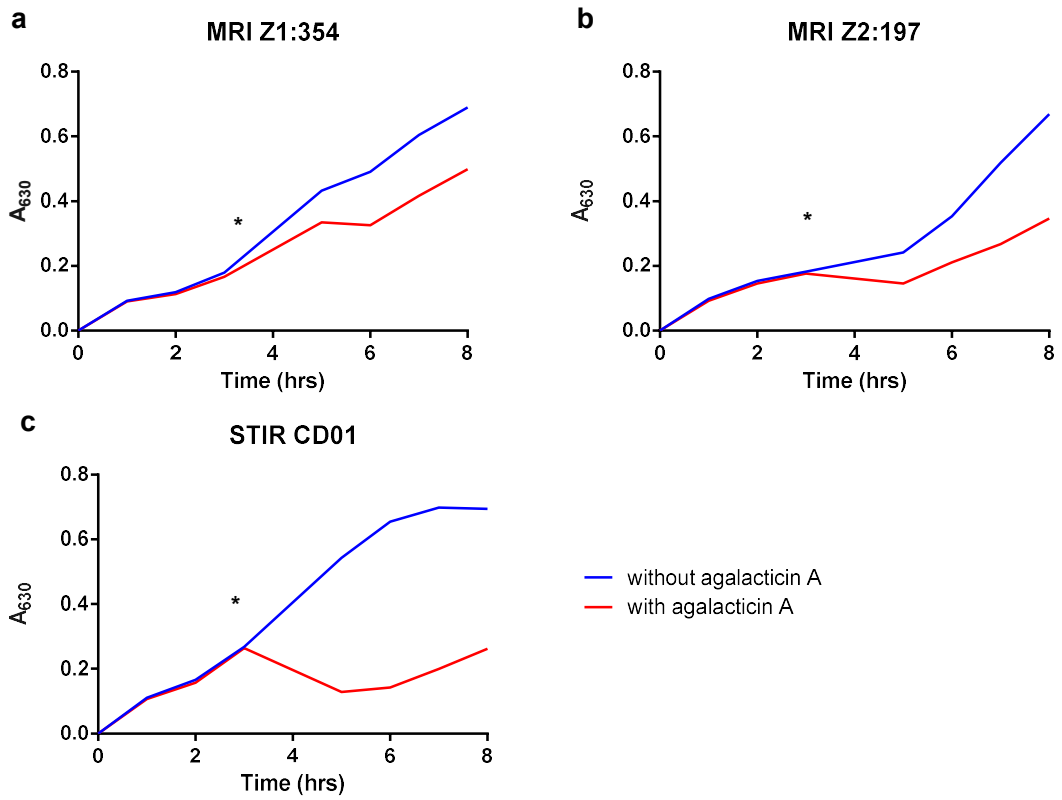

Figure 5-4 Liquid growth of GBS strains with (red) and without (blue) the addition of agalacticin A. Agalacticin A was added to cells in BHI after 3 hours (*) of growth at a final concentration of 3 μM. Growth of GBS MRI Z1:354 (a), MRI Z2:197 (b) and STIR CDO1 (c) was measured by optical density (at 600 nm) every 60 minutes. Growth curves were performed in triplicate with three technical replicates in each replicate.

As in solid media, the susceptibility to agalacticin A varies between isolates, however it can be seen within the liquid media that the fish isolate STIRCD01 is the most susceptible to agalacticin A (Figure 5-4) at a 3 μM concentration. It can also be seen that agalacticin A is able to reduce the growth of two isolates, CD01 and 197, at nanomolar concentrations showing a reduction in growth with 120 nm of agalacticin A (Figure 5-5).

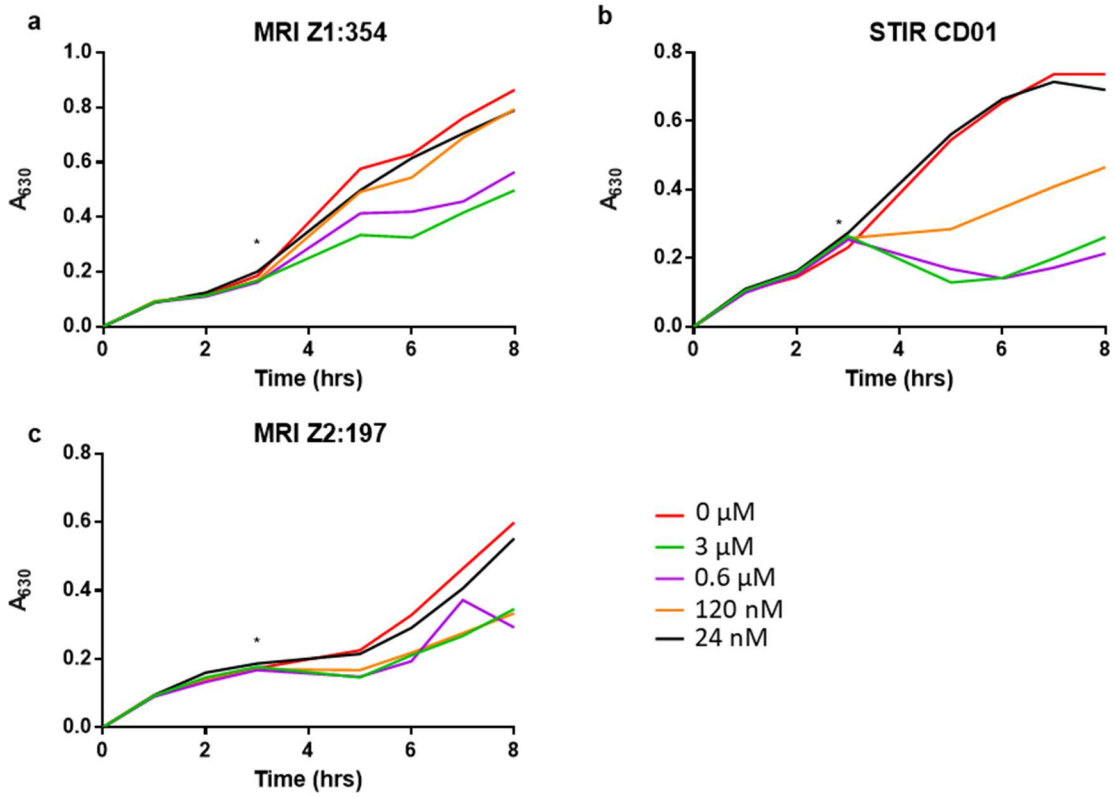

Figure 5-5 Liquid growth curves of GBS strains with different concentrations of agalacticin A. Agalacticin A was added to cells in BHI after 3 hours (*) of growth at a final concentration of 3 µM. a) MRI Z1:354 b) MRI Z2:197 and c) STIR CDO1 with agalacticin A added at mid-log phase (*) at final concentrations of 3 µM (green), 0.6 µM (purple), 120 nM (orange), 24 nM (black), no agalacticin (red). Growth curves were performed in triplicate with three technical replicates in each replicate.

5.2.3 Recombinant agalacticin A has enzymatic activity

5.2.3.1 *In vitro* β-lactamase activity assay

Agalacticin A is predicted to be similar in structure to lysostaphin and ZooA (see 5.2.5). Both proteins are known to act by cleaving the peptide bonds of peptidoglycan causing cell lysis. ß-lactamases are enzymes which cleave ß-lactam antibiotics, such as ampicillin or nitrocefin, by hydrolysing the ß-lactam ring. ß-lactam antibiotics mimic the structure of D-alanyl-D-alanine in order to interact with penicillin binding proteins to disrupt peptidoglycan synthesis. The hydrolysis of beta-lactam antibiotics can therefore be equated to the hydrolysis of the D-alanyl-D-alanine bond in the peptidoglycan layer, as suggested by Heath et al. (2004). Nitrocefin is a yellow coloured peptide antibiotic with a ß-lactam

ring which, when hydrolysed, changes colour to red, this change can be measured at a wavelength of 492 nM giving a quantitative measure of hydrolysis [185].

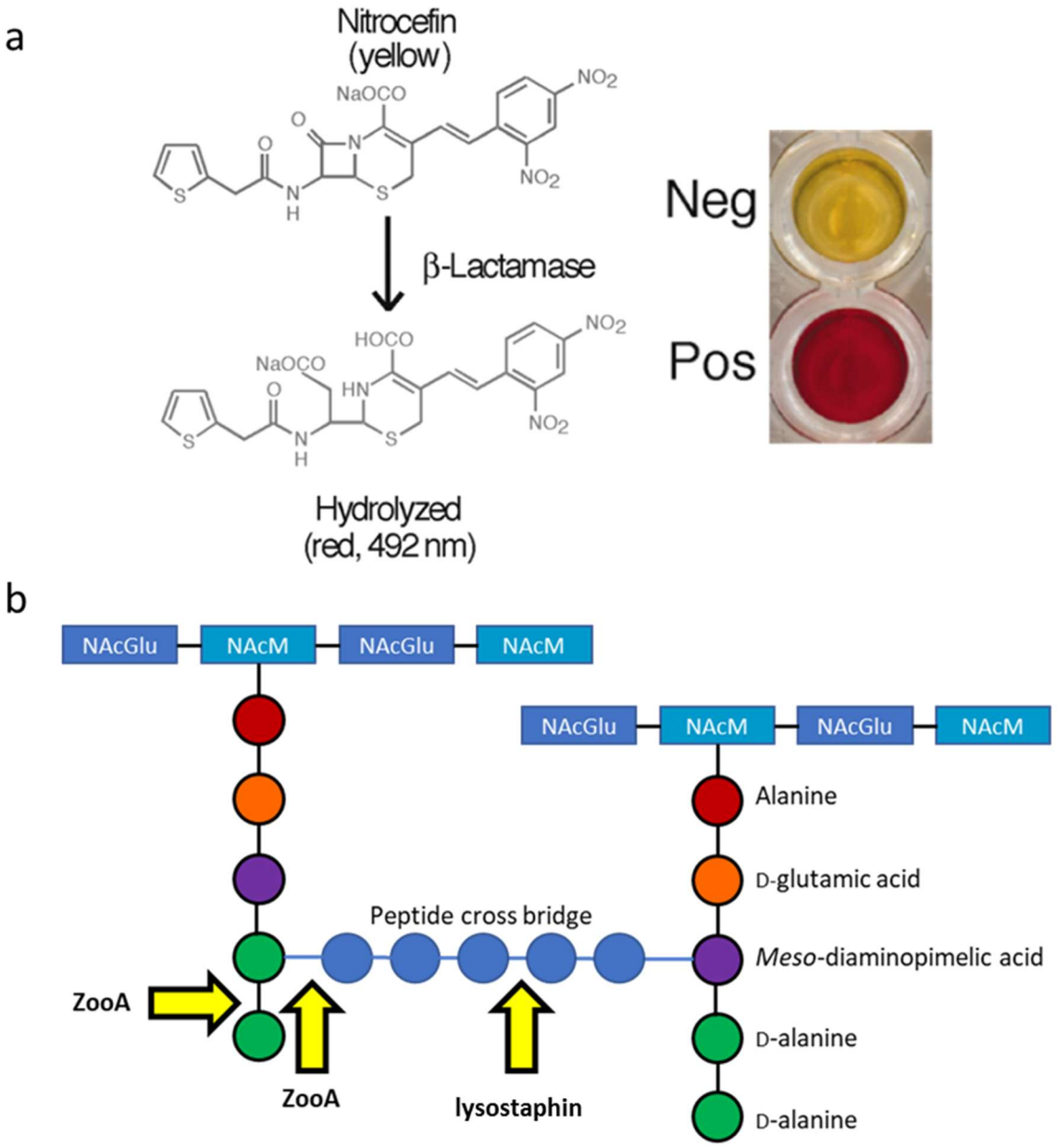

Figure 5-6: Schematic diagram to show the hydrolysis of nitrocefin and the points of hydrolysis on the peptidoglycan. a) Chemical reaction of nitrocefin from yellow to red with the addition of β-lactamases (reproduced from [185] with permission from the Nature publishing group). b) Schematic diagram of peptidoglycan highlighting the peptidoglycan cleavage sites of ZooA (D-ala-L-alanine) and lysostaphin (glycine-glycine) (adapted from [96] under a creative commons licence).

Previous work by Heath et al (2004) showed that ZooA could cleave nitrocefin in a dose-dependent manner, supporting the hypothesis that ZooA acts like a penicillin binding protein and can cleave D-alanyl-D-alanine peptide bonds within peptidoglycan [104]. Recombinant agalacticin A was incubated with nitrocefin for 30 minutes and the absorbance at 490 nM was measured.

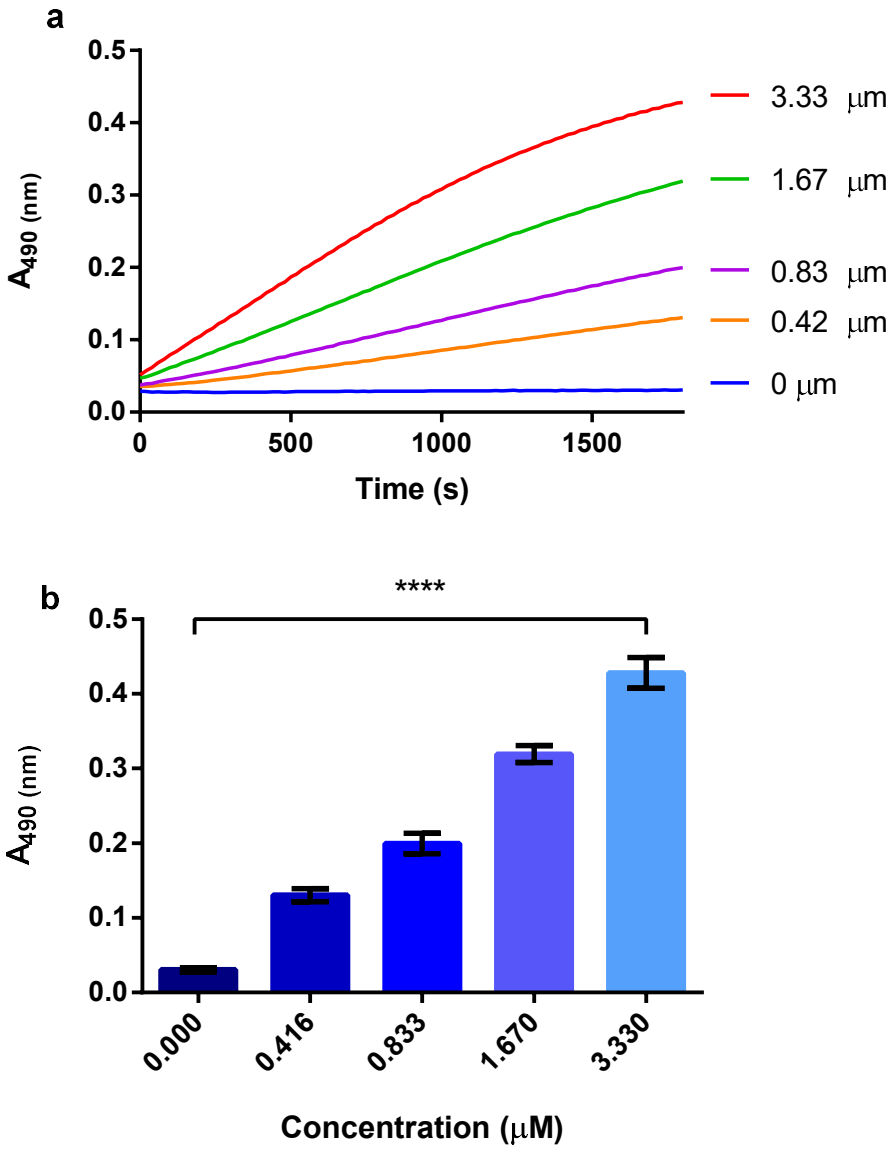

Figure 5-7 Nitrocefin cleavage by agalacticin A shows a concentration dependent hydrolysis of the β-lactam ring. a) Nitrocefin hydrolysis by agalacticin A at 3.33 μM (red), 1.67 μM (green), 833 nM (purple), 416 nM (orange) and in the absence of agalacticin A (blue). b) Absorbance at 490 nM of nitrocefin after 30 minutes of incubation with agalacticin A showing a significant difference ($p < 0.0001$) when all conditions were compared (ANOVA). Multiple comparisons (Bonferroni correction) show a significant difference ($p < 0.001$) between every condition. Absorbance was measured at 490 nm rather than the optimal 492 nm due to limitations in the plate reader filters.

It can be seen in Figure 5-7 that when incubated with agalacticin A the ß-lactam ring of nitrocefin is hydrolysed, as indicated by the increase in absorbance at 490 nm. After incubation with agalacticin A for 30 minutes the absorbance at 490 nm was seen to be significantly different between each of the concentrations of agalacticin A, showing that agalacticin A hydrolyses nitrocefin in a dose-dependent manner (Figure 5-7b). These results suggest a similarity in the mechanism of action between ZooA and agalacticin A [104]. These data show that recombinant agalacticin A is enzymatically active *in vitro* and acts in a similar way to ZooA by hydrolysing peptide bonds. It has previously been suggested by Xing et al. (2017) that the catalytic domain of ZooA can hydrolyse the D-alanyl-L-alanine peptide bonds within the *Streptococcal* peptidoglycan. Due to the similarity of the nitrocefin structure to peptide bonds it can be predicted that agalacticin A is likely to act by hydrolysing peptide bonds within the *Streptococcal* peptidoglycan.

5.2.4 Predicted structural model of agalacticin A

After the discovery of the producing strain *S. agalactiae* MRI Z2-093, agalacticin A was initially examined bioinformatically using sequence and structural alignments. It was discovered that agalacticin A was a homologue of ZooA with an N-terminal cytotoxic domain and a C-terminal target-recognition domain (Figure 5-8). The model, created using I-TASSER, suggested that the N-terminal cytotoxic domain is similar in structure to other M23 metalloproteases, such as lysostaphin; however, the TRD shows little regular secondary structure and no close homologues (Figure 5-8).

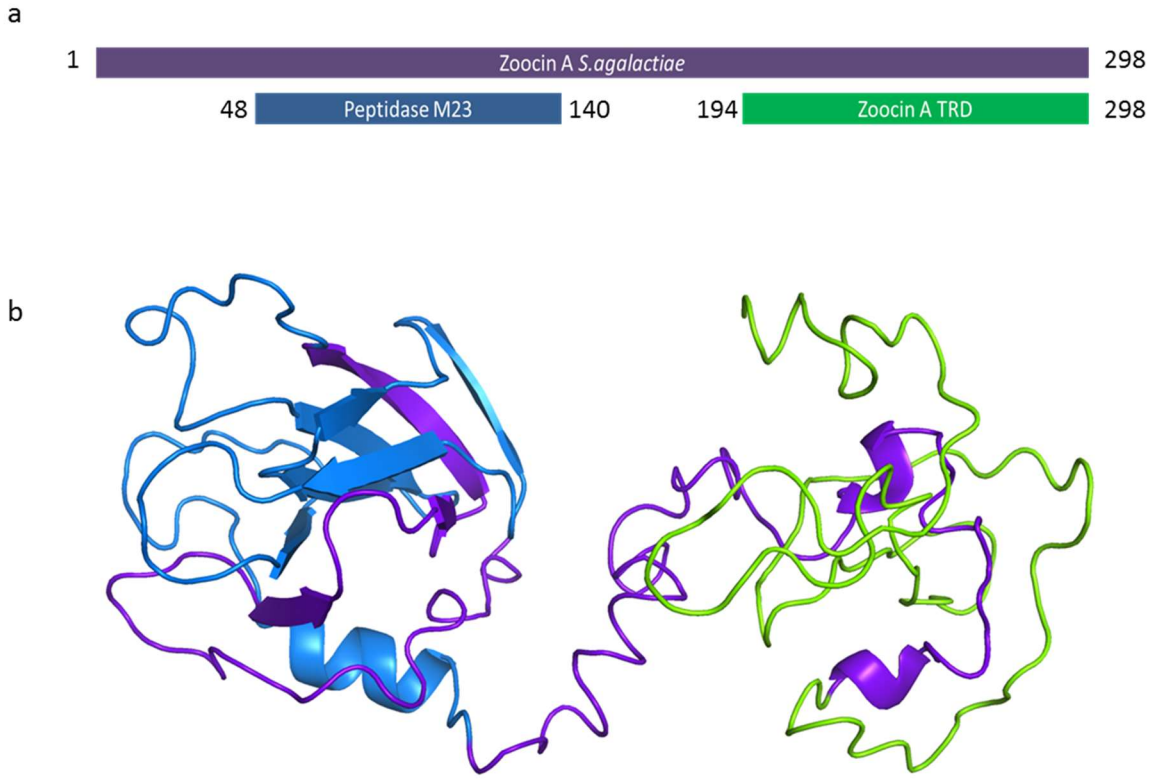

Figure 5-8 Sequence alignment shows similarities to both M23 peptidases and the target recognition domain of ZooA. a) Schematic diagram showing homologous proteins for both the N- and C-terminal domains. b) I-TASSER model highlighting the amino acids homologous to an M23 peptidase in the N-terminal (blue) and the target recognition domain of ZooA (green).

Agalacticin A from GBS has the characteristic cytotoxic domain, with the same HXXXD, HXH active site motif in the N-terminal cytotoxic domain. As with ZooA, LytM and lysostaphin the cytotoxic domain of agalactin A is predicted to be structurally and functionally similar to an M23 metalloprotease and zinc dependent. Classical amino acid sequence alignments show a small amount of similarity between agalacticin A and lysostaphin with only around 25% sequence identity. However, when a structural sequence alignment is performed with the I-TASSER model of agalacticin A and lysostaphin it is clear that despite the sequence disparity they are predicted to be structurally similar (Figure 5-9). This was also seen with an alignment of the NMR structure of ZooA and lysostaphin (not shown). This structural similarity further supports the idea that agalacticin A may be homologous in activity to both ZooA and lysostaphin.

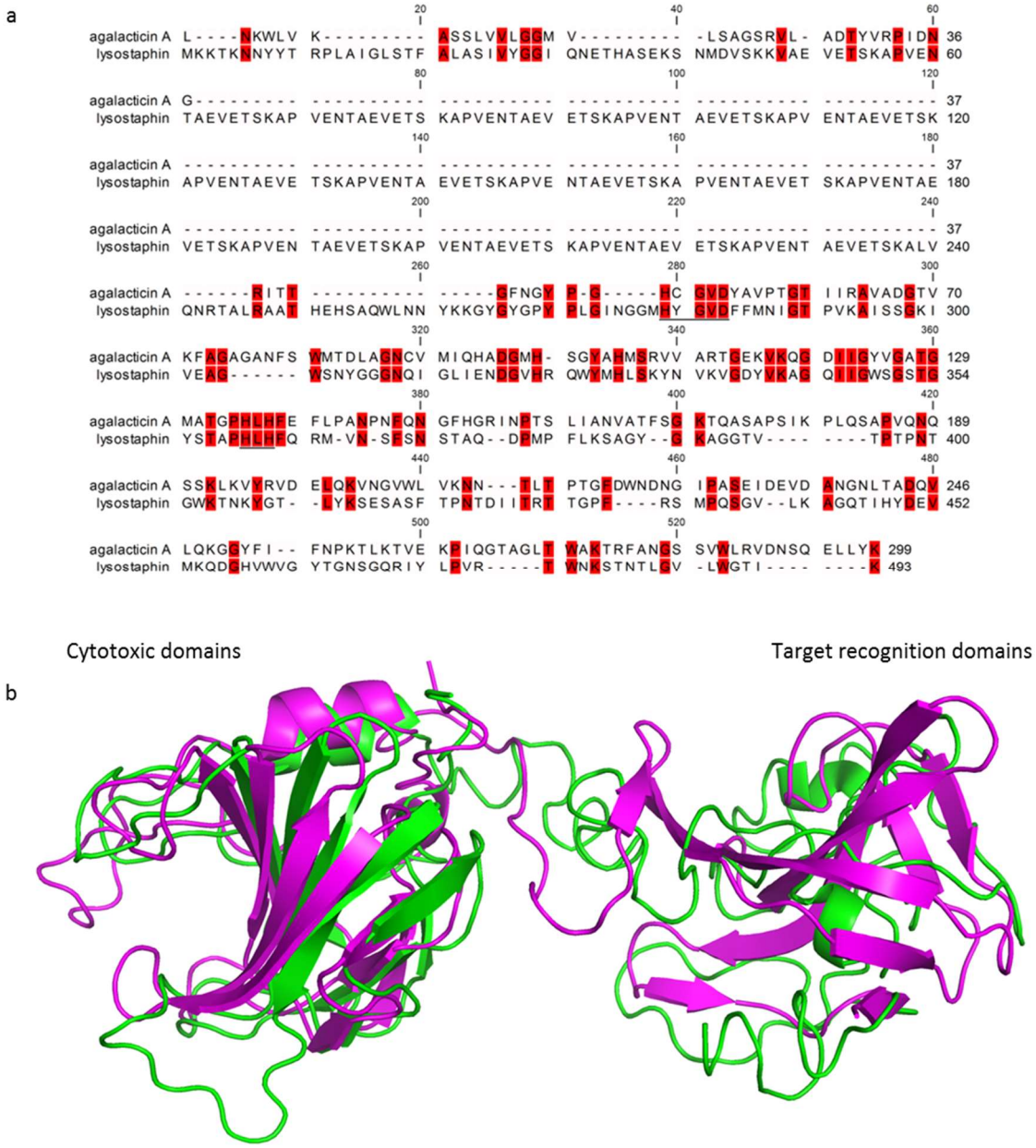

Figure 5-9 Structural alignment of lysostaphin in pink (PDB ID 4LXC) and I-TASSER model of agalacticin A (green) showing structural similarity in the cytotoxic domains and dissimilarity in the TRD. a) Amino acid sequence alignment performed by CLC workbench with conserved residues highlighted in red and the active site motifs underlined. b) PyMOL was used to structurally align the I-TASSER model of agalacticin A and lysostaphin (PDB ID 4LXC) based on the secondary and tertiary structures. The cytotoxic domain shows an alignment of the C-terminal domain of lysostaphin is aligned with the N-terminal domain of agalactin A, the TRD shows the alignment of the C-terminal of agalacticin A and the N-terminal of lysostaphin.

5.2.5 Structural characterisation of agalacticin A

5.2.5.1 Analytical ultracentrifugation

NMR spectroscopy has previously been used to solve the structures of the TRD and cytotoxic domains of ZooA individually, however no work to date has examined the interaction between these domains or the overall protein structure [99,183]. Recent work examining lysostaphin has shown that the flexible inter-domain linker region allows the two domains to move independently, giving elongated and compact conformations [97]. The current model of agalacticin A is similar to that of both ZooA and lysostaphin, which suggests that it might be flexible and potentially elongated in solution.

In order to confirm that agalacticin A is monomeric in solution, as predicted, sedimentation velocity AUC was used to examine the oligomeric state of the protein. Agalacticin A was tested at a range of concentrations from 0.3 to 1.5 mg ml^{-1} at 49000 rpm and the sedimentation coefficient for each was determined. Data acquired at three representative concentrations are shown in Figure 5-10.

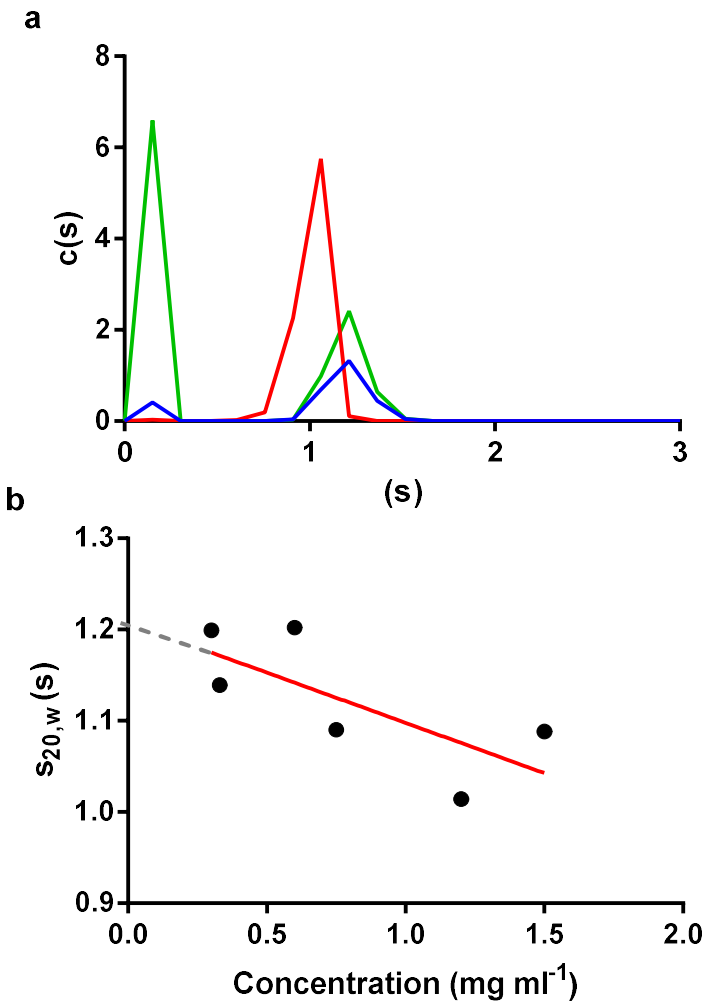

Figure 5-10 AUC analysis of agalacticin A shows the particle is monodisperse in solution a) Continuous c(s) distributions for agalacticin A at concentrations of 1.2 mg ml^{-1} (red), 0.6 mg ml^{-1}(green) and 0.3 mg ml^{-1} (black) at 4°C. b) Extrapolation of sedimentation coefficients corrected to standard conditions ($s_{20,w}$) give an $s^0_{20,w}$ of 1.205.

The sedimentation coefficient for each concentration was calculated in order to extrapolate to the absolute sedimentation coefficient ($S^0_{20,w}$), which was determined to be 1.21.

To assess how well the experimental data correspond to the I-TASSER model of agalacticin A, hydrodynamic bead modelling was used to examine the hypothetical sedimentation coefficient and radius of gyration (R_g) of the model. Hydrodynamic calculations were performed using US-SOMO [149] in which each atom within a structure is replaced by a bead, i.e. a bead to represent the main chain and a separate bead for the side-chain of the amino acid residues. The

volume of the bead is calculated based both on the residue and the amount of hydration predicted for that residue [149].

The hydrodynamic bead model of agalactin A gave a predicted sedimentation coefficient of 2.82 *s* and a predicted R_g of 23.7 Å. This predicted sedimentation coefficient is greater than the experimental $S^0_{20,w}$ of 1.21 *s*. This lower experimental value suggests that agalacticin A may be more flexible in solution than the model predicts. Moreover, agalacticin A could be found in multiple conformations, some of which may be elongated. The continuous *s* distribution confirms that agalactin A is monomeric and therefore is a good candidate for small angle X-ray scattering (SAXS).

5.2.5.2 SAXS analysis of agalacticin A

Results from the AUC experiments suggested that there was the potential for agalacticin A to be flexible or in multiple conformations. Small angle X-ray scattering (SAXS) was used to determine both the overall structural envelope of agalacticin A as well as the inter-domain flexibility.

Scattering data were obtained at concentrations of 10, 5, 2.5 and 1.25 mg ml^{-1} using a bioSAXS robot and 45 µl of each sample was analysed. The quality of the data was analysed by examining the excess kurtosis of each frame. The excess kurtosis is a way of examining the data set corresponds to a normal, expected distribution. If the excess kurtosis suddenly increases this suggests that the sample is radiation damaged and the frames after this increase are omitted. Agalacticin A at 2.5 mg ml^{-1} was analysed as this sample generated the best quality scattering data and the largest number of frames without radiation damage (Figure 5-11). Scattering data for Agalaciticin A was also collected using SEC-SAXS to confirm the bioSAXS data. As the scattering data was identical to the data presented here it is not shown.

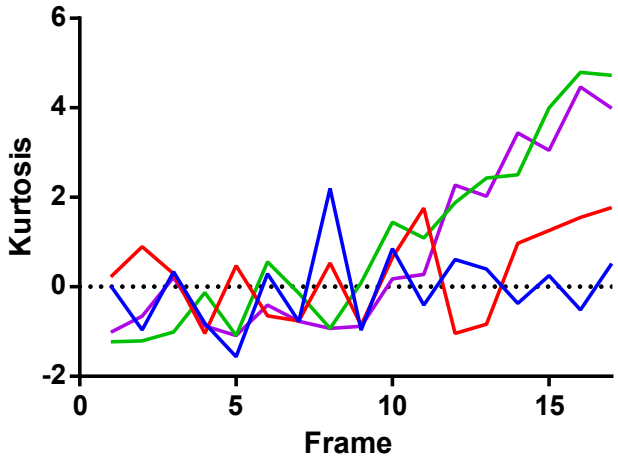

Figure 5-11 Measure of the excess kurtosis for each scattering frame for agalacticin A at four concentrations. Excess kurtosis for each frame was measured for agalacticin A at 10 mg ml^{-1} (purple), 5 mg ml^{-1} (green), 2.5 mg ml^{-1} (red) and 1.25 mg ml^{-1} (blue).

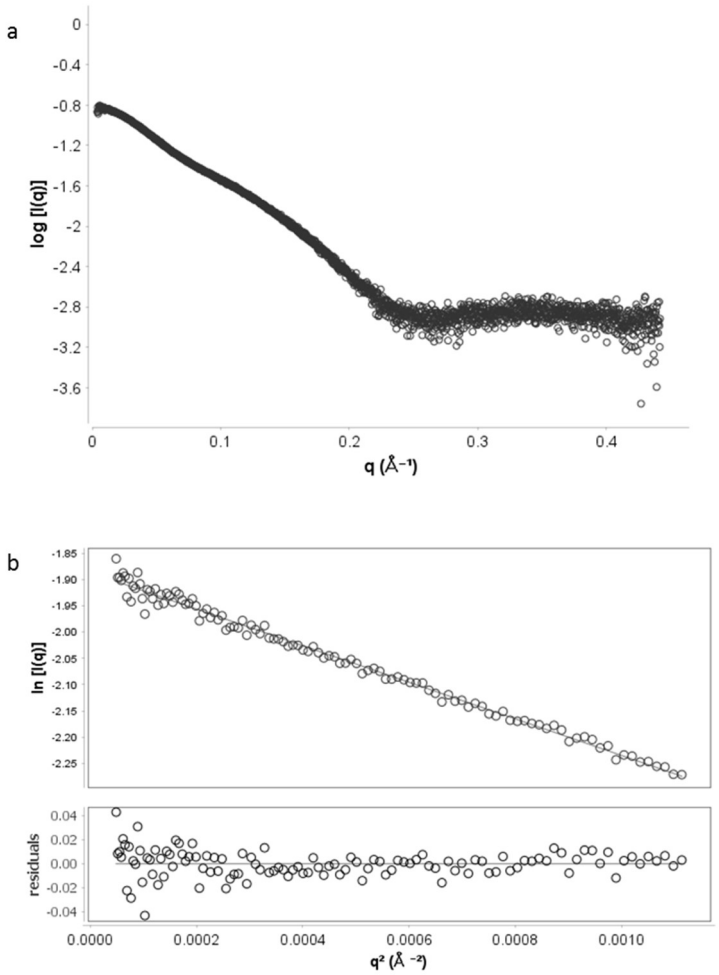

Figure 5-12 Scattering data obtained for agalacticin A (2.5 mg ml^{-1}) show a non-aggregated sample a) q vs log I(q) b) Guinier analysis of the low q range suggests a Rg of 31.9 Å.

Guinier analysis of agalacticin A (Figure 5-12b) gives a predicted molecular weight of 29.9 kDa which is similar to the molecular weight calculated from the sequence, of 30.4 kDa, suggesting that agalacticin A is monomeric in solution. However, the Guinier analysis also suggests a R_g of 31.9 Å which is larger than the predicted R_g of 23.7 Å from the hydrodynamic bead model [149]. This discrepancy between the theoretical and experimental R_g suggests that agalacticin A may be more elongated in solution than the model predicted. This could be due to the presence of the flexible linker region between the two domains (Figure 5-8).

5.2.5.3 In solution data suggest that agalacticin A is elongated and flexible

Kratky analysis examines the scattering data within the high q range in order to predict whether the protein is compact or intrinsically flexible in solution. If a particle is spherical the data will form a Gaussian distribution with the peak occurring around √3. The Kratky analysis of agalacticin A shows a Gaussian distribution, with the peak occurring at an R_g greater than √3 (Figure 5-13a). This suggests that the particle is structured but elongated in solution, which is consistent with the I-TASSER model of agalacticin A (Figure 5-8).

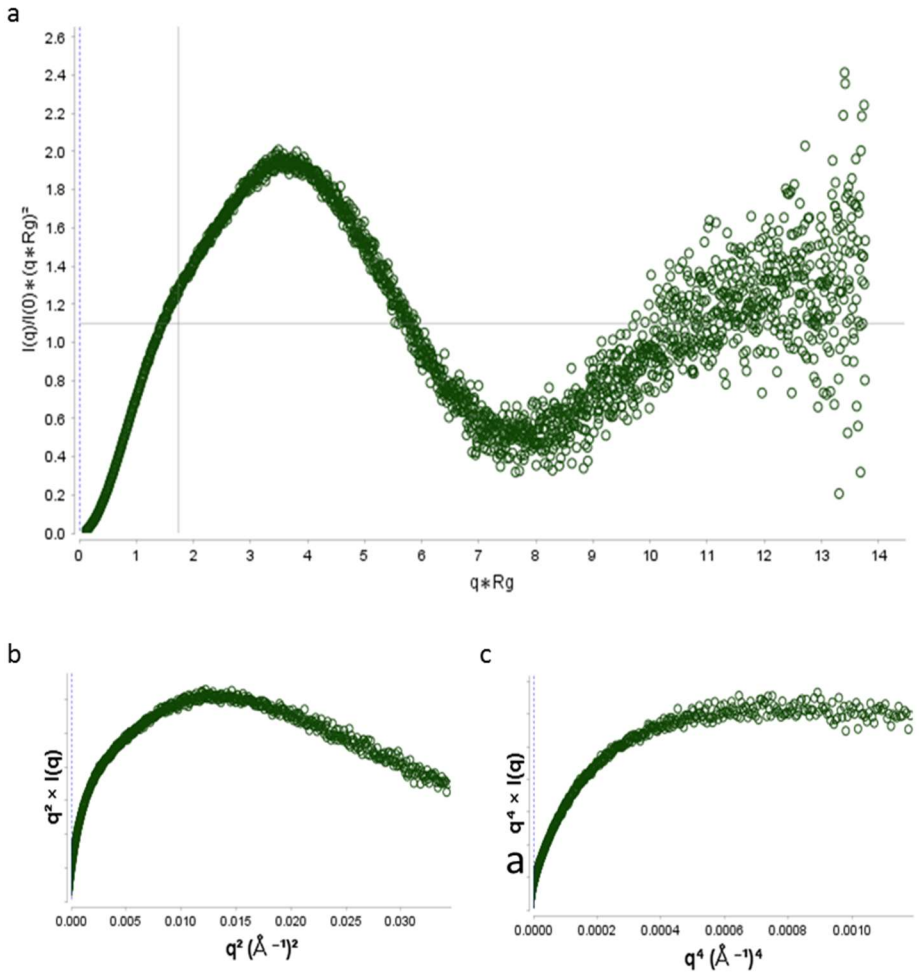

Figure 5-13 Flexibility analysis suggests agalacticin A is elongated and flexible in solution. a) Dimensionless Kratky analysis with √3 shown by crosshairs, as the peak of the data occurs at a greater value than √3 this suggests that the particle is elongated in solution b) Krakty-Debye plot and c) Porod-Debye plot at q= 0.1858 showing the plateau occurring first in the Porod-Debye plot suggesting the particle is flexible.

SAXS data can yield information about the flexibility and shape of a particle in solution. By raising q to the powers of 2 and 4 and examining the data at the low q range the particle can be seen to be either flexible or compact in solution. The flexibility of agalacticin A can be determined by examining the Porod-Debye plot (Figure 5-13c) and the Kratky-Debye plot (Figure 5-13b) in conjunction. By lowering the q value, the plot which plateaus at the highest q value can be used to classify the protein as flexible or compact. It can be seen in Figure 5-13 that the plateau first occurs in the Porod-Debye plot (Figure 5-13c) suggesting that agalacticin A is flexible.

5.2.5.4 Low resolution structure of agalacticin A

A dummy atom model of agalacticin A was created based on the pair-set p*(r)* distribution of the particle using DAMMIF (Figure 5-14). This distribution is created through an indirect Fourier transformation of the scattering data by which the maximum dimensions (D_{max}) of the particle can be found.

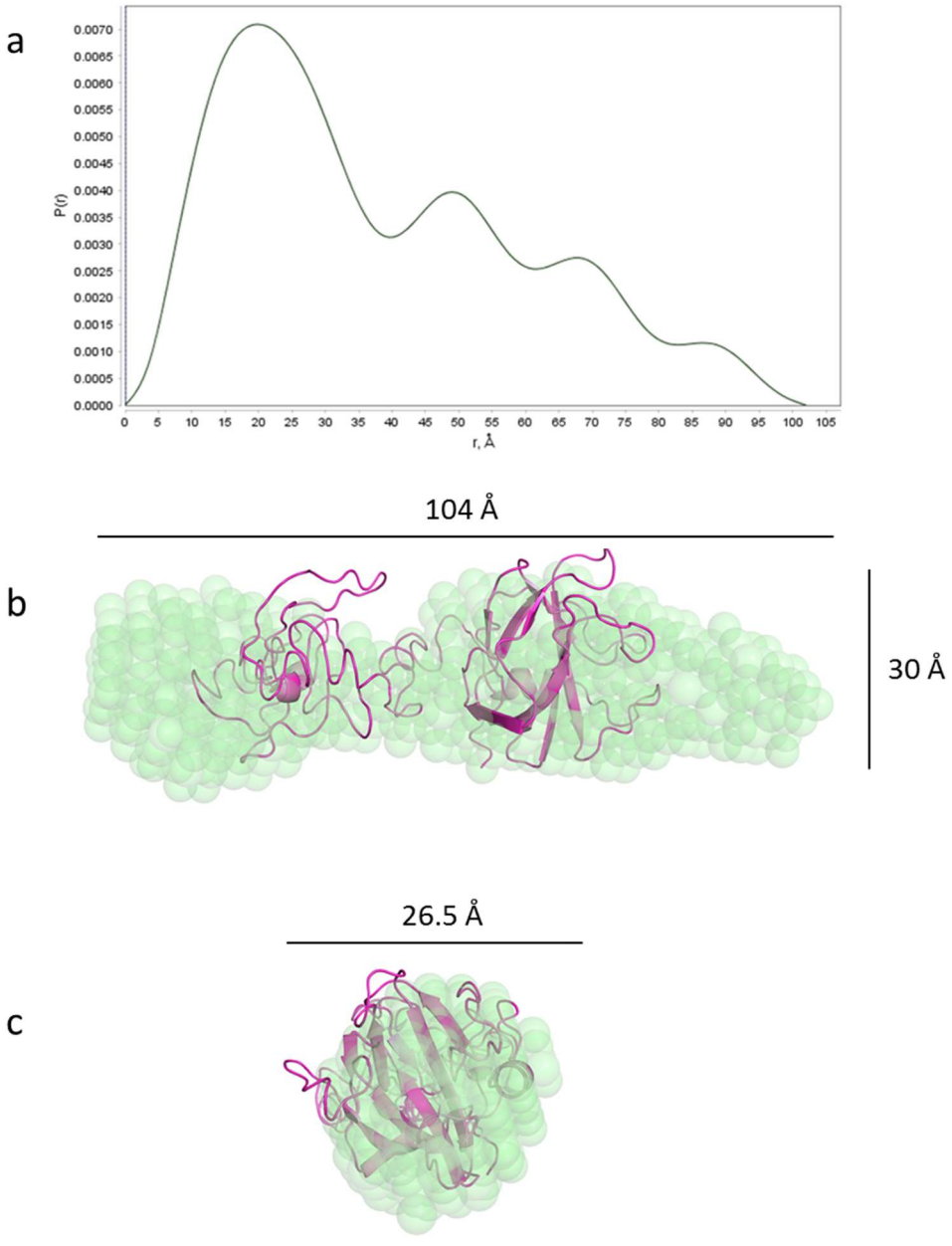

Figure 5-14 DAMMIF model of Agalacticin A a) p(*r*) distribution for agalacticin A scattering data showing a D_{max} value of 108 Å b) and c) DAMMIF model of agalacticin A (green) overlaid with the I-TASSER model of agalacticin A (pink) using SUPCOMB showing the similarity in structure with the C-terminal TRD on the left hand side and the compact N-terminal cytotoxic domain on the right hand side with the two dimensional measurements shown.

The p(*r)* distribution of the particle gave a D_{max} of 108 Å which is longer than the predicted model at approximately 74 Å in length. Due to the difference between the experimental D_{max} and the dimension of the I-TASSER model, this further suggests that agalacticin A may be elongated in solution or in multiple conformations. The undulations in the p(*r*) distribution are consistent with the domain separation shown in the model but may also suggest that the particle is found in multiple conformations within solution.

The N-terminal domain of agalacticin A is thought to be structured and compact, like the cytotoxic domains of other M23 metalloproteases such as lysostaphin. The flexible linker region between the two domains is unstructured and therefore it is likely to be flexible and the potential for elongation around this region. This is consistent with the SAXS data which shows agalacticin A is flexible in solution.

5.2.5.5 SAXS data suggest a flexible linker region

SAXS analysis of agalacticin A suggests that agalacticin A is both flexible and elongated in solution. Previous work has suggested that the linker region may be flexible due to the abundance of proline and threonine residues [184]. Ensemble optimisation modelling (EOM) was used to examine the inter-domain flexibility (see Chapter 3) around the flexible linker region to determine if this allows for the movement of each of the domains independently.

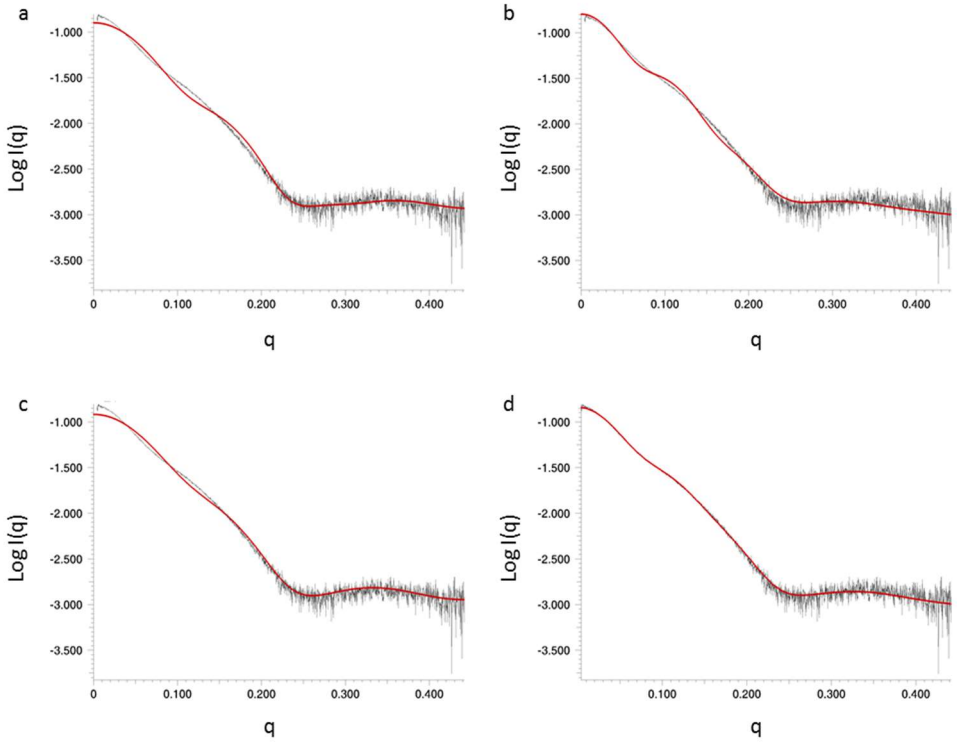

Figure 5-15 CRYSOL fit to experimental SAXS data from models of agalacticin A in multiple conformations. Predicted SAXS curves (red) for each predicted model and a combination of models were compared with the experimental SAXS curves (black). a) Compact model of agalacticin A, X^2= 51.925 b) Elongated model of agalacticin A X^2=23.807 c) I-TASSER model of agalacticin A, X^2= 52.557 d) Combined models of agalacticin A calculated by EOM, X^2= 3.407.

CRYSOL was used to examine the fit of the current predicted agalacticin A model to the SAXS data, as well as modelling two other predicted conformations and a population in multiple conformations to determine the best fit. The results shown in Figure 5-15 show that the best fit to the experimental data comes from a population in multiple conformations. The best fit to the experimental data for agalacticin A was calculated using EOM, modelling multiple conformations of agalacticin A giving a fit with a X^2 value of 3.407 (Figure 5-15d).

The pool of EOM models has D_{max} values that range from 63 Å to 105 Å, however it is clear from the frequency distribution that agalacticin A can be found in two distinct populations in solution (Figure 5-16). The compact population shows a peak D_{max} of 78.5 Å whilst the other peak suggests an elongated population with the peak occurring around 101 Å (Figure 5-16). Furthermore, the R_g for these two populations clearly support both the predicted I-TASSER model of agalacticin

A with a peak R_g of 25 Å, similar to the hydrodynamic model prediction of 23.4 Å as well as the experimental data showing a R_g of 33 Å which is similar to the experimental R_g of 31.4 Å.

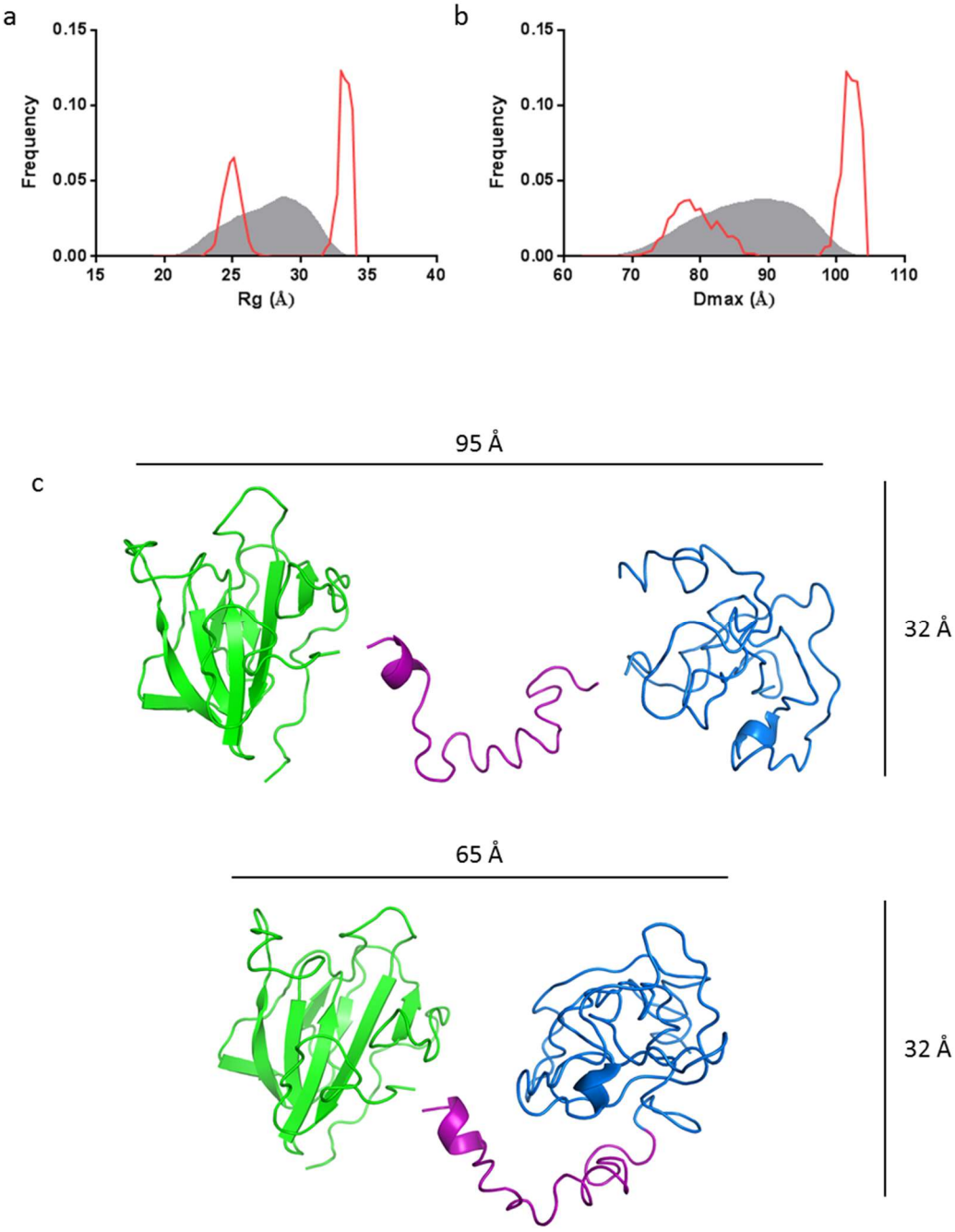

Figure 5-16 EOM modelling of agalacticin A suggests that it is flexible and elongated in solution. a) R_g and b) D_{max} population of the EOM models which best fit the experimental data (red) shown in comparison to the pool of generated models (grey) showing two distinct populations c) Cartoon representations of the elongated and compact models representing the two EOM populations with the cytotoxic C-terminal domain in green, flexible linker in purple and the TRD in blue.

These data, shown in Figure 5-16, further suggest the elongation and flexibility of agalacticin A are found within the flexible linker region. The representative models of the two EOM populations show a compact structure, similar to the I-TASSER model of agalacticin A (Figure 5-16c) and an elongated structure with the flexible linker region predicted to be extended.

Elastic network modelling (ENM) was used to compute the normal modes of agalacticin A [186]. ENM uses computational modelling to determine potential conformational changes of a molecule. Using this method, the flexibility of agalacticin A was found to be centred around the flexible inter-domain linker region, further supporting the model that agalacticin A may become compact and elongated around this central region (Figure 5-17).

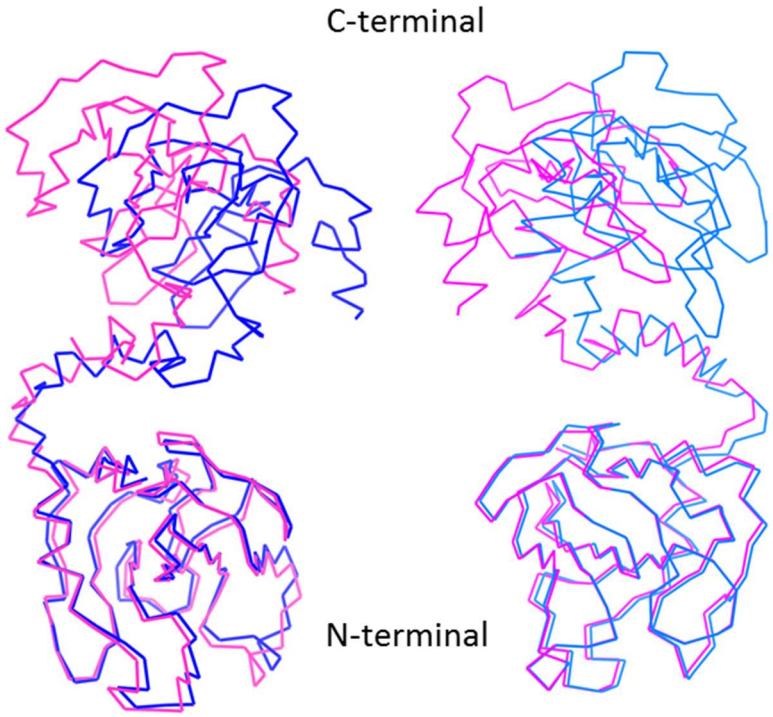

Figure 5-17 Illustration of the elastic network modelling conformational changes suggesting the movement of domains around the flexible linker region. ENM was conducted using ELNemo [186] to determine the potential conformational changes of agalacticin A. Two representative models are shown here with the N-terminus of each of the extreme conformational changes aligned to show the movement of the C-terminal domain around the flexible linker region.

5.2.5.6 Crystallisation trials

A high-resolution structure of agalacticin A has yet to be solved and therefore crystal trays were set up for agalacticin A at both 10 mg ml^{-1} and 5 mg ml^{-1}. Optimisation trays PACT, JSCG, Morpheus and Memphsis were set up and incubated at 16°C and checked weekly for 2 months. After 2 months crystals started to appear however none of these grew large enough to collect a data set.

5.2.6 The active site of agalacticin A

5.2.6.1 Similar structural predictions

The active site of M23 metalloproteases has been characterised by the presence of a zinc ion co-ordinated by three histidines and an aspartic acid [95] found in two motifs (Figure 5-9). The NMR structure of the cytotoxic domain of ZooA (PDB ID 2LS0) was solved by Timkovich et al. (2017) showing the presence of a zinc ion in the predicted active site of ZooA. This conserved active site can be seen in the high-resolution crystal structure of LytM (PDB ID 4ZYB), NMR structure of ZooA and the I-TASSER model of agalacticin A. Therefore, it is predicted that the active site of agalacticin A will consist of the same residues as those found in other M23 metalloproteases (Figure 5-18).

A high-resolution structure of the M23 peptidase LytM, a homologue of the lysostaphin from *S. aureus* was published by Grabowska et al. (2015) showing the active site of LytM and the positions of each amino acid involved in both activity and zinc ion binding [94]. This active site has been shown to involve three histidine residues (H210, H291 and H293) and an aspartic acid (D214) which corresponds to the active site motifs shown in Figure 5-1 [94]. Using structural and sequence alignments the active site residues of agalacticin A were predicted to be H23, D27, H109 and H111 (Figure 5-18).

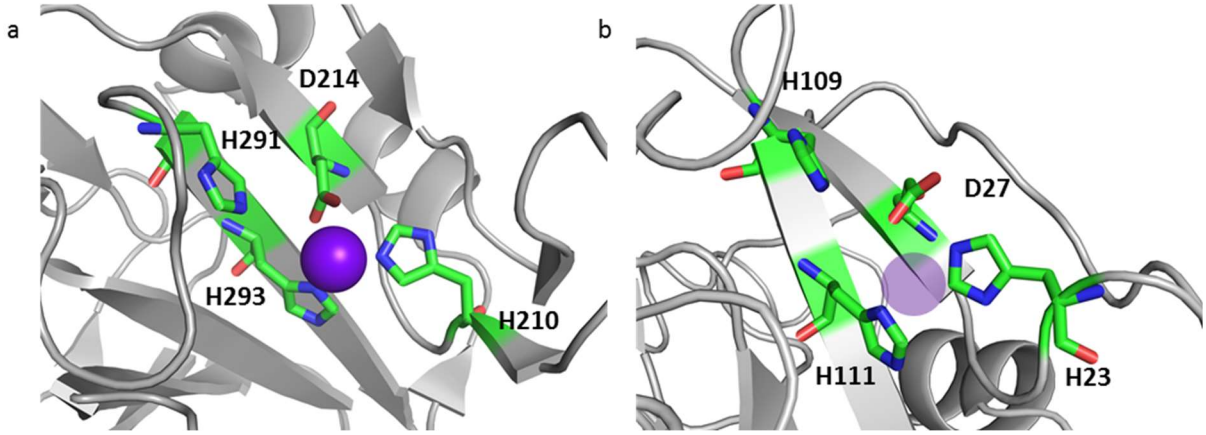

Figure 5-18 Cartoon representation of LytM and agalacticin A predicted active sites. a) High resolution structure of the active site of LytM with residues used in the active site shown as sticks, image adapted from Grabowska et al (2015) and reproduced under a creative commons license [94]. b) I-TASSER model of agalacticin with the predicted active site residues highlighted as sticks and labelled to compare with the LytM structure. The zinc ion is represented by a purple sphere.

Two active site residues, H23 and H109, were successfully mutated to alanine by site-directed mutagenesis as well as the non-active site residue C63. It was shown that these mutations had no effect on the overall protein structure (see 5.2.8). Previous work with ZooA had also mutated C74 (corresponding to C63 in agalacticin A) to create an active site more similar to that of lysostaphin, however this mutation had no effect on enzymatic activity. Initial tests of activity were performed against three GBS strains.

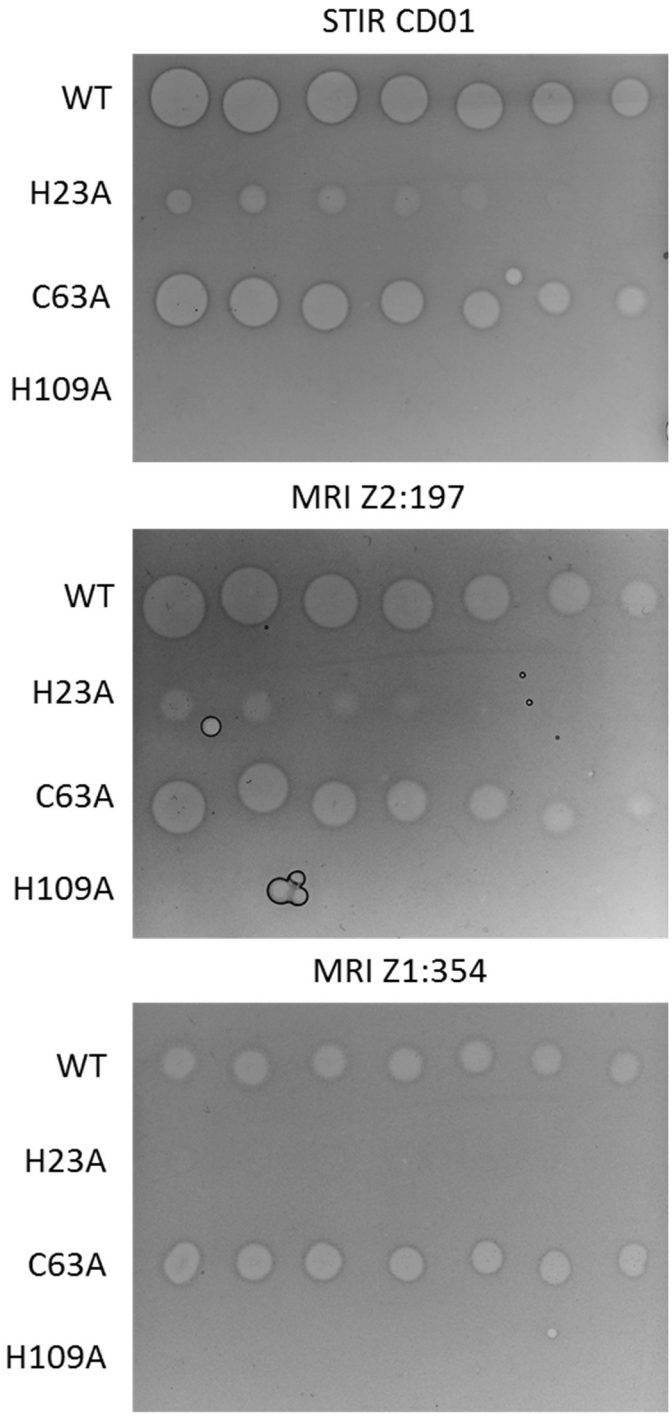

Figure 5-19 Soft agar overlays of three GBS species comparing the activity of mutant agalacticin A proteins. Overlays of GBS on BHI agar plates were spotted with 2µl of agalacticin A at 2-fold decreasing concentrations from left to right from 67µM -1 µM.

Initial tests showed no difference in potency for C63A compared to the wild-type (WT) agalacticin A, whereas there was a reduction in activity for both H23A and H109A against all three strains. The mutation at H109 completely eradicated activity (Figure 5-19) suggesting that it may be essential for activity. This supports the hypothesis that these residues are part of the active site of

agalacticin A. H23 and H109 correspond to H279 and H360 respectively in the LytM active site, further supporting the hypothesis that these are important for activity.

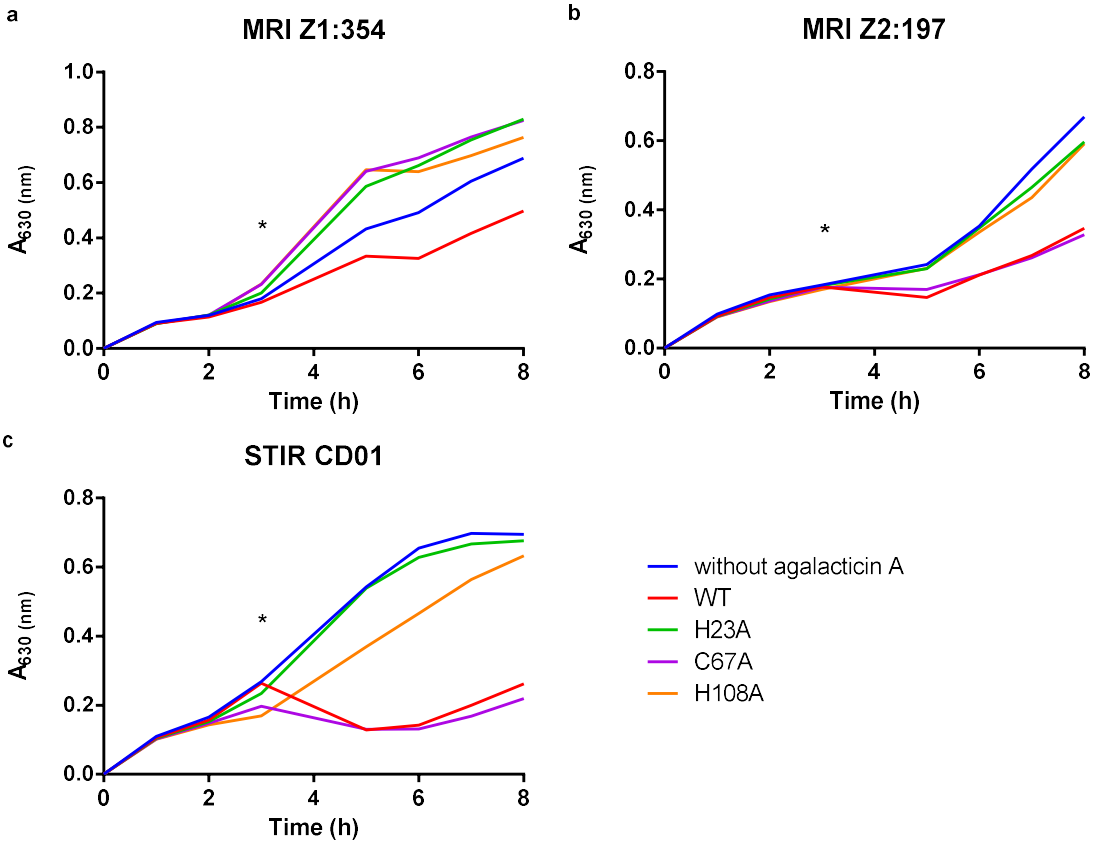

Figure 5-20 Growth curves showing the optical density of the three species of GBS in response to administration of WT and mutant agalacticin. MRI Z1:354 (a), MRI Z2:197 (b) and STIR CD01 (c) were grown in BHI with measurements taken at 630 nm for 8 hours total growth. Agalacticin A was administered at 3 μM total concentrations after 3 hours of initial growth (*). Growth was monitored without any agalacticin (blue) and in the presence of WT agalacticin (red), H23A (green), C63A (purple) and H109A (orange). Each growth curve was performed in triplicate with three technical replicates per replicate.

To test the activity of agalacticin A in liquid culture both the wild-type agalacticin A (WT) and mutants were added at mid-log phase of growth to each of the three strains. It can be seen that H109A and H23A do not inhibit the growth of any of the strains compared with the WT thus confirming that there is no difference in activity between liquid and solid media (Figure 5-20).

Interestingly C63A is active against both CD01 and 197 in liquid culture confirming the results of the solid agar test, but in liquid culture it is inactive against 354 which is contrary to the results shown in the spot-tests. This could potentially be due to small changes in the active site caused by the mutation. It is likely that there is some small difference in the protein which prevents it from effectively lysing the cells. Furthermore, this strain is the least susceptible to agalacticin A in both liquid and solid culture and therefore any disruption in activity could result in uninhibited growth.

5.2.7 *In vitro* assessment of enzymatic activity of agalacticin mutants

As previously shown in Figure 5-7, agalacticin A can hydrolyse nitrocefin, therefore the activity of agalacticin A mutants were tested in the same way. Agalacticin A and its mutants were incubated with nitrocefin for 30 minutes and the optical density at 490 nm was measured (Figure 5-21).

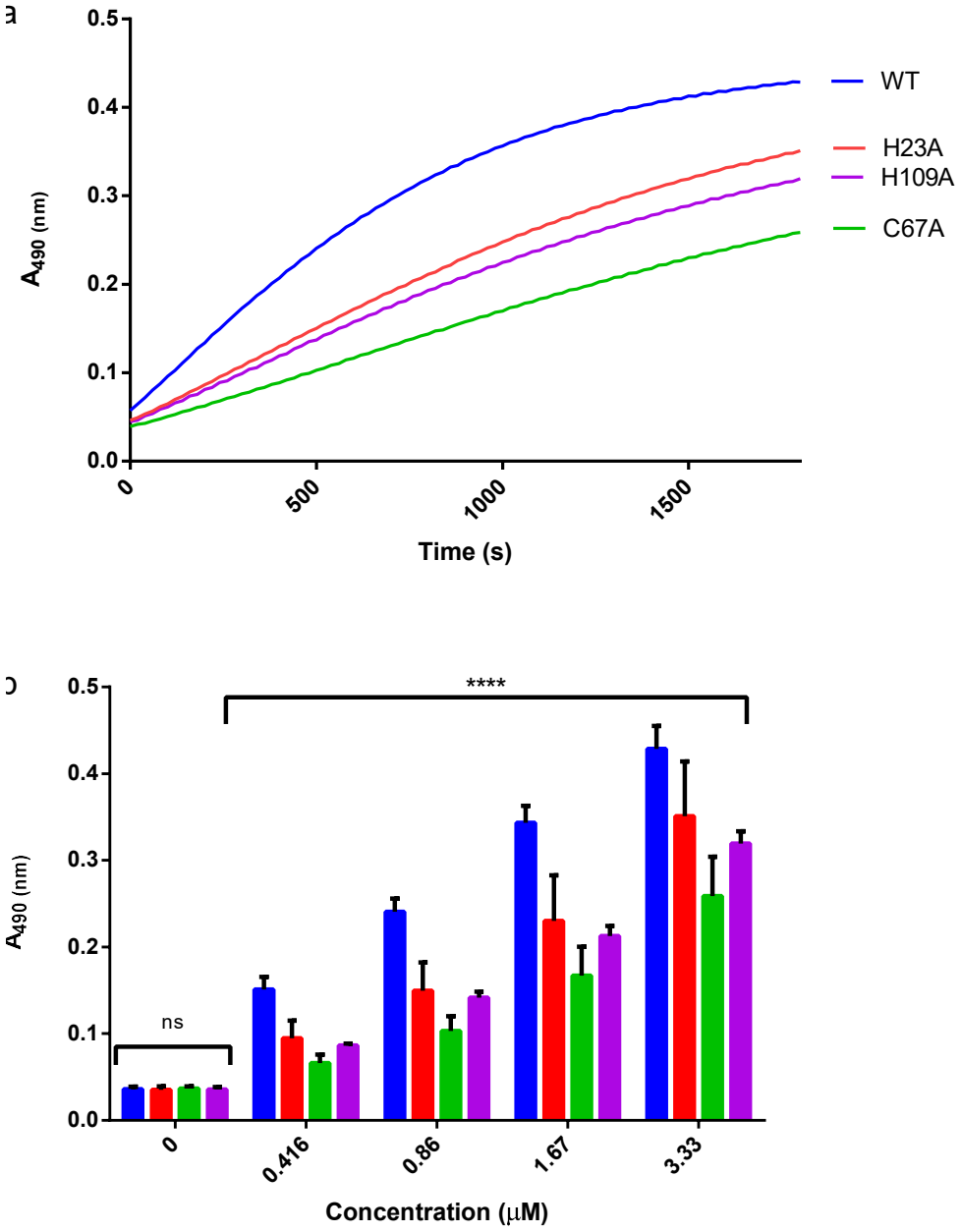

Figure 5-21 Nitrocefin degradation assay comparing WT agalacticin A with that of the mutants. a) Time course of nitrocefin degradation over 30 minutes at 37°C with 3.33 μM of agalacticin A(blue), H23A (red), C63A (green) and H109A (purple) with the absorbance measured at 490 nm. b) Absorbance values at 490 nm after incubation with agalacticin A(blue), H23A (red), C63A (green) and H109A (purple) at 4 concentrations of agalacticin A after 30 minutes. A significant difference ($p<0.0001$) was observed between each of the concentrations, multiple comparisons also showed a significant difference ($p<0.001$) between each of the mutants at each concentration, with the exception of 0 μM.

As with the WT, there is a dose dependent enzymatic rate at which each of the agalacticin A mutants hydrolyses nitrocefin (Figure 5-21). Interestingly, although

the nitrocefin assay confirmed a reduction in enzymatic activity of the mutants it did not fully confirm the results of both the spot tests and the liquid growth curves as each mutant had residual activity, including H109A.

H109A was inactive against all three strains of GBS in both solid and liquid media and it is apparent from the nitrocefin assay that it does retain some enzymatic activity, even at low concentrations, this activity is significantly lower than that of the WT. This suggests that although enzymatic activity with the single substitution is possible *in vitro*, the disruption in activity is too great to prevent lysis of bacterial cells.

Cytotoxicity assays show that agalacticin A with the C63A mutation was as potent against each strain of GBS as the WT, however it has been shown to have reduced enzymatic activity against nitrocefin *in vitro*. The amino acid substitution C63A was based on the work by Xing et al. (2017) who substituted the C74 residue of ZooA with an alanine to create an active site more structurally similar to that seen in lysostaphin. It was found by Xing et al. (2017) that this substitution had little effect on enzymatic activity based on the hydrolysis of purified peptidoglycans rather than ß-lactamase activity [100]. Lysostaphin is an endopeptidase which cleaves the amide bonds between the pentaglycine cross-bridges within a peptidoglycan, however it does not show any ß-lactamase activity due to its affinity for glycyl-glycine bonds [96,187,188]. It is clear from the nitrocefin assay that agalacticin A has ß-lactamase activity. This is consistent with the prediction that agalacticin A, like ZooA, hydrolyses the peptide cross-bridges within *Streptococcal* species as these are composed of alanine residues rather than the glycine residues found in *Staphyloccocus* peptidoglycan layers [189,190].

The alteration of C63 to an alanine residue shows no effect on activity *in vivo*, though within the nitrocefin assay there is a reduction in activity compared with both the WT and the other two mutations. The NMR structure of ZooA C74A [183] showed that this amino acid substitution increased the dimensions of the substrate binding groove. This disruption of the binding groove may explain the discrepancy between the *in vivo* and *in vitro* results due to slight differences in the bonds it may be targeting, however, there is no clear explanation for this

difference in activity. More work is needed to decipher this difference both biochemically and structurally as this still remains unclear.

5.2.8 Circular dichroism of mutants

Circular dichroism (CD) was used to compare the secondary (far UV) and tertiary (near UV) structure of WT agalacticin A with the mutant proteins to determine if the amino acid substitution had any effect on the structure (Figure 5-22).

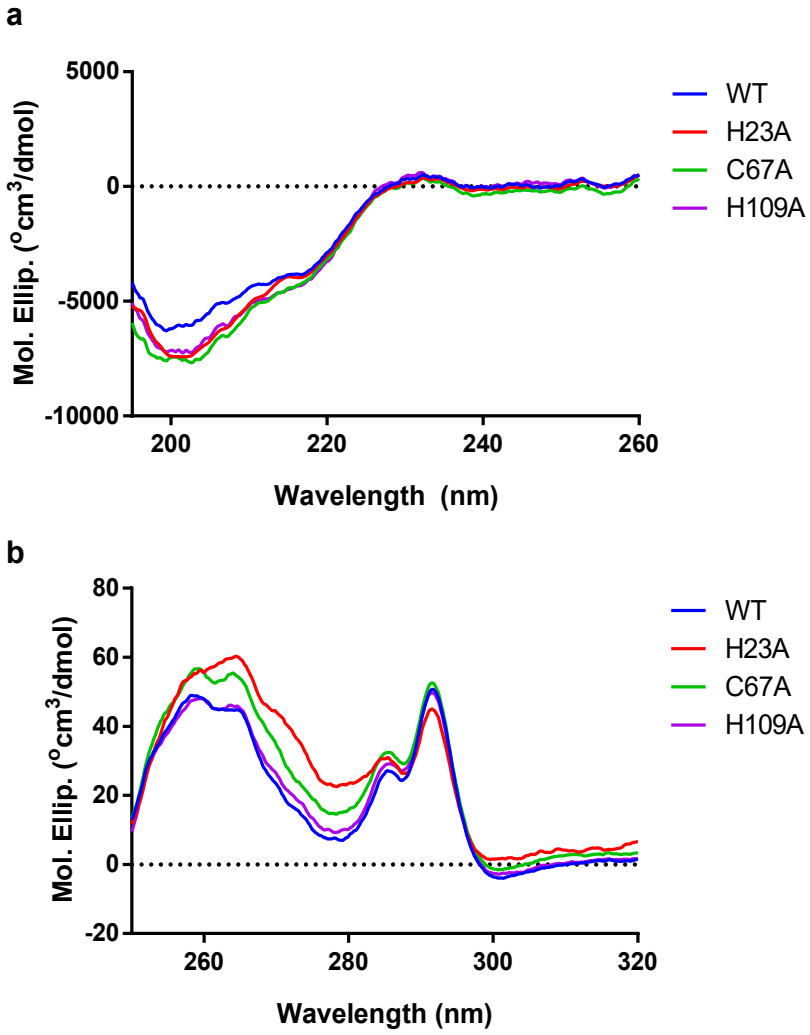

Figure 5-22: Circular dichroism spectra for agalacticin A and mutants in both far (a) and near (b) UV. Spectra for agalacticin A WT and mutants comparing the secondary and tertiary structures of the proteins of the WT (blue) against H23A (red), C63A (green) and H109A (purple) plotted against the molar ellipticity.

There are small differences in the secondary and tertiary structures of agalacticin A and the mutants, the difference seen in H23A may be explained by the positioning of the residue in the centre of a ß-strand, therefore the replacement of a histidine with an alanine in this position may cause some misfolding. The discrepancy in the secondary structure can be seen between the C63A, H23A and the WT protein, but there is no difference between the H109A and the WT protein. The lack of activity by the substitution of H109 with an alanine residue is therefore due to the single amino acid change rather than a difference in structure. The difference in far UV spectra between H23A and WT agalacticin is harder to explain without further biophysical characterisation.

5.2.9 *In vivo Galleria* model of agalacticin activity

Agalacticin A has proven to be a potent novel antibiotic against GBS infection *in vitro*. In order to test the potential of agalacticin A *in vivo* against GBS, *Galleria mellonella* were used as a model organism for infection. The use of *G. mellonella* as a model for *Streptococcal* infection is well established and therefore a good candidate for testing the effectiveness of agalacticin A *in vivo* [191]. The H109A mutant was used as an inactive control *in vivo* as it shows the most structural similarity to the WT within the CD spectrum but has been shown to be enzymatically inactive. Agalacticin A and H109A were tested against clinically relevant *S. agalactiae* strains which had been well established in this model MRI Z2:366 and STIR CD25.

G. mellonella were injected with GBS MRI Z2:366 (2 $x10^6$ CFU) and STIR CD25 (4.33 $x10^6$ CFU) and incubated for 2 hours before being administered with 20 µg (67 nM) of WT agalacticin A, H109A agalacticin or PBS. *G. mellonella* were incubated at 37^oC and monitored at 12 and 24 hours.

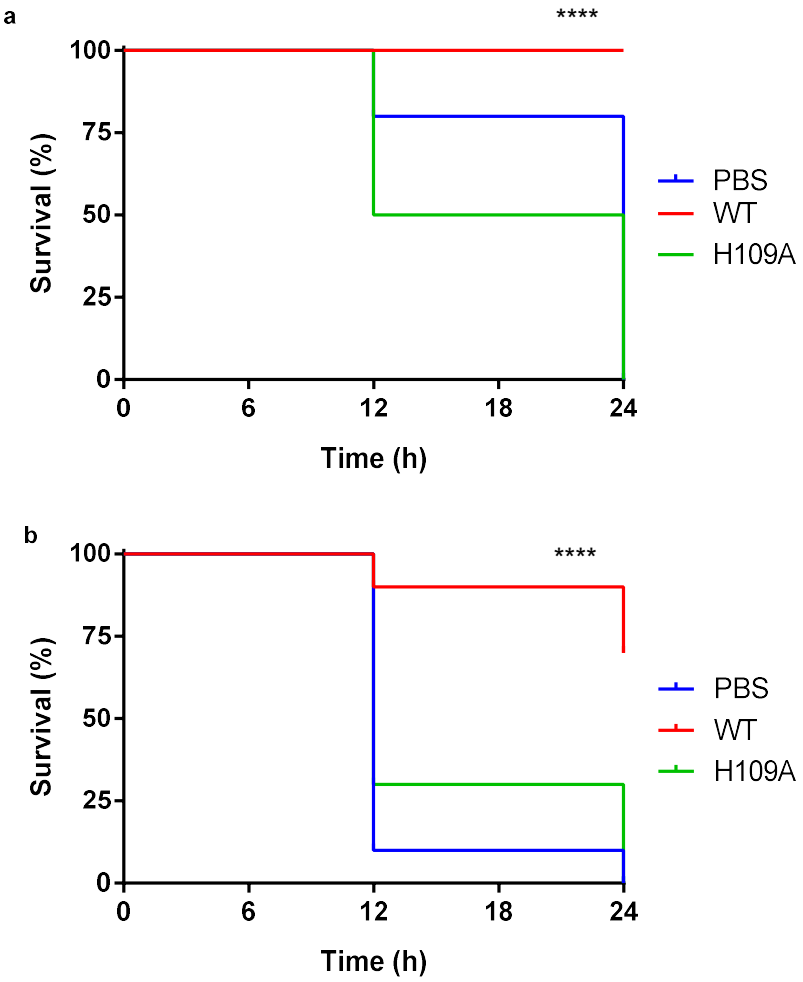

Figure 5-23: Survival curves of *G. mellonella* after GBS infection. Larvae were treated two hours post infection with agalacticin A at 67 nM concentration. Survival curves for larvae infected with MRI Z2-366 (a) and STIR CD25 (b) show that survival rates are higher when larvae are treated with WT agalacticin (red) as compared to mock treatment with PBS (blue) and treatment with the inactive H109A agalacticin A mutant (green). Mantel-Cox comparisons show a significant difference ($p < 0.001$) between treatments in both strains.

The administration of WT agalacticin A increased survival rates of *G. mellonella* after 24 hours in comparison with both no treatment and treatment with the inactive H109A (Figure 5-23). After infection with GBS MRI Z2:366, treatment with WT agalacticin A resulted in 100% survival compared with larvae treated with PBS or H109A groups which succumbed 24 hours after infection. In the case of STIR CD25 infection there was a small increase in survival at 12 hours post-infection with H109A in comparison with no treatment. This is consistent with the *in vitro* nitrocefin data showing the presence of some enzymatic activity. After 24 hours there was still no survival with either no treatment or treatment

with H109A compared to 70% survival when treated with the WT agalacticin A. This is further support for the hypothesis that H109A is part of the active site of agalacticin A and required for activity.

In order to examine the longevity of treatment *G. mellonella* were infected with GBS MRI Z2:366, treated after two hours and survival was observed over 72 hours.

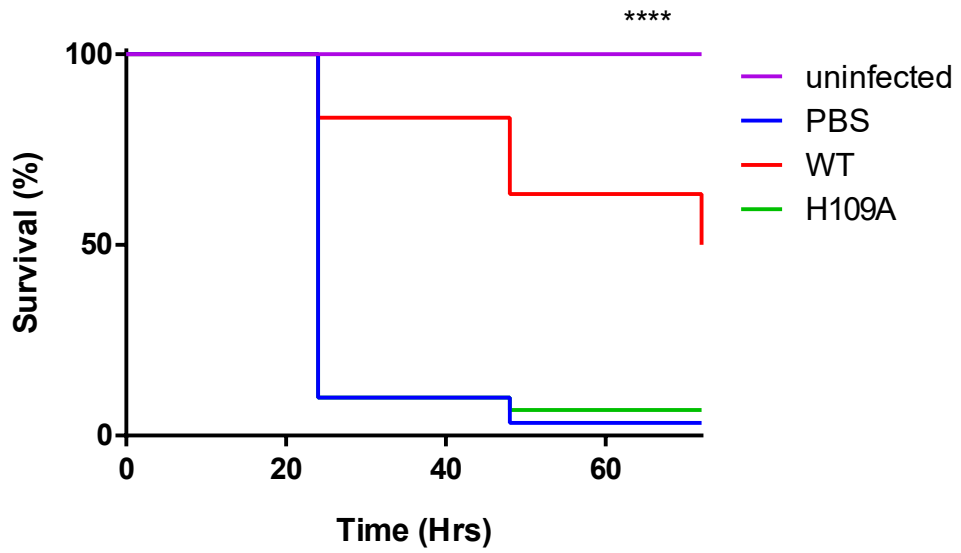

Figure 5-24 Survival curves of *G. mellonella* after GBS infection. *G. mellonella* infected with *S. agalactiae* MRI Z2:366 and treated after 2 hours with WT agalacticin (red), agalacticin A H109A (green) and no treatment (blue), with mock infection shown in purple. Mantel-Cox comparisons show a significant difference of $p<0.001$ between treatments.

It can be seen in Figure 5-24 that treatment with WT agalacticin A increases the survival of *G. mellonella* larvae infected with GBS, rescuing 50% of infected larvae after 72 hours. This is a significant increase in survival compared with both the mock treatment group and treatment with the inactive H109A mutant. Survival of *G. mellonella* with treatment by agalacticin A shows that agalacticin A is a good candidate for further *in vivo* study to tackle GBS infection.

5.3 Conclusions

Agalacticin A is a novel bacteriocin which is active against *Streptococcus* and some *Enterococcus* species. Agalactin A is thought to be similar in structure and

function to ZooA and lysostaphin. Prior to this work it was known that ZooA was a M23 metallopeptidase capable of cleaving D-alanyl-D-alanine and D-alanyl-L-alanine bonds within *Streptococcus* peptidoglycan in order to cause cell lysis [100,104,184]. The TRD and cytotoxic domains of ZooA have been solved using NMR spectroscopy showing that both domains individually are globular and joined by a linker region [99,100].

This work has shown the inter-domain flexibility and overall structure of agalacticin A, confirming its similarity to lysostaphin and ZooA. SAXS data have shown that agalacticin A is flexible and elongated in solution with the flexible linker region allowing for independent movement of the two domains. Recent work by Tossavainen et al. (2018) has examined the overall structure and flexibility of lysostaphin in solution using SAXS. This work determined that lysostaphin is flexible in solution and that the flexibility is found within the inter-domain linker region [97]. The work presented in this chapter suggests that agalacticin A is similar to lysostaphin in solution with the flexibility of the protein found in the inter-domain linker region. An X-ray crystal or NMR solution structure of the entire protein would be beneficial in order to assess the overall structure of agalacticin A and to examine the elongated and compact forms in more detail.

Previous work has reported that ZooA is active against the D-alanyl-D-alanine bonds within the peptidoglycan [104], however it has also been reported that ZooA can hydrolyse the D-alanyl-L-alanine bonds [100]. Work presented here supports the idea that agalacticin A, like ZooA, is able to hydrolyse the the D-alanyl-D-alanine bonds of both nitrocefin and *Streptococcal* peptidoglycan. The active site of agalacticin A has been found through the use of site-directed mutagenesis; however more mutations are needed to confirm all the residues necessary for activity. It would also be beneficial to examine the exact position within the peptidoglycan that agalacticin A cleaves. Understanding the interaction and cleavage sites of agalacticin A would help further characterise agalacticin A and understand potential mechanisms of resistance.

Agalacticin A has been shown to be an effective treatment of GBS infection in *G. mellonella* models suggesting that it has the potential to be developed as a novel therapeutic to combat *Streptococcus* infection in other organisms.

Chapter 6 Concluding remarks

6.1 Key findings

6.1.1 Pectocins and the Fus system

The initial aims of this study were to better understand the interaction and uptake of pectocins M1 and P by the Fus uptake system in *P. atrosepticum*. It has been shown previously that FusA is essential for pectocin M1 uptake, however this work has shown that it is also essential for the uptake of pectocin P. The parasitisation of the ferredoxin uptake system within *Pectobacterium* spp. appears to be a universal trait of ferredoxin-containing pectocins. This work also suggests that the presence of the ferredoxin domain is necessary for the uptake of these pectocins due to its interaction with the FusA receptor.

The N-terminal domain of pectocins is necessary for the interaction with FusA, with a chimeric protein suggesting that the presence of the N-terminal domain is sufficient for receptor binding and potentially for uptake. Through the use of docking modelling it was predicted that the N-terminal domain of pectocin M1 is likely to interact with the long extracellular loops of FusA. This model has been supported through the use of mutagenesis studies showing that the extracellular loops of FusA and the N-terminal of pectocin M1 interact. This work further confirmed the predicted binding site of pectocin M1, showing that it is likely to consist of both large and polar residues [124].

Previous work has shown that pectocin M2 is is flexible in solution which is unusual for M-type bacteriocins [123]. Moreover, the structures of pectocin M2 in both a bent and elongated conformation in conjunction with docking modelling suggested that these conformations were necessary for receptor binding and translocation respectively [123,124]. The flexibility observed for pectocin M2 can be found in all three of the known pectocins, suggesting that this flexibility is a universal feature. Using SAXS it was shown that both pectocin M1 and P are likely to be found in multiple conformations in solution. This data is supported by their uptake through the lumen of FusA which would only be possible if both were able to elongate. This flexibility is unusual amongst most Gram-negative bacteriocins, with the uptake of some reliant on unfolding rather than domain flexibility [63,192].

The elongation of the pectocins is necessary for uptake due to the dimensions of the lumen of FusA. However, the uptake of these pectocins can only occur if the N-terminal plug domain of FusA is entirely removed from the barrel. SANS data suggests that the plug domain of FusA can exit the barrel and remain folded in solution. Although these data are not conclusive they suggest that the plug domain remains intact when exiting the barrel rather than partially unfolding. It is thought that the majority of TonB-dependent outer membrane receptors undergo a partial unfolding of the plug domain to allow for substrate uptake [63,78]. However, for a large folded substrate the unfolding or entire removal of the plug domain seems necessary. Therefore, it is thought that, in the case of FusA, the most likely solution is the exit of the plug domain from the barrel whilst remaining folded.

The distinct structure of ferredoxin-containing bacteriocins suggests a novel mechanism of uptake for Gram-negative bacteriocins in the absence of an IUTD. Without the presence of this TonB-box containing peptide it was not known whether pectocin M1 would be able to interact with the PMF of the inner membrane. Work here suggests that pectocin M1 is able to interact with FusB, an inner membrane homologue of TonB, suggesting a novel uptake mechanism. This interaction has been shown *in vitro*, however work to examine this *in vivo* is necessary to determine the importance of this interaction for uptake. In order to further investigate this interaction, it would be beneficial to examine the C-terminal folded domain of FusB and its interaction with pectocin M1. This would allow for the interaction site to be determined using NMR spectroscopy as well as reducing the flexibility and likelihood of self-association due to the removal of the highly flexible N-terminal.

It is known that pectocin M1 is active against *P. atrosepticum* LMG2386 at low concentrations. Contrastingly, pectocin P is only active against *P. atrosepticum* LMG2386 down to a concentration of 8 μM. Therefore, it is not known whether the reduced potency of pectocin P is due to the enzymatic activity or a reduced efficiency in uptake. The N-terminal domains of pectocin P and pectocin M1, although similar, are not identical. Therefore, it would be interesting to see if the N-terminal of pectocin M1 would increase the level of uptake of pectocin P and enhance its potency against *Pectobacterium* strains. This approach would

also allow for the N-terminal of pectocin M1 to be examined as a delivery system as the uptake of the bacteriocin could be observed.

6.1.2 Agalactin A is a homologue of lysostaphin and ZooA.

This work has gone some way to confirming the active site of agalacticin A. As the structure of M23 metalloproteases is highly conserved it was predicted that the active site residues of agalacticin A would be homologous to those found in lysostaphin, LytM and ZooA [94]. This work has shown that both the substitution of H23 and H109 with alanine reduces enzymatic activity compared to the WT. This reduction in activity is consistent with the active sites found in homologues from other M23 metalloproteases and therefore further suggests that agalacticin A is similar to both ZooA and lysostaphin [94].

Agalacticin A, like its homologues, targets species closely related to the producing strain. This targeting is predicted to be due to the presence of the TRD at the C-terminus of the protein, similarly to lysostaphin which requires the TRD to interact with the target cell [97]. The enzymatic activity of both ZooA and agalacticin A suggest that it may enzymatically active against any cells that possess alanine peptide cross-bridges, such as enterococcus spp. [104,183]. This TRD may be necessary for activity but it may also be possible to create chimeric proteins allowing agalacticin A to target a wider number of Gram-positive species or to target another specific pathogen by altering the TRD.

It has been shown in this work that agalacticin A, like lysostaphin, is flexible in solution. The ability of agalacticin A and lysostaphin to elongate and contract may be important for both target recognition and enzymatic activity [97]. The removal or partial removal of the flexible linker domain of agalacticin A may allow for the importance of this flexibility to be examined. Although the flexibility and overall structure of agalacticin A can be shown using SAXS, the high-resolution structure of agalactin A would be highly beneficial in understanding its detailed mechanism of killing.

6.2 Future work

6.2.1 The role of the *fus* operon in the uptake of pectocins

Although this work has gone some way to examining the interaction of pectocin M1 with the proteins encoded on the *fus* operon, the uptake of these proteins is far from understood. Future work should focus on elucidating the roles of both FusB and FusC in the uptake and processing of pectocins in order to determine if these are essential. It would also be beneficial to examine the role of this operon in virulence; work within this thesis has shown that FusA is not essential for virulence of *P. atrosepticum* LMG2386 in both *N. benthamania nahG* or tuber infections. However, this may not be the case for all *Pectobacterium* strains carrying the *fus* operon. It is likely that the inability of *P. atrosepticum* to acquire iron from a host source is compensated for by the production of siderophores.

It has been shown in other closely related species that siderophore production is upregulated under the iron limiting conditions of infection [193,194]. It would be interesting to determine if the deletion of the *fus* system increased the production of siderophores or led to an upregulation of other iron scavenging pathways to retain iron uptake. Moreover, under iron-limiting conditions, this strain of *P. atrosepticum* does not appear to use ferredoxins as an iron source to enhance growth [117], however this is not the case for all *Pectobacterium* spp. Therefore, it would be interesting to examine if the virulence of strains which do exhibit this enhanced growth is affected by the deletion of the *fus*A gene.

The conformational change needed for pectocin M1 to both bind and be taken up by the FusA is predicted from the NMR spectroscopy data, however the mechanism by which this occurs remains unclear. It is known that pectocin M1, like pectocin M2, can be found in multiple conformations within solution in the absence of FusA [123]. This suggests that the conformational change may not be dependent on the interaction with the outer membrane receptor. However if, as predicted, the pectocin M1 can only interact with FusA in a bent conformation a conformational change would be required upon receptor binding for uptake [124]. Future work should focus on the conformational change of pectocin M1 in

the absence and presence of FusA in order to determine this mechanism. This flexibility should also be examined for pectocin P, it may be that this conformational change is more reliant on receptor interaction as the SAXS data suggest that only a small percentage of the population may be elongated in solution.

Moreover, more data is needed to determine the mechanism by which the plug domain from FusA is removed in solution. As the removal of the plug domain is normally reliant on the presence of the TonB complex it is unusual that the SANS data suggest that it can exit the barrel in the absence of the TonB interaction. Moreover, future work should focus on whether the predicted TonB-box of FusA interacts with TonB in the periplasm, or in fact interacts with FusB. In order to fully examine this, the use of atomic force microscopy would allow for the removal of the plug to be examined. AFM has been successfully used to examine the plug domain rearrangement of BtuB upon its interaction with TonB [76], therefore the same approach could be used to determine if the plug domain of FusA is removed or unfolded upon its interaction with TonB or FusB.

6.2.2 Development and discovery of novel antimicrobials

This work has shown the potential of both Gram-negative and Gram-positive bacteriocins as antimicrobials. Both pectocin M1 and agalacticin A are potent antimicrobials against *Pectobacterium* and GBS respectively when tested *in vitro*. It has been shown that agalacticin A is successful in reducing infection in *G. mellonella* and increasing survival rates suggesting that it may be a candidate for further testing.

Pectocins have the potential to be used as potent antibiotics, however work here has shown that further optimisation and development is needed in order to examine the optimum conditions for both delivery and disease prevention. It has been shown previously that bacteriocins against plant pathogens such as *Pseudomonas syringe* are effective in the prevention of infection, specifically olive knot [195]. Previous work has shown that the production of T4 lysozyme by potato plants significantly reduces the susceptibility of the plant to infection by *P. atrosepticum* without a detectable effect on the rhizosphere microbiota

[196–198]. Therefore, the potential for bacteriocins to be used to prevent infection by phytopathogens has been shown. It is also possible that the N-terminal domain of pectocin M1 could be used to import antimicrobial compounds, such as vancomycin, which are normally ineffective against Gram-negative bacteria due to the presence of the outer membrane. Furthermore, the ability to deliver a cocktail of chimeric bacteriocins could potentially reduce the emergence of resistance within *Pectobacterium* spp. The presence of ferredoxin-containing bacteriocins encoded by other phytopathogens suggests that a universal mechanism of bacteriocin uptake may have the potential to be exploited.

The use of bacteriocins within the food industry has the potential to reduce the amount of food lost to bacterial pathogens every year. Within recent years protein bacteriocins have been used to prevent the spread of *Salmonella* infection through treatment of meat as well as the use of endolysins to prevent the spoilage of dairy products [199]. This work has explored the structural and functional characteristics of bacteriocins from both Gram-positive and Gram-negative bacteria. This work has gone some way to showing the efficacy of these bacteriocins against their target organisms and that agalacticin A has the potential to be developed as a therapeutic against GBS infection. Pectocins, although potent *in vitro* against *Pectobacterium* spp. have not been shown to effectively clear infection in leaf or tuber tissue in this study, however optimisation of these infection models may yet show that they can be effective *in vivo*.

Appendix 1 Sequence alignments of FusA to known proteins highlighting the conserved TonB-box

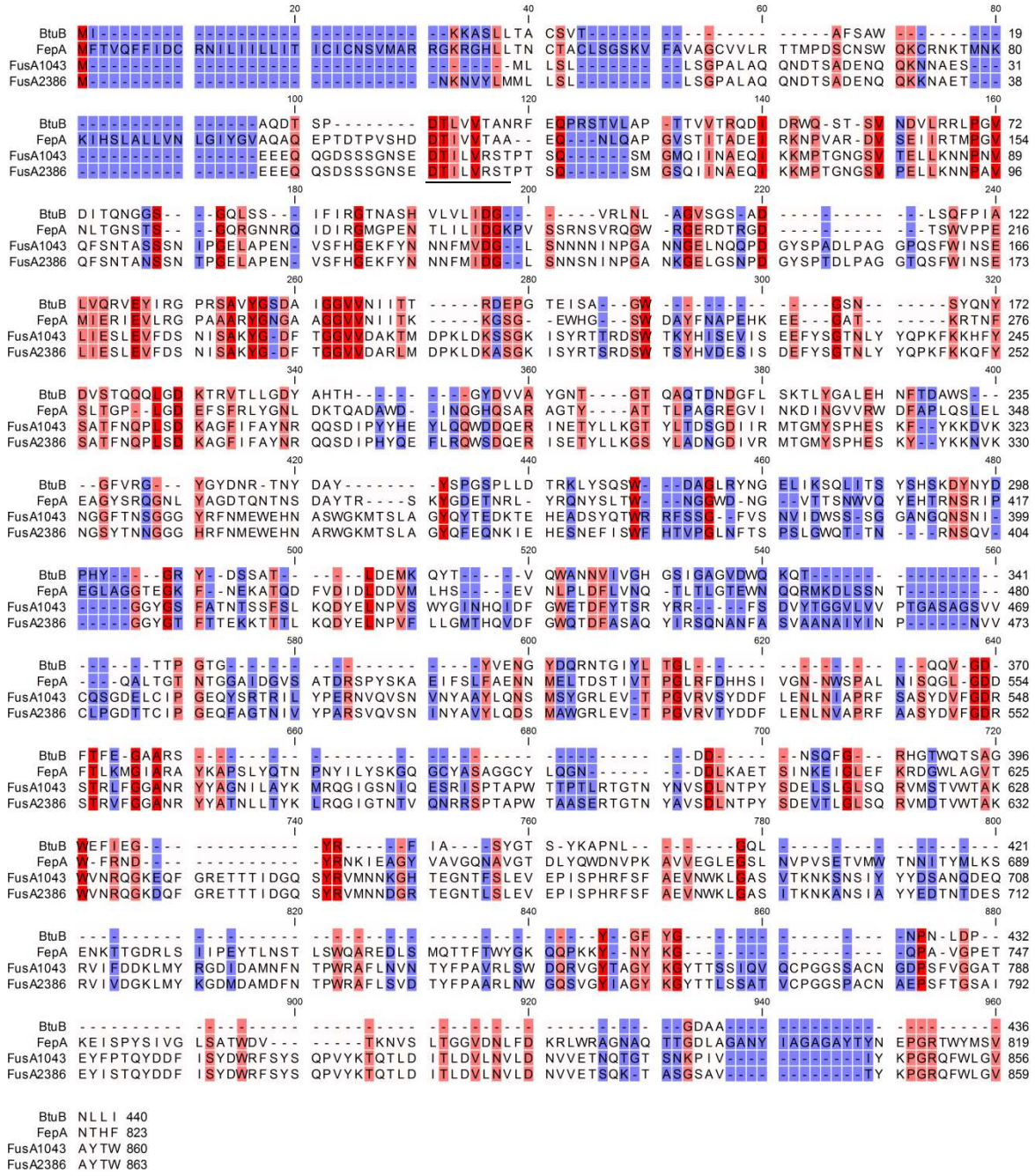

Appendix 1a Sequence alignments of FusA with TonB-dependent receptors from *E. coli*. Amino acid sequence alignment of FusA from *P. atrosepticum* LMG2386, SCRI1043 with BtuB and FepA from *E. coli* with the TonB-box conserved motif underlined. Conserved residues are shown in Red and unconserved residues shown in blue, with residues shared by three or two proteins highlighted in pink and white respectively.

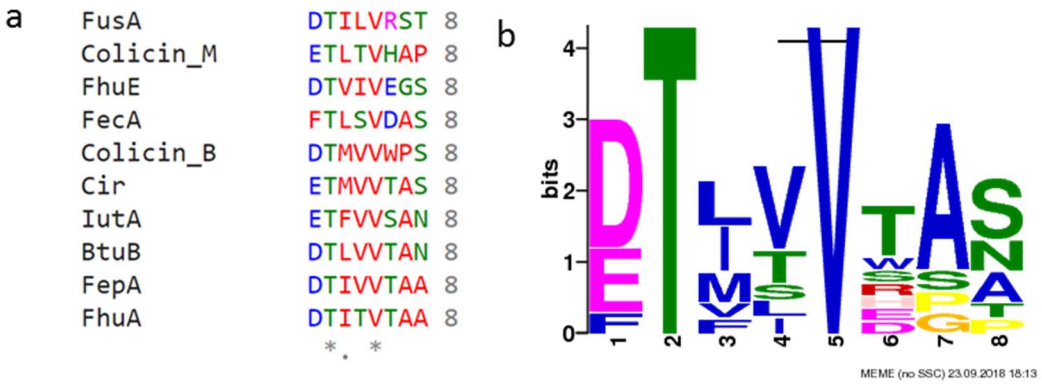

Appendix 1b Conserved TonB-box motifs based on sequence homology with other known TonB-dependent receptors. a) TonB-box sequences from $FusA_{2386}$ and known TonB-boxes from TonB-dependent receptors and colcins (sequences taken from [85] and aligned using Clustal Omega) with colours representing conserved properties. b) Graphical representation of the sequences shown in a using MEME [200]

MMLLSLLSGPALAQQNDTSADENQQKNNAESEEEQQGDSSSGNSEDTILVRSTPTSQSMGMQIINA
EQIKKMPTGNGSVTELLKNNPNVQFSNTASSSNIPGELAPENVSFHGEKFYNNNFMVDGLSNNNN
INPGANNGELNQQPDGYSPADLPAGGPQSFWINSELIESLEVFDSNISAKYGDFTGGVVDAKTMDP
KLDKSSGKISYRTTRDSWTKYHISEVISEEFYSGTNLYYQPKFKKHFYSATFNQPLSDKAGFIFAYNR
QQSDIPYYHEYLQQWDDQERINETYLLKGTYLTDSGDIIRMTGMYSPHESKFYKKDVKNGGFTNS
GGGYRFNMEWEHNASWGKMTSLAGYQYTEDKTEHEADSYQTWRRFSSGFVSNVIDWSSSGGA
NGQNSNIGGYGSFATNTSSFSLKQDYELNPVSWYGINHQIDFGWETDFYTSRYRRFSDVYTGGVL
VVPTGASAGSVVCQSGDELCIPGEQYSRTRILYPERNVQVSNVNYAAYLQNSMSYGRLEVTPGVRV
SYDDFLENLNIAPRFSASYDVFGDRSTRLFGGANRYYAGNILAYKMRQGIGSNIQESRISPTAPWTT
PTLRTGTNYNVSDLNTPYSDELSLGLSQRVMSTVWTAKWVNRQGKEQFGRETTTIDGQSYRVMN
NKGHTEGNTFSLEVEPISPHRFSFAEVNWKLGASVTKNKSNSIYYYDSANQDEQRVIFDDKLMYRG
DIDAMNFNTPWRAFLNVNTYFPAVRLSWDQRVGYTAGYKGYTTSSIQVQCPGGSSACNGDPSFV
GGATEYFPTQYDDFISYDWRFSYSQPVYKTQTLDITLDVLNVLDNVVETNQTGTSNKPIVIYKPGR
QFWLGVAYTW

Appendix 1c Amino acid sequence of $FusA_{1043}$. Amino acids corresponding to the N-terminal plug domain are shown in blue, the C-terminal barrel shown in purple. The red underlined residues (STPTS) are the first five amino acids of the protein used for SANS experiments. The eight residues underlined in green correspond to those of the predicted TonB-box.

Appendix 2 N-terminal domain of pectocin M1

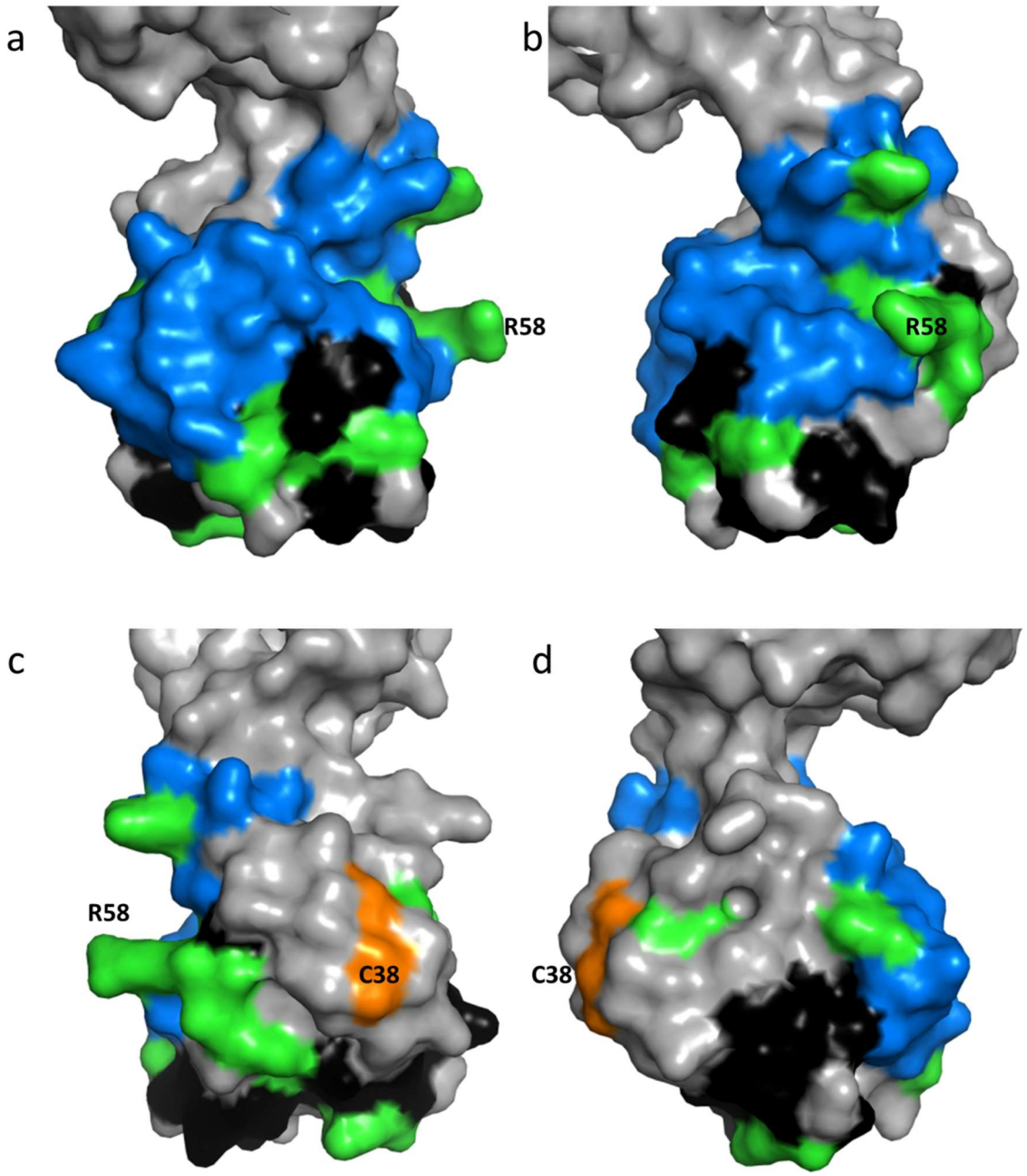

Appendix 2 N-terminal domain of pectocin M1 showing the surface, with colours indicating chemical shift perturbations as measured by NMR spectroscopy and described in Chapter 4. Residues showing a CSP of >0.02 p.p.m. shown in blue, 0.01-0.02 p.p.m shown in green and <0.01 p.p.m shown in black with those residues bound to the iron-sulphur cluster shown in orange. Panels show the four face of pectocin M1 for example panel b is a 90^{o} to the left rotation of panel a, with residues R58 and C38 shown as a reference.

Appendix 3 Absence of the iron-sulphur cluster disrupts both receptor binding and protein uptake.

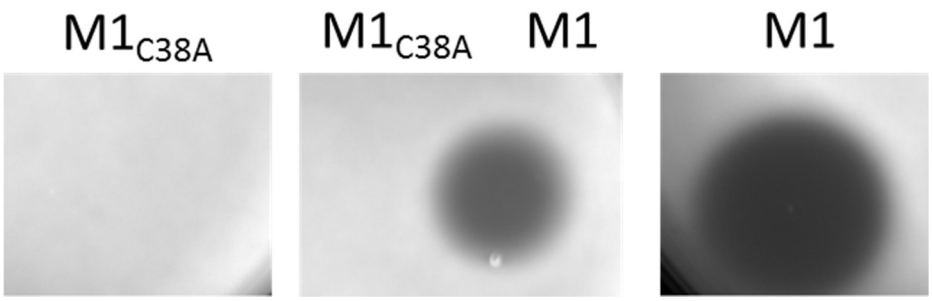

Appendix 3a Competition assay between pectocin M1 and pectocin $M1_{C38A}$ (at a concentration of 3 mg ml^{-1})showing that C38A does not cause cell lysis or compete with pectocin M1 for the FusA outer membrane receptor likely due to its improper folding (shown in Figure 4-7).

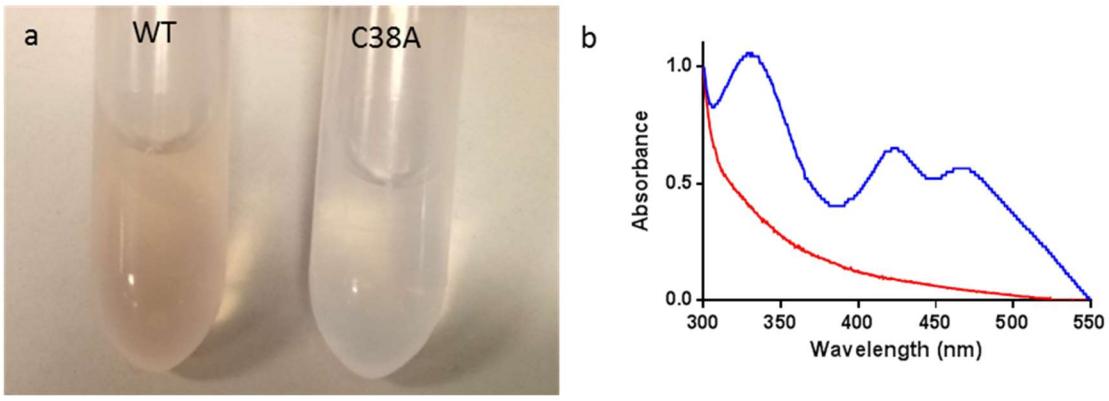

Appendix 3b Mutation of residue C38 to an alanine prevents the binding of an iron-sulphur cluster. a) Light image of WT pectocin M1 and pectocin $M1_{C38A}$ showing the lack of the distinctive red colour indicating the absence of the iron-sulphur cluster. b) Absorbance spectra of pectocin M1 (blue) and pectocin $M1_{C38A}$ showing the lack of distinctive peaks associated with the presence of the iron-sulphur cluster.

Chapter 7 References

1 Esquinas-Alcázar, J. (2005) Protecting crop genetic diversity for food security: political, ethical and technical challenges. *Nat. Rev. Genet.,* **6**, 946–953.

2 Chakraborty, S. and Newton, A. C. (2011) Climate change, plant diseases and food security: An overview. *Plant Pathol*., **60**(1) 2-14

3 Strange, R. N. and Scott, P. R. (2005) Plant disease: a threat to global food security. *Annu. Rev. Phytopathol*. **43**, 83–116.

4 Buttimer, C., McAuliffe, O., Ross, R. P., Hill, C., O'Mahony, J. and Coffey, A. (2017) Bacteriophages and Bacterial Plant Diseases. *Front. Microbiol.,* **8**, 1–15.

5 Keefe, G. P. (1997) *Streptococcus agalactiae* mastitis: a review. *Can. Vet. J.,* **38**, 429–37.

6 Oekre, E.-C. (2006) Crop losses to pests. *J. Agric. Sci.,* **144**, 31–43.

7 Soto, E., Wang, R., Wiles, J., Baumgartner, W., Green, C., Plumb, J. and Hawke, J. (2015) Characterization of Isolates of *Streptococcus agalactiae* from Diseased Farmed and Wild Marine Fish from the U.S. Gulf Coast, Latin America, and Thailand. *J. Aquat. Anim. Health,* **27**, 123–134.

8 Simonsen, K. A., Anderson-Berry, A. L., Delair, S. F. and Davies, H. D. (2014) Early-onset neonatal sepsis. *Clin. Microbiol. Rev.,* **27**, 21–47.

9 Shane, A. L., Sánchez, P. J. and Stoll, B. J. (2017) Neonatal sepsis. *Lancet*, **390**, 1770–1780.

10 Watts, J. E. M., Schreier, H. J., Lanska, L. and Hale, M. S. (2017) The Rising Tide of Antimicrobial Resistance in Aquaculture: Sources, Sinks and Solutions. *Mar. Drugs,* **15**.

11 Kimura, K., Nagano, N. and Arakawa, Y. (2015) Classification of group B *Streptococci* with reduced β-lactam susceptibility (GBS-RBS) based on the amino acid substitutions in PBPs. *J. Antimicrob. Chemother.*, **70**, 1601–1603.

12 Davidsson, P. R., Kariola, T., Niemi, O. and Palva, E. T. (2013) Pathogenicity of and plant immunity to soft rot *Pectobacterium*. *Front. Plant Sci.,* **4**, 1–13.

13 Pérombelon, M. C. M. (2002) Potato diseases caused by soft rot *Erwinias*: An overview of pathogenesis. *Plant Pathol.* **51**, 1–12.

14 Ma, B., Hibbing, M. E., Kim, H.-S., Reedy, R. M., Yedidia, I., Breuer, J., Breuer, J., Glasner, J. D., Perna, N. T., Kelman, A., et al. (2007) Host range and molecular phylogenies of the soft rot enterobacterial genera *Pectobacterium* and *Dickeya*. *Phytopathology* **97**, 1150–1163.

15 Czajkowski, R., Pérombelon, M. C. M., van Veen, J. A. and van der Wolf, J. M. (2011) Control of blackleg and tuber soft rot of potato caused by *Pectobacterium* and *Dickeya* species: a review. *Plant Pathol.,* **60**, 999–1013.

16 Kim, H.-S., Ma, B., Perna, N. T. and Charkowski, A. O. (2009) Phylogeny and virulence of naturally occurring type III secretion system-deficient *Pectobacterium* strains. *Appl. Environ. Microbiol.,* **75**, 4539–49.

17 Hogan, C. S., Mole, B. M., Grant, S. R., Willis, D. K. and Charkowski, A. O. (2013) The Type III Secreted Effector DspE Is Required Early in *Solanum tuberosum* Leaf Infection by Pectobacterium carotovorum to Cause Cell Death, and Requires Wx(3–6)D/E Motifs. *PLoS One* **8**, e65534.

18 Czajkowski, R., Ozymko, Z., de Jager, V., Siwinska, J., Smolarska, A., Ossowicki, A., Narajczyk, M. and Lojkowska, E. (2015) Genomic, Proteomic and Morphological Characterization of Two Novel Broad Host Lytic Bacteriophages ΦPD10.3 and ΦPD23.1 Infecting Pectinolytic Pectobacterium spp. and Dickeya spp. *PLoS One* **10**, e0119812.

19 Baz, M., Lahbabi, D., Samri, S., Val, F., Hamelin, G., Madore, I., Bouarab, K., Beaulieu, C., Ennaji, M. M. and Barakate, M. (2012) Control of potato soft rot caused by Pectobacterium carotovorum and Pectobacterium atrosepticum by Moroccan actinobacteria isolates. World J. Microbiol. Biotechnol. **28**, 303–311.

20 Meziani, S., Oomah, B. D., Zaidi, F., Simon-Levert, A., Bertrand, C. and Zaidi-Yahiaoui, R. (2015) Antibacterial activity of carob *(Ceratonia siliqua L.*) extracts against phytopathogenic bacteria *Pectobacterium atrosepticum. Microb. Pathog*. **78**, 95–102.

21 Faure, D. and Dessaux, Y. (2007) Quorum sensing as a target for developing control strategies for the plant pathogen *Pectobacterium*. *Eur. J. Plant Pathol.***119** (3) 353-365

22 Kreikemeyer, B., Valentin-Weigand, P., Bergmann, S., Spellerberg, B. and Shabayek, S. (2018) Group B *Streptococcal* Colonization, Molecular Characteristics, and Epidemiology. *Front Microbiol.* **9** Article 437

23 Rosinski-Chupin, I., Sauvage, E., Mairey, B., Mangenot, S., Ma, L., Da Cunha, V., Rusniok, C., Bouchier, C., Barbe, V. and Glaser, P. (2013) Reductive evolution in *Streptococcus agalactiae* and the emergence of a host adapted lineage. *BMC Genomics* **14** Article 252

24 Almeida, A., Rosinski-Chupin, I., Plainvert, C., Douarre, P.-E., Borrego, M. J., Poyart, C. and Glaser, P. (2017) Parallel Evolution of Group B *Streptococcus* Hypervirulent Clonal Complex 17 Unveils New Pathoadaptive Mutations. *mSystems,* **2** (5) e00074-17.

25 Delannoy, C. M., Crumlish, M., Fontaine, M. C., Pollock, J., Foster, G., Dagleish, M. P., Turnbull, J. F. and Zadoks, R. N. (2013) Human *Streptococcus agalactiae* strains in aquatic mammals and fish. *BMC Microbiol.* **13** Article 41

26 Sun, J., Fang, W., Ke, B., He, D., Liang, Y., Ning, D., Tan, H., Peng, H., Wang, Y., Ma, Y., et al. (2016) Inapparent *Streptococcus agalactiae* infection in adult/commercial tilapia. *Sci. Rep.,* **6**, 26319.

27 Barkema, H. W., Green, M. J., Bradley, A. J. and Zadoks, R. N. (2009) Invited review: The role of contagious disease in udder health. *J. Dairy Sci.,* **92**, 4717–29.

28 Patras, K. A. and Nizet, V. (2018) Group B Streptococcal Maternal Colonization and Neonatal Disease: Molecular Mechanisms and Preventative Approaches. *Front. Pediatr.,* **6**, 27.

29 Melin, P. (2011) Neonatal group B *streptococcal* disease: from pathogenesis to preventive strategies. *Clin. Microbiol. Infect.* **17**, 1294–1303.

30 Kalimuddin, S., Chen, S. L., Lim, C. T. K., Koh, T. H., Tan, T. Y., Kam, M., Wong, C. W., Mehershahi, K. S., Chau, M. L., Ng, L. C., et al. (2017) 2015 Epidemic of Severe *Streptococcus agalactiae* Sequence Type 283 Infections in Singapore Associated With the Consumption of Raw Freshwater Fish: A Detailed Analysis of Clinical,

Epidemiological, and Bacterial Sequencing Data. *Clin. Infect. Dis.,* **64**, S145–S152.

31 Santos, L. and Ramos, F. (2016) Analytical strategies for the detection and quantification of antibiotic residues in aquaculture fishes: A review. *Trends Food Sci. Technol.* **52**, 16–30.

32 Cabello, F. C. (2006) Heavy use of prophylactic antibiotics in aquaculture: a growing problem for human and animal health and for the environment. *Environ. Microbiol.,* **8**, 1137–1144.

33 Heelan, J. S., Hasenbein, M. E. and McAdam, A. J. (2004) Resistance of group B *streptococcus* to selected antibiotics, including erythromycin and clindamycin. *J. Clin. Microbiol.,* **42**, 1263–4.

34 Garland, S. M., Cottrill, E., Markowski, L., Pearce, C., Clifford, V., Ndisang, D., Kelly, N. and Daley, A. J. Antimicrobial resistance in group B *streptococcus*: the Australian experience.*J Med Microbiol.* **60** (pt2) 230-235

35 Smith, P. (2008) Antimicrobial resistance in aquaculture. *Rev. sci. tech. Off. int. Epiz.* **27** (1) 243-264

36 Bolukaoto, J. Y., Monyama, C. M., Chukwu, M. O., Lekala, S. M., Nchabeleng, M., Maloba, M. R. B., Mavenyengwa, R. T., Lebelo, S. L., Monokoane, S. T., Tshepuwane, C., et al. (2015) Antibiotic resistance of *Streptococcus agalactiae* isolated from pregnant women in Garankuwa, South Africa. *BMC Res. Notes* **8**, 364.

37 Johri, A. K., Paoletti, L. C., Glaser, P., Dua, M., Sharma, P. K., Grandi, G. and Rappuoli, R. (2006) Group B *Streptococcus*: global incidence and vaccine development. *Nat. Rev. Microbiol.,* **4**, 932–42.

38 Hibbing, M. E., Fuqua, C., Parsek, M. R. and Peterson, S. B. (2010) Bacterial competition: surviving and thriving in the microbial jungle. *Nat. Rev. Microbiol.*, **8**, 15–25.

39 Ghoul, M. and Mitri, S. (2016) The Ecology and Evolution of Microbial Competition. *Trends Microbiol.,* **24**, 833–845.

40 Kleanthous, C. (2010) Swimming against the tide: progress and challenges in our understanding of colicin translocation. *Nat. Rev. Microbiol.*, **8**, 843–848.

41 Ghequire, M. G. K., Buchanan, S. K. and De Mot, R. (2018) The ColM Family, Polymorphic Toxins Breaching the Bacterial Cell Wall. *mBio* **9**(1) e02267-17

42 Jack, R. W., Tagg, J. R. and Ray, B. (1995) Bacteriocins of Gram-positive bacteria. *Microbiol. Rev.,* **59**, 171–200.

43 Cascales, E., Buchanan, S. K., Duché, D., Kleanthous, C., Lloubès, R., Postle, K., Riley, M., Slatin, S. and Cavard, D. (2007) Colicin biology. *Microbiol. Mol. Biol. Rev.* **71**, 158–229.

44 Behrens, H. M., Six, A., Walker, D. and Kleanthous, C. (2017) The therapeutic potential of bacteriocins as protein antibiotics. *Emerg. Top. life Sci.* **1**, 65–74.

45 Heng, N. C. K., Wescombe, P. A., Burton, J. P., Jack, R. W. and Tagg, J. R. (2007) The Diversity of Bacteriocins in Gram-Positive Bacteria. In Riley M.A., Chavan M.A. (eds) Bacteriocins, pp 45–92, Springer Berlin Heidelberg, Berlin, Heidelberg.

46 Tong, Z., Ni, L. and Ling, J. (2014) Antibacterial peptide nisin: A potential role in the inhibition of oral pathogenic bacteria. *Peptides* **60**, 32–40.

47 Hansen, J. N. and Sandine, W. E. (1994) Nisin as a model food preservative. *Crit. Rev. Food Sci. Nutr.* **34**, 69–93.

48 Rebuffat, S. (2011) Bacteriocins from Gram-Negative Bacteria: A Classification? In Prokaryotic Antimicrobial Peptides, pp 55–72, Springer New York, New York, NY.

49 Zeth, K. (2012) Structure and uptake mechanism of bacteriocins targeting peptidoglycan renewal. *Biochem. Soc. Trans.,* **40**, 1560–5.

50 Kim, Y. C., Tarr, A. W. and Penfold, C. N. (2014) Colicin import into E. coli cells: A model system for insights into the import mechanisms of bacteriocins. *Biochim Biophys Acta.* **1843***(*8) 1717-31

51 Jakes, K. S. and Cramer, W. A. (2012) Border Crossings: Colicins and Transporters. *Annu Rev Genet* **46** 209-31

52 Housden, N. G., Hopper, J. T. S., Lukoyanova, N., Rodriguez-Larrea, D., Wojdyla, J. A., Klein, A., Kaminska, R., Bayley, H., Saibil, H. R., Robinson, C. V, et al. (2013) Intrinsically disordered protein threads through the bacterial outer-membrane porin OmpF. *Science*, **340**, 1570–4.

53 James, R., Penfold, C. N., Moore, G. R. and Kleanthous, C. (2002) Killing of *E. coli* cells by E group nuclease colicins. *Biochimie.***84**(5-6) 381-9

54 Parret, Annabel, H, A. and De Mot, R. (2002) Bacteria killing their own kind: novel bacteriocins of *Pseudomonas* and other γ-proteobacteria. *Trends Microbiol.* **10**, 107–112.

55 Michel-Briand, Y. and Baysse, C. (2002) The pyocins of *Pseudomonas aeruginosa*. *Biochimie* **84**(5-6) 499-510

56 Silhavy, T. J., Kahne, D. and Walker, S. (2010) The bacterial cell envelope. *Cold Spring Harb. Perspect. Biol.* **2**, a000414.

57 Collins, E. S., Whittaker, S. B.-M., Tozawa, K., MacDonald, C., Boetzel, R., Penfold, C. N., Reilly, A., Clayden, N. J., Osborne, M. J., Hemmings, A. M., et al. (2002) Structural dynamics of the membrane translocation domain of colicin E9 and its interaction with TolB. *J. Mol. Biol.,* **318**, 787–804.

58 Kurisu, G., Zakharov, S. D., Zhalnina, M. V, Bano, S., Eroukova, V. Y., Rokitskaya, T. I., Antonenko, Y. N., Wiener, M. C. and Cramer, W. A. (2003) The structure of BtuB with bound colicin E3 R-domain implies a translocon. *Nat. Struct. Biol.* **10** (11) 948-54

59 Housden, N. G., Loftus, S. R., Moore, G. R., James, R. and Kleanthous, C. (2005) Cell entry mechanism of enzymatic bacterial colicins: Porin recruitment and the thermodynamics of receptor binding.*Proc Natl Acad Sci USA* **102**(39) 13849-54.

60 Jakes, K. S. (2014) Daring to be different: Colicin n finds another way. *Mol Microbiol* **92**, 435–439.

61 Johnson, C. L., Ridley, H., Marchetti, R., Silipo, A., Griffin, D. C., Crawford, L., Bonev, B., Molinaro, A. and Lakey, J. H. (2014) The antibacterial toxin colicin N binds to the inner core of lipopolysaccharide and close to its translocator protein. *Mol. Microbiol.,* **92**, 440–52.

62 Ridley, H. and Lakey, J. H. (2015) Antibacterial toxin colicin N and phage protein G3p compete with TolB for a binding site on TolA. *Microbiology,* **161**, 503–15.

63 White, P., Joshi, A., Rassam, P., Housden, N. G., Kaminska, R., Goult, J. D., Redfield,

C., Mccaughey, L. C., Walker, D., Mohammed, S., et al. (2017) Exploitation of an iron transporter for bacterial protein antibiotic import. *Proc. Natl. Acad. Sci.* **114**, 12051–12056.

64 Nader, M., Journet, L., Meksem, A., Guillon, L. and Schalk, I. J. (2011) Mechanism of Ferripyoverdine Uptake by *Pseudomonas aeruginosa* Outer Membrane Transporter FpvA: No Diffusion Channel Formed at Any Time during Ferrisiderophore Uptake. *Biochemistry,* **50**, 2530–2540.

65 Jakes, K. S. and Finkelstein, A. (2010) The colicin Ia receptor, Cir, is also the translocator for colicin Ia. *Mol. Microbiol.,* **5**, 567–78.

66 Freed, D. M., Lukasik, S. M., Sikora, A., Mokdad, A. and Cafiso, D. S. (2013) Monomeric TonB and the Ton box are required for the formation of a high-affinity transporter-TonB complex. *Biochemistry,* **52**, 2638–48.

67 Sarver, J. L., Zhang, M., Liu, L., Nyenhuis, D. and Cafiso, D. S. (2018) A Dynamic Protein–Protein Coupling between the TonB-Dependent Transporter FhuA and TonB. *Biochemistry,* **57**, 1045–1053.

68 Schauer, K., Rodionov, D. A. and de Reuse, H. (2008) New substrates for TonB-dependent transport: do we only see the 'tip of the iceberg'? *Trends Biochem. Sci.,* **33**, 330–338.

69 Devanathan, S. and Postle, K. (2007) Studies on colicin B translocation: FepA is gated by TonB. *Mol. Microbiol.* **65**, 441–53.

70 Kim, M., Fanucci, G. E. and Cafiso, D. S. (2007) Substrate-dependent transmembrane signaling in TonB-dependent transporters is not conserved. *Proc. Natl. Acad. Sci. U. S. A.,* **104**, 11975–80.

71 Endriss, F. and Braun, V. (2004) Loop deletions indicate regions important for FhuA transport and receptor functions in *Escherichia coli*. *J. Bacteriol.,* **186**, 4818–23.

72 Newton, S. M. C., Igo, J. D., Scott, D. C. and Klebba, P. E. (1999) Effect of loop deletions on the binding and transport of ferric enterobactin by FepA. *Mol. Microbiol.* **32**, 1153–1165.

73 Fuller-Schaefer, C. A. and Kadner, R. J. (2005) Multiple extracellular loops contribute to substrate binding and transport by the *Escherichia coli* cobalamin transporter BtuB. *J. Bacteriol.,* **187**, 1732–9.

74 Eisenhauer, H. A., Shames, S., Pawelek, P. D. and Coulton, J. W. (2005) Siderophore Transport through *Escherichia coli* Outer Membrane Receptor FhuA with Disulfide-tethered Cork and Barrel Domains. *J Biol Chem.* **280**(34) 30574-80

75 Gumbart, J., Wiener, M. C. and Tajkhorshid, E. (2007) Mechanics of force propagation in TonB-dependent outer membrane transport. *Biophys. J*. **93**, 496–504.

76 Hickman, S. J., Cooper, R. E. M., Bellucci, L., Paci, E. and Brockwell, D. J. (2017) Gating of TonB-dependent transporters by substrate-specific forced remodelling. *Nat. Commun.,* **8**, 14804.

77 Oke, M., Sarra, R., Ghirlando, R., Farnaud, S., Gorringe, A. R., Evans, R. W. and Buchanan, S. K. (2004) The plug domain of a neisserial TonB-dependent transporter retains structural integrity in the absence of its transmembrane β-barrel. *FEBS Lett.*

564, 294–300.

78 Udho, E., Jakes, K. S. and Finkelstein, A. (2012) The TonB-dependent Transporter FhuA in Planar Lipid Bilayers: partial exit of its plug from the barrel. *Biochemistry* **51**, 6758–6759.

79 Ferguson, A. D. and Deisenhofer, J. (2002) TonB-dependent receptors-structural perspectives. *Biochim. Biophys. Acta* **1565**, 318–332.

80 Usher, K. C., Ozkan, E., Gardner, K. H. and Deisenhofer, J. (2001) The plug domain of FepA, a TonB-dependent transport protein from *Escherichia coli*, binds its siderophore in the absence of the transmembrane barrel domain. *Proc. Natl. Acad. Sci. U. S. A.* **98**, 10676–81.

81 Locher, K. P., Rees, B., Koebnik, R., Mitschler, A., Moulinier, L., Rosenbusch, J. P. and Moras, D. (1998) Transmembrane Signaling across the Ligand-Gated FhuA Receptor: Crystal Structures of Free and Ferrichrome-Bound States Reveal Allosteric Changes. *Cell* **95**, 771–778.

82 Celia, H., Noinaj, N., Zakharov, S. D., Bordignon, E., Botos, I., Santamaria, M., Barnard, T. J., Cramer, W. A., Lloubes, R. and Buchanan, S. K. (2016) Structural insight into the role of the Ton complex in energy transduction. *Nature,* **538**, 60–65.

83 Domingo, S., Weber, A., Howard, S. P., Welte, W. and Drescher, M. (2010) The proline-rich domain of TonB possesses an extended polyproline II-like conformation of sufficient length to span the periplasm of Gram-negative bacteria. *Protein Sci.* **19**, 625–630.

84 Karlsson, M., Hannavy, K. and Higgins, C. F. (1993) A sequence-specific function for the N-terminal signal-like sequence of the TonB protein. *Mol. Microbiol.,* **8**, 379–388.

85 Fischer, E., Günter, K. and Braun, V. (1989) Involvement of ExbB and TonB in transport across the outer membrane of *Escherichia coli*: phenotypic complementation of exb mutants by overexpressed tonB and physical stabilization of TonB by ExbB. *J. Bacteriol.,* **171**, 5127–34.

86 Jana, B., Manning, M. and Postle, K. (2011) Mutations in the ExbB Cytoplasmic Carboxy Terminus Prevent Energy-Dependent Interaction between the TonB and ExbD Periplasmic Domains. *J. Bacteriol.* **193**, 5649–5657.

87 Freed, D. M., Lukasik, S. M., Sikora, A., Mokdad, A. and Cafiso, D. S. (2013) Monomeric TonB and the Ton box are required for the Formation of a High-Affinity Transporter-TonB Complex. *Biochemistry* **52**, 2638–2648.

88 Philippe, J., Gallet, B., Morlot, C., Denapaite, D., Hakenbeck, R., Chen, Y., Vernet, T. and Zapun, A. (2015) Mechanism of β-lactam action in *Streptococcus pneumoniae*: the piperacillin paradox. *Antimicrob. Agents Chemother.,* **59**, 609–21.

89 Tipper, D. J. (1985) Mode of action of β-lactam antibiotics. *Pharmacol. Ther.* **27**, 1–35.

90 Sauvage, E., Kerff, F., Terrak, M., Ayala, J. A. and Charlier, P. (2008) The penicillin-binding proteins: structure and role in peptidoglycan biosynthesis. *FEMS Microbiol. Rev.* **32**, 234–258.

91 Meziane-Cherif, D., Stogios, P. J., Evdokimova, E., Savchenko, A. and Courvalin, P.

(2014) Structural basis for the evolution of vancomycin resistance D,D-peptidases. *Proc. Natl. Acad. Sci. U. S. A.,* **111**, 5872–7.

92 Nikolaidis, I., Favini-Stabile, S. and Dessen, A. (2014) Resistance to antibiotics targeted to the bacterial cell wall. *Protein Sci.,* **23**, 243–59.

93 Vollmer, W., Blanot, D. and De Pedro, M. A. (2008) Peptidoglycan structure and architecture. *FEMS Microbiol. Rev.,* **32**, 149–167.

94 Grabowska, M., Jagielska, E., Czapinska, H., Bochtler, M. and Sabala, I. (2015) High resolution structure of an M23 peptidase with a substrate analogue. *Sci Rep* **5** Article 14833

95 Sabala, I., Jagielska, E., Bardelang, P. T., Czapinska, H., Dahms, S. O., Sharpe, J. A., James, R., Than, M. E., Thomas, N. R. and Bochtler, M. (2014) Crystal structure of the antimicrobial peptidase lysostaphin from *Staphylococcus simulans*. *FEBS J.* **281**, 4112–4122.

96 Do Carmo De Freire Bastos, M., Coutinho, B. G., Lívio, M. and Coelho, V. (2010) Lysostaphin: A *Staphylococcal* Bacteriolysin with Potential Clinical Applications. *Pharmaceuticals* **3**, 1139–1161.

97 Tossavainen, H., Raulinaitis, V., Kauppinen, L., Pentikäinen, U., Maaheimo, H. and Permi, P. (2018) Structural and Functional Insights Into Lysostaphin-Substrate Interaction. *Front. Mol. Biosci.,* **5**, 60.

98 Baba, T. and Schneewind1, O. (1996) Target cell specificity of a bacteriocin molecule: a C-terminal signal directs lysostaphin to the cell wall of *Staphylococcus aureus. EMBO J.***15**(18) 4789-97

99 Chen, Y., Simmonds, R. S., Young, J. K. and Timkovich, R. (2013) Solution structure of the recombinant target recognition domain of zoocin A. *Proteins Struct. Funct. Bioinforma.,***81**, 722–727.

100 Xing, M., Simmonds, R. S. and Timkovich, R. (2017) Solution structure of the Cys74 to Ala74 mutant of the recombinant catalytic domain of Zoocin A. *Proteins Struct. Funct. Bioinforma*. **85**, 177–181.

101 Gargis, S. R., Heath, H. E., Heath, L. S., Leblanc, P. A., Simmonds, R. S., Abbott, B. D., Timkovich, R. and Sloan, G. L. (2009) Use of 4-Sulfophenyl Isothiocyanate Labeling and Mass Spectrometry To Determine the Site of Action of the Streptococcolytic Peptidoglycan Hydrolase Zoocin A. *Appl. Environ. Microbiol.* **75**, 72–77.

102 Simmonds, R. S., Simpson, W. J. and Tagg, J. R. (1997) Cloning and sequence analysis of zooA, a *Streptococcus zooepidemicus* gene encoding a bacteriocin-like inhibitory substance having a domain structure similar to that of lysostaphin. *Gene,* **189**, 255–261.

103 Chen, Y., Simmonds, R. S. and Timkovich, R. (2013) Proposed docking interface between peptidoglycan and the target recognition domain of zoocin A. *Biochem. Biophys. Res. Commun.,* **441**, 297–300.

104 HEATH, L. (2004) The streptococcolytic enzyme zoocin A is a penicillin-binding protein. *FEMS Microbiol. Lett.* **236**, 205–211.

105 Akesson, M., Dufour, M., Sloan, G. L. and Simmonds, R. S. (2007) Targeting of *streptococci* by zoocin A. *FEMS Microbiol. Lett.,* **270**, 155–161.

106 Lester, K. and Simmonds, R. S. (2012) Zoocin A and lauricidin in combination reduce *Streptococcus mutans* growth in a multispecies biofilm. *Caries Res.,* **46**, 185–93.

107 Dufour, M., McLeod, F. S. A. and Simmonds, R. S. (2011) Zoocin A facilitates the entry of antisense constructs into *Streptococcus mutans*. *FEMS Microbiol. Lett.,* **317**, 93–99.

108 Zeth, K., Römer, C., Patzer, S. I. and Braun, V. (2008) Crystal Structure of Colicin M, a Novel Phosphatase Specifically Imported by *Escherichia coli., J. Biol. Chem.* **283**, 25324–25331.

109 Touzé, T., Barreteau, H., El Ghachi, M., Bouhss, A., Barnéoud-Arnoulet, A., Patin, D., Sacco, E., Blanot, D., Arthur, M., Duché, D., et al. (2012) Colicin M, a peptidoglycan lipid-II-degrading enzyme: potential use for antibacterial means? *Biochem. Soc. Trans.,* **40**, 1522–7.

110 Ghequire, M. G. K., Öztürk, B. B., Alfons, E. and Stams, J. M. (2018) A Colicin M-Type Bacteriocin from *Pseudomonas aeruginosa* Targeting the HxuC Heme Receptor Requires a Novel Immunity Partner. *Appl. Environ. Microbiol.* **84**, 716–734.

111 Ghequire, M. G. K. and De Mot, R. (2015) Distinct colicin M-like bacteriocin-immunity pairs in *Burkholderia*. *Sci. Rep.,* **5**, 17368.

112 Usón, I., Patzer, S. I., Rodríguez, D. D., Braun, V. and Zeth, K. (2012) The crystal structure of the dimeric colicin M immunity protein displays a 3D domain swap. *J. Struct. Biol.* **178**, 45–53.

113 Pilsl, H., Glaser, C., Gross, P., Killmann, H., Olschläger, T. and Braun, V. (1993) Domains of colicin M involved in uptake and activity. *Mol. Gen. Genet.* **240**, 103–12.

114 Chérier, D., Giacomucci, S., Patin, D., Bouhss, A., Touzé, T., Blanot, D., Mengin-Lecreulx, D. and Barreteau, H. (2016) Pectocin M1 (PcaM1) Inhibits *Escherichia coli* Cell Growth and Peptidoglycan Biosynthesis through Periplasmic Expression. *Antibiotics,* **5**, 36.

115 Patin, D., Barreteau, H., Auger, G., Magnet, S., Crouvoisier, M., Bouhss, A., Touzé, T., Arthur, M., Mengin-Lecreulx, D. and Blanot, D. (2012) Colicin M hydrolyses branched lipids II from Gram-positive bacteria. *Biochimie,* **94**, 985–990.

116 Patzer, S. I., Albrecht, R., Braun, V. and Zeth, K. (2012) Structural and mechanistic studies of pesticin, a bacterial homolog of phage lysozymes. *J. Biol. Chem*. **287**, 23381–96.

117 Grinter, R., Milner, J. and Walker, D. (2012) Ferredoxin containing bacteriocins suggest a novel mechanism of iron uptake in *Pectobacterium spp. PLoS One* **7**, e33033.

118 Meyer, J. (1988) The evolution of ferredoxins. *Trends Ecol. Evol.,* **3**, 222–226.

119 HANKE, G. and MULO, P. (2013) Plant type ferredoxins and ferredoxin-dependent metabolism. *Plant. Cell Environ.* **36**, 1071–1084.

120 Andreini, C., Banci, L., Bertini, I., Elmi, S. and Rosato, A. (2007) Non-heme iron through the three domains of life. *Proteins Struct. Funct. Bioinforma.*, **67**, 317–324.

121 Fukuyama, K. (2004) Structure and Function of Plant-Type Ferredoxins. *Photosynth. Res.,* **81**, 289–301.

122 Bertini, I., Luchinat, C., Provenzani, A., Rosato, A. and Vasos, P. R. (2002) Browsing

gene banks for [2Fe-2S] ferredoxins and structural modeling of 88 plant-type sequences: an analysis of fold and function. *Proteins* **46**, 110–27.

123 Grinter, R., Josts, I., Zeth, K., Roszak, A. W., McCaughey, L. C., Cogdell, R. J., Milner, J. J., Kelly, S. M., Byron, O. and Walker, D. (2014) Structure of the atypical bacteriocin pectocin M2 implies a novel mechanism of protein uptake. *Mol. Microbiol.* **93**, 234–46.

124 Grinter, R., Josts, I., Mosbahi, K., Roszak, A. W., Cogdell, R. J., Bonvin, A. M. J. J., Milner, J. J., Kelly, S. M., Byron, O., Smith, B. O., et al. (2016) Structure of the bacterial plant-ferredoxin receptor FusA. *Nat. Commun*. **7**, 13308.

125 Mosbahi, K., Wojnowska, M., Albalat, A. and Walker, D. (2018) Bacterial iron acquisition mediated by outer membrane translocation and cleavage of a host protein. *Proc. Natl. Acad. Sci. U. S. A.,* **115**, 6840–6845.

126 Grinter, R., Hay, I. D., Song, J., Wang, J., Teng, D., Dhanesakaran, V., Wilksch, J. J., Davies, M. R., Littler, D., Beckham, S. A., et al. (2018) FusC, a member of the M16 protease family acquired by bacteria for iron piracy against plants. *PLOS Biol*. **16**, e2006026.

127 Okinaka, Y., Yang, C.-H., Perna, N. T. and Keen, N. T. (2002) Microarray Profiling of *Erwinia chrysanthemi* 3937 Genes That are Regulated During Plant Infection. *Mol. Plant-Microbe Interact.* **15**, 619–629.

128 Schneider, E. and Hunke, S. (1998) ATP-binding-cassette (ABC) transport systems: Functional and structural aspects of the ATP-hydrolyzing subunits/domains. *FEMS Microbiol. Rev.,* **22**, 1–20.

129 Kikhney, A. G. and Svergun, D. I. (2015) A practical guide to small angle X-ray scattering (SAXS) of flexible and intrinsically disordered proteins. *FEBS Lett.* **589**, 2570–2577.

130 Pauw, B. R. (2013) Everything SAXS: small-angle scattering pattern collection and correction. *J. Phys. Condens. Matter,* **25**, 383201.

131 Singh, P. S. (2017) Small-Angle Scattering Techniques (SAXS/SANS). In Membrane Characterisation, In Membrane Characterization, pp 95–111.

132 Gabel, F. (2017) Applications of SANS to Study Membrane Protein Systems, *Adv Exp Med Biol.* **1009** 201-214

133 Breyton, C., Gabel, F., Lethier, M., Flayhan, A., Durand, G., Jault, J.-M., Juillan-Binard, C., Imbert, L., Moulin, M., Ravaud, S., et al. (2013) Small angle neutron scattering for the study of solubilised membrane proteins. *Eur. Phys. J.* **36**, 71.

134 Jordan, A., Jacques, M., Merrick, C., Devos, J., Forsyth, V. T., Porcar, L. and Martel, A. (2016) SEC-SANS: size exclusion chromatography combined in situ with small-angle neutron scattering. *J. Appl. Crystallogr.,* **49**, 2015–2020.

135 Malaby, A. W., Chakravarthy, S., Irving, T. C., Kathuria, S. V., Bilsel, O. and Lambright, D. G. (2015) Methods for analysis of size-exclusion chromatography–small-angle X-ray scattering and reconstruction of protein scattering. *J. Appl. Crystallogr.* **48**, 1102–1113.

136 Fischer, H., de Oliveira Neto, M., Napolitano, H. B., Polikarpov, I., Craievich, A. F. and IUCr. (2010) Determination of the molecular weight of proteins in solution from a

single small-angle X-ray scattering measurement on a relative scale. *J. Appl. Crystallogr.,* **43**, 101–109.

137 Debye, P., Anderson, H. R., Brumberger, H. and Brumberger, A. H. (1957) Theory of Scattering by an Inhomogeneous Solid Possessing Fluctuations in Density and Anisotropy. *Light Scatt. Solut. J. Appl. Phys.* **28**, 1093.

138 Rambo, R. P. and Tainer, J. A. (2011) Characterizing flexible and intrinsically unstructured biological macromolecules by SAS using the Porod-Debye law. *Biopolymers* **95**, 559–571.

139 Tria, G., Mertens, H. D. T., Kachala, M. and Svergun, D. I. (2015) Advanced ensemble modelling of flexible macromolecules using X-ray solution scattering. *IUCrJ* **2**, 207–217.

140 Receveur-Brechot, V. and Durand, D. (2012) How random are intrinsically disordered proteins? A small angle scattering perspective. *Curr. Protein Pept. Sci.,* **13**, 55–75.

141 Franke, D. and Svergun, D. I. (2009) DAMMIF, a program for rapid ab-initio shape determination in small-angle scattering. *J. Appl. Cryst.* **42**, 342–346.

142 Bernadó, P., Mylonas, E., Petoukhov, M. V, Blackledge, M. and Svergun, D. I. (2007) Structural Characterization of Flexible Proteins Using Small-Angle X-ray Scattering. *J Am Chem Soc* **129**(17) 5656-64

143 Xu, M., McCanna, D. J. and Sivak, J. G. (2015) Use of the viability reagent PrestoBlue in comparison with alamarBlue and MTT to assess the viability of human corneal epithelial cells. *J. Pharmacol. Toxicol. Methods,* **71**, 1–7.

144 Petoukhov, M. V, Franke, D., Shkumatov, A. V, Tria, G., Kikhney, A. G., Gajda, M., Gorba, C., Mertens, H. D. T., Konarev, P. V and Svergun, D. I. (2012) New developments in the ATSAS program package for small-angle scattering data analysis. *J. Appl. Cryst.* **45**, 342–350.

145 Franke, D., Petoukhov, M. V., Konarev, P. V., Panjkovich, A., Tuukkanen, A., Mertens, H. D. T., Kikhney, A. G., Hajizadeh, N. R., Franklin, J. M., Jeffries, C. M., et al. (2017) *ATSAS 2.8* : a comprehensive data analysis suite for small-angle scattering from macromolecular solutions. *J. Appl. Crystallogr.,* **50**, 1212–1225.

146 Yang, J., Yan, R., Roy, A., Xu, D., Poisson, J. and Zhang, Y. (2015) The I-TASSER Suite: protein structure and function prediction. Nat. Methods **12**, 7–8.

147 Svergun, D., Barberato, C. and Koch, M. H. J. (1995) CRYSOL – a Program to Evaluate X-ray Solution Scattering of Biological Macromolecules from Atomic Coordinates. J. Appl. Cryst **28**, 768–773.

148 Sreerama, N. and Woody, R. W. (2000) Estimation of Protein Secondary Structure from Circular Dichroism Spectra: Comparison of CONTIN, SELCON, and CDSSTR Methods with an Expanded Reference Set. Anal. Biochem. **287**, 252–260.

149 Brookes, E., Demeler, B., Rosano, C. and Rocco, M. (2010) The implementation of SOMO (SOlution MOdeller) in the UltraScan analytical ultracentrifugation data analysis suite: enhanced capabilities allow the reliable hydrodynamic modeling of virtually any kind of biomacromolecule. *Eur. Biophys. J.,* **39**, 423–435.

150 Czajkowski, R., Pérombelon, M., Jafra, S., Lojkowska, E., Potrykus, M., van der Wolf,

J. and Sledz, W. (2015) Detection, identification and differentiation of *Pectobacterium* and *Dickeya* species causing potato blackleg and tuber soft rot: a review. *Ann. Appl. Biol*. **166**, 18–38.

151 Lechenet, M., Dessaint, F., Py, G., Makowski, D. and Munier-Jolain, N. (2017) Reducing pesticide use while preserving crop productivity and profitability on arable farms. *Nat. Plants,* **3**, 17008.

152 Gasteiger, E., Hoogland, C., Gattiker, A., Duvaud, S., Wilkins, M. R., Appel, R. D. and Bairoch, A. (2005) Protein Identification and Analysis Tools on the ExPASY Server. In The Proteomics Protocols Handbook (Walker, J. M., ed.), pp 571–607.

153 Choi, Y., Weiss, G. A., Collins, P. G. and Edu, C. Single Molecule Recordings of Lysozyme Activity. *Phys Chem Chem Phys*. **15**(36) 14879-95

154 Shugar, D. (1952) The measurement of lysozyme activity and the ultra-violet inactivation of lysozyme. *Biochim. Biophys. Acta* **8**, 302–308.

155 Rakin, A., Boolgakowa, E. and Heesemann, J. (1996) Structural and functional organization of the Yersinia pestis bacteriocin pesticin gene cluster. *Microbiology,* **142**, 3415–3424.

156 Yang, J., Yan, R., Roy, A., Xu, D., Poisson, J. and Zhang, Y. (2015) The I-TASSER Suite: protein structure and function prediction. *Nat. Methods* **12**, 7–8.

157 Svergun, D. I., Petoukhov, M. V and Koch, M. H. (2001) Determination of domain structure of proteins from X-ray solution scattering. *Biophys. J.,* **80**, 2946–53.

158 Kozin, M. B., Svergun, D. I. and IUCr. (2001) Automated matching of high- and low-resolution structural models. *J. Appl. Crystallogr.,* **34**, 33–41.

159 Papadakos, G., Housden, N. G., Lilly, K. J., Kaminska, R. and Kleanthous, C. (2012) Kinetic basis for the competitive recruitment of TolB by the intrinsically disordered translocation domain of colicin E9. *J. Mol. Biol.* **418**, 269–80.

160 Koebnik, R., Locher, K. P. and Van Gelder, P. (2000) Structure and function of bacterial outer membrane proteins: barrels in a nutshell. *Mol. Microbiol.,* **37**, 239–253.

161 Noinaj, N., Guillier, M., Banard, T. J. and Buchanan, S. K. (2010) TonB-dependent transporters: regulation, structure and function. *Annu. Rev. Microbiol.* **64**, 43–60.

162 Tang, K., Jiao, N., Liu, K., Zhang, Y. and Li, S. (2012) Distribution and Functions of TonB-Dependent Transporters in Marine Bacteria and Environments: Implications for Dissolved Organic Matter Utilization. *PLoS One* **7**, e41204.

163 Schauer, K., Rodionov, D. A. and de Reuse, H. (2008) New substrates for TonB-dependent transport: do we only see the 'tip of the iceberg'? *Trends Biochem. Sci.*, **33**, 330–338.

164 Schons, V., Atkinson, R. A., Dugave, C., Graff, R., Mislin, G. L. A., Rochet, L., Hennard, C., Kieffer, B., Abdallah, M. A. and Schalk, I. J. (2005) The Structure−Activity Relationship of Ferric Pyoverdine Bound to Its Outer Membrane Transporter: Implications for the Mechanism of Iron Uptake. *Biochemistry* **44**, 14069–14079.

165 Pawelek, P. D., Croteau, N., Ng-Thow-Hing, C., Khursigara, C. M., Moiseeva, N., Allaire, M. and Coulton, J. W. (2006) Structure of TonB in Complex with FhuA, *E. coli*

Outer Membrane Receptor. *Science* **312**(5778) 1399-402.

166 Kozin, M. B., and Svergun, D. I. (2001) Automated matching of high- and low-resolution structural models. *J. Appl. Crystallogr.,* **34**, 33–41.

167 Brillet, K., Journet, L., Célia, H., Paulus, L., Stahl, A., Pattus, F. and Cobessi, D. (2007) A β Strand Lock Exchange for Signal Transduction in TonB-Dependent Transducers on the Basis of a Common Structural Motif. *Structure,* **15**, 1383–1391.

168 Postle, K., Kastead, K. A., Gresock, M. G., Ghosh, J. and Swayne, C. D. (2010) The TonB dimeric crystal structures do not exist in vivo. *MBio*, **1**(5) e00307-10

169 Howard, S. P., Herrmann, C., Stratilo, C. W. and Braun, V. (2001) In Vivo Synthesis of the Periplasmic Domain of TonB Inhibits Transport through the FecA and FhuA Iron Siderophore Transporters of *Escherichia coli. J. Bacteriol.* **183**, 5885–5895.

170 Brautigam, C. A. (2015) Calculations and Publication-Quality Illustrations for Analytical Ultracentrifugation Data. *Methods Enzymol.,* **562**, 109–133.

171 Christie, J. M., Hitomi, K., Arvai, A. S., Hartfield, K. A., Mettlen, M., Pratt, A. J., Tainer, J. A. and Getzoff, E. D. (2012) Structural Tuning of the Fluorescent Protein iLOV for Improved Photostability. J. Biol. Chem. **287**, 22295–22304.

172 Buckley, A. M., Petersen, J., Roe, A. J., Douce, G. R. and Christie, J. M. (2015) LOV-based reporters for fluorescence imaging. *Curr. Opin. Chem. Biol.,* **27**, 39–45.

173 Ganz, T. (2009) Iron in innate immunity: starve the invaders. *Curr. Opin. Immunol.,* **21**, 63–67.

174 van Wees, S. C. M. and Glazebrook, J. (2003) Loss of non-host resistance of Arabidopsis NahG to *Pseudomonas syringae pv. phaseolicola* is due to degradation products of salicylic acid. *Plant J.* **33**, 733–742.

175 Raoul des Essarts, Y., Cigna, J., Quêtu-Laurent, A., Caron, A., Munier, E., Beury-Cirou, A., Hélias, V. and Faure, D. (2015) Biocontrol of the Potato Blackleg and Soft Rot Diseases Caused by *Dickeya dianthicola*. *Appl. Environ. Microbiol.,* **82**, 268–78.

176 Grinter, R., Milner, J. and Walker, D. (2013) Beware of proteins bearing gifts: Protein antibiotics that use iron as a Trojan horse. *FEMS Microbiol. Lett.* **338**, 1–9.

177 Carvalho-Castro, G. A., Silva, J. R., Paiva, L. V, Custódio, D. A. C., Moreira, R. O., Mian, G. F., Prado, I. A., Chalfun-Junior, A. and Costa, G. M. (2017) Molecular epidemiology of Streptococcus agalactiae isolated from mastitis in Brazilian dairy herds. *Braz. J. Microbiol.,* **48**, 551–559.

178 Rea, M. C., Ross, R. P., Cotter, P. D. and Hill, C. (2011) Classification of Bacteriocins from Gram-Positive Bacteria. In Prokaryotic Antimicrobial Peptides, pp 29–53, Springer New York, New York, NY.

179 Rollema, H. S., Kuipers, O. P., Both, P., de Vos, W. M. and Siezen, R. J. (1995) Improvement of solubility and stability of the antimicrobial peptide nisin by protein engineering. *Appl. Environ. Microbiol.,* **61**, 2873–8.

180 Jack, R. W., Tagg, J. R. and Ray, B. (1995) Bacteriocins of Gram-Positive Bacteria. *Microbiol. Rev.***59**(2) 171-200

181 Bastos, M. do C. de F., Coutinho, B. G. and Coelho, M. L. V. (2010) Lysostaphin: A Staphylococcal Bacteriolysin with Potential Clinical Applications. *Pharmaceuticals* **3**, 1139–1161.

182 Zhao, H.-L., Chen, X.-L., Xie, B.-B., Zhou, M.-Y., Gao, X., Zhang, X.-Y., Zhou, B.-C., Weiss, A. S. and Zhang, Y.-Z. (2012) Elastolytic Mechanism of a Novel M23 Metalloprotease Pseudoalterin from Deep-sea Pseudoalteromonas sp. CF6-2: Cleaving not only glycyl bonds in the hydrophobic regions but also peptide bonds in the hydrophilic regions involved in cross-linking. *J Biol Chem* **287**(47) 39710-20

183 Xing, M., Simmonds, R. S. and Timkovich, R. (2016) Solution structure of the Cys74 to Ala74 mutant of the recombinant catlytic domain of Zoocin A. *Proteins*. **85**(!) 177-181

184 Chen, Y., Simmonds, R. S., Sloan, G. L. and Timkovich, R. (2008) The metal binding site of zoocin A. *J. Biol. Inorg. Chem.,* **13**, 855–60.

185 Galarneau, A., Primeau, M., & L.-E. T. and Michnick, S. W. (2002) β-Lactamase protein fragment complementation assays as in vivo and in vitro sensors of protein–protein interactions. *Nat. Biotechnol.* **20**, 619–622.

186 Suhre, K. and Sanejouand, Y.-H. (2004) ElNemo: a normal mode web server for protein movement analysis and the generation of templates for molecular replacement. Nucleic Acids Res., **32**, W610–W614.

187 Climo, M. W., Ehlert, K. and Archer, G. L. (2001) Mechanism and suppression of lysostaphin resistance in oxacillin-resistant *Staphylococcus aureus. Antimicrob. Agents Chemother.,* **45**, 1431–7.

188 Kusuma, C., Jadanova, A., Chanturiya, T. and Kokai-Kun, J. F. (2007) Lysostaphin-resistant variants of *Staphylococcus aureus* demonstrate reduced fitness in vitro and in vivo. *Antimicrob. Agents Chemother.,* **51**, 475–82.

189 Schleifer, K. and Kandler, O. (1972) Peptidoglycan Types of Bacterial Cell Walls and their Taxonomic Implications. *Bacteriol. Rev.***36** (4) 407-77

190 Kim, S. J., Chang, J. and Singh, M. (2015) Peptidoglycan architecture of Gram-positive bacteria by solid-state NMR. *Biochim Biophys Acta* **1848** (1ptB) 350-362

191 Velikova, N., Kavanagh, K. and Wells, J. M. (2016) Evaluation of *Galleria mellonella* larvae for studying the virulence of *Streptococcus suis*. *BMC Microbiol.,* **16**, 291.

192 Mills, A. and Duong, F. (2017) Lipopolysaccharides promote binding and unfolding of the antibacterial colicin E3 rRNAse domain. *Biochim. Biophys. Acta* **1859**, 2454–2460.

193 Dellagi, A., Segond, D., Rigault, M., Fagard, M., Simon, C., Saindrenan, P. and Expert, D. (2009) Microbial Siderophores Exert a Subtle Role in *Arabidopsis* during Infection by Manipulating the Immune Response and the Iron Status. *Plant Physiol*. **150**, 1687–1696.

194 Dellagi, A., Rigault, M., Segond, D., Roux, C., Kraepiel, Y., Cellier, F., Briat, J.-F., Gaymard, F. and Expert, D. (2005) Siderophore-mediated upregulation of Arabidopsis ferritin expression in response to *Erwinia chrysanthemi* infection. *Plant J.* **43**, 262–272.

195 Lavermicocca, P., Lonigro, S. L., Valerio, F., Evidente, A. and Visconti, A. (2002) Reduction of olive knot disease by a bacteriocin from *Pseudomonas syringae pv. ciccaronei*. *Appl. Environ. Microbiol.,* **68**, 1403–7.

196 Heuer, H., Kroppenstedt, R. M., Lottmann, J., Berg, G. and Smalla, K. (2002) Effects

of T4 lysozyme release from transgenic potato roots on bacterial rhizosphere communities are negligible relative to natural factors. *Appl. Environ. Microbiol.,* **68**, 1325–35.

197 Liu, B., Zeng, Q., Yan, F., Xu, H. and Xu, C. (2005) Effects of transgenic plants on soil microorganisms. *Plant Soil,* **271**, 1–13.

198 Düring, K., Porsch, P., Fladung, M. and Lörz, H. (1993) Transgenic potato plants resistant to the phytopathogenic bacterium *Erwinia carotovora*. *Plant J.,* **3**, 587–598.

199 García, P., Rodríguez, L., Rodríguez, A. and Martínez, B. (2010) Food biopreservation: Promising strategies using bacteriocins, bacteriophages and endolysins. *Trends Food Sci. Technol.***21**(8) 373-382

200 Bailey, T. L. and Elkan, C. (1994) Fitting a mixture model by expectation maximization to discover motifs in biopolymers. *Proceedings. Int. Conf. Intell. Syst. Mol. Biol.* **2**, 28–36.